

**Multi-Scale Fluctuations
in Non-Equilibrium Systems:
Statistical Physics and Biological Application**

DISSERTATION

zur Erlangung des akademischen Grades

**Doctor rerum naturalium
(Dr. rer. nat.)**

vorgelegt

dem Bereich Mathematik und Naturwissenschaften der Technischen
Universität Dresden

von

Felix Jonathan Meigel

geboren am 27. Juli 1994 in München

Max-Planck-Institut für Physik komplexer Systeme

Februar 2023

Eingereicht am 9. Februar 2023

Verteidigt am 15. Juni 2023

Gutachter:

Prof. Dr. Frank Jülicher

Prof. Dr. Steffen Rulands

Prof. Dr. Benjamin Friedrich

Abstract

Understanding how fluctuations continuously propagate across spatial scales is fundamental for our understanding of inanimate matter. This is exemplified by self-similar fluctuations in critical phenomena and the propagation of energy fluctuations described by the Kolmogorov-Law in turbulence. Our understanding is based on powerful theoretical frameworks that integrate fluctuations on intermediary scales, as in renormalisation group or coupled mode theory. In striking contrast to typical inanimate systems, living matter is typically organised into a hierarchy of processes on a discrete set of spatial scales: from biochemical processes embedded in dynamic subcellular compartments to cells giving rise to tissues. Therefore, the understanding of living matter requires novel theories that predict the interplay of fluctuations on multiple scales of biological organisation and the ensuing emergent degrees of freedom. In this thesis, we derive a general theory of the multi-scale propagation of fluctuations in non-equilibrium systems and show that such processes underlie the regulation of cellular behaviour. Specifically, we draw on paradigmatic systems comprising stochastic many-particle systems undergoing dynamic compartmentalisation.

We first derive a theory for emergent degrees of freedom in open systems, where the total mass is not conserved. We show that the compartment dynamics give rise to the localisation of probability densities in phase space resembling quasi-particle behaviour. This emergent quasi-particle exhibits fundamentally different response kinetics and steady states compared to systems lacking compartment dynamics. In order to investigate a potential biological function of such quasi-particle dynamics, we then apply this theory to the regulation of cell death. We derive a model describing the subcellular processes that regulate cell death and show that the quasi-particle dynamics gives rise to a kinetic low-pass filter which suppresses the response of the cell to fast fluctuations in cellular stress signals. We test our predictions experimentally by quantifying cell death in cell cultures subject to stress stimuli varying in strength and duration.

In closed systems, where the total mass is conserved, the effect of dynamic compartmentalisation depends on details of the kinetics on the scale of the stochastic many-particle dynamics. Using a second quantisation approach, we derive a commutator relation between the kinetic operators and the change in total entropy. Drawing on this, we show that the compartment dynamics alters the total entropy if the kinetics of the stochastic many-particle dynamics violate detailed balance. We apply this mechanism to the activation of cellular immune responses to RNA-virus infections. We show that dynamic compartmentalisation in closed systems gives rise to giant density fluctuations. This facilitates the emergence of gelation under conditions that violate theoretical gelation criteria in the absence of compartment dynamics. We show that such multi-scale gelation of protein complexes on the membranes of dynamic mitochondria governs the innate immune response.

Taken together, we provide a general theory describing the multi-scale propagation of fluctuations in biological systems. Our work pioneers the development of a statistical physics of such systems and highlights emergent degrees of freedom spanning different scales of biological organisation. By demonstrating that cells manipulate how fluctuations propagate across these scales, our work motivates a rethinking of how the behaviour of cells is regulated.

Zusammenfassung

Unser Verständnis von unbelebter Materie basiert auf der Schlussfolgerung von den Wechselwirkungen zwischen den Bestandteilen der Materie auf materielle Eigenschaften. Insbesondere, wie sich Fluktuationen kontinuierlich über räumliche Skalen ausbreiten, ist grundlegend für unser Verständnis unbelebter Materie, was kritische Phänomene oder das Kolmogorov-Gesetz in Turbulenz verdeutlichen. Die Beschreibung der Propagation von Fluktuationen erfordert theoretische Formalismen, wie Renormierungsgruppentheorie oder die Theorie gekoppelter Moden, welche Fluktuationen über auf alle Zwischenskalen hinweg integrieren. Im Gegensatz dazu ist lebende Materie in einer Hierarchie von Prozessen auf diskreten räumlichen Skalen organisiert, von biochemischen Prozessen, die in dynamische subzelluläre Kompartimente eingebettet sind, bis hin zu Zellen, aus denen Gewebe entstehen. Um lebende Materie zu verstehen, sind neue Theorien erforderlich, die das emergente Verhalten vorhersagen, das sich aus dem Zusammenspiel von Fluktuationen über mehrere Skalen biologischer Organisation ergibt. In dieser Arbeit leiten wir eine allgemeine Theorie der Ausbreitung von Fluktuationen in Nicht-Gleichgewichtssystemen über mehrere Skalen hinweg ab und zeigen, dass solche Prozesse das Verhalten von Zellen regulieren. Anhand von paradigmatischen Systemen, die aus stochastischen Vielteilchensystemen mit dynamischer Kompartimentierung bestehen, leiten wir eine Theorie für emergente Freiheitsgrade in offenen Systemen ab, in denen die Gesamtmasse nicht konserviert ist. Wir zeigen, dass Kompartimentdynamik zu einer Lokalisierung von Wahrscheinlichkeitsdichten im Phasenraum führt, die einem Quasiteilchenverhalten ähnelt. Dieses Quasiteilchen weist eine grundlegend andere Reaktionskinetik und einen anderen stationären Zustand auf als Systeme ohne Kompartimentdynamik. Um die biologische Funktion einer solchen Quasiteilchendynamik zu untersuchen, wenden wir die Theorie auf die Regulierung des Zelltods an. Wir leiten ein Modell ab, das die subzellulären Prozesse beschreibt, die den Zelltod regulieren, und zeigen, dass die Quasiteilchendynamik zu einem kinetischen Tiefpassfilter führt, der die Reaktion der Zelle auf schnelle Fluktuationen in zellulären Stresssignalen unterdrückt. Um unsere Vorhersagen zu testen, quantifizieren wir Apoptose in Zellkulturen, die Stressreizen unterschiedlicher Stärke und Dauer ausgesetzt sind. In geschlossenen Systemen, in denen Masseerhaltung gilt, hängt die Wirkung der dynamischen Kompartimentierung von Details der Kinetik auf der mikroskopischen Skala ab. Mithilfe eines Besetzungszahldarstellungsansatzes leiten wir eine Kommutatorbeziehung zwischen den kinetischen Operatoren und der Änderung der Gesamtentropie ab. Die Kompartimentdynamik beeinflusst die Gesamtentropie, wenn die Kinetik auf der kleinsten Skala das detaillierte Gleichgewicht stört. Wir wenden diesen Mechanismus auf den Nachweis von RNA-Viren durch das angeborene Immunsystem an. Außerdem zeigen wir, dass kompartimentierte Systeme extreme Dichtefluktuationen aufweisen, was das Entstehen eines Gel unter Bedingungen ermöglicht, die gegen theoretische Gel-Bildungskriterien in statisch kompartmentalisierten Systemen verstoßen. Wir belegen, dass eine solche mehrskalige Gelierung von Proteinkomplexen auf der mitochondrialen Membran die angeborene Immunantwort von Zellen reguliert. Zusammengefasst liefern wir eine allgemeine Theorie, die die Ausbreitung von Fluktuationen in biologischen Systemen auf mehreren Skalen beschreibt. Unsere Arbeit leistet Pionierarbeit in der Entwicklung einer statistischen Physik von multiskalen Systemen und beschreibt emergente Freiheitsgrade, die sich über verschiedene Skalen der biologischen Organisation erstrecken. Wir zeigen, dass Zellen die Ausbreitung von Fluktuationen über diese Skalen hinweg manipulieren können, was uns herausfordert, die Frage nach der Regulation von Zellverhalten neu zu denken.

Acknowledgments

I would like to express my deep gratitude to all those who have supported me throughout my academic journey and the completion of this thesis. This achievement would not have been possible without the unwavering support and guidance of many individuals who have made a significant impact on my life.

I would like to express my sincere gratitude to Professor Dr Steffen Rulands for his invaluable support which went beyond just scientific guidance. Throughout my PhD, Professor Rulands provided me with a mentor-mentee relationship which gave me the freedom to explore different aspects of my PhD project while also providing scientific guidance. I had stimulating meetings with him on a regular basis, which provided me with new perspectives on my research. I particularly appreciated his encouragement to think outside the box and his ability to draw analogies between various systems, in order to demonstrate the value of understanding physics. Beyond the scientific guidance, Prof. Rulands taught me a lot about presentation skills and how to communicate science in inter-disciplinary environments. I am also thankful for the personal support he gave me on a number of occasions when I was struggling with fundamental doubts.

I am grateful to Professor Dr Frank Jülicher for his numerous constructive comments which identified superficialities and imprecise formulations in projects. I am particularly grateful to Professor Jülicher for creating a stimulating and productive scientific environment in which projects and ideas are discussed critically and yet constructively. I have learned from Professor Jülicher to be rigorous and unambiguous in my assumptions and scientific reasoning.

I had the privilege to supervise the Bachelor thesis project of Josef Kaenders and the Master thesis project of Rushikesh Shinde during my PhD. I particularly enjoyed the scientific discussions I had with Mr. Kaenders, which largely inspired the findings of Chapter 5 of this thesis. I would like to express my gratitude to Mr. Kaenders for his structured approach to implementing the dynamics of compartmentalised systems in numerical routines, as this provided a strong foundation for my work. I am also thankful to Rushikesh Shinde for our conversations on the core mechanisms and assumptions of thermodynamics. Through our discussions, Mr. Shinde motivated me to question my own understanding of thermodynamics and, in doing so, indicated directions for my own research projects, in particular the results presented in chapter 4.

I want to thank our experimental collaborator PD. Dr. med. Philipp Mergenthaler and Lina Hellwig for the many discussions about the biology and physiological dynamics of apoptosis. In particular, I want to express my gratitude to PD. Dr. med. Philipp Mergenthaler and Lina Hellwig for conducting numerous experiments to test our theoretical predictions experimentally.

Throughout my thesis, Professor Dr Karen Alim offered me the chance to engage in regular scientific dialogue. During these meetings, Professor Alim not only provided me with guidance on how to undertake research, but also encouraged me to pursue my projects with her unwavering enthusiasm for science. Furthermore, I am immensely grateful to Professor Alim for her patience and commitment to helping me publish the findings of

my master's thesis, even after I had left her research group.

I am grateful to Aida Hashtroud, Adolfo Alsina and Johanna Dickmann for the many conceptual discussions I had about my research projects during my PhD. Not only did I gain new insights into my research projects whenever I was stuck, but their support and guidance also provided me with renewed motivation at each and every meeting.

I am also thankful to Christian Hanauer, Ali Tahaei and Jonathan Bauermann for their scientific discussions and valuable comments, and to Mirna Kramar, Leonie Bastin and Nico Schrammar for inspiring discussions. I am particularly indebted to Aida Hashtroud, Matteo Ciarchi, Yiteng Dang, Kathrin Laxhuber, and Ali Tahaei for their instructive comments on my thesis. I wish to thank the entire scientific PKS environment and the Rulands group in particular for creating a stimulating research environment. My appreciation also goes to Ulrike Burkert and the administration of the MPI PKS for their help with all the bureaucratic matters.

I want to thank my family for the unconditional support that I have received. My parents always supported me in all possible ways. I could have never wished for better parents. I also want to thank my brother for being there, when I needed help. I thank my grandparents, who have financially supported me in my studies. In this regard, I specifically want to thank my grandfather Prof. Dr. med. Wilhelm Meigel, who always was an inspiration for me. Finally, I would like to thank my hamster, to whom I dedicate this thesis. Your unwavering support throughout this endeavour was truly invaluable and I apologise for the frustration which I may have inadvertently directed towards you. I thank you from the bottom of my heart for always bringing a more optimistic perspective to my life. I would not have been able to make it this far without your support and I will never forget how you supported me in the last years.

Contents

1. Introduction	1
1.1. Propagation of fluctuations in inanimate matter	1
1.2. The multi-scale organisation of living matter	3
1.3. Research question and main findings of the thesis	7
2. Theory of collective degrees of freedom in open compartmentalised systems	11
2.1. Introduction	11
2.2. Literature review of compartmentalised systems: dynamics on distinct spatial scales	12
2.2.1. Mathematical framework for stochastic reaction network kinetics	13
2.2.2. Compartment dynamics within the framework of population balance equations	14
2.2.3. Smoluchowski aggregation-fragmentation dynamics	17
2.3. Compartmentalised stochastic systems within the framework of Master equations	19
2.4. Effective dynamics of open compartmentalised systems	22
2.4.1. Flux approximation of compartment fusion	23
2.4.2. Generalisations on the flux approximation of compartment fusion	29
2.4.3. Flux approximation of compartment fragmentation	34
2.4.4. Flux approximation of compartment growth and shrinkage	35
2.4.5. Effective ensemble dynamics and their limitations	36
2.5. Emergence of a single, collective degree of freedom	38
2.5.1. Qualitative effects of compartment dynamics	38
2.5.2. Compartment fusion and fragmentation give rise to a collective degree of freedom	40
2.5.3. Discussion on how the collective degree of freedom resembles a quasi-particle	43
2.6. Equations of motion for the quasi-particle	44
2.7. Kinetic properties of the quasi-particle	48
2.7.1. Mechanic analogue of the quasi-particle	48
2.7.2. Response kinetics of the quasi-particle	49
2.8. Discussion	51
3. Application to multi-scale fluctuations in the regulation of cell death	55
3.1. Introduction	55
3.2. Literature review on organelle and signalling pathway dynamics	56
3.2.1. Cell signalling pathways	56
3.2.2. Biology of organelles	57
3.2.3. Biology of cell death decision-making	59
3.3. The regulation of cell death in the framework of compartmentalised systems	62
3.3.1. Modelling the Bcl2 reaction network	63
3.3.2. Effective model of the apoptotic signalling pathway	65

3.4.	Quasi-particle kinetics in the regulation of cell death	69
3.5.	Fluctuating stimuli and the emergence of a kinetic low-pass filter	78
3.6.	Improvement of the sensitivity and specificity of apoptotic decision-making	81
3.7.	Testing for the predicted quasi-particle kinetics in experiments	83
3.7.1.	Test for the localisation of mitochondria in the concentration phase space	85
3.7.2.	Observing sigmoidal response kinetics of the quasi-particle in ex- periments	87
3.7.3.	Testing for the sigmoidal progression of apoptosis in cell culture experiments	87
3.8.	Discussion of applying quasi-particle kinetics to apoptotic decision-making	90
3.8.1.	Is a separation of timescales a plausible choice for organelle-associated signalling pathways?	90
3.8.2.	Potential therapeutic strategies for facilitating and mitigating apop- tosis by mitochondrial dynamics	92
3.9.	Discussion on quasi-particle kinetics in signalling pathways beyond apoptosis	93
3.9.1.	Application to the regulation of oxidative phosphorylation	93
3.9.2.	Application to the regulation of protein synthesis (mTORC1 pathway)	94
3.9.3.	Application to endosomal maturation	94
3.9.4.	Application to cellular innate immune signalling (MAVS pathway) .	95
3.10.	Conclusion	96
4.	Towards a thermodynamics of closed compartmentalised systems	97
4.1.	Introduction	97
4.2.	Literature review on the thermodynamics of compartmentalisation	99
4.2.1.	The definition of entropy	99
4.2.2.	Gibbs' paradox	103
4.2.3.	Maxwell's demon	105
4.3.	Model definition: How compartment dynamics induce temporal ordering .	107
4.3.1.	The connection between dynamic compartmentalisation and the modification of system constraints	107
4.3.2.	Temporal order induced by compartment fragmentation	108
4.3.3.	Compartment fusion and fragmentation dynamics	112
4.4.	The ideal gas subject to dynamic compartmentalisation	112
4.4.1.	Understanding the ideal gas as stochastic many-body dynamics . .	112
4.4.2.	Finite-sized ideal gas ensembles as a multi-variate random variables	113
4.4.3.	Simulation of the ideal gas subject to sequential and synchronous compartment fragmentation	116
4.4.4.	Proof of entropic neutrality under dynamic compartmentalisation .	118
4.4.5.	The ideal gas as a special case?	124
4.5.	Stochastic many-body dynamics subject to dynamic compartmentalisation	124
4.5.1.	Refinement on boundary conditions	125
4.5.2.	Describing compartment dynamics in the formalism of the Second quantisation	126
4.5.3.	Quantised gases subject to sequential compartment fragmentation .	132
4.5.4.	Reversible polymerisation dynamics subject to sequential compart- ment fragmentation	137

4.6.	Effects of dynamic compartmentalisation on the total system’s entropy . . .	142
4.6.1.	Discussing thermodynamic inconsistencies	142
4.6.2.	Linking microscopic interaction rules with entropic neutrality under dynamic compartmentalisation	145
4.6.3.	Breaking entropic neutrality by performing work on the system . . .	146
4.6.4.	Effect of compartment dynamics beyond compartment fusion and fragmentation on the total entropy	152
4.7.	Technical and biological relevance of dynamic compartmentalisation	152
4.8.	Discussion	155
5.	Multi-scale fluctuations facilitate gelation in the innate immune response	159
5.1.	Introduction	159
5.2.	Literature review on gelation in reversible polymerisation kinetics	160
5.2.1.	Physical modelling of fusion and fragmentation kernels	161
5.2.2.	Gel-forming solutions to the Smoluchowski aggregation-fragmentation equation	163
5.3.	Reversible polymerisation subject to dynamic compartmentalisation	165
5.4.	Dynamic compartmentalisation facilitates the formation of giant aggregates	167
5.4.1.	Dynamic compartmentalisation increases the frequency of large ag- gregates	168
5.4.2.	Testing different aggregation and fragmentation kernels	175
5.4.3.	System size scaling shows characteristics of gelation	179
5.5.	Application to the cellular immune response to RNA-virus infections . . .	181
5.5.1.	Innate immune signalling	181
5.5.2.	Discussion on how multi-scale gelation facilitates cellular anti-viral responses	183
5.6.	Discussion	185
6.	Conclusion and outlook	189
6.1.	Discussion of the main findings of this thesis	190
6.1.1.	Deriving effective dynamics of open compartmentalised systems . . .	190
6.1.2.	Collective response kinetics in the regulation of cell death	191
6.1.3.	Thermodynamics of closed compartmentalised systems	192
6.1.4.	Extremal fluctuations and multi-scale gelation	194
6.2.	Outlook and future research perspectives	195
A.	Mathematical concepts	199
A.1.	Master Equation	199
A.2.	Compartment dynamics in the framework of Master equations	200
A.3.	Stochastic two-body interaction dynamics	203
A.4.	Waddington’s epigenetic landscape as a metaphor for signalling pathways .	204
A.5.	Modification of Kramer’s escape rate due to compartment dynamics	206
A.6.	Modification of Kramer’s escape rate due to heterogeneous size distributions	207
A.7.	Pre- and post-modifications in apoptotic signalling pathway	208
B.	Numerical routines	209
B.1.	Numerical routine for the simulation of compartmentalised systems	209
B.2.	Optimisation of the numerical routine to account for gelation dynamics . .	210

Contents

B.3. Routine for the efficient numerical investigation of finite-sized ideal gas ensembles	211
List of Figures	213
Bibliography	215

1. Introduction

1.1. Propagation of fluctuations in inanimate matter

The Encyclopedia Britannica defines Physics as the "science that deals with the structure of matter and the interactions between the fundamental constituents of the observable universe" [1]. Our universe exhibits a large variety of structures of matter across a vast range of spatial scales: atoms organised in lattice structures form solid crystal structures, interacting water molecules constitute as ice, liquid, or gas depending on temperature, and stars interact through gravitational forces to form galaxies. A key question in Physics is to understand how the constituents of matter interact to give rise to phenomena on much larger spatial scales. The advent of classical Physics can be attributed to the work of Galileo Galilei, Johannes Kepler, and Nicolaus Copernicus [2], who described the mechanics of our solar system by introducing mathematics as the language of physics, allowing for measurable predictions [3]. The orbital mechanics of planets in the solar system can be seen as an epitome of how seemingly simple laws can explain complex phenomena in nature. This example has since been an inspiration to physicists to describe the interactions of ever smaller constituents of matter by describing their interactions through simple laws [4]. Yet, as one approaches the microscopic realm with an increasingly large number of constituents, the complexity of predicting macroscopic behaviour from microscopic interaction laws rises drastically. This effectively prohibited the understanding of systems composed of more than a few tens of particles, [5], and required the development of theories that were able to bridge the gap between microscopic interactions and their consequences on the macroscopic properties of matter.

Statistical physics overcame this barrier by providing a statistical formalism to link microscopic rules to macroscopic material properties, such as temperature, pressure, and magnetisation [6, 7]. This is based on the idea that the behaviour of large numbers of particles can be described by random variables with associated probabilities. Using this approach, statistical physics makes predictions about the macroscopic properties of matter by calculating summary statistics such as averages from the random variables describing microscopic states. Random deviations of constituents from their average state are termed fluctuations. How such fluctuations propagate in space, as encoded in correlation functions, is central to understanding macroscopic material properties.

For example, the fluctuation-dissipation theorem, [8], is a fundamental principle in statistical physics. In thermal equilibrium it relates the correlation of fluctuations of a material to its response to external perturbations. As an example, Brownian motion is the random movement of particles suspended in a fluid caused by collisions of these particles with the molecules of the fluid. The fluctuation-dissipation theorem relates the velocity fluctuations caused by Brownian motion to a drag as a body is moved through a fluid [8, 9]. Another example is Johnson electronic noise related to the random thermal motion of electrons in a conductor. The fluctuation-dissipation theorem relates Johnson noise to electrical resistance in circuits [10, 11].

The fluctuation-dissipation theorem exemplifies the importance of understanding how

1. Introduction

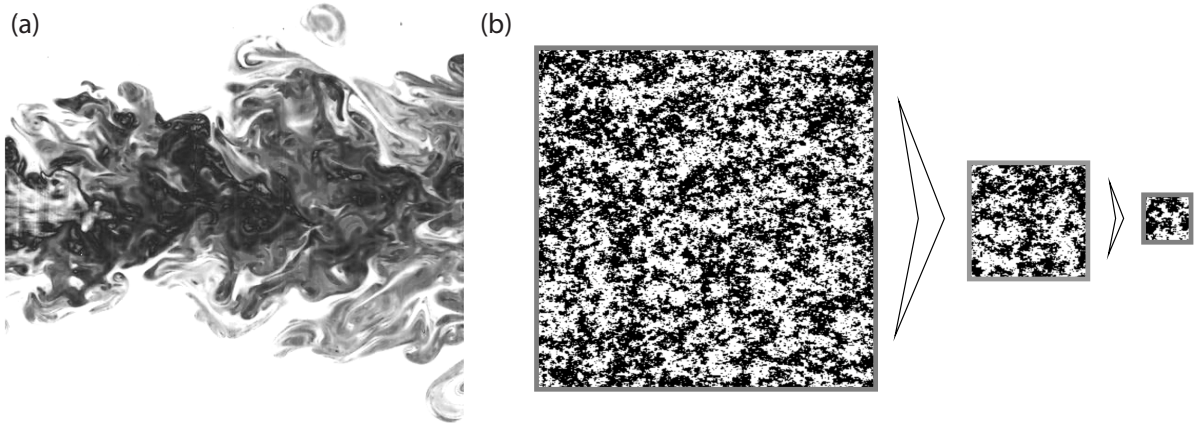


Fig. 1.1.: Our understanding of inanimate matter relies on how fluctuations propagate through scales (a) The energy cascade describes how macro-scale fluctuations introduced into an inertial fluid generate eddies which then break down into progressively smaller structures until the energy is dissipated as thermal fluctuations on the micro-scale. The image is adapted from [19]. (b) Renormalisation group theory is used to understand how the behaviour of a system changes as its scale changes, and to predict the behaviour of the system at different scales based on its behaviour at a single scale. The theory is based on the idea of to summarise over and "renormalise" the parameters of the system at different scales, so that they reflect the behaviour of the system at that scale. The image is adapted from [20].

fluctuations propagate in space for understanding macroscopic properties of matter. Particularly striking examples for the importance of understanding the propagation of fluctuations arise in the theories of phase transitions and non-equilibrium matter; compare also with Fig. 1.1 for an illustration. In turbulent flow, macroscale perturbations are applied to a viscous fluid, such as through stirring, which lifts the fluid into a non-equilibrium state. This generates swirls which break down into progressively smaller structures until the energy stored in these swirls is dissipated as thermal fluctuations on a smaller scale [12–14]. This continuous propagation of velocity fluctuations down from the macroscopic scale is termed the energy cascade.

Critical phenomena are another prominent example where the interplay between fluctuations on vastly different spatial scales gives rise to macroscopic phenomenology [15–17]. Preparing a physical system at a critical point leads to two experimental observations [18]: Firstly, the system is scale invariant, resulting in observations from different distances being statistically similar, and therefore all length scales being equally represented. Mathematically, this implies that fluctuations are correlated throughout the system, with the correlation length being infinite. Secondly, as the critical point is approached, many thermodynamic properties, such as magnetic susceptibility, specific heat and compressibility, change in accordance with a power law. Moreover, the same macroscopic behaviour can be observed at critical points of different physical systems; this phenomenon is referred to as universality. For example, magnets made of different materials may exhibit the same power laws.

These phenomena have motivated the development of theoretical methods that allow making predictions about macroscopic states of matter by integrating the effect of fluctuations from a range of different length scales [15–18]. In the theory of phase transitions and critical phenomena, renormalisation group theory has led to a general understand-

ing of the origins of scaling behaviour and universality in phase transitions. In order to understand these observations, a naive approach of averaging over large length scales to write down a macroscopic theory is not adequate, as all length scales are relevant at the critical point. Consequently, a method which allows for the derivation of macroscopic descriptions through the incorporation of all length scales is necessary. Renormalisation group theory achieves this by systematically deriving a macroscopic description from a microscopic description, length scale by length scale.

Underlying renormalisation is the fundamental idea of coarse graining. That is, at each step we integrate out the smallest length scale from the partition function. For example, in a magnetic lattice system, blocks of lattice points can be combined to represent a block by an effective lattice point, a technique known as block spin renormalisation [17]. The magnetic moment of this effective lattice point is usually taken to be the average of all magnetic moments in the block. Following the averaging, the lengths are rescaled to their original values and the fields are renormalised, so that the energy scale conforms to that of the original system. If the original system is described by a Hamiltonian¹, then these three steps yield a new Hamiltonian that describes the system at the coarsened scale. Because of scale invariance, the new Hamiltonian is assumed to be structurally identical, but with changed parameters [16, 17].

Repeating this procedure leads to a renormalisation flow describing how the Hamiltonian changes continuously from the microscopic to the macroscopic level. Close to the critical point, this renormalisation flow converges to the vicinity of fixed points which describe the macroscopic properties of the Hamiltonian. All microscopic systems that flow into the same fixed point show the same macroscopic properties, which is the foundation of universality [18]. The stability of the fixed point with respect to small changes in model parameters is quantitatively associated with the exponents describing the power-law behaviour of the system in the vicinity of the critical point. In summary, how fluctuations propagate through a continuous spectrum of spatial scales and theories describing these processes have been fundamental to our understanding of inanimate matter.

In striking difference to inanimate matter, living matter is organised into a hierarchy of non-equilibrium processes on a distinct set of spatial scales, ranging from biochemical processes embedded in dynamic subcellular compartments to cells forming tissues. This raises the question of whether the propagation of fluctuations within and across these scales influences the properties of living matter. Thus, understanding living matter necessitates developing novel theories that can predict the effective emergent behaviour arising from the interplay of non-equilibrium fluctuations on multiple levels of biological organisation.

1.2. The multi-scale organisation of living matter

Living matter is fundamentally different from many forms of inanimate matter in two different ways: First, living matter operates far from thermal equilibrium. Thermodynamics equilibrium describes states of a system in which the system is termed to be balanced, as there is no net flow of energy or matter between subsystems [6, 21]. In contrast, in a non-equilibrium state, the system changes between states or is subject to steady transformation due to a non-vanishing net flow of energy or matter between sub-

¹The Hamiltonian is the mathematical function that describes the total energy of the system in terms of its position and momentum or position and spin, respectively [17].

1. Introduction

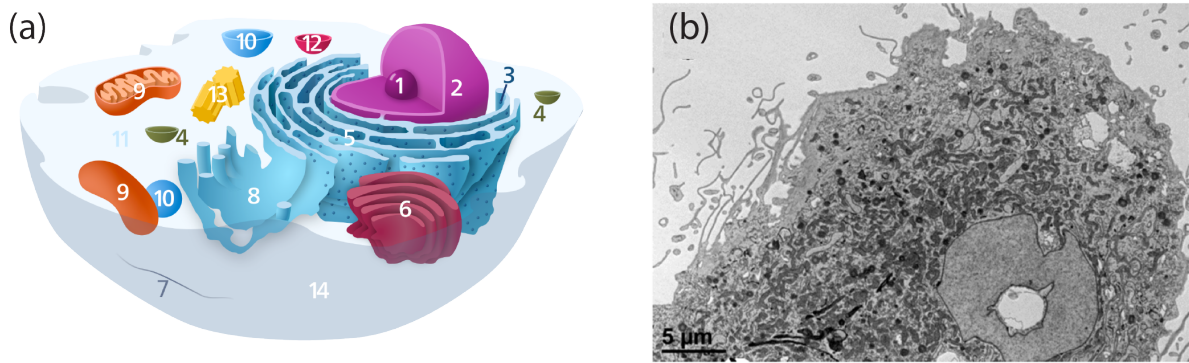


Fig. 1.2.: Organelles structure the interior of cells into highly dynamic compartments Organelles are subcellular structures that form small compartments in cell cytosol. These compartments exhibit altered chemical reaction environments which is, for example, needed for the degradation or synthesis of some bio-molecules [37, 38]. (a) is adapted from [39] and shows a sketch of different types of organelles. (1) Nucleolus, (2) nucleus, (3) ribosomes (dots on rough reticulum walls), (4) vesicle, (5) rough endoplasmic reticulum, (6) golgi apparatus, (7) cytoskeleton, (8) smooth endoplasmic reticulum, (9) mitochondrion, (10) vacuole, (11) cytosol, (12) lysosome, (13) centriole, (14) cell membrane. (b) shows a transmission electron microscopy image of macrophage-tumor cell fusions. Dark lines are organelle membranes and extended darker regions demonstrate the plethora of various organelles inside a cell. The image is adapted from [40].

systems. Non-equilibrium states are realised if the system is externally perturbed from its equilibrium state [22–24]. If a perturbation is removed after a transient time, the system relaxes back to its equilibrium state. In order to investigate non-equilibrium systems, the theories of classical thermodynamics were extended to discuss flows of energy and matter in non-equilibrium states. For example, Onsager theory describes the relaxation of weakly perturbed non-equilibrium systems by assuming that the perturbed state is governed by the same fluctuations as in equilibrium [22]. Onsager relations are a set of linear response relations that link the thermodynamic forces to the corresponding flows in non-equilibrium systems. They are, however, limited to systems that are close to thermodynamic equilibrium and cannot account for far-from-equilibrium dynamics [22, 24].

If the system is subject to steady external outflow and inflow of energy or matter, the system is driven to operate out of equilibrium [25]. The external driving can be applied by inconsistent boundary conditions [17]. For example, a thermodynamic system can be driven out of equilibrium by applying inconsistent boundary conditions on the macroscopic level, for example by heating the walls of a container to different temperatures. In many biological systems energy is dissipated on the level of individual components [26–29]. Examples range from motor proteins that transport cargo through the cell by converting chemical fuel to active movement [30] to birds that migrate in flocks [31]. These systems have inspired a novel field of research termed active matter [27–29, 32–34]. In recent years, it was found that active systems exhibit a wide range of new dynamical phenomena with examples ranging from swarming [31], to kinetic phase transitions [35], and motion-induced phase separation [36]. By this, active matter provides fundamental insight in the dynamics of living matter and it has opened up new theoretical and experimental roads in non-equilibrium physics.

In addition to operating far from thermal equilibrium, living matter also fundamentally

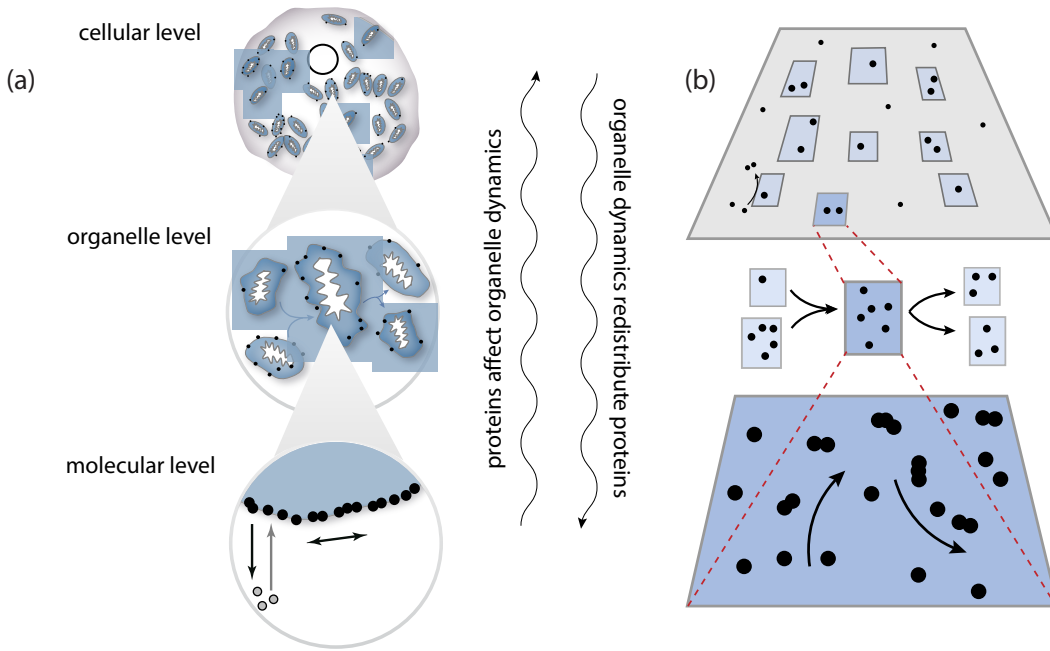


Fig. 1.3.: The functioning of living matter relies on the interplay between dynamics on different spatial scales (a) The propagation of fluctuations through distinct scales of biological organisation can be illustrated using the example of the regulation of cell death [41]. Apoptosis is mediated by a protein termed Bax, which stochastically binds and unbinds to the mitochondrial membrane, where it undergoes oligomerisation dynamics. If the Bax membrane concentration is high, Bax forms pores in the membrane and releases the apoptosis-inducing toxin cytochrome c, thus evoking the degradation of individual mitochondria. However, by mitochondrial fusion and fragmentation, Bax is redistributed among mitochondria, suppressing the spontaneous accumulation of Bax and, in turn, the degradation of mitochondria. (b) This provides an abstract illustration of the propagation of fluctuations in compartmentalised systems, whereby the compartment dynamics induce fluctuations on many-particle dynamics enclosed in the compartments, and by this alter the dynamics on the molecular scale. The statistics of the fluctuations, in turn, depend on the dynamics on the molecular scale, setting the basis of the propagation of fluctuations between different scales of biological organisation.

differs in its spatial organisation from inanimate matter. Living matter is organised into a hierarchy of non-equilibrium processes on a distinct set of spatial scales of biological organisation: Biochemical processes on the molecular scale are embedded in dynamic subcellular compartments, termed organelles. These organelles are highly dynamic and thereby exchange molecules among each other. Cells interact and give rise to tissues, which form individuals that interact in populations [42].

Since processes on each of these organisational scales are coupled, fluctuations on a given scale induce fluctuations on other scales. We will refer to this interdependence of fluctuations as the propagation of fluctuations across scales. The propagation of fluctuations across spatial scales can be best illustrated by considering specific biological examples. The development and maintenance of biological tissues relies on a tight coordination between many cells. In order to give rise to complex and highly specialised structures, such as the heart or the brain, the behaviour of each individual cell must be tightly regulated. Signals from the cell's environment need to be accurately interpreted

1. Introduction

and translated into appropriate cell behaviour in terms of proliferation, differentiation, death or migration [43]. These behaviours are collectively referred to as cell fate. Historically, research on the processes underlying the regulation of cell fate has focussed on molecular processes, such as the expression of genes in gene regulatory networks [44–46]. More recently, chemical modifications of the DNA and histones have been investigated in the context of cell fate decision [47–49], i.e. the proteins the DNA is wrapped around. The focus on the molecular scale has in recent years intensified with technological breakthroughs in sequencing technologies that allow probing a broad variety of molecular states of cells with unprecedented detail [50–52].

Cells are, however, hierarchically structured into processes happening on different scales. Many fundamental processes in cells occur in or on subcellular compartments termed organelles [37, 38, 53]. Organelles serve as hubs for biomolecule synthesis, degradation, and metabolic conversion, as well as a platform for various pathways involved in the processing of internal and external signals; compare also with Fig. 1.2. These molecular processes involve chemical reaction networks mediating the formation of protein complexes [54, 55] and underlie central cellular functions, such as cell death [56] or the response to viruses [57]. For example, cell death is triggered by the formation of protein complexes on the outer membrane of organelles termed mitochondria [41, 56]. The concentration of these complexes is increased if the cell is subjected to stress. If the complex concentration extends beyond a threshold concentration, the complexes form pores in the mitochondrial membrane [58], which mediate the release of toxins from the mitochondria that trigger the disassembly of the cell.

Mitochondria themselves are highly dynamic compartments which actively migrate in the cytosol of cells and undergo fusion and fragmentation dynamics on a timescale of minutes [59–63]. These fusion and fragmentation events lead to the redistribution of protein complexes between mitochondria, such that the stochastic dynamics on the organelle scale induce fluctuations in protein complex concentrations on the molecular scale. Vice versa, the concentration of protein complexes on mitochondrial membranes influences the rates of fusion and fragmentation processes, such that fluctuations on the molecular scale also give rise to fluctuations on the organelle scale. Other examples that rely on the formation of protein complexes on organelle membranes as central regulators of cellular behaviour follow similar dynamics. Examples include the metabolic regulation of aerobic metabolism [64, 65], the metabolic regulation of protein synthesis [66, 67], and the cellular innate immune response to RNA-virus infection [57, 68]. These examples therefore illustrate how fluctuations propagate across vastly different spatial scales in biological systems.

Since copy numbers in biological systems are typically small, quantitative descriptions usually must account for strong number fluctuations [69, 70]. Therefore, the dynamics on a given spatial scale can be effectively described in the framework of non-equilibrium statistical physics in general and stochastic processes in particular. The theory of stochastic processes provides a framework for describing the stochastic time evolution on a given spatial scale either by stochastic differential equations, where the deterministic time evolution is supplemented by noise summarising many inaccessible microscopic degrees of freedom [17, 71]. Or by the deterministic time evolution of probability distributions in the form of Master equations [17]. The description of stochastic systems, where fluctuations can propagate across a hierarchy of spatial scales, is, however, mathematically cumbersome. Although attempts have been made in deriving mathematical expressions for summary statistics [72–77], there is no understanding of the effective physical degrees

of freedom emerging from the multi-scale propagation of fluctuations. Since, as in the examples of critical phenomena and turbulence discussed above, these degrees of freedom might determine macroscopic properties of living matter and, specifically, underlie the regulation of cell fate behaviour. Therefore, understanding living matter requires a theoretical framework that is able to integrate the propagation of fluctuations across different scales of biological organisation. Such a framework would extend beyond the notion of emergence, as illustrated in Fig. 1.3.

1.3. Research question and main findings of the thesis

Just as for inanimate matter, understanding living matter requires novel theories that predict the emergent degrees of freedom arising from the interplay between fluctuations on multiple scales of biological organisation. In this thesis, we derive general theories of the multi-scale propagation of fluctuations in non-equilibrium systems and provide theoretical and empirical evidence for their biological function in the biological context of cell death and the innate immune system. Specifically, we use the paradigmatic framework of stochastic many-body systems subject to dynamic compartmentalisation. We follow the approach taken in statistical physics and distinguish between open systems, where we allow for the creation and annihilation of constituents, and closed systems, where mass is conserved, see Fig. 1.4; While dynamic compartmentalisation is central for the systems we study in this thesis, we will consider compartment dynamics as effectively imposed and only mention in biological applications the non-equilibrium mechanisms that give rise to compartment dynamics.

This thesis is structured as follows. In the chapters 2 and 3, we discuss open compartmentalised stochastic systems, while chapters 4 and 5 consider the dynamics of closed compartmentalised systems. The chapters 2 and 4 are concept-driven and aim to establish statistical physics concepts of compartmentalised systems, with an emphasis on analytic investigations. In the chapters 3 and 5 we build on the preceding chapters and investigate potential biological functions by deriving predictions for different biological contexts. We test these predictions using perturbation experiments. This thesis approaches the propagation of fluctuations in compartmentalised systems from four different perspectives, each necessitating the introduction of related, yet distinct, mathematical frameworks and biological concepts. To enhance the readability of this thesis, the mathematical and biological concepts required for each chapter are introduced at the start of the respective chapter. Yet, the chapters of this thesis are not arranged in a juxtaposed manner and we will build upon the insight gained from preceding chapters.

In chapter 2, we investigate the emergence of collective dynamics in open compartmentalised systems. We formally define compartment dynamics within the framework of Master equations and derive effective dynamics for its temporal evolution. We introduce a flux approximation for compartment fusion and fragmentation, which allows for analytical tractability and enables us to draw comparison to other physical systems. We find a structural equivalence of the effective dynamics to McKean-Vlasov equations describing collective resonance modes in plasma physics. We show that the combined effects of compartment fusion and fragmentation lead to the localisation of probability densities, which describe the probability of an individual compartment occupying a specified position in the concentration phase space. To capture the effective ensemble dynamics, we introduce a collective degree of freedom, which characterises the collective motion of the localised probability densities in the concentration phase space. Given that this motion closely

1. Introduction

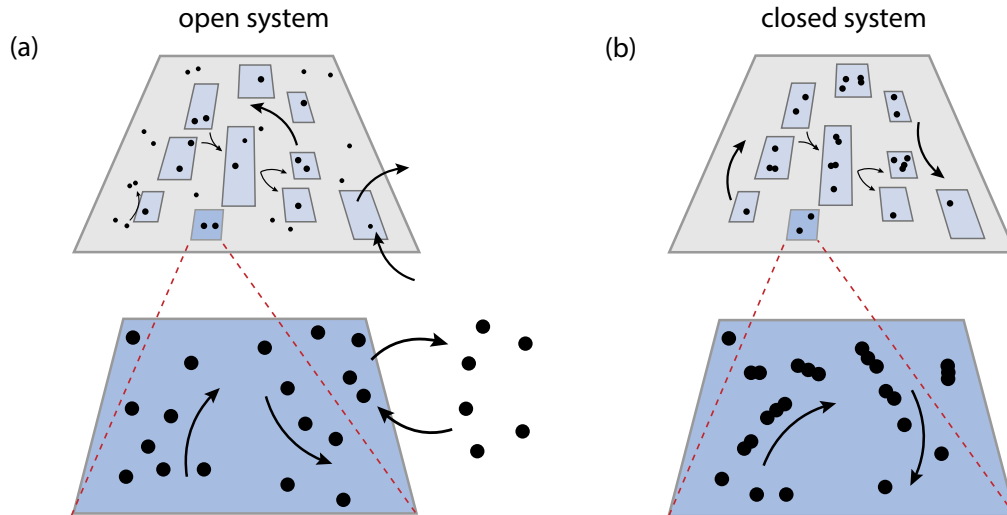


Fig. 1.4.: Illustration of open and closed compartmentalised stochastic systems. We follow the approach taken in statistical physics and distinguish between open systems (a) and closed systems (b). For open compartmentalised systems we do not impose mass conservation. Instead, we explicitly allow for the creation and annihilation of particles and compartment mass. This, for example, manifests by the binding and unbinding of particles to containers from a reservoir, or the growth or degradation of compartments. In contrast, for closed compartmentalised systems, we demand the conservation of mass on the level of the stochastic many-body dynamics as well as on the level of the compartments. Note that density fluctuations between compartments are permitted in closed systems.

resembles that of an individual compartment in concentration phase space, we term this degree of freedom ‘quasi-particle’. We derive effective equations of motion for this quasi-particle and show how its kinetic properties differ qualitatively from the dynamics of a single compartment. Furthermore, we demonstrate that the quasi-particle kinetics differ fundamentally from those of single-scale stochastic biochemical systems, raising the question of whether and how they are used to perform functions in biological systems.

In chapter 3, we apply these findings in the biological context of the decisions of cells to commit programmed cell death, which is a prominent biological example of an open system exhibiting multi-scale fluctuations. We first review the biology of organelle dynamics and signalling pathways in the context of cell death decision-making and then present a model describing the regulation of the accumulation dynamics of Bax protein complexes to the mitochondrial outer membrane. We apply the quasi-particle theory derived in chapter 2 to this model and show that the response of the accumulation of Bax complexes to stress signals shows a sigmoidal response. This gives rise to a kinetic low-pass filter which suppresses transient noise fluctuations yet allows cells to respond to trends in stress levels on long timescales. To experimentally test our theoretical predictions, we predict a transition from sigmoidal to exponential-like responses with increasing apoptotic stimulus strength, which is characteristic of the quasi-particle-like response kinetics. Evidence of this kinetic behaviour is found in experiments conducted by our experimental collaborators Philipp Mergenthaler and Lina Hellwig. Finally, we discuss the plausibility of our findings and their potential therapeutic implications, and consider the direct translatability of our findings to other organelle-associated signalling pathways.

In chapter 4, we investigate the thermodynamics of closed compartmentalised systems,

where the total mass of the system is conserved. Specifically, we focus on the total entropy and demonstrate that the effect of dynamic compartmentalisation depends on details of the kinetics on the scale of the stochastic many-particle dynamics. Using a second quantisation approach, we derive a commutator relation between the kinetic operators and the change in total entropy. We prove that, in particular, the total entropy of the ideal gas is not affected by dynamic compartmentalisation. Turning to many-particle dynamics that admit reactions among the particles, we demonstrate how specific compartment fragmentation rules can act as implicit measurements and we show how compartment fusion and fragmentation alter the total system's entropy. Furthermore, we demonstrate that the compartment dynamics alter the statistics of realised microstates if the kinetics of the stochastic many-particle dynamics violate detailed balance. Importantly, we illustrate how this can be used to facilitate or suppress reaction products of the stochastic reaction dynamics by manipulating the compartment dynamics.

In chapter 5, we apply the theory of closed compartmentalised systems derived in chapter 4 to the cellular innate immune response to RNA-virus infections. We provide a brief overview of the Smoluchowski aggregation-fragmentation dynamics, and discuss the concept of gelation and its connection to diverging moments in the aggregate size distributions. Our simulations illustrate how compartment fusion and fragmentation can facilitate the formation of large aggregates of MAVS proteins and augment their stability. This also gives rise to a power-law decay in density fluctuations. We systematically investigate different kernels describing the reversible aggregation and fragmentation of MAVS protein complexes. We thereby show that compartmentalised systems can exhibit giant density fluctuations. This facilitates the emergence of gelation under conditions that violate theoretical gelation criteria in the absence of compartment dynamics. We show that such multi-scale gelation of protein complexes on the membranes of dynamic mitochondria governs the innate immune response. Finally, we discuss our findings in light of the signalling pathway responsible for inflammation responses following infection of cells with RNA-virus. Our findings suggest that mitochondrial dynamics are essential for efficient inflammation responses. This is supported by previously published experimental data.

2. Theory of collective degrees of freedom in open compartmentalised systems

2.1. Introduction

The Nobel laureate Philip Warren Anderson is the founding father of modern condensed matter physics and among the most influential physicists of the second half of the twentieth century. He dedicated his life to the electronic structure of magnetic and disordered systems and profoundly influenced how generations of physicists think about condensed matter. One of his most influential papers was published in 1972 in *Science* with the title ‘More is different’ [78]. In this paper, Anderson set the concept of emergence as a cornerstone of how to describe (condensed) matter, which today has applications from solid state physics [79–81] to complexity theory [82].

Emergence is the property of physical systems to exhibit phenomena that are not present in the symmetries describing its individual components and the interactions between them [79]. These properties *emerge* from the interactions between the components via quantitative to qualitative transitions, which are also referred to as symmetry breaking [78]. A hallmark of this theory is the discovery of emergent collective dynamics in many-body systems which manifests as the localisations of wave packages, collective excitations of interacting bosons, and quasi-particles formed by interacting fermions. Emergent collective dynamics not only allow for a simplified description of the many-body system but show qualitative new dynamics and behaviour [78, 79].

In this chapter, we ask whether multi-scale fluctuations in dynamically compartmentalised systems give rise to emergent or collective dynamics. To this end, we will use the paradigmatic framework of compartmentalised stochastic systems, which comprise a hierarchical organisation of interacting non-equilibrium dynamics on various distinct spatial scales. As a minimal framework, we study many-body dynamics enclosed in dynamic compartments. In the absence of dynamic compartmentalisation, we can conveniently examine the dynamics of the stochastic many-body dynamics using Master equations. We demonstrate in this chapter how compartment dynamics lead to collective dynamics, which provides an intuitive way to understand multi-scale fluctuations in non-equilibrium systems. We demonstrate how we gain an analytical handle on the collective dynamics as we utilise the framework of population balance equations, as we describe the probability of an individual compartment occupying a specified position in the concentration phase space. Specifically, we show that the combined effects of compartment fusion and fragmentation lead to the localisation of probability densities in the concentration phase space. We find the emergence of a collective degree of freedom, which characterises the collective motion of the localised probability densities in the concentration phase space. We show that this motion closely resembles that of an individual compartment in the concentration phase space. We discuss a conceptual equivalence of the collective ensemble

dynamics with collective excitations and quasi-particle solutions in many-body theory. In this chapter, we focus on deriving an effective description of emergent dynamics in *open* compartmentalised systems, as we do not impose the conservation of mass. Consequently, this chapter is mainly technical. In the following chapter 3, we will focus on an application of our theory in the context of organelle-associated signalling pathways, with particular emphasis on cell death decision-making.

This chapter is structured as follows. We begin this chapter by reviewing mathematical frameworks to describe the dynamics of stochastic many-body dynamics and compartment dynamics in section 2.2. We focus on the description of the stochastic many-body dynamics in terms of reaction kinetics and the compartment dynamics within the framework of population balance equations. In section 2.3, we formally define compartmentalised systems by giving a definition of the full stochastic dynamics within the framework of Master equations. When we derive the ensemble dynamics, we will closely check the quality of the approximations by comparing with the full-stochastic dynamics.

We start the derivation of the effective ensemble dynamics in section 2.4, where we describe the compartmentalised systems within the framework of population balance equations. In particular, we approximate compartment fusion and fragmentation by a flux approximations in section 2.4.1. By marginalising over the compartment properties, we arrive at an effective description in Eq. (2.55), with an approximation of the compartment fusion and fragmentation in the flux approximation in Eq. (2.56). In section 2.5, we discuss the analogy of Eq. (2.55) to McKean-Vlasov equations, which are for example used in plasma physics to describe collective excitations. We then demonstrate the emergence of a collective degree of freedom due to steady compartment fusion and fragmentation dynamics by qualitatively studying the dynamics encoded in Eq. (2.55). Here, we also discuss how this collective degree of freedom resembles a quasi-particle. We proceed in section 2.6 to assess the kinetics of the quasi-particle, by deriving effective equations of motion. Finally, we conclude this chapter in section 2.7 by investigating the kinetic properties of the quasi-particle, and by comparing to the system's dynamics in the absence of compartment fusion and fragmentation dynamics.

2.2. Literature review of compartmentalised systems: dynamics on distinct spatial scales

The defining characteristic of compartmentalised multi-scale systems is the scale hierarchy of dynamics being nested into each other. As such, the analysis of the dynamics of compartmentalised multi-scale systems demands the explicit treatment of the dynamics on different spatial scales as well as the studying of their interplay. Here, we in particular focus on compartmentalised multi-scale systems, which admit dynamics on two spatial scales. For this, we focus on stochastic many-body dynamics enclosed in dynamic compartments. Before we study the interplay between compartment dynamics and the enclosed many-body dynamics, we first focus on the dynamics on specified scales separately.

To this end, we investigate on the stochastic many-body dynamics in the context of stochastic chemical reaction network kinetics. We review how chemical reaction network kinetics are described within the framework of Master equations and review how system size expansions allow for a description in the context of Fokker-Planck equations. For the compartment dynamics, we review the framework of population balance equations.

Allowing for the fusion and fragmentation of compartments as central for dynamic compartmentalisation, we discuss the Smoluchowski-coagulation formalism.

2.2.1. Mathematical framework for stochastic reaction network kinetics

In this thesis, we in particular specify the enclosed stochastic many-body dynamics as stochastic reaction kinetics system. In this subsection, we focus on stochastic chemical reaction networks kinetics, accounting for low copy numbers and intrinsic and extrinsic noises sources on the subcellular scale [70, 83–85] without explicitly discussing their spatial evolution. Next, we closely follow [85]. We consider a well stirred mixture of $N \geq 1$ chemical species $\{S_1, S_2, \dots, S_N\}$ inside a fixed volume Ω that chemically interact at a constant temperature, through $M \geq 1$ reaction channels $\{R_1, R_2, \dots, R_M\}$. We define with $X_i(t)$ the number of S_i molecules in the system. Each reaction is defined by

$$R_j \equiv \sum_i^N s_{ij} S_i \xrightarrow{k_j} \sum_i^N r_{ij} S_i, \quad (2.1)$$

where k_j is the rate of the reaction, and s_{ij} and r_{ij} stoichiometric coefficients. The state change vector $\vec{V}_j = (V_{1j}, \dots, V_{Nj})$ is defined by its components $V_{ij} = r_{ij} - s_{ij}$. While $\{S_1, S_2, \dots, S_N\}$ defines the molecules interacting in the signalling pathway, $\{R_1, R_2, \dots, R_M\}$ define the dynamics of the signalling pathway. We introduce the dependence on an external signal $\eta(t)$ in this general definition of chemical reaction networks by setting a dependence between the reaction rate and the signal $k_j(\eta(t))$ to a subset $j \in R_{\text{sig}}$. This formalism is equivalent to either externally manipulating the kinetic properties of chemical reactions, or externally controlling the concentration of a chemical species. The propensity of each reaction is given by $a_j(\vec{X}(t)) = k_j h(\vec{X}(t))$, where $h(\vec{X}(t))$ is the number of distinct combinations of R_j . The time evolution of joint probability function $P(\vec{X}, t)$ is then given by

$$\frac{\partial}{\partial t} P(\vec{X}, t) = \sum_j^M \left[a_j(\vec{X} - \vec{V}_j) P(\vec{X} - \vec{V}_j, t) - a_j(\vec{X}) P(\vec{X}(t)) \right], \quad (2.2)$$

see also the appendix on the Master equation formalism in A.1. We introduce a change of variables, as we express the state of the system in terms of a concentration $\vec{x}(t) = \vec{X}(t)/\Omega$ and formally $\vec{v} = \vec{V}/\Omega$. By rescaling the propensity while omitting combinatorial factors arising from identical species, we find $\tilde{a}_j = \Omega a_j$. The probability function is rescaled by $\tilde{P}(\vec{x}, t) = \Omega^N P(\vec{X}, t)$. We series expand Eq. (2.2) around $\vec{x}(t)$ with the small variable v_{ij} , which is also referred to the Kramers-Moyal expansion [83, 84]

$$\frac{\partial}{\partial t} \tilde{P}(\vec{x}, t) = \sum_{n=1}^{\infty} (-1)^n \left(\frac{1}{\Omega} \right)^{n-1} \sum_{\vec{m} \in Q(n)} \frac{1}{\prod_i^N m_i! \prod_i^N \partial x_i^{m_i}} \left[\left[\sum_{j=1}^M \prod_i^N V_{ij}^{m_i} \tilde{a}_j(\vec{x}) \right] \tilde{P}(\vec{x}, t) \right]. \quad (2.3)$$

For large volumes Ω^{-n+1} higher order terms vanish. The Fokker-Planck approximation corresponds to the truncation of the Kramers-Moyal expansion at the second order. To

2. Theory of collective degrees of freedom in open compartmentalised systems

this end, we define the drift vector \vec{F} and the noise matrix \mathbf{D} via

$$F_i(\vec{x}, t, \eta(t)) = \sum_{j=1}^M V_{ij} \tilde{a}_j(\vec{x}, t, \eta(t)), \quad D_{ik}(\vec{x}, t, \eta(t)) = \frac{1}{\Omega} \sum_{j=1}^M V_{ij} V_{kj} a_j(\vec{x}, t, \eta(t)), \quad (2.4)$$

where the subscript $\eta(t)$ refers to the dependence of the reaction rate on the external signal $\eta(t)$. Note, that here the noise matrix $\mathbf{D}_{\eta(t)}$ describes dispersive dynamics in the concentration phase space and not in a spatial sense, as we have excluded any spatial notion from our analysis by assuming well-mixed conditions. Making use of the drift vector $\vec{F}_{\eta(t)}$ and the noise matrix $\mathbf{D}_{\eta(t)}$, we find

$$\begin{aligned} \frac{\partial}{\partial t} \tilde{P}(\vec{x}, t) &\approx - \sum_{i=1}^N \frac{\partial}{\partial x_i} [F_i(\vec{x}, t, \eta(t)) \tilde{P}(\vec{x}, t)] + \frac{1}{2} \sum_{i,k}^N \frac{\partial}{\partial x_i} \frac{\partial}{\partial x_k} [D_{ik}(\vec{x}, t, \eta(t)) \tilde{P}(\vec{x}, t)] \\ &= -\nabla \cdot \vec{F}_{\eta} \tilde{P}(\vec{x}, t) + \frac{1}{2} \nabla \cdot (\nabla \cdot \mathbf{D}_{\eta(t)})^{\top} \tilde{P}(\vec{x}, t), \end{aligned} \quad (2.5)$$

where the second line is equal to the first line by making use of a vector notion. The formulation in terms of a multi-dimensional Fokker-Planck Equation allows for an equivalent formulation in terms of Itô stochastic differential equations. For this, we make use of the Cholesky decomposition $\mathbf{D}(\vec{x}, t) = \mathbf{C}(\vec{x}, t) \mathbf{C}^{\top}(\vec{x}, t)$ to find

$$\frac{d}{dt} \vec{x} = \vec{F} + \mathbf{C} \vec{\xi}(t), \quad (2.6)$$

where $\vec{\xi}(t)$ is an (uncorrelated) Gaussian white noise vector. This set of coupled stochastic differential equations is also referred to as Chemical Langevin Equations. In the thermodynamic limit, $\Omega \rightarrow \infty$, the noise vanishes and the system is described by a set of coupled deterministic differential equations, which corresponds to a formulation on the basis of reaction rates. Notably, both the drift vector \vec{F} and the noise matrix \mathbf{D} encode both the chemical reaction rates k_j and the current state of the system.

Here, we formally allowed for the creation and annihilation of species from a bath. As such, our system is not mass-conserving. Note, that in general, the formulation in terms of Langevin Equations or in terms of Fokker-Planck equations allows for the conservation of the mass of the system if the system is specified accordingly [86]. Yet, caution should be taken when reaction kinetics in a closed system are considered, where the total mass is conserved. In this case, it is necessary to consider the full structure of the noise diffusion matrix. In any case, the set of coupled Langevin Equations offers an intuitive approach to the dynamics encoded in the stochastic reaction networks and allows for straightforward numerical implementation. In contrast, the Fokker-Planck approximation is more beneficial for statistical analysis.

2.2.2. Compartment dynamics within the framework of population balance equations

Dynamic compartmentalisation is a fundamental aspect of the multi-scale organization of biological systems. Dynamic compartmentalisation is displayed in numerous examples, ranging from populations of interacting individuals to tissues composed of cells, to organelles that compartmentalise the cytosol. While the dynamics of each scale are driven by different physical mechanisms, they can be effectively captured by the same statistical

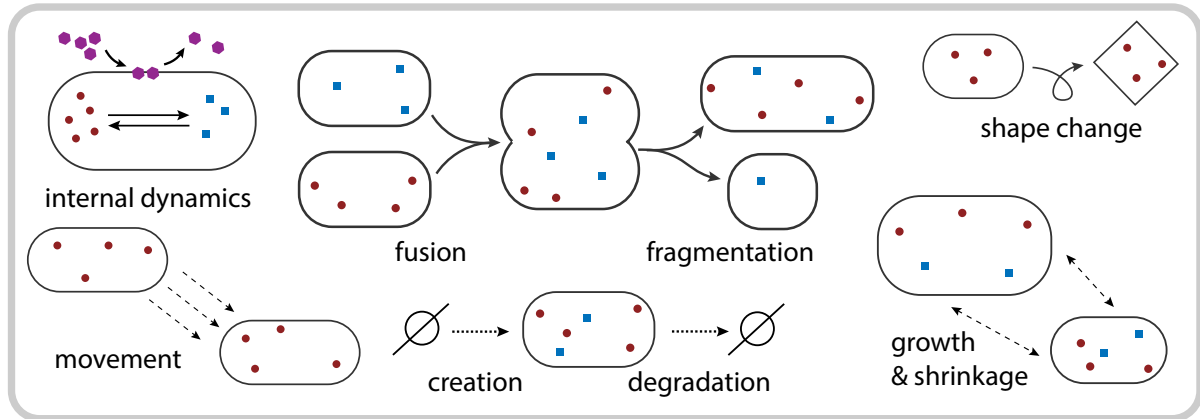


Fig. 2.1.: Various compartment dynamics. This schematic illustrates the multitude of different compartment dynamics, ranging from compartment growth, degradation, fusion, and shape change, up to internal dynamics. Note, that the list of compartment dynamics illustrated here is not extensive. Squares, dots, and hexagons refer to stochastic many-body dynamics associated with the compartments. In particular, the framework of population balance equations, presented in section 2.2.2, is suited to capture the effects of compartment dynamics.

description. In this section, we formalise the compartment dynamics.

While discrete population models suggest the framework of agent-based dynamics, organelle dynamics demand the temporal remodelling, merging, and splitting of compartments. See for an illustration of compartment dynamics Fig. 2.1. These processes can be addressed through population balance equations. Here, we distinguish two distinct levels of population dynamics: a kinetic description through Master equations, and a statistical description in terms of smooth distribution functions for large populations. This statistical description is obtained through the Master equation when the population size limit is correctly drawn [87]. Here, we focus on smooth distribution functions, as this formalism facilitates analytical tractability and links compartment dynamics to Smoluchowski aggregation-fragmentation dynamics¹. Complementary to the approach presented in this section, we presented a definition of the full stochastic dynamics of the system in section 2.3.

Population balance equations are popular in different branches of science ranging from chemical engineering [89], atmospheric modelling [90], to colloidal physics [91–93], and biology [94–96]. Population balance equations describe the temporal evolution of *populations* on a statistical level. Here, we closely follow [87] and define a phase space \mathbb{D} composed by the physical space of coordinates \vec{r} and the property space $\vec{\zeta} = (\xi_1, \xi_2, \dots)$ which refers to compartment properties like size, shape, or the state of the internal dynamics. Here, we assume that compartment properties are described by continuous variables, as $x_i \in \mathbb{R}$. We describe the ensemble of compartments by the number density distribution function $f(\vec{r}, \vec{\zeta}, t)$ in the phase space \mathbb{D} , where $f(\vec{r}, \vec{\zeta}, t)d\vec{r}d\vec{\zeta}$ refers to the ensemble of entities in the range $(d\vec{r}, d\vec{\zeta})$ around $(\vec{r}, \vec{\zeta})$. The conservation of mass then implies

$$\int_{\mathbb{D}} \frac{D}{Dt} f(\vec{r}, \vec{\zeta}, t) d\vec{r} d\vec{\zeta} = \int_{\mathbb{D}} (\Sigma_B - \Sigma_D) d\vec{r} d\vec{\zeta}, \quad (2.7)$$

¹This formalism is also referred to as Smoluchowski’s coagulation formalism [88].

2. Theory of collective degrees of freedom in open compartmentalised systems

where D/Dt refers to the substantial derivative, Σ_B and Σ_D to birth and death term respectively, and the integration was taken over an arbitrary volume \mathcal{D} . Approximating both the spatial dynamics and the internal dynamics of the compartments in terms of Fokker-Planck equations, the drift and diffusive fluxes in both the real space and property space read

$$\vec{d}_r = \vec{F}_r f - D_r \nabla_r f \quad \text{and} \quad \vec{d}_\zeta = \vec{F}_\zeta f - D_\zeta \nabla_\zeta f, \quad (2.8)$$

where the subscript refers to either the real space or the property space, \vec{d} is the flux displacement vector, \vec{F} is the drift vector and the matrix D comprises the diffusion coefficients. In a differential form, the conservation of mass then implies

$$\frac{\partial f}{\partial t} + \nabla_r \cdot (\vec{F}_r f) - \nabla_r \cdot (D_r \nabla_r f) + \nabla_\zeta \cdot (\vec{F}_\zeta f) - \nabla_\zeta \cdot (D_\zeta \nabla_\zeta f) = \Sigma_B - \Sigma_D. \quad (2.9)$$

In this formulation, we already account for the multi-scale character of dynamic compartmentalisation, as we explicitly account for both the dynamics of compartments, as well as for the internal dynamics. Next, we will extend on birth and death terms, which allows accounting for both the synthesis and degradation, as well as for the fusion and fragmentation of compartments. To this end, we employ Smoluchowski's coagulation formalism and start by focusing on the fusion of compartments. Formally, the fusion of two compartments results in a removal of the two fusing compartments and the addition of the fused compartments to the ensemble, and thus manifests in coupled birth and death terms. For the birth term, we need to define how compartment properties $\vec{\zeta}$ change upon the fusion of compartments. We formally define $\vec{\zeta} = \Upsilon(\vec{\zeta}', \vec{\zeta}'')$ for the compartment properties $\vec{\zeta}$ of a compartment resulting from the fusion of two compartments with $\vec{\zeta}'$ and $\vec{\zeta}''$. In the continuum limit, the birth and the death term yield

$$\begin{aligned} \Sigma_{D,\text{fus}}(\vec{r}, \vec{\zeta}, t) &= \int d\vec{r}' d\vec{\zeta}' a(\vec{r}', \vec{\zeta}', \vec{r}, \vec{\zeta}, t) f^{[2]}(\vec{r}', \vec{\zeta}', \vec{r}, \vec{\zeta}, t), \\ \Sigma_{B,\text{fus}}(\vec{r}, \vec{\zeta}, t) &= \frac{1}{2} \int d\vec{r}' d\vec{\zeta}' \int d\vec{\zeta}'' a(\vec{r}', \vec{\zeta}', \vec{r}, \vec{\zeta}'', t) f^{[2]}(\vec{r}', \vec{\zeta}', \vec{r}, \vec{\zeta}'', t) \delta(\Upsilon(\vec{\zeta}', \vec{\zeta}'') - \vec{\zeta}), \end{aligned} \quad (2.10)$$

where $a(\vec{r}', \vec{\zeta}', \vec{r}, \vec{\zeta}, t)$ is the fusion rate of two compartments specified by $(\vec{r}', \vec{\zeta}')$ and $(\vec{r}, \vec{\zeta})$, and $f^{[2]}(\vec{r}', \vec{\zeta}', \vec{r}, \vec{\zeta}, t)$ is the entity-pair distribution function. $\delta(\vec{x})$ refers to the multi-dimensional δ -function. The factor 1/2 in the birth term corrects for doubling counting. Based on this formulation, a number of approximations are applied: A mean-field approximation is applied as the entity-pair distribution is expressed as the product of the number density $f^{[2]}(\vec{r}', \vec{\zeta}', \vec{r}, \vec{\zeta}, t) \approx f(\vec{r}', \vec{\zeta}', t) f(\vec{r}, \vec{\zeta}, t)$. As compartments need to be in close spatial proximity for a fusion, local homogeneity is assumed with $f(\vec{r}', \vec{\zeta}', t) \approx f(\vec{r}, \vec{\zeta}, t)$. Carrying out the integration of \vec{r}' over $a(\vec{r}', \vec{\zeta}', \vec{r}, \vec{\zeta}, t)$ reduces the fusion rate to $\kappa(\vec{r}, \vec{\zeta}', \vec{\zeta}, t)$, which is referred to as the collision kernel. This yields

$$\begin{aligned} \Sigma_{D,\text{fus}}(\vec{r}, \vec{\zeta}, t) &= \int d\vec{\zeta}' \kappa(\vec{r}, \vec{\zeta}', \vec{\zeta}, t) f(\vec{r}, \vec{\zeta}', t) f(\vec{r}, \vec{\zeta}, t), \\ \Sigma_{B,\text{fus}}(\vec{r}, \vec{\zeta}, t) &= \frac{1}{2} \int d\vec{\zeta}' d\vec{\zeta}'' \kappa(\vec{r}, \vec{\zeta}', \vec{\zeta}'', t) f(\vec{r}, \vec{\zeta}', t) f(\vec{r}, \vec{\zeta}'', t) \delta(\Upsilon(\vec{\zeta}', \vec{\zeta}'') - \vec{\zeta}). \end{aligned} \quad (2.11)$$

Analogously, the fragmentation of compartments also results in both birth and death terms. Here, we define the break-up kernel $b(\vec{r}, \vec{\zeta}', \vec{\zeta}'', t)$ as rate at which a compartment

with properties $\vec{\zeta} = \Upsilon(\vec{\zeta}', \vec{\zeta}'')$ splits in compartments specified by $\vec{\zeta}'$ and $\vec{\zeta}''$,

$$\begin{aligned}\Sigma_{\text{D,frag}}(\vec{r}, \vec{\zeta}, t) &= f(\vec{r}, \vec{\zeta}, t) \int d\vec{\zeta}' d\vec{\zeta}'' b(\vec{r}, \vec{\zeta}', \vec{\zeta}, t) \delta(\Upsilon(\vec{\zeta}', \vec{\zeta}'') - \vec{\zeta}), \\ \Sigma_{\text{B,frag}}(\vec{r}, \vec{\zeta}, t) &= \int d\vec{\zeta}' b(\vec{r}, \vec{\zeta}', \vec{\zeta}, t) f(\vec{r}, \Upsilon(\vec{\zeta}', \vec{\zeta}), t).\end{aligned}\tag{2.12}$$

Taken together, this formalism encompasses various compartment dynamics, such as movement \vec{d}_r , internal changes \vec{d}_ζ , growth/shrinkage \vec{d} , degradation/synthesis Σ_{B} and Σ_{D} and fusion/fragmentation, expressed as integral terms in Σ_{B} and Σ_{D} .

Concluding on this section, the description of compartmentalised stochastic reaction kinetics systems in terms of population balance equations constitutes a statistical description in the continuum limit of infinitely many compartments using smooth distribution functions. Additionally, a mean-field approximation and the assumption of local homogeneity for the coagulation dynamics are assumed. As the framework of population balance equations allows for analytical tractability there are a few examples, where specific chemical reaction networks in dynamic compartments were analysed [75, 96–98]. Note that the noise contributions induced by the randomness of discrete compartment dynamics and finite system size, as well as the spatial setting of compartments, are not accounted for within the framework of population balance equations.

There are few examples where stochastic dynamics in compartments with a spatial setting have been studied [74–77]. To account for the stochasticity induced by compartment dynamics on a mesoscale description, compartment dynamics have been discussed in the context of counting processes. While these models allow for the computational accessibility of the dynamics, analytical tractability is only recovered by assuming moment closure approximations [72].

The full stochastic evolution of a finite system is when tracking the dynamics on the basis of stochastic transition rates, as formalised the framework of Master equations, see section 2.3. While this is a useful approach for numerical simulations, it lacks analytical tractability. In this chapter, we thus consider both a full stochastic framework for numerical simulations and the framework of population equations in order to gain analytical insight. Specifically, we corroborate our analytical findings through finite-size full stochastic simulations. For an intuitive understanding of the phenomenology of compartment aggregation-fragmentation dynamics, we next provide a case example of Smoluchowski aggregation dynamics.

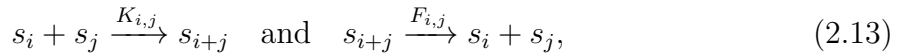
2.2.3. Smoluchowski aggregation-fragmentation dynamics

To describe the fusion and fragmentation dynamics of compartments, we consider the framework of reversible aggregation based on the seminal work of Marian Smoluchowski [88]. Smoluchowski developed this framework to describe the time evolution of the number density $f(s, t)$ of particles as they coagulate. Here, we follow closely the introduction into the formalism provided by [99], who refer to it as *reversible polymerisation* due to its predominate application in the context of the aggregation of molecules.

Smoluchowski aggregation-fragmentation dynamics are used to describe the aggregation and fragmentation processes through population balance equations in a mean-field description. We refer to objects created by aggregation as *aggregates* and refer to aggregates of unit size as *building blocks*. This formalism is applicable to describe the aggregation of polymers, organelle dynamics and more generally, compartment dynamics.

2. Theory of collective degrees of freedom in open compartmentalised systems

In particular, the formalism comprises two types of reactions



which describe the aggregation of two aggregates of size s_i and s_j to an aggregate of the size s_{i+j} and conversely its fragmentation. Within the framework of chemical reactions, the aggregation and fragmentation processes are represented by the aggregation rate, $K_{i,j}$, and the fragmentation rate, $F_{i,j}$, respectively. These rates are usually dependent on the sizes of the respective aggregates and are thus referred to as aggregation and fragmentation kernels. In this thesis, we focus on the symmetric case of reciprocal interactions, with $K_{i,j} = K_{j,i}$ and $F_{i,j} = F_{j,i}$.

The Smoluchowski aggregation-fragmentation formalism generally allows the description of the size distribution of aggregates in a continuous manner. In this study, however, we consider the special case of discrete size distributions, as sizes are multiples of the unit building block $s_k = ks_1$. This special case is particularly suited to the aggregation of molecules to polymers and constitutes an approximation for compartment dynamics. The primary benefit of this formalism is the restriction of the creation of arbitrarily small aggregates, as well as its numerical and analytical tractability. In the discrete setting, the set of coupled population balance equations is

$$\begin{aligned} \frac{df(s_k, t)}{dt} = & \frac{1}{2} \sum_{i+j=k} K_{i,j} f(s_i, t) f(s_j, t) - f(s_k, t) \sum_j K_{k,j} f(s_j, t) \\ & + \sum_j F_{k,j} f(s_{k+j}, t) - \frac{1}{2} f(s_k, t) \sum_{i+j=k} F_{i,j}. \end{aligned} \quad (2.14)$$

Note that these dynamics in general not fulfil the detailed balance condition

$$K_{i,j} f(s_i, t) f(s_j, t) = F_{i,j} f(s_{i+j}, t) \quad (2.15)$$

which demands a dependence between the aggregation and the fragmentation kernel. Further note, that reversible aggregation dynamics are mass conserving and hence

$$\mathcal{N} = \sum_k kf(s_k, t) \quad (2.16)$$

is a conserved quantity.

There exist a multitude of different physics models for the aggregation and the fragmentation kernels, with only a subset admitting analytic solutions. We will further elaborate on this in section 5.2, where we also elaborate on general qualitative insights that can be made by classifying the aggregation and fragmentation kernels. Here, we next focus on the special case of constant aggregation and fragmentation kernels, $F_{i,j}/K_{i,j} = \varphi/\mu = \lambda^{-1}$. This specific kernel choice was previously discussed in the context of organelle dynamics [100], fragmentation dynamics, fulfils the detailed balance condition, and admits an analytic solution. The analytic solution in steady state is of the type

$$f_{ss}(s_k, t) = \lambda^{-1} \beta^k, \quad (2.17)$$

2.3. Compartmentalised stochastic systems within the framework of Master equations

where β is derived by the normalisation condition $\mathcal{N} = 1$ and evaluates to

$$\beta = 1 + \frac{1}{2\lambda} - \sqrt{\frac{1}{\lambda} + \frac{1}{4\lambda^2}}. \quad (2.18)$$

The existence of an analytic solution allows us to verify the accuracy of our numerical routines. Furthermore, we observe that the size distribution is approximately described by an exponential decay in aggregate size. This will be utilised in section 2.4.2.3 to derive effective ensemble dynamics. While we mostly consider constant and finite aggregation and fragmentation kernels in this chapter 2, we focus on the derivation of general aggregation and fragmentation kernels in chapter 5. Having provided a brief overview of the mathematical concepts, we now move on to investigate the effective dynamics of compartmentalised stochastic reaction kinetics systems.

2.3. Compartmentalised stochastic systems within the framework of Master equations

In order to reflect on the multi-scale nature of compartmentalised stochastic reaction kinetics systems, we explicitly consider both the dynamics of the chemical reactions taking place in (or on) the compartments, as well as the dynamics of the compartments themselves. At the molecular level, we describe the changes in concentrations of chemical species over time within each compartment. At the compartment level, we account for mesoscopic changes, such as the growth and shrinkage of compartments, or the fragmentation and fusion of compartments. Here, we provide a microscopic model definition as we employ the powerful framework of Master equations. We will in particular use this framework of Master equations to investigate the phenomenology of the system through numerical simulations.

We formally define the state of a compartmentalised stochastic reaction kinetics system by a finite set of compartments \mathbb{S} . Each compartment is characterised by a concentration vector \vec{c}_i and macroscopic compartment properties \vec{o}_i ,

$$\mathbb{S} = \begin{bmatrix} \vdots \\ [\vec{c}_i, \vec{o}_i] \\ \vdots \end{bmatrix}. \quad (2.19)$$

with a total number of n compartments. Compartment properties account for characteristics like size, mass, shape, and spatial position. The size of a compartment is defined as $v_i = \vec{o}_{1,i}$. The concentration vector \vec{c}_i specifies the composition of molecular species in this compartment, where $\vec{c}_i v_i = \vec{n}_i$ is the number of molecular species. We take into account the density dependencies of chemical reactions by considering concentrations rather than copy numbers. Moreover, we assume that molecular species diffuse quickly within the compartment, disregarding concentration gradients and assuming well-mixed conditions.

We distinguish different classes of transitions between states $\mathcal{T}_{\mathbb{S} \rightarrow \mathbb{S}'}$, accounting for the dynamics on the scale of stochastic reactions and compartment dynamics. On the scale of stochastic reactions (molecular scale), changes in the concentration of molecular species are due to chemical reactions, such as chemical modifications of proteins, complex formation and reversible oligomerisation processes, see also section 2.2.1. Formally, a chemical

2. Theory of collective degrees of freedom in open compartmentalised systems

reaction $C_j + C_k + C_l \xrightarrow{k_\alpha} C_n + C_m$ reduces the concentrations of reactant molecular species $c_{i;j}$, $c_{i;k}$, and $c_{i;l}$ and increases the concentrations of product species $c_{i;m}$ and $c_{i;n}$ at a rate k_α on compartment i . The full dynamics are encoded in a chemical reaction network. We associate each reaction with a transition rate $\mathcal{T}_{k_\alpha,i}$. For an individual compartment, the dynamics are described by a chemical Master equation, see Eq. (2.2) in section 2.2.1, also compare for example with [17]. We formally collect transition rates only affecting the molecular level as \mathcal{Q} , and acknowledge external signals $\vec{\eta}(t)$ perturbing the rates of chemical reactions by writing $\mathcal{Q}_{\eta(t)}$.

On top of stochastic chemical reaction dynamics in each compartment, compartments can also undertake compartment dynamics, such as fusion, fragmentation, growth, movement and degradation. These compartment processes are formally defined as those which affect the properties \vec{o}_i of compartments and can be further classified into two distinct classes. Macroscopic compartment properties, such as shape and movement, can only be changed by compartment dynamics, resulting in transitions between different states $\mathcal{T}_{\vec{o}_i \rightarrow \vec{o}'_i}$. We summarise these processes formally with operator \mathcal{S} .

Compartment processes such as compartment growth and shrinkage, degradation and synthesis, or compartment fusion and fragmentation, however, affect both the macroscopic properties of compartments and the concentrations of molecular species (\vec{c}_i, \vec{o}_i) . For example, compartment growth leads to a decrease in the density of molecular species, which is reflected in a change in concentrations. Consequently, the growth and shrinkage of compartments affect the collision rates and thus the reaction rates. Such changes in reaction rates are consistently taken into consideration when dealing with chemical reactions by using concentration instead of occupation numbers.

In contrast, when a compartment is degraded, both the compartment itself and its content are removed from set \mathcal{S} . This naturally affects both the compartment properties and the number of molecular species. The fusion of two compartments with different concentrations \vec{c}_i and \vec{c}_j results in a single compartment with an averaged concentration. This is supported by the assumption of well-mixed conditions, accounting for instantaneous mixing. In analogous terms, also the synthesis of compartments and the fragmentation of compartments changes both compartment properties \vec{o}_i and the concentration compositions \vec{c}_i . Summarising all the transitions with respect to both macroscopic compartment properties and the concentration of molecular species yields the operator \mathcal{R} .

Accounting for the stochasticity of compartment dynamics and chemical reactions at finite numbers, we define the probability of finding the system in a specified state $P(\mathcal{S})$, which evolves according to a Master equation $\partial_t P(\mathcal{S}) = \mathcal{L}P(\mathcal{S})$. \mathcal{L} accounts for transitions either due to chemical reactions or compartment dynamics; it is composed of the transitions defined in the classes $\mathcal{Q}_{\eta(t)}$, \mathcal{S} , and \mathcal{R} , and is in symbolic notation:

$$\partial_t P(\mathcal{S}) = \left(\mathcal{Q}_{\eta(t)} + \mathcal{S} + \mathcal{R} \right) P(\mathcal{S}). \quad (2.20)$$

We distinguish intra-scale fluxes $(\mathcal{Q}_{\eta(t)}P(\mathcal{S}), \mathcal{S}P(\mathcal{S}))$ and inter-scale fluxes $(\mathcal{R}P(\mathcal{S}))$, as depicted in Fig. 2.2. Intra-scale fluxes only affect the dynamics on the specified scale. While we allow the dependence of inter-scale fluxes on the properties of the compartment on a different scale², inter-scale fluxes $\mathcal{R}P(\mathcal{S})$ directly set the dynamics on the different spatial scales into an interplay. While we formally defined transitions in \mathcal{R} as compartment

²For example, we account for the compartment size by considering concentrations. Vice versa, we could set also a dependence of the compartment processes in \mathcal{S} on the concentration compositions, for example by linking the concentration to the motility of the compartment.

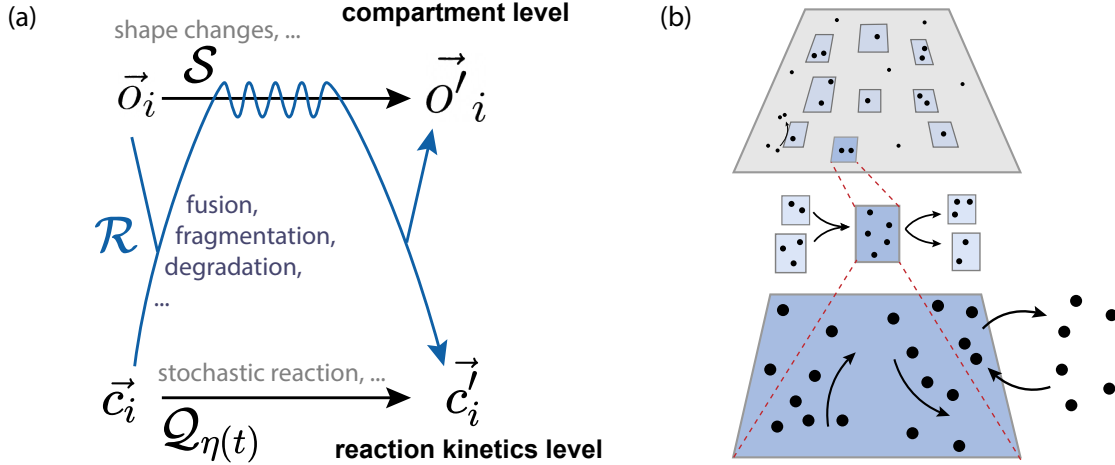


Fig. 2.2.: Illustration of the multi-scale organisation of compartmentalised systems (a) A schematic illustrates the structure of Eq. (2.20). A list of the detailed form of the terms of the Master equation is given in appendix A.2. (b) Illustration of an open compartmentalised system, also illustrating that dynamics happen on different spatial scales.

dynamics, these transitions not only depend on both compartment properties and the chemical composition (\vec{c}_i, \vec{o}_i) , but directly change the composition of chemical species \vec{c}_i . An analogy can be drawn to hybrid systems, wherein microscopic dynamics are perturbed by *jump* perturbations. In the multi-scale setup, the stochastic reaction dynamics constitute the level of microscopic dynamics which are perturbed by time-discrete compartment dynamics.

Note, that here we refer to *open* compartmentalised systems, as we do not impose the conservation of mass, neither on the level of compartment dynamics nor on the level of the stochastic reaction kinetics dynamics. This, for example, allows for the continuous binding and unbinding of molecules to and from a compartment, as illustrated in Fig. 2.2 (b), where compartments are embedded and in contact with an external reservoir.

For further analysis, we specify how compartment fusion and fragmentation change the concentrations within each compartment. With regard to compartment fusion, the copy numbers of the molecular species \vec{n}_i and \vec{n}_j are added together to give $\vec{n}_l = \vec{n}_i + \vec{n}_j$ and the compartments sizes $v_l = v_i + v_j$, which induces changes in the concentration vectors $\vec{c}_l = (v_i \vec{c}_i + v_j \vec{c}_j) / (v_i + v_j)$. Conversely, for compartment fragmentation, the number of molecular species is randomly distributed across each daughter compartment. If the mother compartment is described by (\vec{c}_l, \vec{o}_l) , we consider a random splitting into the two daughter compartments, with $v_i + v_j = v_l$, $(v_i, v_j < v_l)$, where $v_i B(v_j)$ is a random variable based on the initial size v_j specified by a break-up distribution $B(v_j)$. Furthermore, each molecular species is subjected to a binomial splitting procedure, with $n_{i;i} = \text{Binom}(n_{l;i}, v_i/v_j)$, where the success probability is proportional to the size of compartment i ($p = v_i/v_j$), and $n_{j;i} = n_{l;i} - n_{i;i}$. The concentration compositions on each daughter compartment then follow from scalar multiplication with the respective sizes of the compartments.

While we have only presented a symbolic notation of the dynamics above, a full Master equation can be directly translated from it. This Master equation, however, is lengthy. We

detail out the terms in appendix A.2. Note, that this Master equation provides a formal definition of the system’s dynamics. Its extensive form renders it difficult to inspect and analyse further, hence, numerical routines for it are necessary. The numerical routines are elucidated on in appendix B.1. In section 2.4, analytical approximations to the system’s dynamics are presented in the form of population balance equations.

Concluding on this section, with the model presented in this section, we want to investigate if compartment dynamics can give rise to emergent degrees of freedom and if compartment dynamics can qualitatively alter the dynamical behaviour and the response of the system to external perturbations. To answer this question, we in the further of this chapter, we will employ a combination of numerical investigates and analytic calculations.

2.4. Effective dynamics of open compartmentalised systems

In this section, we derive effective equations for the dynamics of open compartmentalised systems on the basis of population balance equations. We consider compartment fusion and fragmentation in the context of a *flux approximation* and explain how the temporal evolution of our system can be accurately described on an ensemble level. This effective ensemble description offers physical interpretations, with its analysis revealing the emergence of a collective degree of freedom due to compartment dynamics. The collective degree of freedom, which resembles a quasi-particle state for the ensemble, will be studied in following section 2.5. Additionally, we will explore the kinetic properties of this collective degree of freedom in section 2.7, in order to predict how compartmentalised stochastic reaction kinetics systems respond to external perturbations.

The description of system dynamics in terms of Master equations facilitates direct implementation into numerical routines, see appendix B.1, however, the multitude of transition rates in Eq. (2.20) impedes any analytic treatments of the dynamics. Analytical approximations present the opportunity for an intuitive approach to system dynamics, granting a qualitative description of the system without the need for large-scale simulations. In this section, we utilise the population balance equations framework, as introduced in section 2.2.2, to derive analytical approximations for compartment fusion and fragmentation in terms of probability fluxes. We effectively integrate out the compartment degrees of freedom by marginalising over the compartment properties \vec{o}_i and obtain an effective description of the system at the molecular species level. This approach allows for an intuitive understanding of how the dynamics of *open* compartmentalised stochastic reaction kinetics systems are impacted by compartment dynamics, with a simple calculation of the qualitative dynamics of these systems. Note that this subsection is largely technical, with the purpose of outlining the approximations taken to obtain effective equations for the dynamics of open compartmentalised systems. Throughout this section, comparisons are made between analytic approximations and numerical simulations for corroboration and emphasis is given to the conditions under which approximations must be used cautiously and require further refinement.

In line with the formalism of population balance equations presented in section 2.2.2, we consider the continuum limit of an infinite number of compartments and describe the compartments using a number density distribution function³. Recalling the structure of

³Note, that in this approximation, we make no assumption about the timescale of processes, but continuous fluxes arise due to the assumption of the continuum limit in the number of compartments.

population balance equation Eq. (2.9), this yields

$$\frac{\partial f}{\partial t} + \nabla_r \cdot (\vec{F}_r f) - \nabla_r \cdot (D_r \nabla_r f) + \nabla_\zeta \cdot (\vec{F}_\zeta f) - \nabla_\zeta \cdot (D_\zeta \nabla_\zeta f) = \Sigma_B - \Sigma_D.$$

We identify the property vector $\vec{\zeta} = (\vec{c}, \vec{o})$ as the combination of the concentration vector and the compartment properties. In our analysis, we neglect the spatial evolution of the system and move to a mean-field description. In the context of organelle-associated signalling pathways, this approximation is motivated by the rapid movement of organelles through the cytosol. The spatial translocation of organelles is facilitated by molecular motors on the cytoskeleton, leading to rapid spatial reorganization and changes in the neighbourhood of organelles. We assume independence between the chemical composition and shape of compartments, thus formally marginalising over the compartment shape. The compartment properties are then completely described by their size, $\vec{o}_i \equiv v_i$.

A key assumption of the subsequent analysis is that the chemical reactions network is approximated as set of coupled stochastic differential equations, with the stochastic fluxes described using a Fokker-Planck approximation, as outlined in section 2.2.1. To account for variations in compartment size, the noise matrix $\mathbf{D}_{\text{eff}} = \mathbf{D}/v_i$ is made to depend on the size of the respective compartment. In particular, the drift and diffusion flux on the left side of the population balance equation are associated with the chemical reaction dynamics. This leads to the simplification of the population balance equation to

$$\boxed{\frac{\partial f}{\partial t} = -\nabla_c (\vec{F}_{\eta(t)} f) + \nabla_c \left(\left(\nabla_c \mathbf{D}_{\eta(t), \text{eff}} \right)^\top f \right) + \Sigma_B - \Sigma_D,} \quad (2.21)$$

where the number density distribution function $f(\vec{c}, v, t)$ defines the frequency to find compartments with a specified concentration composition \vec{c} and size s at time t . The birth and the death term (Σ_B, Σ_D) summarise the compartment dynamics.

Compartment degradation and synthesis are, by definition, birth and death terms. In contrast, compartment growth involves both birth and death terms, as compartments are formally removed and replaced with compartments containing the same chemical species \vec{n}_i , but with an altered size. If compartment growth is considered a continuous process, it can be represented by an additional drift that changes both the concentration and size of the compartments $-\nabla_{c,v} \cdot (\vec{F}_{\text{growth}} f)$, which is elaborated on in more depth in section 2.4.4. Similarly, fusion and fragmentation also contain coupled birth and death terms. Next, we approximate the fusion and fragmentation terms by first focusing on a simplified system, in which compartment dynamics are restricted to fusion and fragmentation, and the reaction kinetics are reduced to 1-dimensional dynamics with $\vec{c} = c$. Assessing the quality of the approximation of the fusion and fragmentation flux first in this simplified setting, we subsequently relax on the assumptions to account for the full complexity of Eq. (2.21). This approach allows us to keep track of and assess the quality of the approximations we make.

2.4.1. Flux approximation of compartment fusion

In order to build an intuitive understanding of how fusion and fragmentation affect one-dimensional ensemble statistics, we simplify the population balance equation in Eq. 2.21 by neglecting compartment dynamics apart from fusion and fragmentation. We denote

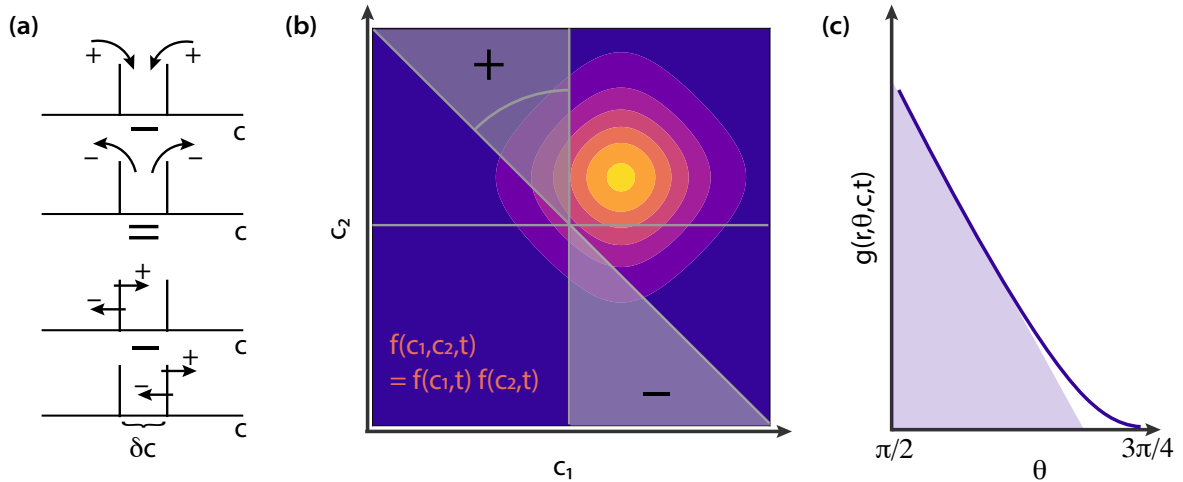


Fig. 2.3.: Graphically illustration of approximation steps made for in the flux approximation of compartment fusion (a) Schematic that illustrates the relation between the flux formulation and the structure of a balancing equation. (b) Schematic that illustrates the double integral using a geometric notion. Colour-coded are the iso-lines of the product $f(c_1, t)f(c_2, t)$. The two index sets subtracted against each other are illustrated. The arc along $g(r, \theta, c, t)$ is represented as a grey line. (c) Schematic of the triangulation approximation in Eq. (2.29).

the rate of compartment fusion by μ and the rate of compartment fragmentation by φ . To begin, we consider the limit of fast compartment fragmentation, $\mu/\varphi \ll 1$. We set a delta-distributed break-up probability $B(v) = \delta(v' - 0.5v)$, such that compartments always split in equal-sized daughters. In order to prevent compartments from splitting into infinitesimal dust, we limit the fragmentation kernel with a Heaviside step function $\Theta(v - v_0)$, so that only compartments larger than v_0 undergo fragmentation. The compartment dynamics are thus given by compartments that immediately fragment after a fusion event, such that we effectively find a delta-peaked size distribution $p(v, t_0) = \delta(v_0)$. In this limit, we neglect the compartment size and assume $f(\vec{c}, v, t) \equiv f(\vec{c}, t)$. At the same time, we still assume that the fused compartment state is preserved sufficiently long to allow for a complete mixing in the fused compartment state. With these assumptions, we symbolically write fusion and fragmentation in terms of two compartments as

$$(\vec{c}_i, \vec{c}_j) \xrightarrow{\text{fus. \& frag.}} (\vec{c}_l + \vec{\xi}, \vec{c}_l - \vec{\xi}), \quad \text{with } \vec{c}_l = \frac{\vec{c}_i + \vec{c}_j}{2}, \quad (2.22)$$

where \vec{c}_l is the averaged concentration and $\vec{\xi}$ account for the imperfect splitting. Assuming a small Gaussian contribution $\vec{\xi}$ to be negligible⁴ in comparison with the noise induced by chemical binding dynamics, we set it to zero in this subsection and elaborate on its functional form and strength in section 2.4.3. Note that, however, the statistics of fragmentation-induced noise plays a pivotal role in *close* compartmentalised systems, which we investigate in chapter 4.

Setting the fusion kernel independent of compartment size and composition,

⁴By construction, the noise induced by imperfect splitting is following a binomial distribution, which has a variance $\sigma^2 = np(1-p)$ and vanishes like the chemical reaction noise with $1/\sqrt{n}$. Assuming that fusion and fragmentation happens on slower time-scales than chemical reactions renders noise due to chemical reactions larger than noise induced by imperfect splitting.

2.4. Effective dynamics of open compartmentalised systems

$K(\vec{c}, \vec{c}', v, v') = \mu$, we initially focus on one-dimensional systems ($\vec{c} \rightarrow c$). We will relax these assumptions in the subsequent analysis. Under this approximation, we find that the fusion and subsequent fragmentation of compartments follows the Smoluchowski aggregation formalism, with source and sink terms describing the respective *jump into* and *jump out of* a state c by

$$\begin{aligned} \frac{\partial f(c, t)}{\partial t} = & \frac{\partial}{\partial c} \left(-F(c, t, \eta(t))f(c, t) + \frac{1}{2} \frac{\partial}{\partial c} (D(c, t, \eta(t))f(c, t)) \right) \\ & + \frac{\mu}{2} \int_0^\infty dc_1 f(c_1, t) \int_0^\infty dc_2 f(c_2, t) \delta\left(\frac{1}{2}(c_1 + c_2) - c\right) \\ & - \mu f(c, t). \end{aligned} \quad (2.23)$$

By making use of a mean-field approximation, we assumed that the two-point number density function, $f(c_1, c_2, t) = f(c_1, t)f(c_2, t)$, is the product of the one-point number density functions. Furthermore, we assumed that the processes of creation and removal of compartments are coupled, as for every two removed due to fragmentation, two new compartments are created. Therefore, instead of computing the jumps in and out of points in phase space, we made use of Gauss' theorem and considered the derivative of the virtual flux J_{fus} , as illustrated in Fig. 2.3 (a). This yields

$$\frac{\partial f(c, t)}{\partial t} = \frac{\partial}{\partial c} \left(-F(c, t, \eta(t))f(c, t) + \frac{1}{2} \frac{\partial}{\partial c} (D(c, t, \eta(t))f(c, t)) \right) - \frac{\partial}{\partial c} J_{\text{fus}}(c), \quad (2.24)$$

with the fusion flux $J_{\text{fus}}(c)$ defined by

$$\frac{J_{\text{fus}}(c)}{\mu} = \frac{1}{2} \int dc_1 \int dc_2 f(c_1, t) f(c_2, t) \Theta((c_1 - c)(c - c_2)) \text{sgn}(c' - c), \quad (2.25)$$

where we defined $c' = (c_1 + c_2)/2$. Here, $\Theta(c)$ refers to the Heaviside Theta function and $\text{sgn}(c)$ to the sign function. Next, we cast the definition of the $\Theta(c)$ and $\text{sgn}(c)$ in two index sets, over which the two-point number density is integrated

$$\begin{aligned} I_+(c) &= \{(c_1, c_2) | c_1 < c \wedge \frac{c_1 + c_2}{2} > c\}, \\ I_-(c) &= \{(c_1, c_2) | c_1 > c \wedge \frac{c_1 + c_2}{2} < c\}, \end{aligned}$$

which yields

$$\frac{J_{\text{fus}}(c)}{\mu} = \int_{I_+(c)} dc_1 dc_2 f(c_1, t) f(c_2, t) - \int_{I_-(c)} dc_1 dc_2 f(c_1, t) f(c_2, t). \quad (2.26)$$

We perform a variable transformation to spherical coordinates

$$\begin{aligned} c_1 &= \cos(\theta)r + c, \\ c_2 &= \sin(\theta)r + c, \end{aligned}$$

as we express c_1 and c_2 as functions of radius coordinate r and an angle coordinate θ . In

2. Theory of collective degrees of freedom in open compartmentalised systems

these coordinates, the fusion flux yields

$$\frac{J_{\text{fus}}(c)}{\mu} = \int_{\pi/2}^{3\pi/4} d\theta \int_0^\infty dr r f(\cos(\theta)r + c, t) f(\sin(\theta)r + c, t) - f(-\cos(\theta)r + c, t) f(-\sin(\theta)r + c, t). \quad (2.27)$$

In this formulation, we find symmetries of double integral, as the integral over the radius vanishes for $\theta = 3\pi/4$. Conversely, if $f(\tilde{c}+c, t)^2 \geq f(\tilde{c}+2c, t)f(\tilde{c}, t)$, $\forall \tilde{c}, c \in \mathbb{D}$, the integral over the radius has the maximal absolute value for $\theta = \pi/2$ and decreases monotonically in the range $\theta \in [\pi/2, 3\pi/4]$ by construction; Here \mathbb{D} refers to the support of the distribution f . Note, that this condition is in particular true for $f(c) \propto e^{-V(c)}$, and $V(c)$ a convex function. This is illustrated in Fig. 2.3 (b). We next make use of these symmetries, as we approximate the double integral. To this end, we perform the integral over the angle before the integral radial coordinate. For brevity of notation, we introduce

$$g(r, \theta, c, t) \equiv f(\cos(\theta)r + c, t) f(\sin(\theta)r + c, t) - f(-\cos(\theta)r + c, t) f(-\sin(\theta)r + c, t). \quad (2.28)$$

For the integral over θ , we linearise the $g(r, \theta, c, t)$ in θ for $\theta \in [\pi/2, 3\pi/4]$. $|g(r, \theta, c, t)|$ is a monotonically decreasing function in $\theta \in [\pi/2, 3\pi/4]$ by construction, if $f(m+x, t)^2 \geq f(m+2x, t)f(m, t)$, $\forall m, x \in \mathbb{D}$. We approximate the integral over $\theta \in [\pi/2, 3\pi/4]$ by a triangle, as we linearise $|g(r, \theta, c, t)|$ at $\theta = \pi/2$ and compute the intersection with $h(\theta) = 0$. This is illustrated in Fig. 2.3 (c). The intersection is approximately given by

$$\Delta\theta \approx \left| \frac{f(c, t)}{f'(c, t)} \right| \frac{r}{r + \left| \frac{f(c, t)}{f'(c, t)} \right|}, \quad (2.29)$$

where $f'(c, t) = \partial_c f(c, t)$ refers to the derivative with respect to the concentration. This approximation for $\Delta\theta$ renders an approximation for the double integral as

$$\frac{J_{\text{fus}}(c)}{\mu} \approx \int_0^\infty dr \frac{1}{2} \Delta\theta g(r, \pi/2, c, t) = \frac{1}{2} \left| \frac{f(c, t)}{f'(c, t)} \right| \int_0^\infty dr \frac{r}{r + \left| \frac{f(c, t)}{f'(c, t)} \right|} g(r, \pi/2, c, t). \quad (2.30)$$

We note, that for c a constant, the fraction in the integral over the radius renders a constant.

Based on this, we next introduce three approximations of the fusion flux, which vary in their quality in assessing either the fluxes close to the mean of the distribution or in the tails of the distribution. While in the following we will mostly employ the approximation assess the fusion flux close to the mean of the distribution, for completeness we also state the approximation for the fusion flux in the tail of the distribution. We introduce the *short range approximation*

$$\boxed{\frac{J_{\text{fus, sr}}(c)}{\mu} \approx \frac{1}{2} \int_0^\infty dr r g(r, \pi/2, c, t) = \frac{1}{2} f(c, t) \int_{\mathbb{D}} dc' f(c', t) (c' - c),} \quad (2.31)$$

which is especially suited to estimate the flux close to the mean of the distribution $f(c)$,

and a *long range approximation*

$$\frac{J_{\text{fus, lr}}(c)}{\mu} \approx \left| \frac{f(c)}{f'(c)} \right| \frac{1}{2} \int_0^\infty dr g(r, \pi/2, c, t) = \frac{1}{2} f(c, t) \left| \frac{f(c, t)}{f'(c, t)} \right| \int_{\mathbb{D}} dc' f(c', t) \text{sgn}(c' - c), \quad (2.32)$$

which is especially suited to depict the correct behaviour in the tails of the distribution. Note, that the fraction $|f(c)/f'(c)|$ vanishes in the tails of the distribution $f(c)$, if $f(c)$ is exponentially decaying with $f(c) \propto \exp(-c/k)$ for $c \rightarrow \infty$. Based on this, we additionally introduce the *stable tail long range approximation*

$$\frac{J_{\text{fus, stlr}}(c)}{\mu} \approx \frac{k}{2} f(c, t) \int_{\mathbb{D}} dc' f(c', t) \text{sgn}(c' - c), \quad (2.33)$$

which we will show to be in particular useful for the estimation of tails in steady-state distributions. Note, that k can be determined by self-consistent steady-state solutions. By comparing the Fokker-Planck equation for a many-body system with two-particle interaction potentials, we note the structural equivalence, see appendix A.3 and [101]. We thus identify the short-range approximation with an effective two-body interaction potential $w_{i,j;sr} = (c_i - c_j)^2$ and the stable tail long-range approximation with $w_{i,j;stlr} = |c_i - c_j|$. Our findings suggest that the combination of compartment fusion and subsequent fragmentation act as a steady attractive force in the concentration phase-space between all compartments. We will further explore the implications of this interpretation in section 2.5.2.

In order to simplify the approximations further, we define a normalisation factor $N(t) = \int dc f(c, t)$. We normalise $p(c, t) = f(c, t)/N(t)$ to a probability distribution, and define $N(t)\langle c(t) \rangle = \int dcc f(c, t)$ as the mean of the distribution $f(c, t)$. Furthermore, we define the cumulative distribution $\Phi(c, t) = \int_\infty^c dc' f(c')$, and, by performing the integral in the fusion flux approximations, we find that the short-range approximation describes a steady attraction towards the mean

$$J_{\text{fus, sr}}(c) \approx \frac{\mu}{2} N f(c, t) (\langle c \rangle - c), \quad (2.34)$$

while the long range approximation describes a steady attraction to the median, as

$$J_{\text{fus, stlr}}(c) \approx \frac{\mu k}{2} f(c, t) \left| \frac{f(c, t)}{f'(c, t)} \right| N(2\Phi(c, t) - 1). \quad (2.35)$$

The compartments in the tail of the distribution $x \rightarrow \infty$ are attracted to the centre of the distribution with different functional dependencies for the long-range and the short-range approximations. Notably, the functional dependence in the long-range approximation has a weaker effect on tails that decay slower than exponentially, and a stronger effect on tails that decay faster than exponentially. Consequently, the fusion fluxes create exponentially decaying tails in a steady state in the absence of compartment or additional drift terms. This motivates the introduction of the stable tail long-range approximation in Eq. (2.35).

In the absence of drifts, $F_{\eta(t)}(c, t) = 0$, and constant diffusion, $D_{\eta(t)}(c, t) = D$, the short-range approximation of the fusion flux and the stable tail long range approximation admit analytical solutions. We make use of analytical solutions to test the goodness of the approximations. To this end, we simulate a finite-sized ensemble of Brownian random walkers, which undergo random averaging events due to fusion and subsequent immediate

2. Theory of collective degrees of freedom in open compartmentalised systems

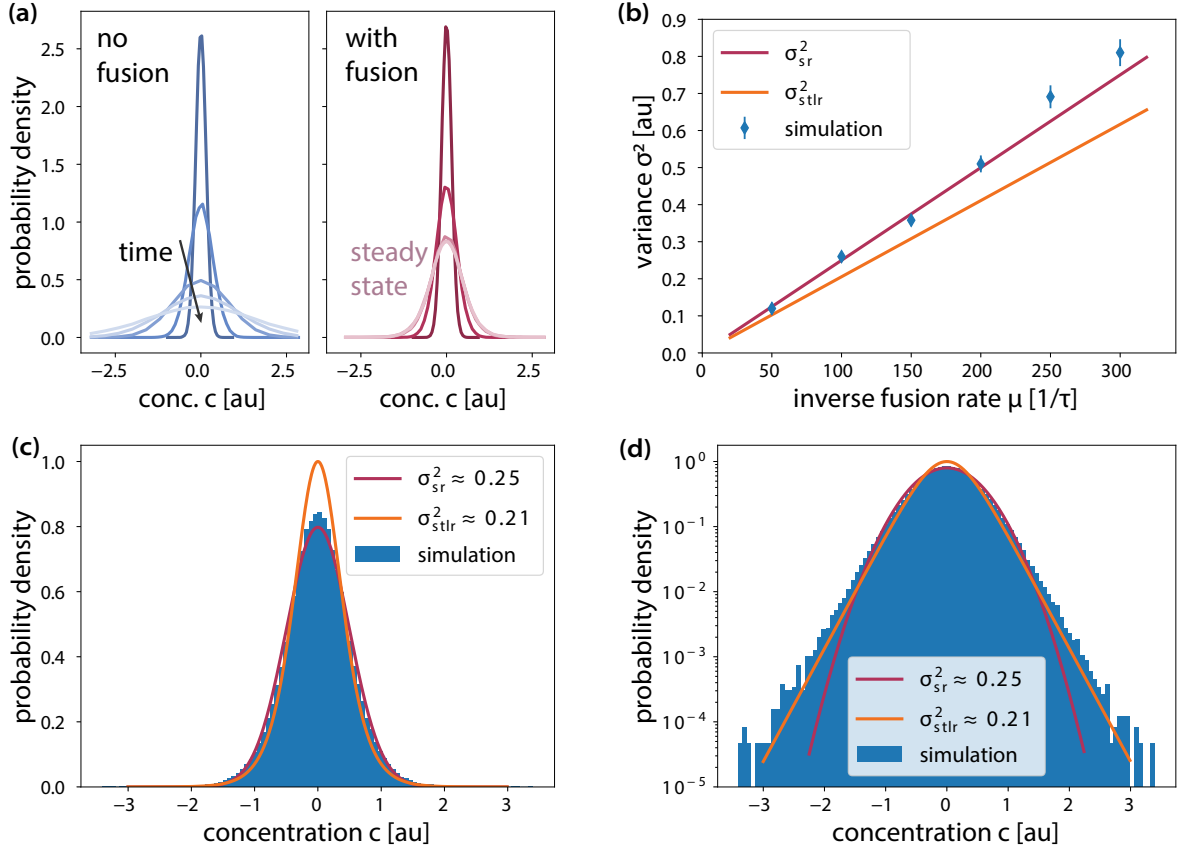


Fig. 2.4.: Corroboration of the fusion flux approximation by full stochastic numerical simulations Numerical simulations are conducted by simulating random walkers in a flat potential with constant diffusion coefficient using over-damped Langevin equations. Random walkers are initialised at time $t = 0$ at position $c_0 = 0$. Compartment fusion and subsequent fragmentation is modelled as stochastic, time-discrete averaging events between two randomly chosen random walkers. μ refers to the rate of the averaging events. All results are present in simulation units, where τ refers to the time-discrete updating step. (a) While the random walkers without "compartment fusion and fragmentation" disperse, the random averaging events give rise to steady state distribution with finite dispersion. (b) Eq. (2.34) and Eq. (2.35) predict the variance of the steady state in simulation units. Note, that the estimates are fully defined by the simulation parameters and admit no free fit parameter. Both approximations correctly predict the functional dependence of the fusion rate μ . Furthermore, the long-range approximations give a good quantitative assessment of the variance. Errorbars show the standard deviation. (c) The short-range approximation furthermore captures the shape of the steady state well close to the mean of the distribution. (d) The stable tail long-range approximation, in contrast, captures the tail of the distribution with the correct function dependence on c .

fragmentation, as introduced above. With these approximations, the population balance equation then yields

$$\partial_t f(c, t) = \partial_c [-J_{\text{fus}} + D \partial_c f(c, t)]. \quad (2.36)$$

Without any loss of generality, we normalise $\int_{-\infty}^{\infty} dc f(c) = 1$ and initialise the random walkers at $p(c, t_0) = \delta(c)$ at the origin. Our analysis predicts that the ensemble statistics

will approach a steady state with finite variance, as opposed to an ensemble of random walkers in the absence of fusion and fragment. The simulations reveal that the variance increases linearly with time in the absence of compartment fusion and fragmentation, whereas the variance reaches a fixed value if compartment fusion and fragmentation are taken into consideration. The steady-state distribution for the short-range approximation is

$$f_{\text{sr}; \text{ss}}(c) = \sqrt{\frac{\mu}{4\pi D}} \exp\left(-\frac{\mu}{4D}c^2\right), \quad (2.37)$$

which predicts a variance $\sigma_{\text{sr}}^2 = 2D/\mu$. The steady-state distribution for the stable tail long-range approximation is

$$f_{\text{stlr}; \text{ss}}(c) = \sqrt{\frac{\mu}{8D}} \frac{1}{\cosh\left(x\sqrt{\frac{2D}{\mu}}\right)^2}, \quad (2.38)$$

which predicts a variance $\sigma_{\text{stlr}}^2 = \pi^2/12 \cdot 2D/\mu$. We test our theoretical predictions through numerical simulations. We consider a finite set of random walkers which undergo pairwise averaging events at a rate of μ . Fig. 2.4 (a) shows that, in agreement with our prediction, the dynamics approach a steady state when averaging is present, i.e. when compartment fusion and fragmentation occurs. In contrast, the variance in the set of random walkers without interactions shows the expected diffusive spreading and no steady state is approached. Fig. 2.4 (b) demonstrates that we correctly predict the variance of the steady state distribution as a function of the fusion rates. Note that our prediction admits no free fit parameters. Fig. 2.4 (c,d) show that we correctly predict the shape of the distribution $f(c, t)$. The short-range approximation correctly describes the shape close to the mean of the distribution, while the long-range stable tail approximation is well-suited to assess the tail of the distribution.

2.4.2. Generalisations on the flux approximation of compartment fusion

In the preceding section, we considered approximations of the fusion flux in order to capture compartment fusion and the subsequent fragmentation. We focused on one-dimensional systems, constant fusion kernels and a delta-peaks size distribution. Here, we relax on these assumptions.

2.4.2.1. Accounting for general fusion kernels

We can straightforwardly relax the assumption of a constant fusion kernel, allowing for arbitrary kernels dependent on the concentrations $K(c, c', t)$. To this end, we draw $K(c, c', t)$ initially into the double integral of the fusion flux and redefine $\tilde{g}(r, \theta, c, t) = K(c, c', t)g(r, \theta, c, t)$ in Eq. (2.28). However, arbitrary fusion fluxes potentially break the symmetries of the double integral which were exploited in the approximation. For fusion kernels of the form $K(c, c', t) = \kappa(c, t)\kappa(c', t)$, with $\kappa(c, t)$ an algebraic function, the approximations still hold and the short range approximation yields

$$J_{\text{fus, sr}}(c) \approx \frac{1}{2} f(c, t) \kappa(c, t) \int_{\mathbb{D}} dx f(x, t) \kappa(x, t) (x - c). \quad (2.39)$$

2.4.2.2. Accounting for finite fragmentation rates

As we assume a fast fragmentation rate ($\varphi \gg \mu$), we account for compartments of varying sizes. Additionally, we relax the assumption on the break-up probability defining the position where fragmentation is happening. Specifically, we assume that the break-up probability is uniformly distributed over the compartment volume. This requires refinement of the fusion flux integral in Eq. (2.23) by taking into account the number density $f(c, v, t)$, adjusting the averaging by rescaling the variable x' accordingly, and tracking the masses that move across position c :

$$\frac{\tilde{J}_{\text{fus}}(c, v_1, v_2)}{\mu} = \int dc_1 \int dc_2 v_1 \left[f(c_1, v_1, t) f(c_2, v_2, t) \Theta((c - c_1)(c' - c)) \text{sgn}(c' - c) \right], \quad (2.40)$$

with $c' = (v_1 c_1 + v_2 c_2)/(v_1 + v_2)$. Here, we kept the compartment masses v_1 and v_2 fixed. The full fusion flux is then computed by integrating over the masses as

$$J_{\text{fus}}(c) = \int dv_1 \int dv_2 \tilde{J}_{\text{fus}}(c, v_1, v_2). \quad (2.41)$$

Here, the subscript 'v' refers to *size*, to distinguish this fusion flux approximation from the approximation made in section 2.4.1. Accounting for different masses directly translates into the two index sets

$$I_+(c, v_1, v_2) = \{(c_1, c_2) | c_1 < c \wedge \frac{c_1 v_1 + c_2 v_2}{v_1 + v_2} > c\},$$

$$I_-(c, v_1, v_2) = \{(c_1, c_2) | c_1 > c \wedge \frac{c_1 v_1 + c_2 v_2}{v_1 + v_2} < c\},$$

which yields

$$\frac{\tilde{J}_{\text{fus}}(c)}{\mu} = \int_{I_+} dc_1 dc_2 v_1 f(c_1, v_1, t) f(c_2, v_2, t) - \int_{I_-} dc_1 dc_2 v_1 f(c_1, v_1, t) f(c_2, v_2, t). \quad (2.42)$$

We thus find, that the approximation of the fusion flux accounting for different masses follows the analogous structure as presented in section 2.4.1, if the two compartment masses v_1 and v_2 are considered fixed. When converting to polar coordinates, we find the analogous equation Eq. (2.27) with the integration boundary of the integral over the angle varied to $\theta \in [\pi/2, \pi/2 + \alpha]$, where the upper boundary is determined by $\alpha = \arctan(v_2/v_1)$. Analogous to the triangle approximation in section 2.4.1, we approximate that both fractions $v_2/v_1 > 1$ and $v_2/v_1 < 1$ effectively reduce the value of the integral. In the picture of the triangle, for $v_2/v_1 < 1$, we find that the upper boundary $\pi/2 + \alpha < 3\pi/4$. In this case, the triangle is not integrated over the full baseline. Conversely, for $v_2/v_1 > 1$ the integration includes negative values. We approximate each integral $\mathcal{I}_\theta(r, \theta, c, v_1, v_2, t)$ by

$$\begin{aligned} \mathcal{I}_\theta(r, \theta, c, v_1, v_2, t) &\approx \mathcal{I}_\theta(r, \pi/4, c, v_1, v_2, t) \left(1 - \left(\arctan\left(\frac{v_2}{v_1}\right) \frac{4}{\pi} n - 1 \right)^2 \right) \\ &= \mathcal{I}_\theta(r, \pi/4, c, v_1, v_2, t) \Lambda(v_1, v_2) \end{aligned} \quad (2.43)$$

which describes an adjustment of the triangle area by the fraction of the reduced or extended baseline. With this, the approximation of the fusion flux shows the same structure as in Eq. (2.30),

$$\frac{J_{\text{fus}, v}(c)}{\mu} \approx \int dv_1 \int dv_2 v_1 \Lambda(v_1, v_2) \frac{1}{2} \left| \frac{f(c, v_2, t)}{f'(c, v_2, t)} \right| \int_0^\infty dr \frac{r}{r + \left| \frac{f(c, v_2, t)}{f'(c, v_2, t)} \right|} g(r, \pi/2, c, v_1, v_2, t). \quad (2.44)$$

While this approximation show the same functional form as in the case of compartments of the same size, the above equation is analytically difficult to capture if the joint distribution $f(c, v_1, t)$ of mass and concentration is considered. In the next step, we further simplify this expression by marginalising over the different compartment sizes.

2.4.2.3. Marginalising over compartment sizes

To allow for an analytic treatment of Eq. (2.44), we further approximate $\frac{J_{\text{fus}, v}(c)}{\mu}$ by marginalising over the different compartment sizes. To this end, we employ a mean-field approximation, approximating $f(c, v, t) = f(c, t)m(v, t)$. We assume compartment fusion to be independent of the compartment sizes and the fragmentation rate to be proportional to the size of the splitting compartment, as introduced in section 2.2.3. The distribution $f(c, t)$ thus describes the mass density, that is the number of compartments with concentration c at time t in units of multiples of compartment building block mass. Under these assumptions, the size distribution $m(v, t)$ is approximately given by an exponential distribution $m(v, t) \propto a^2 e^{-a(t)v}$, where a^2 adjust for measuring the $m(v, t)$ in terms of multiples of the building blocks. With these assumptions, the fusion flux approximates to

$$\frac{J_{\text{fus}, mv}(c)}{\mu} \approx \frac{a}{3} \left| \frac{f(c, t)}{f'(c, t)} \right| \int_0^\infty dr \frac{r}{r + \left| \frac{f(c, t)}{f'(c, t)} \right|} g(r, \pi/2, c, t). \quad (2.45)$$

Here the subscript ‘mv’ indicates the marginalisation over the compartment size. We find that the fusion flux marginalised over different compartment sizes is proportional to the fusion flux in the approximation of singular compartment size $J_{\text{fus}, mv}(c) \propto J_{\text{fus}}(c)$ and rescaled only by a numerical factor $\gamma(\langle v \rangle)$ which is a function of the average mass.

To consistently account for the marginalisation of the number density $f(c, v, t) \rightarrow f(c, t) = \int dv f(c, v, t)$ in the population balance equation in Eq. (2.55), it is necessary to also marginalise the other terms. The drift term can be drawn out of the integral, whereas the diffusion $D_{\eta(t)}(c, v)$ has a size dependence of $D_{\eta(t)}(c, v) = D_{\eta(t)}(c)/v$. Taking advantage of the same size distribution as for the marginalisation of the fusion flux, $m(v, t) \propto a^2 \exp[-a(t)v]$, and assuming a mean-field approximation, we obtain

$$D_{\eta(t), \text{eff}}(c) = \int dv m(v, t) \frac{D_{\eta(t)}(c)}{v} \approx \frac{D_{\eta(t)}(c)}{\langle v \rangle}. \quad (2.46)$$

Furthermore, the birth and death terms in Eq. (2.55), which take into account compartment degradation, synthesis and growth, must be marginalised under the same assumption in order to obtain a self-consistent approximation of the population balance equation.

We tested the approximations of marginalising over different sizes using the same model considered in section 2.4.1 and Fig. 2.4. This model featured an absence of a drift term, a

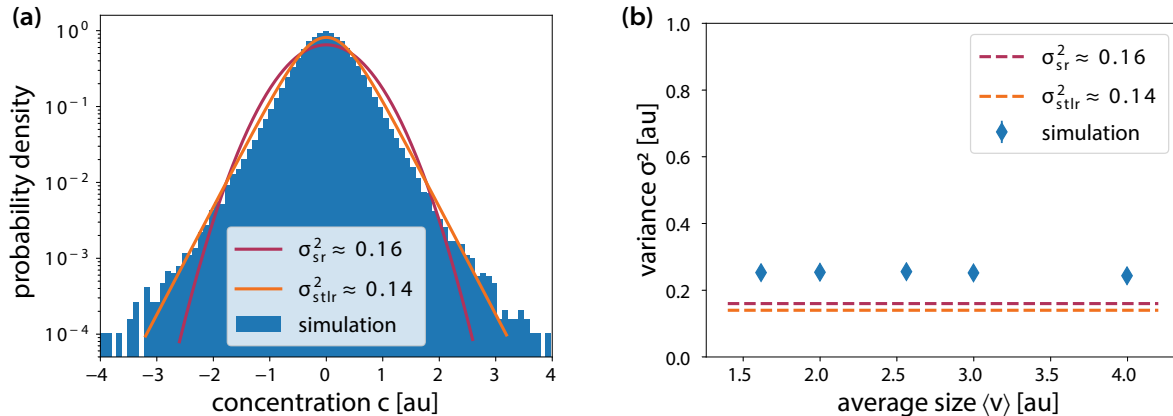


Fig. 2.5.: Corroboration of the fusion flux approximation accounting for the marginalisation over compartment sizes Simulations are analogous to Fig. 2.4, but additional finite fragmentation rates $\varphi < \infty$ are assumed, results in compartments with various sizes. While the enclosed dynamics are modelled by Langevin Equations, the compartment dynamics simulated as full stochastic processes, also compare with appendix B.1. All results are present in simulation units, where τ refers to the time-discrete updating step. (a) Considering the normalised mass density distribution function $f(c, t) / \int f(c, t) dc$, Eq. (2.34) and Eq. (2.35) still give qualitative good estimates of the steady-state distribution. (b) Based on our analysis, we predict the variance of the steady state to be independent of the average compartment size $\langle v \rangle$. Errorbars show the standard deviation. We verify this prediction with numerical simulations. Compartment size is evaluated in multiples of the compartment unit size.

constant diffusion coefficient $D(c) = D$, a constant fusion kernel $K(c', c, v', v, t) = \mu$, and finite fragmentation rates $\phi < \infty$. We rescaled the diffusion coefficient to $D(c, v, t) = D/v$ and predicted an effective diffusion constant that scales inversely with the average system size, i.e. $D_{\text{eff}} \propto 1/\langle v \rangle$. Additionally, we defined an effective fusion rate which summarised all the prefactors in front of the approximation of the fusion integral and found a reciprocal scaling $\mu_{\text{eff}} \propto 1/\langle v \rangle$. Therefore, we predicted that the distribution $f(c, v, t)$ should remain fixed as the fragmentation rate φ was varied. As expected, our results demonstrated that the short-range approximation and the stable-tail long-ranged approximation in Eq. (2.34,2.35) accurately approximated the marginalised number density $f(c, t)$, see Fig. 2.5 (a). Furthermore, in line with our prediction, the variance remained approximately constant, see Fig. 2.5 (b).

The results of the marginalisation presented in this section rely upon the assumption of a size distribution. Should other compartment fusion and fragmentation dynamics be considered, the approximations made in the context of the marginalisation need to be reviewed and adjusted accordingly. The approximation holds well in the model studied in Fig. 2.5, however, additional processes which introduce a correlation between the concentration and the size distribution reduce the efficacy of the mean-field approximation. This is especially true when fusion kernels with an explicit concentration dependence are taken into account, in which case the size marginalisation should be applied with caution. Thus far, we have only focused on effective one-dimensional models. In the next stage, we will generalise the approximation to include $d > 1$ dimensional dynamics.

2.4.2.4. Accounting for multi-variate concentration vectors

The approximation of the fusion flux in section 2.4.1, Eq. (2.34), relied on the assumption of a 1-dimensional dynamics in the concentration c . We note, that the fusion of two compartments creates the virtual displacement of compartment masses along a 1-dimensional line in the concentration phase space. We used in the approximation of the double integral, that this agrees with the dimension of the phase space for 1-dimensional dynamics.

We note, that also in higher dimensional dynamics the fusion of two compartments creates a virtual displacement along a one-dimensional line. To approximate the fusion flux at a specified point \vec{c}_{fus}^* in the concentration phase space, we hence need to account for mass displacements due compartment fusion across $\vec{c}^{*\top}$ in all possible directions. To this end, we consider a parametrisation of a d -dimensional concentration phase space in spherical coordinates, making use of a radial coordinate r and $d - 1$ angle coordinates $\phi_1, \dots, \phi_{d-1}$, where $r \in [0, \infty)$, $\phi_1, \dots, \phi_{d-2} \in [0, \pi]$, and $\phi_{d-1} \in [0, 2\pi)$, as

$$\begin{aligned} c_1 &= c_1^* + r \cos(\phi_1) \\ c_2 &= c_2^* + r \sin(\phi_1) \cos(\phi_2) \\ &\dots \\ c_{d-1} &= c_{d-1}^* + r \sin(\phi_1) \cdots \cos(\phi_{d-1}) \\ c_d &= c_d^* + r \sin(\phi_1) \cdots \sin(\phi_{d-1}). \end{aligned}$$

We define a line in the multi-dimensional phase space, by fixing all angle variables $\phi_1, \dots, \phi_{d-1}$ and allowing the radial coordinate to assume values in $r \in (-\infty, \infty)$, as $\vec{l}(r, \phi_1, \dots, \phi_{d-1})$. For the brevity of notation, we collect the angle variables in a vector $\vec{\alpha} = (\phi_1, \dots, \phi_{d-1})^\top$, and write $\vec{l}_{\vec{\alpha}}(r)$. For every line, we define a unit vector $\vec{e}_{\vec{\alpha}}$, which points in the same direction as the line $\vec{l}_{\vec{\alpha}}(r)$. Along every line $\vec{l}_{\vec{\alpha}}(r)$, the virtual displacement of compartments attribute to the total flux $\vec{J}_{\text{fus}}(\vec{c}^*)$. To account for this, we define the fusion flux along a specified line as $\vec{J}_{\text{fus}, \vec{\alpha}}(\vec{c}^*)$. Note, that the fusion flux along the one-dimensional line can be approximated by Eq. (2.34). Instead of varying the coordinated one-dimensional concentration c , here the radial coordinate r is varied, while the angle variables $\vec{\alpha}$ are considered fixed. By construction the flux decomposes into $\vec{J}_{\text{fus}, \vec{\alpha}}(\vec{c}^*) = J_{\text{fus}, \vec{\alpha}}(\vec{c}^*) \cdot \vec{e}_{\vec{\alpha}}$. The total flux is recovered by

$$\vec{J}_{\text{fus}}(\vec{c}^*) = \int d\vec{\alpha} J_{\text{fus}, \vec{\alpha}}(\vec{c}^*) \cdot \vec{e}_{\vec{\alpha}}, \quad (2.47)$$

where all angles are integrated over the range $\phi_i \in [0, \pi]$ to cover the full phase space.

The definition in Eq. (2.47) correctly accounts for correlations in the different molecular species in the concentration vector \vec{c} , yet it does not admit further analytical treatment. We next approximate Eq. (2.47), by setting a mean-field approximation on the concentrations, such that $f(\vec{c}, v, t) = \prod_j^d f_j(c_j, v, t)$. In consistency with this approximation, we set the formal independence of averaging events due to compartment fusion. In this approximation, the fusion flux factorises, such that each component is

$$\vec{J}_{\text{fus}, i}(\vec{c}^*) \approx \mu \frac{1}{3\langle v \rangle} \left| \frac{f(\vec{c}^*, t)}{f'(\vec{c}^*, t)} \right| \int_0^\infty dr \frac{r}{r + \left| \frac{f(\vec{c}^*, t)}{f'(\vec{c}^*, t)} \right|} g_i(r, \pi/2, c_i^*, t) \left(\prod_{j \neq i} f_j(c_j^*, t) \right) \quad (2.48)$$

2. Theory of collective degrees of freedom in open compartmentalised systems

in analogy to Eq. (2.30), and $g_i(r, \pi/2, \vec{c}_i^*, t)$ constructed with the single component number density $f_i(c_i, t)$. Here, we made use of the marginalisation of different compartment sizes introduced in section 2.4.2.3. Note, that this in particular allows for the simple generalisation of the short-range approximation of the fusion flux in Eq. (2.34), which yields

$$\boxed{\vec{J}_{\text{fus, sr}}(\vec{c}) \approx -\frac{\mu}{3\langle v \rangle} f(\vec{c}, t) \nabla_c \int_{\mathbb{D}} d\vec{x} f(\vec{x}, t) (\vec{x} - \vec{c})^2}, \quad (2.49)$$

and the stable tail long range approximation in Eq. (2.35) yields

$$\vec{J}_{\text{fus, stlr}}(\vec{c}) \approx -\frac{\mu}{3\langle v \rangle} f(\vec{c}, t) \nabla_c \int_{\mathbb{D}} d\vec{x} f(\vec{x}, t) (\vec{k} \cdot |\vec{x} - \vec{c}|), \quad (2.50)$$

where $|\vec{x}|$ refers to the vector of absolute values and \vec{k} specifies the exponential decay in the different dimensions. Specifically, the short-range approximation is a straightforward generalisation of the one-dimensional fusion flux approximation as the d -dimensional mean is considered. Note, that the generalisation of the long-range approximation formally defines a generalisation of the d -dimensional median.

With this, we have generalised the approximation of the fusion flux to include multi-dimensional dynamics as we consider the multi-dimensional number density distribution $f(\vec{c}, v, t)$, general compartment fusion kernel $K(c, c', v, v', t)$, and finite fragmentation rates $\varphi < \infty$, which implies compartments of varies size over which we marginalised. In the next section 2.4.3, briefly turn to fluxes induced by compartment fragmentation and compartment growth and shrinkage. After this, we summarise the technical steps we followed to derive effective ensemble dynamics to grant an overview about the approximations made in this section 2.4. We interpret the consequence of the effective ensemble dynamics in the context of compartmentalised stochastic reaction kinetics systems in section 2.5.

2.4.3. Flux approximation of compartment fragmentation

In the previous section, we focused on a flux approximation for compartment fusion. Compartment fusion constitutes an averaging process between two compartments. In this section, we study compartment fragmentation, which we link to a binomial splitting process, as introduced in section 2.4.1. As such, compartment fragmentation increases differences between compartments and we link compartment fragmentation with a noise contribution. In Eq. (2.22), we have introduced the notation $\vec{\xi}_{\text{frag}}$ to refer to the noise due to compartment fragmentation. Next, we first discuss the strength of this noise component and then investigate how this can be incorporated into a flux approximation.

Starting on the discussion of the strength of the noise component, we first note that fragmentation noise is proportional to the rate of compartment fragmentation. Further note, that for compartment size distributions in steady state, the rate of compartment fusion and fragmentation coincide. For this reason, we set $\vec{\xi}_{\text{frag}} \propto \mu$. Furthermore, the definition of compartment fragmentation as a binomial splitting process sets the full statistics of the fragmentation noise. Let $b_i(n, p) \sim \text{Binom.}(n_i, p)$ refer to a set of independent binomial random variables with parameter n_i and success probability p . The fragmentation noise is then given by $\vec{\xi}_{\text{frag}} = \mu \vec{b}(\vec{n}, p)$, where \vec{n} is the number of copy numbers, as $\vec{n} = \vec{c}s$. We approximate the binomial splitting noise with a Gaussian random variable, which allows for further analytic treatment. To this end, we assess the variance of the binomial noise

vector. We find

$$\vec{\sigma}_{\vec{c}}^2 \approx \left(\frac{\pi}{8}\right)^2 \frac{\vec{c}}{\langle v \rangle}, \quad (2.51)$$

where we already transformed to a notation in terms of concentration marginalised over different compartment sizes. For this result, we assumed a uniform splitting probability. By construction, the mean of the fragmentation noise is $\langle \vec{\chi}_{\text{frag}} \rangle = 0$. Furthermore, we assume that noise is temporally uncorrelated. With this, we have fully defined the statistics of the Gaussian noise vector.

We note, that the noise vector has a square root dependence on the concentration, and thus is multiplicative noise. As such, we here take the Itô-convention and associate with compartment fragmentation a diffusion flux

$$\vec{J}_{\text{frag}} \approx -\frac{\mu}{\langle v \rangle} \frac{\pi}{8} (\nabla_{\vec{c}} \vec{c}) f(\vec{c}, t) \vec{e}_i, \quad (2.52)$$

where e_i are the orthonormal basis vectors. We find, that the fragmentation flux approximation has the same functional form as the diffusion flux in the enclosed stochastic reaction kinetics. Yet, as we generally assume that the compartment dynamics happen on a longer timescale than the enclosed reaction kinetics, we assume that for *open* compartmentalised systems, the diffusion term of the enclosed stochastic reaction kinetics is dominating. We next turn to derive a flux approximation for compartment growth and shrinkage.

2.4.4. Flux approximation of compartment growth and shrinkage

Similar to the approach of expressing compartment fusion and fragmentation as fluxes in the phase space rather than through a formulation of birth and death terms, we note that compartment growth and shrinkage can also be seen as a displacement of compartments in the phase space rather than a removal and subsequent addition. While compartment fusion and fragmentation are mass-conserving processes, this is not true for compartment growth and shrinkage. Therefore, we need to take into account the changes in compartment mass when deriving the compartment growth and shrinkage fluxes. Generally speaking, compartment growth and shrinkage can be defined as:

$$\frac{d}{dt} v_i = G_i(\vec{c}_i, v_i, t). \quad (2.53)$$

Where we specified on compartment i . In the following, we drop the index i as we assume that the dynamics governing compartment growth and shrinkage are identical for all compartments. For deterministic, time-continuous function $G(\vec{c}, v, t)$, and accounting for the definition $\vec{c} = \vec{n}/s$, where \vec{n} is the copy number of molecular species unaffected by compartment size, we can directly deduce:

$$-\nabla \vec{J}_g \approx +\nabla_{\vec{c}} \vec{c} \frac{G(\vec{c}, v, t)}{v} f(\vec{c}, v, t) - \partial_v G(\vec{c}, v, t) f(\vec{c}, v, t). \quad (2.54)$$

Note that by definition, the fluxes due to growth and shrinkage in generally admit no simple marginalisation over the sizes due to the dependence of the growth rate on both

size and compartment concentration $G(\vec{c}, v, t)$.

2.4.5. Effective ensemble dynamics and their limitations

In sections 2.4.1 and 2.4.3 we investigated the approximation of the effects of compartment fusion and fragmentation in the context of the population balance equation presented in the beginning of section 2.4. In this section, we summarise the central approximations in the derivation of the effective ensemble dynamics again, to grant a comprehensive overview and allow us to assess situations in which the approximations break down.

We started this section 2.4 by approximating the dynamics of compartmentalised stochastic reaction kinetics systems within the framework of population balance equations, as seen in Eq. (2.21). In doing so, we have assumed a continuum approximation in the number of compartments, considering the continuous number density distribution function $f(\vec{c}, \vec{o}, t)$. This framework allows us to decompose the chemical reaction dynamics of the signalling pathway and the effects of compartment dynamics into distinct components. We have further assumed that the spatial position of compartments and their shape have no influence on the chemical reaction kinetics of the signalling pathways, marginalising over the compartment properties \vec{o} and only accounting for the different sizes of compartments through the number density distribution $f(\vec{c}, v, t)$.

Making use of system size expansion on the level of the chemical reaction kinetics, we derived drift and diffusion fluxes in the concentration phase space, see section 2.2.1. We then applied a mean-field approximation, assuming a well-mixed system for the reaction kinetics in each compartment. This enabled us to make a continuum approximation in the concentration \vec{c} . The compartment dynamics were expressed by birth and death terms, which account for, for example, degradation and synthesis, or fusion and fragmentation of compartments. We left these terms unspecified to account for general compartment dynamics. We noted that compartment growth and shrinkage, as well as fusion and fragmentation, are processes where compartment masses are displaced in the property phase space (\vec{c}, v) , as compartments are removed from the number density distribution function $f(\vec{c}, v, t)$ and subsequently compartments with changed properties are added. In the continuum limit of $f(\vec{c}, v, t)$, this leads to continuous virtual displacement fluxes. Notably, the continuous fluxes formally arise from the continuum approximation in the number of compartments without making any assumptions on the timescale of the compartment dynamics.

In section 2.4.1, we derived an approximation for the fluxes induced by compartment fusion and fragmentation. In particular, the approximation of the fusion flux incorporated several approximations. To ensure clarity of the argument, we first derived the flux in a highly simplified model context, assuming one-dimensional dynamics in the concentration c , constant fusion kernels $K(c, c', v, v', t) = \mu$, and the limit of fast compartment fragmentation rates $\varphi \rightarrow \infty$, where all compartments effectively have the same size. Additionally, we assumed that the concentrations of fused compartments mix instantaneously, which is consistent with the assumption of well-mixed conditions for the chemical reaction kinetics. In these limits, a geometrical interpretation of the fusion flux can be given by assuming a mean-field approximation in which the two-point distribution $f(c, c', t)$ of two compartments with concentration c and c' , factorises to $f(c, t)f(c', t)$. This resulted in two approximations, referred to as the *short range approximation* (Eq. (2.34)) and the *stable tail long range approximation* (Eq. (2.35)). The former is especially suited for calculating the fusion flux close to the mode of the distribution $f(c, t)$, while the latter is

more appropriate for the tails of the distribution $f(c, t)$. Furthermore, the geometrical interpretation enables us to assess the accuracy of the approximations and identify the conditions under which they are likely to fail. In particular, it can be observed that the approximation of the fusion flux is valid for distributions $f(c, v, t)$ with exponential tails, although caution should be exercised when dealing with distributions with algebraic tails.

We corroborated the approximations of the fusion flux by numerical simulations, yielding good qualitative and quantitative agreement when considering stochastic, time-discrete compartment fusion and fragmentation dynamics, see Fig. 2.4. Importantly, we derived estimates for the distribution $f(c, t)$ with no free parameters. Building upon the insight gained from the approximation of the fusion flux in this limit, we demonstrated how to directly account for concentration-dependent fusion kernels. Next, we relaxed the assumption of infinitely fast fragmentation rates $\varphi < \infty$, thereby allowing for various compartment sizes.

By making a mean-field approximation, wherein $f(c, v, t) = f(c, t)m(v, t)$ is factorised, we presented an approximation of the marginalisation of the fusion flux approximation across different compartment sizes. Assuming a particular compartment size distribution $m(v, t)$ for this approximation, the marginalisation yielded the functional form of the fusion flux approximations found in the limit of fast fragmentation rates, $\varphi \rightarrow \infty$. In this approximation, the various compartment sizes had a numeric prefactor in front of the integral fusion flux approximation, which was dependent on the average compartment size. Furthermore, to be consistent in the description, we also introduced an approximation for the marginalisation of the diffusion flux of the chemical reaction dynamics. We compared our analytical prediction with numerical simulations of finite-sized compartment ensembles with stochastic, time-discrete compartment fusion and fragmentation dynamics, finding good qualitative and quantitative agreement between our theoretical predictions and the numerical results, see Fig. 2.5. Note, that also other terms of the compartment dynamics in the population balance equation Eq. (2.21) need to be consistently marginalised, e.g. growth terms or degradations terms.

In the last step, we generalised the fusion flux to d -dimensional dynamics in the concentration phase space. We derived a formal approximation of the fusion flux, accounting for the correlations among molecular species in the concentration vector \vec{c}_i . This was done by making use of the one-dimensional fusion integrals and integrating over the phase space dimensionality for each point. Whilst this formal definition is complex, we derived a mean-field approximation, by factorising $f(\vec{c}, v, t) = \prod_j^d f_j(c_j, v, t)$. This approximation provides a straightforward generalisation of the physical insight that we gained on the one-dimensional system in Eq. (2.34,2.35). In section 2.4.4, we demonstrated how compartment growth and shrinkage can be represented as fluxes in the context of the population balance equation.

Summarising our findings, we find size marginalised effective ensemble dynamics

$$\boxed{\begin{aligned} \frac{\partial f}{\partial t} = & -\nabla_c(\vec{F}_{\eta(t)}f) + \nabla_c\left(\left(\nabla_c\mathbf{D}_{\text{eff},\eta(t)}\right)^\top f\right) - \nabla_c\vec{J}_{\text{fus, eff}}[f] \\ & - \nabla_c\vec{J}_{\text{frag, eff}}[f] + \tilde{\Sigma}_{\text{B}}[f] - \tilde{\Sigma}_{\text{D}}[f], \end{aligned}} \quad (2.55)$$

where $\tilde{\Sigma}_{\text{B}}$ and $\tilde{\Sigma}_{\text{D}}$ refer to the size-marginalised contributions of further compartment dynamics like compartment degradation or synthesis, on which we have not specified. Note, that here we have formally included the growth and shrinkage fluxes in the birth and death terms for brevity of notation. In the following, we will especially focus on

2. Theory of collective degrees of freedom in open compartmentalised systems

an approximation of the fusion flux, which we termed *short-range* approximation and a fragmentation flux approximation according to the Eq. (2.34,2.35),

$$\vec{J}_{\text{fus, eff}}[f] \approx -\frac{\mu}{3\langle v \rangle} f(\vec{c}, t) \nabla_c \int_{\mathbb{D}} d\vec{x} f(\vec{x}, t) (\vec{x} - \vec{c})^2, \quad (2.56a)$$

$$\vec{J}_{\text{frag, eff}}[f] \approx -\frac{\mu}{\langle v \rangle} \frac{\pi}{8} (\nabla_c \vec{c}) f(\vec{c}, t) \vec{e}_i \quad (2.56b)$$

Here, we assume a compartment size marginalisation constant and compartment fusion kernels proportional to the compartment size, as well as fragmentation rates proportional to the compartment size. Furthermore, we employ a mean-field approximation on the level of molecular species, factorising $f(\vec{c}, t) = \prod_j f_j(c_j, t)$. These effective ensemble equations permit us to assess how the compartment dynamics influence the kinetics of the reaction network.

2.5. Emergence of a single, collective degree of freedom

In section 2.4, we derived effective ensemble dynamics that allow us to directly assess how compartment dynamics affect the dynamics of compartmentalised stochastic reaction kinetics systems. In this section, we will qualitatively discuss the effects of different compartment dynamics on the kinetics of compartmentalised stochastic systems in the context of Eq. 2.55. We will start by discussing the qualitative effects of different compartment dynamics in section 2.5.1, and then focus on the effects of compartment fusion, which we find to be qualitatively different from other compartment dynamics in section 2.5.2. We will specifically discuss how compartment fusion and fragmentation give rise to a quasi-particle-like, collective degree of freedom, which allows for an intuitive approach to the kinetics of organelle-associated signalling pathways.

2.5.1. Qualitative effects of compartment dynamics

In order to assess the effects of different compartment dynamics qualitatively, we begin by discussing the dynamics in the absence of compartment dynamics. The chemical reaction kinetics on each compartment are described by the changes in the molecular species \vec{c} of the compartmentalised stochastic reaction kinetics system. As introduced in section 2.4, on each compartment, we observe a stochastic trajectory that depicts the change in the concentration of different molecular species as specified by a chemical reaction network. In the approximation of chemical Langevin equations, the changes in the trajectory are split into two qualitative contributions: the drift term describes deterministic changes in the concentration vector \vec{c} , and the diffusion term accounts for the intrinsic stochasticity of chemical reactions at small concentrations and deviations from the deterministic trajectory. Having provided a description for the dynamics on each compartment, we can now make a conceptual shift and consider an ensemble description.

As we consider an ensemble of several compartments, there are variations in the concentration vector \vec{c}_i due to the stochastic noise. To describe this ensemble, we use a number density distribution function $f(\vec{c}, t)$, which estimates the amount of compartment mass with a specified concentration \vec{c} at time t . The temporal changes in the number density are described by a population balance equation, see Eq. (2.21) and Eq. (2.55). This noise causes the distribution $f(\vec{c}, t)$ to spread over the concentration phase space, the details of

which are determined by the interplay of the drift and the diffusion flux. As the variance among the compartments increases, the dynamics are said to *explore* the concentration phase space. The collective configuration of the compartments as an ensemble gives the state of the system \mathbb{S} , so a full knowledge of the distribution function $f(\vec{c}, t)$ is formally needed to assess this state. In practice, when for example considering this model in the context of organelle-associated signalling pathways, statistics of the distribution are often considered, such as the mean, moments, mode, or quantiles, which still formally require the full estimation of the distribution $f(\vec{c}, t)$. Compartment dynamics may directly alter $f(\vec{c}, t)$ and, by extension, the dynamics of the stochastic reaction kinetics. We thus discuss next the qualitative effect of different compartment dynamics.

As derived in Eq. 2.22, the fragmentation of compartments creates a binomial splitting in every molecular species, thereby increasing the variance in the distribution $f(\vec{c}, t)$ by construction. We approximate the effects of compartment fragmentation by adding an additional diffusion flux. Specifically, in a description where we have marginalised over compartment sizes, we interpret the effects of compartment fragmentation as a correction to the diffusion flux of the chemical reaction dynamics. We thus assess that the fragmentation flux yields no qualitatively different dynamics.

For compartment growth and shrinkage, we have derived a flux approximation that depends on the specific growth and shrinkage dynamics in section 2.4.4. Notably, the approximated flux has a deterministic character. Similar to the deterministic drift flux of the chemical reaction kinetics, the growth flux is fully defined at the level of individual compartments. We interpret fluxes due to the growth and shrinkage of compartments as corrections to the drift flux of the chemical reaction kinetics. Also, we assess that these compartment dynamics result in no qualitatively different dynamics.

Degradation and synthesis terms cannot be expressed within the framework of fluxes as they are, by definition, birth and death terms. Note that by controlling source and sink terms, the distribution $f(\vec{c}, t)$ can be remodelled into any arbitrary shape. However, if the distribution $f(\vec{c}, t)$ is effectively determined by the fine-tuning of birth and death terms, the dynamics of the system are dictated by the regulation of synthesis and degradation of compartments, and the chemical reaction kinetics would only have marginal effects. If the degradation and synthesis terms are found to dominate the dynamics, the model assumptions should be carefully reconsidered. It is also worth noting that some specific synthesis and degradation dynamics can be effectively modelled as boundary conditions of the population balance equation: for example, the degradation of compartments upon the accumulation of a critical amount of molecular species \vec{c}^* can be treated as an absorbing boundary condition. Here, we are in particular interested in homeostatic conditions, where we have no explicit coupling between the characteristics of a compartment and its synthesis or degradation. In this case, the synthesis and degradation yield no qualitative effects on the dynamics of the system.

Compartment fusion affects the dynamics of the compartmentalised stochastic reaction kinetics systems in a qualitatively different way. In section 2.4.1, we derived an approximation of the fusion flux, which we termed the *short range approximation* of the fusion flux, and which has the form of an effective two-body interaction potential, compare also with appendix A.3. Identifying the fusion flux with a two-body interaction potential allows us to interpret the effects of the fusion flux by drawing analogies to other physical systems. Furthermore, we can directly assess a qualitative difference between the fusion flux and the drift flux due to the chemical reaction kinetics: while the drift flux is determined by the molecular species of the chemical reactions in a specific compart-

ment, the fusion flux depends on the full distribution $f(\vec{c}, t)$, and therefore on the state of the signalling pathway. Next, we will expand on the discussion of how the combination of compartment fusion and fragmentation affect the dynamics of the compartmentalised stochastic reaction kinetics systems qualitatively.

2.5.2. Compartment fusion and fragmentation give rise to a collective degree of freedom

The effects of compartment fusion are qualitatively distinct to the other compartment dynamics, as this is a genuine two-body interaction. While the other compartment dynamics can be effectively reduced to effects on individual compartments, a two-body interaction adds qualitatively different dynamics to the compartmentalised stochastic reaction kinetics system. The fusion of compartments sets individual compartments into contact with the other compartments in the considered system. By this, we break the assumption of statistical independence of the compartments as correlations among the different compartments are established. Yet, importantly, in the absence of compartment fragmentation, compartment fusion results in the creation of a single, big, fully-fused compartment.

For a fully-fused compartment system, we assume that the diffusion term is effectively suppressed as $s \gg 1$. The kinetics of the fully-fused system can be described by a single degree of freedom, which we interpret as *point particle* moving in the drift field $\vec{F}(\vec{c}, t)$. In contrast, for an ensemble of fragmented compartments without fusion and fragmentation dynamics, the individual compartments *explore* the concentration phase space. In this case, dynamics of the ensemble distribution $f(\vec{c}, t)$ cannot be described by a small number of ensemble characteristics.

Qualitatively different dynamics arise when both compartment fusion and fragmentation are considered; this was presented in section 2.4.1, where the combined effects of fusion and fragmentation were investigated. We find that the fusion and fragmentation of compartments give rise to a steady attraction of individual compartments to the *centre* of the distribution $f(\vec{c}, t)$. The *centre* of the distribution, in particular, refers to the mean of the distribution, if the short-range approximation in Eq. (2.56) is considered. This steady attraction counteracts the dispersion in the distribution, which is caused by the diffusive flux and stochasticity in the chemical reaction kinetics. Although diffusivity gives rise to an effective exploration of the concentration phase space as time progresses, this exploration is counteracted by compartment fusion and fragmentation, which *localise* the ensemble in the concentration phase space. These effects are illustrated in Fig. 2.6, but also Fig. 2.4 and Fig. 2.5. The interplay between dispersive dynamics due to reaction stochasticity and compartment fusion and fragmentation gives rise to an effectively fixed ensemble variance. Notably, the localised ensemble moves collectively with approximated fixed shape through the concentration phase space, see an illustration in Fig. 2.7.

We recognise that equations analogous to Eq. (2.55) in the absence of birth and death terms, and using the approximation of the fusion flux with Eq. (2.56), have been considered in the literature under the name of *McKean-Vlasov Equations* [102–106]. These equations have been particularly studied in the context of collective dynamics of stochastic many-body physics, for example, to describe collective excitations in nuclei plasmas [102, 107, 107–109], notice here also the relation to the Vlasov-Fokker-Planck equation. The linkage to these physical systems is mainly due to the interpretation of compartment fusion and fragmentation giving rise to an effective two-body interaction potential, compare also with [101]. We will now further illustrate this connection by providing an

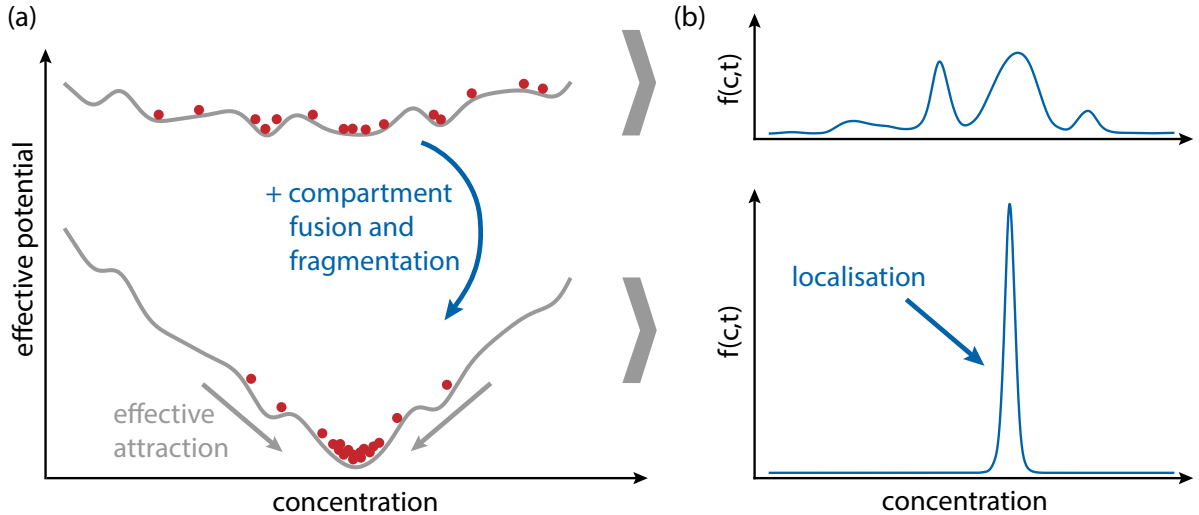


Fig. 2.6.: **Compartment fusion and fragmentation gives rise to a localised distribution, which resembles a quasi-particle** (a) For visualisation, 1-dimensional dynamics in c are considered, which admit the express the dynamics as gradient dynamics. Compartments are represented by red, *particle-like* dots. Dynamics are dictated by an effective multi-welled potential. In the absence of compartment fusion and fragmentation, the compartments stochastically hop between wells. Compartment fusion and fragmentation qualitatively deform the potential, as they give rise to an effective attraction to the mean. (b) The same dynamics as in (a) are presented, but here in terms of the mass density function $f(c, t)$. While the distribution is Boltzmann-like for the system with no compartment fusion and fragmentation, the self-attraction between the compartments due to compartment fusion and fragmentation results in a localisation of the system in the concentration phase-space. Notably, the localisation has finite dispersion. By analogy to other physical systems, we refer to the localised distribution by a quasi-particle-like state, see also section 2.5.2.

analogy to self-gravitating systems [110, 111]. For illustrative purposes, we assume that the chemical drift reactions can be described by gradient dynamics. While this is not generally true, see appendix A.4 and [112], here we consider effective 1-dimensional, integrable dynamics. Note that the insight still applies to general drift kinetics, albeit with the disadvantage of multi-dimensional vector fields being not visually easily approachable.

In Fig. 2.6, we schematically illustrate the effective two-body interaction potential $V(c)$. For the drift kinetics, we consider intricate dynamics with a multi-welled potential landscape, wherein each potential well corresponds to a stable fixed point. Compartments are described by the state of the enclosed stochastic dynamics. Compartments, illustrated as red dots, stochastically escape potential wells and *hop* between them, and by this explore the concentration phase space. The steady-state distribution over the compartments in a set of indefinitely many compartments is a Boltzmann-like distribution, $f_{ss}(c, t) \sim \exp(-\beta^{-1}V(c))$. Here, β^{-1} quantifies the inverse diffusivity of the stochastic dynamics in the compartments. This is illustrated by simulations in Fig. 2.6 (b).

The effective interaction potential gives rise to a local deformation of the potential landscape. This is analogous to self-gravitating systems, where the analogy to a rubber-plane landscape is drawn in which balls deform the landscape. This picture is translated to our system in Fig. 2.6 (a). The localisation in the concentration phase space here is as an analogue to the coalescence dynamics in the self-attracting physical systems. However,

2. Theory of collective degrees of freedom in open compartmentalised systems

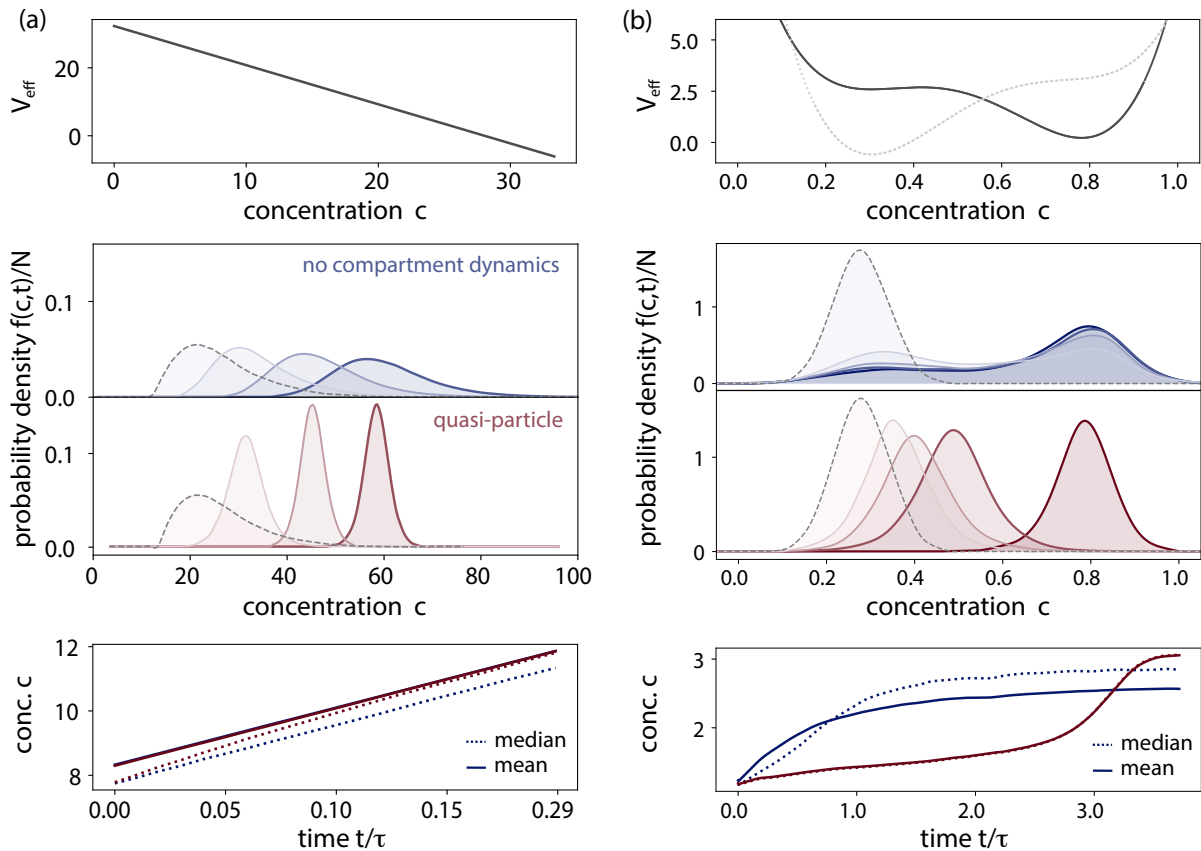


Fig. 2.7.: The quasi-particle moves with a fixed functional shape through the concentration phase space. Here, full stochastic simulations over a finite set of compartments are conducted. On the microscopic level, the dynamics are given by overdamped Langevin Equations with constant diffusion and a potential specified in the plot. Compartment dynamics are taken as full stochastic process, also compare with appendix B.1. The simulations are evaluated in simulation units, where the time is rescaled to fit the relaxation time of the ensemble in absence of compartment fusion and fragmentation. ‘Quasi-particle’ refers to the ensemble with compartment fusion and fragmentation (red), while ‘no compartment dynamics’ refers to the ensemble with no compartment fusion and fragmentation (blue). The rate of compartment fusion is set to $\mu^{-1}/\tau = 0.05$ and the average compartment size is $\langle v \rangle = 2$ in multiples of the compartment unit size. (a) Sliding in a skewed potential. The initial configuration is given by a positively skewed distribution. In blue, a system with no compartment fusion and fragmentation shows dispersive dynamics. In contrast, the quasi-particle state emerges due to compartment fusion and fragmentation and slides down the potential in a fixed functional shape. We find that the median of the distribution is effectively attracted to the mean, as the quasi-particle state emerges. (b) Response in a double-well potential. The old potential is represented by a grey dotted line. Also in more complex potentials, the quasi-particle admits an approximately fixed shape as moves through the concentration phase space. Notably, the quasi-particle admits altered response kinetics, which we elucidate in section 2.6.

we want to emphasise that here the collective dynamics arise in the concentration phase space and not in the real (spatial) space, as the compartment further

2.5.3. Discussion on how the collective degree of freedom resembles a quasi-particle

In this section, we discuss how the collective degree of freedom resembles a quasi-particle. To this end, focus on the characterisation of the collective degree of freedom and also discuss related concepts, such as collective modes and condensates.

Importantly, as we investigate compartmentalised stochastic systems, we consider classical systems and not a quantum-mechanical framework. In the preceding section 2.5.2, a comparison was made to self-aggregating systems [110, 111], which are also in the domain of classical physics. It should, however, be emphasised that the collective degree of freedom is fundamentally different from a condensed form of matter [79]. We want to emphasise that collective dynamics emerge in the concentration phase space and not in the real (spatial) space. The compartments do not aggregate to form a single large aggregate, as the collective degree of freedom emerges. Quasi-particles and collective modes offer a more general way to describe collective dynamics in many-body dynamics.

A quasi-particle in many-body theory is a concept used to describe the behaviour of large numbers of interacting particles [17, 79]. It is conceptualised as an individual particle with clearly defined properties such as mass, charge, and energy. This notion is a practical way of interpreting complex many-body systems, allowing simple models and analytical tools to be employed for analysing their respective properties. Particularly in the field of condensed matter physics, quasi-particles⁵ are used to model the behaviour of electrons, phonons, and other types of excitations in solids. Quasi-particles are mostly studied in the realm of quantum mechanics. Collective modes [114–117], however, differ from quasi-particles in that they describe the coordinated motion of in particles in many-body systems. Collective modes affect the system as a whole, yet preserve its overall properties such as particle number, energy, or momentum. Collective modes can manifest both in quantum systems, such as phonons, and classical systems, as acoustic waves, and are often associated by the wave-like spreading of perturbations. Therefore, collective modes emphasise the coordinated motion of particles, while quasi-particles emphasise the emergent collective dynamics that are ‘particle-like’.

In section 2.5.2, we discussed how compartment fusion and fragmentation can lead to the localisation of probability densities in the concentration phase space. The emergent collective degree of freedom describes the collective movement of the compartments through this concentration phase space. We found that this collective degree of freedom can be characterised in a similar way to that of an individual compartment. In sections 2.6 and 2.7, we will demonstrate that this collective degree of freedom exhibits qualitatively different kinetic properties compared to individual compartments in the absence of compartment fusion and fragmentation. Furthermore, the collective degree of freedom does not display wave-like spreading of perturbations, suggesting that it more closely resembles a quasi-particle than a collective mode.

Quasi-particles are formally characterised by a dispersion relation [17], which describes the relationship between the course of a physical process and the properties of the quantities describing it. In a quantum-mechanical framework, this manifests as a relation

⁵Note that in a part of the literature, quasi-particles are associated with fermionic systems, while their bosonic analogues are referred to as collective excitations [113].

between the energy and momentum of the quasi-particle. In this study, we consider overdamped dynamics in the concentration phase space, and thus cannot formally derive a relation between the energy and momentum of the collective degree of freedom. However, we can link the characteristics of the collective degree of freedom to its kinetics in the phase space. In section 2.6, we demonstrate how the variance of the localised compartment ensemble, whose motion is described by the collective degree of freedom, can be linked to an effective drift on the collective degree of freedom. For this, we derive effective equations of motion, which we argue to serve as an analogue to the dispersion relation.

We emphasise that a mean-field approximation was assumed and that the collective ensemble dynamics are a consequence of this. We anticipate that, when considering a spatial setting of our dynamics, spatially localised collective dynamics will be observed within small neighbourhoods. In the application of our findings to a physical system, a mean-field approximation is suitable if compartments frequently exchange their neighbours; an example of this is organelles which are actively transported through the cytosol by molecular motors attached to the cytoskeleton.

While our collective degree of freedom does not formally originate from a quantum-mechanical framework, but rather from a classical one, we find that it is reminiscent of a quasi-particle in quantum mechanics. We acknowledge the semantic limitations of referring to the collective degree of freedom as a quasi-particle, yet we deem that it emphasises the particle-like motion of the collective degree of freedom in the concentration phase space. Furthermore, we emphasise the fact that the collective degree of freedom displays qualitatively different kinetic properties to the dynamics of individual compartments in the absence of compartment fusion and fragmentation. As such, like the quasi-particle, the collective degree of freedom is inherently a many-body phenomenon. In the following we will refer to the collective degree of freedom as a quasi-particle. Specifically, we will next derive effective equations of motion for the quasi-particle.

2.6. Equations of motion for the quasi-particle

In section 2.5, we have discussed how the compartment dynamics give rise to a collective degree of freedom. We semantically discussed how this collective degree of freedom resembles a quasi-particle state of the system, as the distribution of the compartments is localised in the concentration phase space. Notably, this quasi-particle allows the characterisation of the ensemble distribution $f(\vec{c}, t)$ with a reduced number of variables, providing a simple characterisation of the state of the system. We are particularly interested in how the state of the system changes in response to external perturbations $\eta(t)$ applied on the molecular level. To assess the kinetic properties of the quasi-particle, we derive effective equations of motion in this section. We then investigate on the kinetic properties of the quasi-particle on the basis of these equations in the subsequent section 2.7.

In order to analyse the kinetic properties of the quasi-particle, we begin by recalling that the short-range approximation of the fusion flux, as stated in Eq. (2.56), describes the steady attraction to the mean of the distribution. We will demonstrate that characterising the quasi-particle in terms of the mean, the multivariate generalisation of the median, and the variance of the distribution $f(\vec{c}, t)$ is useful in characterising its kinetic properties. We will focus on the statistics of the collective ensemble state close to the centre of the distribution $f(\vec{c}, t)$ and make use of the short-range approximation of the fusion flux. Additionally, we assume that the further compartment dynamics are independent of \vec{c} , homeostatic conditions hold such that the total compartment mass is conserved and that

the diffusion coefficients $\mathbf{D}_{\text{eff},\eta(t)} = D_{\text{eff},\eta(t)}$ remain constant.

For brevity of notation, we summarise the population balance equation to

$$\partial_t f(\vec{c}, t | \vec{c}_0, t_0) = \nabla[-\vec{F}[\vec{c}, f(\vec{c}, t | \vec{c}_0, t_0)]f(\vec{c}, t | \vec{c}_0, t_0)] + D\nabla^2 f(\vec{c}, t | \vec{c}_0, t_0), \quad (2.57)$$

where (\vec{c}_0, t_0) refers to the initial condition of the distribution. Here, \vec{F} refers to the composite of the approximation of the fusion flux and the deterministic drift component of the stochastic chemical reaction kinetics, whilst the diffusion term accounts for both the diffusion noise in the stochastic reactions and the noise induced by compartment fragmentation. For brevity of notation, we set $f(\vec{c}, t | \vec{c}_0, t_0) \equiv f(\vec{c}, t)$. We define the multivariate generalisation of the median \vec{m} , as the point in the concentration phase space where the stable tail long-range approximation of the fusion flux vanishes. Furthermore, we define a multivariate generalisation of the cumulative distribution $\vec{\Phi}$, where each component is

$$\Phi_i(\vec{x}) = \int_{-\infty}^{\infty} \prod_{j \neq i}^d dc_j \int_{-\infty}^x dc_i f(\vec{c}, t) = \int_{-\infty}^x dc_i q_i(c_i, t). \quad (2.58)$$

In the second equation, we introduced the marginalised density per component $q_i(c_i, t)$ and d refers to the dimensionality of \vec{c} . As Φ_i is by construction a monotonically increasing function, we define the inverse function of the generalised cumulative distribution as $\vec{\Phi}^{-1}$. We define the multi-variate generalisation of the median $\vec{m} = \vec{\Phi}^{-1}(N/2\vec{e}_1)$, where $N = \int d\vec{c} f(\vec{c}, t)$ and \vec{e}_1 is the vector of ones. Applying a mean-field approximation on the flux \vec{F} in line with section 2.4, the integration of the population balance equation yields

$$\partial_t \Phi_i(\vec{c}, t) \approx -F_i[\vec{c}, f(\vec{c}, t)]q_i(c_i, t) + D\partial_{c_i} q_i(c_i, t). \quad (2.59)$$

We note that \vec{m} is a function of the distribution $f(\vec{c}, t)$. We next derive how \vec{m} changes as $f(\vec{c}, t)$ evolves,

$$\partial_t \vec{m} = \partial_t \vec{\Phi}^{-1} \left(\frac{N}{2d} \vec{e}_1 \right). \quad (2.60)$$

Let \vec{m}_0 refer to the multi-variate generalised median at time t_0 . To obtain the temporal derivative of \vec{m} , we linearise $\vec{\Phi}(\vec{c}, t)$ around a point \vec{m}_0 and obtain for each component

$$\begin{aligned} \Phi_i(\vec{m}, t) &= \Phi_i(\vec{m}_0, t_0) + \nabla_c \Phi_i(\vec{m}_0, t_0) \cdot (\vec{m} - \vec{m}_0) \\ &\quad + \partial_t \Phi_i(\vec{m}_0, t_0) \cdot (t - t_0) + \mathcal{O}(\vec{c}^2, t^2). \end{aligned} \quad (2.61)$$

Not that by construction $\partial_{c_i} \Phi_j = 0$ if $i \neq j$. Solving the equation component-wise, m_i is

$$m_i \approx -\frac{\partial_t \Phi_i(\vec{m}_0, t_0) \cdot (t - t_0)}{q_i(m_{0,i})} + m_{0,i}, \quad (2.62)$$

which directly yields

$$\partial_t m_i \approx -\frac{\partial_t \Phi_i(\vec{m}_0, t_{m,0})}{q_i(m_{0,i})}. \quad (2.63)$$

This temporal derivative gives the instantaneous response for \vec{m}_0 at time $t_{m,0}$, and is an approximation for later time points. Using the approximation for $\partial_t \Phi_i(\vec{c}, t)$, the temporal

2. Theory of collective degrees of freedom in open compartmentalised systems

derivative of the generalised median further simplifies to

$$\partial_t m_i \approx F_i[\vec{m}, f(\vec{m}, t)] + \frac{D \partial_{m_i} q_i(m_i, t)}{q_i(m_i, t)}. \quad (2.64)$$

For $\|F_i\| \gg \|D\|$, the first term on the right-hand side of the equation dominates. Note, that D vanishes for large systems sizes due to the rescaling by the system size; Compare for this with section 2.2.1. Inserting the definition of the drift flux due to the chemical reaction kinetics and the fusion flux, the effective equation of motion for the generalised median is

$$\partial_t \vec{m} = \vec{F}_{\eta(t)}(\vec{m}) + \Lambda(\langle \vec{c} \rangle - \vec{m}). \quad (2.65)$$

The drift term $\vec{F}_{\eta(t)}$ refers to the chemical reaction kinetics, where $\eta(t)$ denotes the external signal. The short-range approximation is used for the fusion flux and all prefactors are collected in Λ . The difference between the mean $\langle \vec{c} \rangle$ and the multivariate generalisation of the median \vec{m} quantifies the skewness of the distribution $f(\vec{c}, t)$ as an analogue to a rescaled version of the non-parametric skew in one-dimension. This skewness parameter is referred to as $\vec{s} = \langle \vec{c} \rangle - \vec{m}$ and the fusion flux gives rise to an additional force that pulls the median in the direction of \vec{s} . The rate of compartment fusion $\Lambda \propto \mu$ is directly proportional to the strength of this force. We now proceed to derive the temporal derivative $\partial \langle m \rangle$ of \vec{s} over time.

By integration of the population balance equation in Eq. (2.55), we assume that $f(\vec{c}, t)$ decay exponentially or faster in $\vec{c} \rightarrow \infty$ and find the temporal evolution of the mean is

$$\partial_t \langle c \rangle = \int_{-\infty}^{\infty} d\vec{c} \vec{F}[\vec{c}, f(\vec{c}, t)] f(\vec{c}, t) = \sum_{\alpha} \frac{D^{\alpha} f(\langle \vec{c} \rangle, t)}{\alpha!} \int_{-\infty}^{\infty} d\vec{c} (\vec{c} - \langle \vec{c} \rangle)^{\alpha}. \quad (2.66)$$

Making use of the series expansion of \vec{F} around $\langle \vec{c} \rangle$ with the multi-index notation $\vec{x}^{\alpha} = x_1^{\alpha_1} \cdots x_d^{\alpha_d}$ and the mixed partial derivatives $D^{\alpha} = \partial_{x_1^{\alpha_1}} \cdots \partial_{x_d^{\alpha_d}}$, we assume the existence of a localised ensemble state with finite dispersion. We approximate that the vector field spanned by the drift term \vec{F} is well-approximated around $\langle \vec{c} \rangle$ on the scale of the finite dispersion of the localised ensemble state by a second-order expansion of \vec{F} . With this, $\partial_t \langle \vec{c} \rangle$ approximates to

$$\partial_t \langle \vec{c} \rangle_i \approx F_i(\langle \vec{c} \rangle, t) + \frac{1}{2} \text{tr}(H_{F_i} K_{\vec{c}, \vec{c}}^{\top}). \quad (2.67)$$

Note that the first-order derivative vanishes due to the definition of $\langle \vec{c} \rangle$. Here, we made use of the Hessian matrix H_{F_i} of the i -component of \vec{F} and the variance matrix $K_{\vec{c}, \vec{c}}$. Assuming a mean-field approximation analogous the approximations made for $\partial_t \vec{m}$ in Eq. (2.65), the expression simplifies to

$$\partial_t \langle \vec{c} \rangle \approx \vec{F}(\langle \vec{c} \rangle, t) + \frac{1}{2} (\nabla_{\vec{c}}^2) \vec{F}(\langle \vec{c} \rangle, t) \sum_i \sigma_{ii}^2, \quad (2.68)$$

where σ_{ii}^2 refers to the variance of the marginalised distribution $q_i(c_i, t)$. Note, that the sum $\sum_i \sigma_{ii}^2$ refers to the variance of $f(\vec{c}, t)$, which we approximated as fixed for the localised ensemble state. For brevity of notation, we define $\gamma = \sum_i \sigma_{ii}^2$. The motion of the mean is thus driven by the interplay of the force field and its second derivative.

Assuming the existence of a localised ensemble state, we find that the multi-variate generalisation of the median \vec{m} is steadily attracted to the mean $\langle \vec{c} \rangle$. We hence consider \vec{s} a small parameter and further approximate

$$\vec{F}(\langle \vec{c} \rangle, t) \approx \vec{F}(\vec{m}, t) + (\vec{s} \nabla_c) \vec{F}(\vec{m}, t), \quad \text{and} \quad (2.69)$$

$$\frac{\gamma}{2} (\nabla_c^2) \vec{F}(\langle \vec{c} \rangle, t) \approx \frac{\gamma}{2} (\nabla_c^2) \vec{F}(\langle \vec{m} \rangle, t) + \frac{\gamma}{2} (\vec{s} \nabla_c) (\nabla_c^2) \vec{F}(\langle \vec{m} \rangle, t). \quad (2.70)$$

With this, we find for the temporal evolution of the skewness of the distribution

$$\partial_t \vec{s} = -\Lambda \vec{s} + (\vec{s} \nabla_c) \vec{F}(\vec{m}, t) + \frac{\gamma}{2} (\vec{s} \nabla_c) (\nabla_c^2) \vec{F}(\langle \vec{m} \rangle, t) + \frac{\gamma}{2} (\nabla_c^2) \vec{F}(\langle \vec{m} \rangle, t). \quad (2.71)$$

In the limit of fast compartment fusion and fragmentation, $\Lambda > \|\vec{F}\|$, implying that macroscopic concentration changes happen on slower or similar timescales as compartment fusion and fragmentation, we derive a set of two simple coupled differential equation describing the kinetics of the quasi-particle

$$\partial_t \vec{m} = \vec{F}_{\eta(t)}(\vec{m}) + \Lambda \vec{s} \quad (2.72a)$$

$$\partial_t \vec{s} = -\Lambda \vec{s} + \frac{\gamma}{2} (\nabla_c^2) \vec{F}(\vec{m}, t). \quad (2.72b)$$

For one-dimensional dynamics in the concentration phase space, the equations further simplify to

$$\partial_t m = F_{\eta(t)} + \Lambda s \quad (2.73a)$$

$$\partial_t s = -\Lambda s + \gamma (\partial_{cc} F_{\eta(t)}). \quad (2.73b)$$

We interpret \vec{m} as the position of the quasi-particle and \vec{s} as the internal deformation of the localised ensemble state, which we will elaborate on in the next section. While, the motion of a point particle is dictated solely by the value of $\vec{F}_{\eta(t)}(\vec{m}, t)$, the motion of the quasi-particle is additionally affected by a force proportional to the skewness \vec{s} . This skewness \vec{s} is driven by the second derivative of the vector field $\vec{F}_{\eta(t)}$, which can be linked to the curvature of $\vec{F}_{\eta(t)}$. As the quasi-particle degree of freedom has a finite dispersion, it not only responds to the local value of $\vec{F}_{\eta(t)}(\vec{m}, t)$, but also to the local neighbourhood of \vec{m} , the size of which is determined by the dispersion of the localised ensemble state. This further sets the dynamics of the quasi-particle apart from ensemble dynamics without compartment fusion and fragmentation, where the generalised median or the mean formally depends on the full distribution $f(\vec{c}, t)$. Finally, we assume the limit of fast relaxation in $\partial_t \vec{s} = 0$, which yields:

$$\partial_t \vec{m} = \vec{F}_{\eta(t)}(\vec{m}) + \frac{\gamma}{2} (\nabla_c^2) \vec{F}(\vec{m}, t). \quad (2.74)$$

This simple differential equation allows for the qualitative inference of the dynamics of the quasi-particle through graphical analysis, provided that the dynamics of the force field are qualitatively known. We will demonstrate an example of this graphical analysis in section 3.4. Next, we proceed with a general discussion of the phenomenology of the kinetics encoded by Eq. (2.72) in section 2.7.

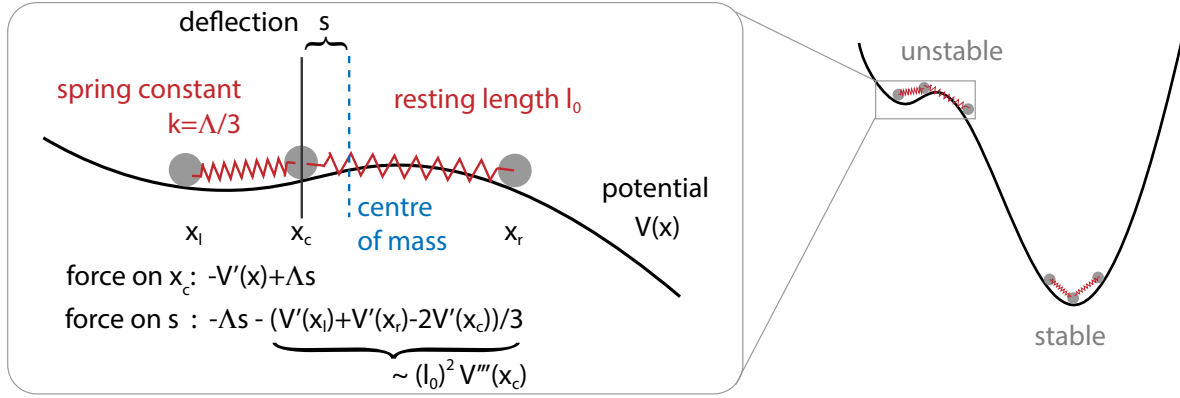


Fig. 2.8.: Illustration of the mechanics analogue to the quasi-particle A system of three coupled, over-damped point-masses recreates the dynamics of the quasi-particle in 1-dimension. The springs are analogous to the steady attraction between compartments due to compartment fusion and fragmentation. We here illustrate how the second derivative on the forces arises in the simple analogue of three coupled point-masses. This in particular renders some minima of a potential unstable.

2.7. Kinetic properties of the quasi-particle

In the preceding section, we derived an effective equation of motion for the quasi-particle, which was introduced in the section before. In this section, we investigate the kinetics of this degree of freedom by introducing a simple, one-dimensional mechanical analogue which provides an intuitive approach to the kinetics. We begin by demonstrating the formal equivalence of this analogue to the set of coupled differential equations in Eq. (2.72). Following this, we discuss the kinetic properties of the analogue and offer an intuitive insight, before considering how this insight translates to the general dynamics of the quasi-particle.

2.7.1. Mechanics analogue of the quasi-particle

In order to facilitate an intuitive approach to the kinetics described by the effective equations of motion for the quasi-particle, we present a one-dimensional, mechanical analogue, which is described by equivalent equations of motion to Eq. (2.73). For this, we consider three point-masses which move with an over-damped motion in a one-dimensional force field and are coupled by ideal springs. For simplicity, we take the one-dimensional force field to be given by a gradient dynamics $F(x) = -V'(x)$. The position of the three point-masses, from left to right, are labelled x_l, x_c , and x_r , as shown in Fig. 2.8. We set the point masses to have equal mass m and the two springs to have rest length l_0 . The over-damped motion of the three point-masses is then described by the equations of motion:

$$\begin{aligned}
 \nu \dot{x}_l + m \ddot{x}_l &= \tilde{F}(x_l) + \tilde{k}(x_l - x_c - l_0) \\
 \nu \dot{x}_c + m \ddot{x}_c &= \tilde{F}(x_c) + \tilde{k}(x_c - x_r - l_0) - \tilde{k}(x_l - x_c - l_0) \\
 \nu \dot{x}_r + m \ddot{x}_r &= \tilde{F}(x_r) - \tilde{k}(x_c - x_r - l_0),
 \end{aligned}$$

where we used the friction coefficient ν , the rescaled force field \tilde{F} and the spring constant \tilde{k} . We define $F = \tilde{F}/\nu$ and $k = 3\tilde{k}/\nu$. In the over-damped limit $m/\nu \ll 1$, the motion of

the centre mass x_c is

$$\dot{x}_c = F(x_c) + k(\langle x \rangle - x_c), \quad (2.75)$$

where $\langle x \rangle = (x_l + x_c + x_r)$ is the centre of mass of the system. We define the deviation of the centre mass to the centre of mass $s = \langle x \rangle - x_c$, which we call the internal deformation of the system, as this deviation is associated with the asymmetric extension of the two ideal springs. In turn, s changes according to

$$\begin{aligned} \dot{s} &= -k(\langle x \rangle - x_c) - F(x_c) + \frac{1}{3}(F(x_l) + F(x_c) + F(x_r)) \\ &= -ks + \frac{1}{3}(F(x_r) + F(x_l) - 2F(x_c)) \\ &\approx -ks + l_0^2 \partial_{xx} F(x_c). \end{aligned} \quad (2.76)$$

We note the formal equivalence between the system of three point masses and the effective equations of motion for the quasi-particle degree of freedom in Eq. (2.72), as the centre mass x_c corresponds to the median and the deviation s is linked to the skewness. Analogous to the quasi-particle, the system of three spring masses accounts for the local curvature of the force field, as the deviation s depends on the second derivative, which is weighted by l_0^2 . It is worth noting that $\sqrt{l_0^2}$ gives an estimate of the width of the three spring masses, which is analogous to taking the root of the summed variances $\sqrt{\gamma}$ in Eq. (2.72), which is an estimate for the width of the localised ensemble state. Focusing on k , we find a correspondence between the strength of the springs and the rate of compartment fusion, which sets the strength of attraction between the median and mean for the quasi-particle. We next study the response kinetics to external perturbations that alter the force field F .

2.7.2. Response kinetics of the quasi-particle

In section 2.7.1, the mechanic analogue was introduced in order to illustrate how the kinetics of the quasi-particle differs qualitatively from that of a single point mass. In this section, we make use of this analogue to discuss the response of the quasi-particle to external perturbations. For this, we consider a force field generated by a gradient dynamics $F(x) = -V'(x)$ and restrict our focus to one-dimensional dynamics. Nonetheless, the insights acquired in this section may be readily translated to multi-variate dynamics and general force-fields.

First, we note that the kinetic properties of the three-point mass system are altered in comparison to those of a point particle: The system has different steady states and fixed points, and different response dynamics on long and short timescales. To understand why the three-point mass system has different steady states, consider the asymmetric double-well potential illustrated in Fig. 2.9. For point masses, both wells of the system are fixed points. However, for the three coupled spring masses, the higher well is not a fixed point of the system. Although the centre mass is located at the bottom of the higher potential well, and experiences no force $F(x_c) = 0$, it still experiences a force due to $s \neq 0$. The left mass slides down the potential and pushes x_c towards the potential barrier at x^* , while the right mass pulls the centre mass down into the next potential. From Eq. (2.73), we find that, in steady state, s typically has finite values of $|s| > 0$, thus perturbing the fixed points of the force field $F(x_{c,ss}) = 0$. This allows for the vanishing

2. Theory of collective degrees of freedom in open compartmentalised systems

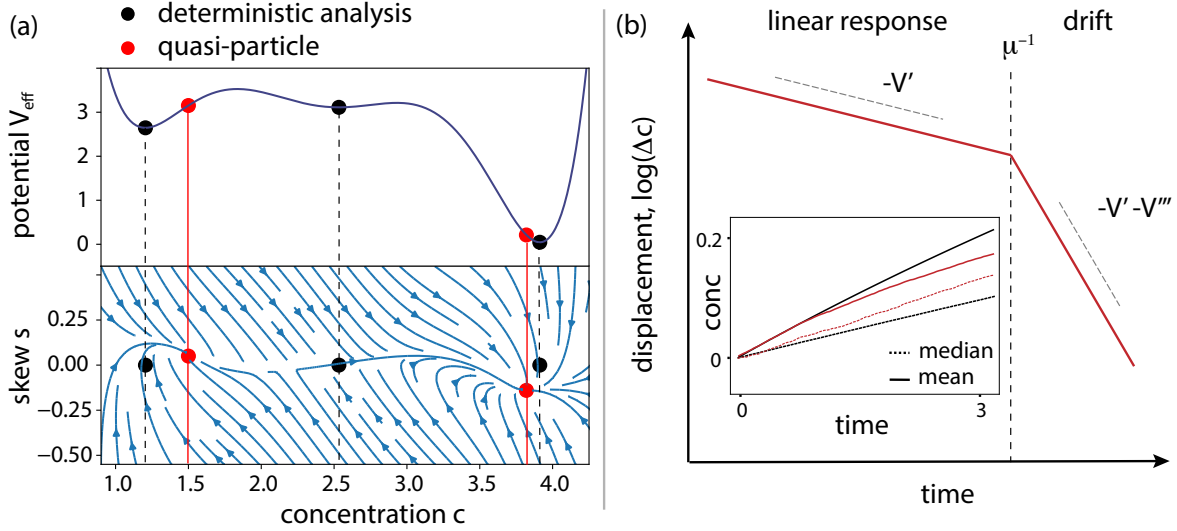


Fig. 2.9.: The quasi-particle exhibits altered kinetic properties (a) The stable fixed points of the quasi-particle are altered compared to the analysis of the deterministic system $\vec{F}(\vec{c}, t)$. This is illustrated as the phase-portrait of Eq. (2.73) is exemplified for a multi-stable potential. Stable fixed points of the quasi-particle are plotted as red dots, and fixed points of $\vec{F}(\vec{c}, t)$ are plotted as black dots. Note, that we formally set $s = 0$ for the fixed points of $\vec{F}(\vec{c}, t)$. (b) The quasi-particle exhibits altered response kinetics on different timescales, as represented by a schematic. The dotted line shows the transition between a linear response regime, to a regime where effective dynamics arise due to the drift in the direction of the skew. The inset shows simulations analogous to Fig. 2.7, which shows the response to a perturbation at $t = 0$. Red refers to the quasi-particle while black refers to a compartment ensemble with no fusion and fragmentation dynamics. Note, that both mean and median initially evolve as in the independent ensemble and we see effective dynamics on large time-scales.

of fixed points, resulting in the three point-masses typically having a smaller number of stable fixed points than a single point-mass.

The altered fixed points imply changes in the long-term dynamics, as the three-point-mass system approaches different states compared to those of single point-masses. Furthermore, the response kinetics on short timescales are also affected. To investigate the response kinetics, we focus on the relaxation dynamics following a general perturbation from $V(x) \rightarrow \tilde{V}(x)$. For the linearised response, we approximate the new potential as follows:

$$-\tilde{F}(x) = \tilde{V}'(x) = \tilde{V}'(m) + \tilde{V}''(m)(x - m) + \mathcal{O}((x - m)^2) \approx \beta_{1,0} + \beta_{1,1}(x - m) \quad (2.77)$$

$$-\tilde{F}''(x) = \tilde{V}'''(x) = \tilde{V}'''(m) + \tilde{V}''''(m)(x - m) + \mathcal{O}((x - m)^2) \approx \beta_{3,0} + \beta_{3,1}(x - m). \quad (2.78)$$

With this, Eq. (2.73) simplifies to

$$\frac{\partial}{\partial t} \begin{pmatrix} m \\ s \end{pmatrix} \approx \begin{pmatrix} -\beta_{1,1} & +k \\ -\gamma\beta_{3,1} & -k \end{pmatrix} \begin{pmatrix} m \\ s \end{pmatrix} - \begin{pmatrix} \beta_{1,0} \\ \gamma\beta_{3,0} \end{pmatrix} \quad (2.79)$$

This matrix equations admits results of the general form

$$\boxed{\begin{pmatrix} m(t) \\ s(t) \end{pmatrix} = c_1 e^{\lambda_1 t} \vec{u}_1 + c_2 e^{\lambda_2 t} \vec{u}_2 - \vec{b}t,} \quad (2.80)$$

where \vec{u}_1, \vec{u}_2 are eigenvectors of the matrix in Eq. (2.79) and $\vec{b}t$ refers to the particular solution of Eq. (2.80). In the limit of strong spring constants, $k \gg |\beta_{1,1}|, |\gamma\beta_{3,1}|$, we observe two distinct eigenvalues: $\lambda_1 \approx k + \gamma\beta_{3,1}$ and $\lambda_2 \approx \beta_{1,1} - \gamma\beta_{3,1}$, which indicate two different relaxation scales. On short timescales, $\tau < k^{-1}$, the point masses behave as if they are uncoupled, resulting in a new value of s . On longer timescales, $\tau > k^{-1}$, a finite value of s gives rise to an additional drift of m .

By comparing to the quasi-particle in the context of compartmentalised stochastic systems, we conclude that the kinetics are altered analogously. Concentration compositions \vec{c}^* that render stable steady states according to the deterministic analysis of the chemical reaction network, $\vec{F}(\vec{c}^*) = 0$, are not necessarily steady states of the quasi-particle. Furthermore, the dynamics on short timescales follow different response kinetics: Compartments respond independently to an external perturbation on timescales shorter than the timescale of compartment fusion and fragmentation. With this, we conclude on the characterisation of the emergent, quasi-particle.

2.8. Discussion

In this chapter, we have demonstrated how compartment dynamics give rise to an emergent, collective degrees of freedom in open compartmentalised stochastic systems. Specifically, compartment fusion and fragmentation counteract the dispersive dynamics of the enclosed stochastic reaction dynamics. In this section, we reflect on our findings and consider their potential technical and biological applications. While this chapter was to a large extent technical, we apply our findings in the following chapter 3 in the context of organelle-associated signalling pathways and cell death decision-making.

We started this section by providing a formal definition of compartmentalised stochastic systems in section 2.3. We showed how the dynamics of the system can be expressed in the formalism of Master equations. While this approach allows for full stochastic numerical simulations, the complexity of the system makes it difficult to analyse the Master equation. To gain a mechanistic understanding of the system, we employed the framework of population-balance equations in section 2.4. We considered two main approximations: assuming a mean-field approximation and formally describing the compartment dynamics in the thermodynamic continuum limit of infinitely many compartments, using the smooth number density function $f(\vec{c}, \vec{o}, t)$. Due to the mean-field approximation, we do not account for the spatial evolution of the system, while the continuum limit approximation formally demands us to investigate *large* systems. This precludes us from estimating additional noise due to the stochasticity of compartment dynamics. When applying our findings to specified systems, we should be aware of the limitations of our approach and reconcile them with the specific research question asked. Note that there have been attempts in the literature to account for spatial placement and stochasticity in population dynamics [72, 118, 119].

A further qualitative restriction of our analysis is that we assume open compartmentalised systems in which we do not impose mass conservation of the enclosed stochastic

2. Theory of collective degrees of freedom in open compartmentalised systems

many-body dynamics. This is primarily due to the stochastic many-body dynamics introduced in section 2.2.1, which allows for the creation and annihilation of molecular species from and to a reservoir. However, if the dynamics of the system is specified accordingly, mass conservation can be accounted for in terms of the chemical Langevin equation, as presented in section 2.2.1. Additionally, in closed compartmentalised systems, we also need to constrain the compartment dynamics to be mass conserving, which effectively prohibits birth and death terms, as well as compartment growth and shrinkage dynamics. As we derived approximations of the fusion and fragmentation fluxes, we did not formally impose mass conservation. Thus, in order to apply Eq. (2.55), we need to refine the approximation scheme applied in this chapter.

Furthermore, note that we, in general, expect very different systems dynamics when considering closed or open compartmentalised systems, as the dynamics are strictly constrained in closed compartmentalised systems. Additionally, we need to take into account correlations between the compartments. This will result in different tail statistics. Moreover, the nature of fluctuations between compartments varies depending on whether the system is open or closed. For open compartmentalised systems, the fluctuations between compartments are induced by the contact with a reservoir, whereas the fluctuations are induced purely by the stochastic binomial splitting procedure during compartment fragmentation for closed compartmentalised systems. These considerations are investigated in more detail in chapters 4 and 5, where we also elaborate on the usefulness of deriving equations similar to Eq. (2.55) for closed compartmentalised systems.

When deriving the flux approximations in Eq. (2.56), we applied mean-field approximations and approximations on the tail statistics of the ensemble. When applying these approximations to specific systems, it is important to evaluate if they are valid or need to be refined, see section 2.4.5. This is particularly relevant for dynamics in which algebraic tails occur, as the triangulation approximation in section 2.4.1 is likely to be inadequate. The same applies for multi-modal distributions; the triangulation approximation in the flux approximations between modes is likely to be inadequate. In cases of multi-variate dynamics in \vec{c} , note that Eq. (2.56) does not accurately account for correlations between components in \vec{c} . If these correlations are found to be essential for the system dynamics, the full multi-variate formulation in Eq. (2.47) should be used.

When we derived the emergence of the collective degree of freedom in section 2.5 and discussed how it resembles a quasi-particle in section 2.5.3. We emphasised that the combined action of compartment fusion and fragmentation are a prerequisite for the emergence of the quasi-particle. We also presented how our findings are robust to other compartment dynamics. However, if compartment fusion and fragmentation occur on timescales much longer than those of other dynamics, their imprint on the system's dynamics is likely to be small. This is particularly the case if the dynamics of the stochastic many-body system enclosed in the compartments changes on timescales faster than those of compartment fusion and fragmentation. Conversely, if dispersive dynamics play a central role in the system's dynamics, we expect to observe the qualitative effects of compartment fusion and fragmentation on the system's dynamics.

Having derived the effective equations of motion in Eq. (2.72) for the quasi-particle in section 2.6, we assumed that the dispersive spreading dynamics were slow compared to the drift dynamics, and that the drift dynamics only changed marginally over the width of the quasi-particle dynamics. We can relax these assumptions with a more refined analysis of effective equations of motion. Here, we suggest that a first refinement should allow for variations in the variance of the localised ensemble configuration, which can be easily

accounted for by considering higher-order corrections. When we investigated the altered kinetic properties of the quasi-particle in section 2.7, we based our findings on the effective equations of motion in Eq. (2.72). Hence, the same assessments hold, however, we expect the qualitative results of altered steady states and altered response kinetics to be generally valid.

We suggest that our findings have direct implications for applications in biological and technical realisations of open compartmentalised systems. In chapter 3, we will investigate in depth the application to organelle-associated signalling pathways, with a particular focus on the cell death decision-making intrinsic apoptotic signalling pathway. We will also briefly discuss to what extent our findings can be directly translated to other organelle-associated signalling pathways. Compartment fusion and fragmentation are central ingredients of our dynamics, but we suggest that general exchange dynamics between compartments or agents can also be treated in the context of the flux approximation presented in Section 2.4.1. Note a structural similarity to the effective equation in [120], which investigated the dynamics of social wasps, and where re-engineering of the exchange dynamics could give us new insight into the system dynamics. In addition to biological applications, technical applications may be found in the fields of finance, where depot fusion and splitting and the assessment of tail statistics are of pivotal interest.

3. Application to multi-scale fluctuations in the regulation of cell death

3.1. Introduction

Our theoretical results concerning open compartmentalised systems provoke two questions: firstly, is there any experimental evidence of quasi-particle¹ kinetics? Secondly, do biological systems make use of such kinetics to perform functions, such as signal processing? In this chapter, we will seek to address these questions in the context of cell fate decisions.

In order to self-organise into complex tissue structures, the fate of cells needs to be precisely regulated. Therefore, the question of how biological systems - and cells in particular - interpret and respond to their environment is a central question in biology. From a biochemical perspective, the central mechanisms by which cells perceive, interpret, and respond to changes in their environment are signalling pathways [121]. In this chapter, we apply our findings from chapter 2 to organelle-associated signalling pathways. These pathways involve biochemical reaction kinetics that occur at dynamic structures that compartmentalise the cytosol of the cell, called organelles, see for example [37, 38, 54]. Organelle-associated signalling pathways are a prime example of compartmentalised stochastic systems. Here, we consider steady binding and binding-release dynamics from the cytosol to organelles and thus consider open compartmentalised systems.

In this chapter, we use the theoretical insights developed in chapter 2 to understand how compartment dynamics qualitatively affect the response kinetics of organelle-associated signalling pathways and examine the functional implications for cell fate decision-making. The binary decision of cells whether or not to initiate programmed death is a prime example of a cell fate decision. We focus on the cell death decision and analyse how the interplay between organelle dynamics and protein complex formation dynamics affects response kinetics to cellular stress signals. We show how the quasi-particle kinetics leads to a low-pass kinetic filter for transient stress signals, thereby significantly improving the quality of the cell death decision. We then explore how our theoretical predictions can be tested experimentally, consider the potential medical applications of our findings, and evaluate the extent to which our findings can be applied to other organelle-associated signalling pathways.

This chapter is structured as follows. We start by giving a brief introduction to the biological concepts of signalling pathways and organelles in section 3.2. We then focus in the same section also on organelle-associated signalling pathways with particular emphasis on

¹In section 2.5.2 we discussed how compartment fusion and fragmentation gives rise to a single, collective degree of freedom, which is reminiscent of a quasi-particle state of the ensemble dynamics. Throughout this chapter, we refer to the collective degree of freedom as a *quasi-particle*.

3. Application to multi-scale fluctuations in the regulation of cell death

cell-death decision-making. We discuss the intrinsic apoptotic signalling pathway in section 3.2.3 and consider the reaction network of Bcl-2 proteins, which act as a bottleneck in apoptotic signalling. In section 3.2.3.2, we explore how the effective dynamics of the protein Bax translocating to the mitochondrial membrane can reduce the complexity of the Bcl-2 reaction network. We then propose an effective model for the organelle-associated signalling pathways of apoptosis, taking into account the stochasticity of Bax translocating and explicitly accounting for the stochastic fusion and fragmentation dynamics of mitochondria. Doing so, we specify on the model dynamics we introduced in section 2.3. We then turn to investigate the response of the system to fixed apoptotic stress stimuli in section 3.4.

Specifically, in section 3.4, we demonstrate that for physiologically plausible parameters, the quasi-particle investigated in chapter 2 is observed. In chapter 2, we investigated the quasi-particle in a general context. Referring to this, section 3.4 considers the kinetics of the quasi-particle within a specified setup of cell death regulation. We find that the quasi-particle shows sigmoidal response kinetics when an apoptotic stress perturbation is applied. This response is initially suppressed on short timescales and facilitated on long timescales when compared to mitochondrial ensembles that show no fusion and fragmentation dynamics. section 3.5 generalises our findings to fluctuating stress signals and concludes that the sigmoidal response kinetics give rise to a kinetic low-pass filter, which suppresses the system's response to short, transient stress fluctuations. The quality of apoptotic decision-making is then assessed by quantifying the specificity and sensitivity of a response in section 3.6. We conclude our investigation of the effect of mitochondrial dynamics on the apoptotic signalling pathway by challenging our theoretical predictions in comparison with experiments in section 3.7. We show that our findings are robust to additional effects in the apoptotic signalling pathway in section 3.7.3. We consolidate our theoretical predictions through experiments performed by our experimental collaborators Philipp Mergenthaler and Lina Hellwig. Finally, we discuss how our findings can be translated to other signalling pathways in section 3.9 and conclude this chapter.

3.2. Literature review on organelle and signalling pathway dynamics

In chapter 2, we adopted a theoretical approach. In this chapter, we study the application of our findings as we study organelle-associated signalling pathways as prime examples of compartmentalised stochastic reaction kinetics systems. To this end, we first provide a general definition of signalling pathways, followed by a brief description of organelles. We then focus specifically on the organelle-associated signalling pathways centred around cell-death decision-making: the intrinsic apoptotic signalling pathway.

3.2.1. Cell signalling pathways

The National Cancer Institute of the United States defines signalling pathways [121] as "a series of chemical reactions in which a group of molecules in a cell work together to control a cell function." These pathways involve a wide range of protein complexes that transmit and translate signals from the environment to changes in cell behaviour. Signals are received as molecules - such as hormones, toxins, or drugs - bind to and modify specific protein receptors in or on the cell. The modification of receptor proteins then activates

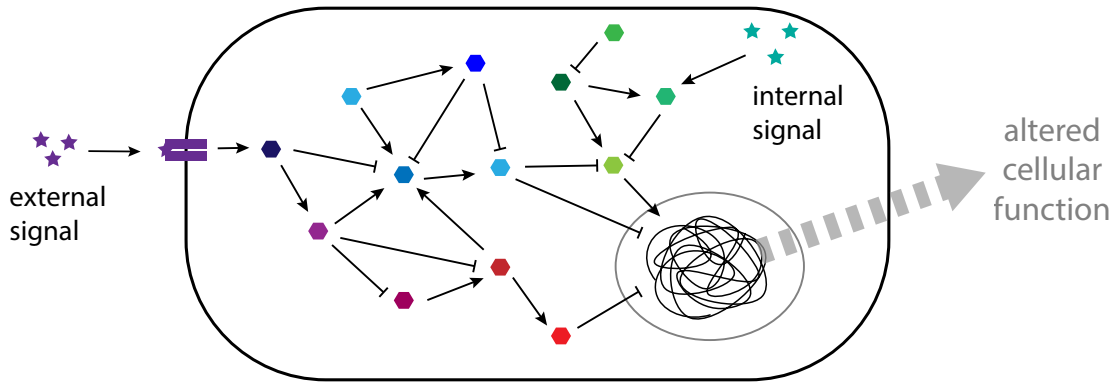


Fig. 3.1.: Schematic of a signalling pathway. Signals can be either intra- or extracellular. By binding and modifying bio-molecules in the signalling pathway, the signal is propagated through a signalling cascade. The signalling cascade generally constitutes as a reaction network, which allows for the integration of various stimuli. At the end of the signalling pathway, changes in the cellular phenotype and cellular behaviour are evoked.

and modifies molecules downstream in the pathway, which in turn again modify other proteins downstream in the signalling pathway. This initiates a signalling cascade, which culminates in changes in gene expression and changes in the behaviour and phenotype of the cell [121]. As signalling pathways describe the complex interplay between various protein complexes and molecules, the concept of signalling pathways is often described with varying levels of detail depending on the specific research question being investigated. This ambiguity in the concept of signalling pathways necessitates a precise definition of constituents and dynamics when discussing them.

Ambiguity in signalling pathways arises from the extent to which molecules are considered part of a signalling cascade. While a signalling pathway formally describes a cascade of events from receptor molecules to a change in cell function, it is common practice to refer to excerpts of full signalling pathways as signalling pathways. This necessitates a precise definition of all constituent molecules. Furthermore, there are various levels of description of signalling pathway dynamics, each with its own level of detail and purpose. For instance, at the coarsest level, signalling pathways can be described using Boolean networks [122, 123], which only focus on the involvement of proteins, while at a more refined level, the qualitative effect of overexpressing a protein species is included [124, 125]. A biophysical understanding of signalling pathways often involves the investigation of temporal changes, which can be described in terms of chemical reaction networks under the assumptions of well-mixed conditions and macroscopic concentrations [126–129]. Relaxing the assumption of well-mixed conditions requires a full spatiotemporal description of signalling pathways [118], while relaxing the assumption of macroscopic concentrations requires the consideration of the stochasticity of individual chemical reactions [85]. In this thesis, we describe excerpts of full signalling cascades as stochastic chemical reaction networks, as introduced in section 2.2.1.

3.2.2. Biology of organelles

Organelles are defined as subcellular structures that perform a specific function within a cell and include a wide range of structures, such as mitochondria, the endoplasmic

3. Application to multi-scale fluctuations in the regulation of cell death

reticulum, ribosomes, flagella, and intracellular condensates like stress granules [37, 38, 130]. The term *organelles* is inspired by the idea that these structures inside a cell are similar to organs in the bodies of multicellular organisms. Organelles can be divided into two categories: membrane-bound and membrane-less organelles [130]. Examples of membrane-bound organelles include mitochondria, the endoplasmic reticulum, and lipid vesicles, which are involved in energy production by oxidative phosphorylation, protein translation, and intracellular material transport, respectively. Examples of membrane-less organelles include flagella, ribosomes, and stress granules, which are associated with cellular locomotion, protein translation, and the storage of mRNA, respectively. In this thesis, we focus on membrane-bound organelles.

Membrane-bound organelles are enclosed by lipid bilayers, which restrict the transport of biomolecules across their membranes, thus creating intracellular compartments that separate bio-molecular reaction processes from the rest of the cytosol. These organelles can vary in terms of function, size, shape, and number [53]; some are involved in the degradation and synthesis of biomolecules (e.g. lysosomes, mitochondria, and the endoplasmic reticulum), while others are involved in the protection of biomolecules (e.g. the nucleus). Generally, they are composed of several discrete compartments, with the exception of the nucleus and endoplasmic reticulum, which display as single organelles within the cell. Additionally, they can take a range of shapes, from small spheres (e.g. lysosomes) to interconnected network-like clusters (e.g. mitochondria). Importantly, membrane-bound organelles are highly dynamic structures, constantly being synthesised, degraded, fused, and actively transported through the cytosol [53]. Moreover, their morphology typically varies between different cell types, under different environmental conditions, and during the cell cycle. Organelles thus structure the interior of the cell into *dynamic* compartments.

When we investigate the dynamic compartmentalisation of the cytosol in relation to membrane-bound organelles, we exclude the dynamics of singular organelles, such as the nucleus and the endoplasmic reticulum, and refer instead to those organelles which are present in large numbers in the same cell. Such organelles undergo a range of dynamic processes, such as transport through the cytosol, biogenesis and growth, degradation, as well as cycles of fusion and fragmentation [53]. The remodelling of their morphologies is often mediated by the constant fusion and fission of organelles [131–133]. Moreover, these dynamics are active processes, requiring the conversion of chemical energy. Membrane-bound organelles are often linked to the cytoskeleton by molecular motors which actively transport them through the cell; while the fusion and fission of lipid membranes is typically regulated by GTPases and ATPases, such as SNARE proteins or proteins of the dynamin superfamily. Consequently, organelle dynamics should be viewed as active processes that rely on the constant consumption of energy and are regulated by the abundance of proteins specific to the dynamics of the organelle in question.

Understanding organelle dynamics as active processes yields questions on the biological function of dynamic compartmentalisation. What are the benefits of steadily remodelling organelle morphology? In this thesis, we investigate this question by deriving general theoretical insight into how dynamic compartmentalisation affects the ensemble statistics of organelles with a special focus on the dynamics of signalling pathways associated with dynamic organelles. We in particular formalise organelle dynamics in the context of dynamic compartmentalisation using either population balance equations, as introduced in section 2.2.2, or by Master equations, as introduced in section 2.3.

3.2.3. Biology of cell death decision-making

In the subsequent sections of this chapter, we will examine the application of our findings concerning quasi-particle kinetics in compartmentalised stochastic reaction kinetics systems in the context of cellular death decision-making. For this, we will briefly review the intrinsic apoptotic signalling pathway, with particular emphasis on the interactions within the Bcl-2 protein family and the specifics of mitochondrial dynamics.

3.2.3.1. Biology of mitochondrial dynamics

Mitochondria are membrane-bound organelles that are present in most eukaryotic cells and are strongly associated with aerobic respiration and the production of adenosine triphosphate [53, 132–134]. As opposed to the ‘bean-shaped’ form often depicted in cartoons, mitochondria have different morphologies depending on the type and state of the cell and are commonly found as reticulated clusters of varying sizes [53]. They consist of a double-membraned structure, containing an outer membrane (MOM) and an inner membrane (MIM). The space between the MOM and the MIM is known as the inter-membrane space, while the MIM encloses the matrix. The MIM is highly folded to form cristae, which increases its surface area. It also houses the proteins of the respiratory chain, and its activity generates a membrane potential across the MIM [64]. Furthermore, mitochondrial DNA and ribosomes are located within the matrix, allowing for the transcription of proteins that form part of the respiratory chain [135]. However, the majority of proteins that make up the structure of mitochondria are synthesised in the cell nucleus. The OMM binds a variety of trans-membrane proteins associated with different signalling pathways, making mitochondria not only important for metabolic regulation in cells, but also for apoptosis, inflammation signalling in response to viral infections, and hormonal signalling [54].

Mitochondria are highly dynamic organelles [59, 60, 138–141], actively traversing the cytosol and undergoing rapid cycles of fusion and fragmentation, commonly referred to as mitochondrial fission. Through this process, they are able to remodel their morphology [59]. Mitochondrial motility relies on the active translocation by molecular motors along the microtubule cytoskeleton, with dynein motors driving the mitochondria towards the minus-end of microtubules, and kinesin motors towards the plus-end, creating a tug-of-war scenario for individual mitochondria [142]. This results in a high degree of mixing, with mitochondria in some cell types exploring up to approximately 80% of the cell content in just 15 minutes [143]. The linkage to the cytoskeleton is also responsible for the observed network-like structures of mitochondrial clusters. Mitochondria are also subject to steady growth and degradation, resulting in a turnover rate with a half-life between nine and 24 days for different tissues in rats [144].

In comparison to the timescale of mitochondrial turnover, rapid events of fusion and fission take place in mitochondria on the timescale of minutes. Mitochondrial fusion is composed of two steps, outer-membrane fusion and inner-membrane fusion, both of which are mediated by GTPases that hydrolyse guanosine triphosphate (GTP) to guanosine diphosphate (GDP). Mnf1 and Mnf2 are responsible for the fusion of the outer mitochondrial membrane while Opa1 is responsible for the fusion of the inner mitochondrial membrane [133, 138]. As outer and inner membrane fusion are two separate events, only partial fusion of mitochondria can occur, in which only the outer membrane fuses. In the context of apoptosis, fusion of the outer membrane is sufficient for the mixing of Bcl-2 proteins; however, depending on the experimental assays, only full fusion events are de-

3. Application to multi-scale fluctuations in the regulation of cell death

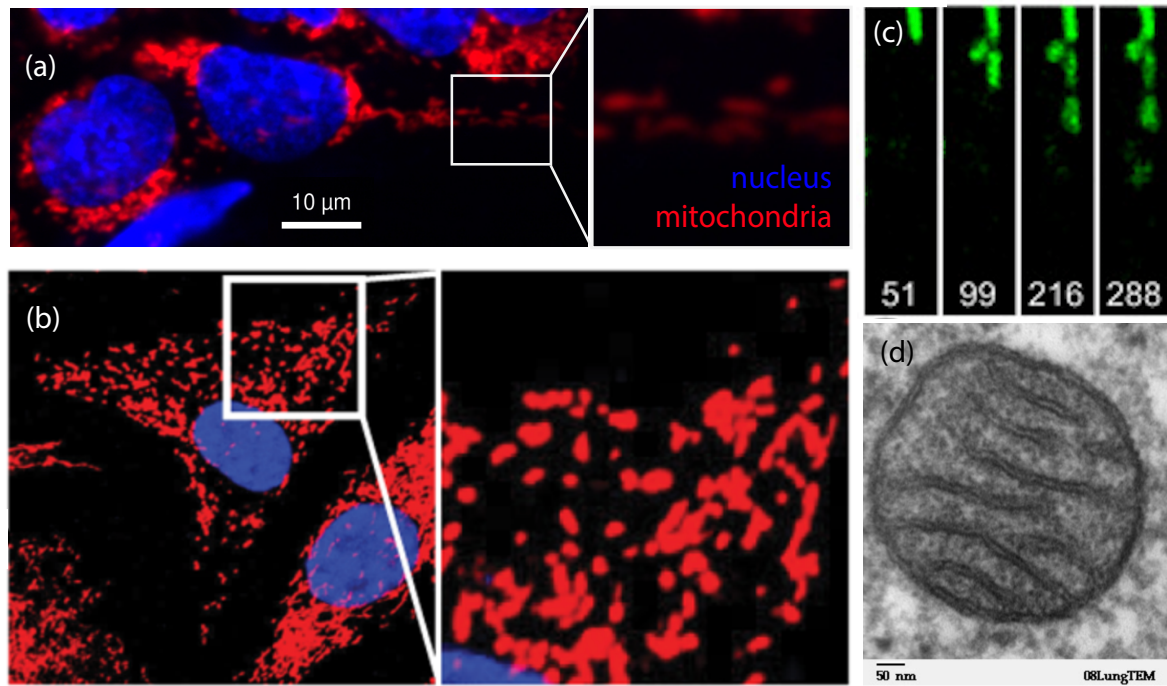


Fig. 3.2.: Mitochondria inside a cell shows as multiple compartments. (a) Fluorescent microscopy image of cell nucleus (DAPI, blue) and mitochondria (TMRE, red) of human induced pluripotent stem cell (hiPSC). Image courtesy Lina Hellwig and Philipp Mergenthaler. (b) Image is adapted from [136] Fig. 1 A. The cell nucleus (DAPI, blue) and mitochondria are dyed (Cyt c antibody, red). (c) Image from [63] from Fig. 2 C demonstrating mitochondrial dynamics. Individual mitochondria are fluorescently labelled (green) and tracked by fluorescent microscopy. When mitochondria fuse, the fluorescent dye spreads in the intermembrane space and thus colours both mitochondria. This experimental setup allows for the quantification of mitochondrial fusion rates. White numbers are the time steps after activation of the fluorescent dye in seconds. This setup demonstrates that mitochondria undergo cycles of fusion and fragmentation on the timescale of minutes. The width of a black strip is $10\ \mu\text{m}$. (d) Transmission electron microscope image of a mitochondrion showing the membrane structure of the outer and the inner membrane. Image adapted from [137].

tectable, thus underestimating the rate of mitochondrial fusion in the context of apoptotic decision-making [62, 145, 146]. Similarly to mitochondrial fusion, fission is also mediated by the GTPase Drp1 for the outer mitochondrial membrane [133, 138]. By regulating the abundance of functional mitochondrial fusion and fission events, the mitochondrial morphology can be modified. Increasing the abundance of fission proteins, or the inhibition of fusion proteins leads to the formation of many small, separated mitochondria with predominantly spherical and tubular shapes, referred to as a fragmented state [59]. Conversely, the suppression of fission proteins, or the increase in fusion proteins, results in the formation of large network-like structures, up to the formation of a single, fully-connected mitochondrion, referred to as a hyperfused morphology.

Mitochondrial morphology is closely related to the number of mitochondria present. In physiological conditions, typically several hundred for morphologies of intermediate and fragmented forms are present inside a mammalian cell [59]. Rates of mitochondrial fusion and fission balance each other in a steady state, resulting in a consistent distribution of mitochondrial sizes [147]. Studies suggest that mitochondrial fusion rate is independent

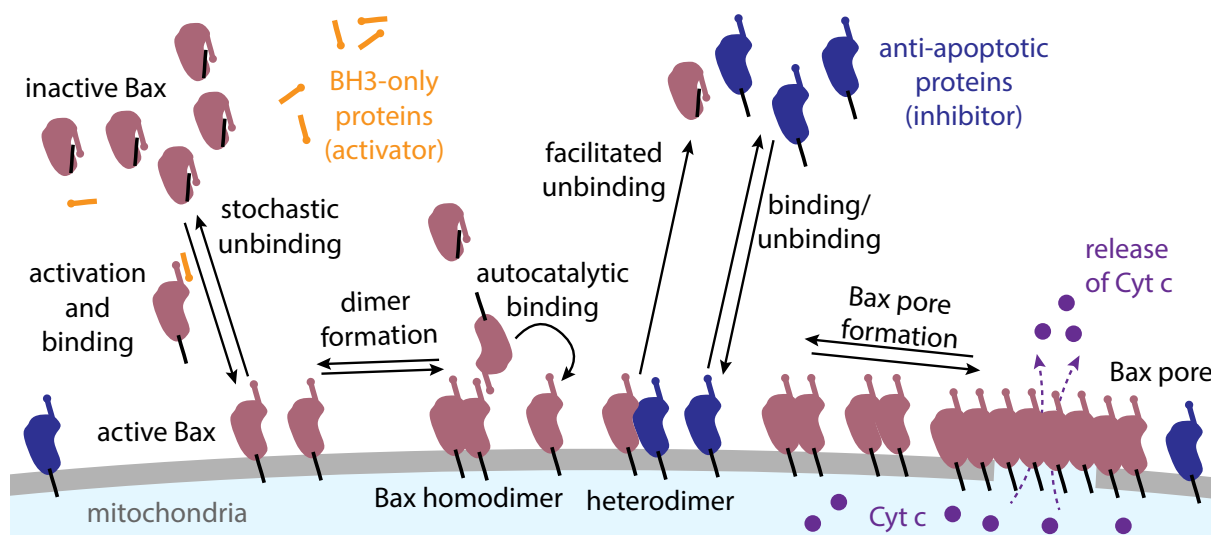


Fig. 3.3.: Schematic of the Bcl-2 reaction network with focus on the Bax activation and pore formation kinetics. This schematic illustrates a coarse-grained version of Bcl-2 reaction network. Here, the central kinetics include the facilitated activation and membrane insertion of inactive Bax by activators and autocatalytic binding. Bax unbinding is facilitated by hetero-dimer formation with inhibitors. Bax homo-dimers accumulate to form pores in the outer mitochondrial membrane, which allow for the release of the cytotoxin Cytochrome c. Compare with [128, 129, 150, 151].

of size, while mitochondrial fission rate is directly proportional to the size of mitochondria [61]. Estimates of mitochondrial fusion rates can range from as low as 0.05 events per minute per mitochondrion in human axons [61], where mitochondrial density is low, to as high as 1.3 events per minute per mitochondrion in HeLa cells [62, 148]. Based on these experimental findings, we consider mitochondria as highly dynamic organelles, which undergo fusion and fission/fragmentation events on the timescale of minutes.

3.2.3.2. Biology of apoptosis (Bcl-2 signalling pathway)

Apoptosis is a form of programmed cell death, by which a cell is fragmented into small vesicles where biomolecules are degraded. By this, apoptosis differs from necrosis, which involves cell rupture and the release of cytotoxic material [149]. It is a highly regulated process that, once initiated, cannot be stopped [41]. The intrinsic apoptotic pathway is activated in response to cell stress and the extrinsic pathway is initiated by external signals via the death receptors (TNF receptor family). Regulation of the intrinsic pathway is achieved by proteins from the Bcl-2 family, which mediate the release of cytochrome c (Cyt c) from mitochondria [41, 150]. Both pathways lead to the activation of caspases, which degrade proteins and mRNA within the cytosol, and trigger the destruction of chromosomal DNA by DNase. In the following, we focus on the intrinsic apoptotic pathway.

The intrinsic apoptotic signalling pathway is initiated by a variety of stress signals, which converge in the regulation of the abundance of proteins of the Bcl-2 family. Proteins of the Bcl-2 family mediate the initiation of apoptosis through the release of Cyt c from mitochondria [150]. Bcl-2 proteins form a pore in the mitochondrial outer membrane [151], facilitating the release of Cyt c, which is a bottle-neck of the intrinsic pathway and inhibition of its release results in inhibition of apoptosis initiation [149]. Cyt c

3. Application to multi-scale fluctuations in the regulation of cell death

in the cytosol then enables the formation of the apoptosome protein complex, which activates different caspases that conduct apoptosis. In this work, we consider the apoptotic signalling pathway with particular emphasis on Bcl-2 protein interaction up to the release of Cyt c.

The Bcl-2 protein family comprises a number of proteins that share Bcl-2 homology (BH) domains. Variations in the number of homology regions are observed amongst family members, while four distinct BH domains (BH1, BH2, BH3, and BH4) are distinguished; compare for the following paragraph with [150]. Additionally, some family members contain trans-membrane domains, which facilitate binding to the mitochondrial outer membrane. The Bcl-2 family is divided into three groups, based on primary function: anti-apoptotic proteins (Bcl-2, Bcl-XL, Bcl-W, Mcl-1), pro-apoptotic pore-formers (Bax, Bak), and pro-apoptotic BH3-only proteins (Bid, Bad, Noxa, Puma). Notably, Bax and Bak both exist in active and inactive forms; homo-dimerisation is inhibited in the inactive form. While Bak is anchored to the mitochondrial outer membrane in both active and inactive forms, Bax is located in the cytosol when inactive and binds to the mitochondrial outer membrane upon activation. Pro-apoptotic BH3-only proteins activate Bax and Bak, while anti-apoptotic proteins deactivate them, form hetero-dimers, and/or bind pro-apoptotic BH3-only proteins. The various anti-apoptotic and pro-apoptotic BH3-only proteins differ in terms of binding affinities, preferred localisation (cytosol or mitochondrial outer membrane), and abundance. Abundance is subject to a variety of cellular signals, such as metabolic conditions, nutrient deprivation, DNA damage and radiation, as well as several toxins. Mitochondrial outer membrane permeabilisation (MOMP) is the process of forming pores in the mitochondrial outer membrane, which leads to the leakage of mitochondrial content into the cytosol; this is linked to mitochondrial lysis and degradation.

We consider the accumulation of Bax or Bak in their active form on the outer mitochondrial membrane to be a hallmark of apoptosis induction, leading to the release of Cyt c into the cytosol [41, 149, 150]. As mitochondria are typically found as a set of clusters of varying sizes, the release of Cyt c for weak apoptotic stimuli might happen only in a subset of the clusters [56, 152–155]. We refer to apoptotic decision-making, as a cell regulates the accumulation of active Bax or Bak over the set of different mitochondria. Specifically, we consider the concentration of activated Bax and Bak overall mitochondria as a proxy for the state of the apoptotic signalling pathway.

3.3. The regulation of cell death in the framework of compartmentalised systems

In order to apply our finding of chapter 2 to cell death decision-making, we next specify on the stochastic reaction dynamics and compartment dynamics. For the stochastic reaction dynamics, we discuss the Bcl-2 reaction network in the context of chemical reaction kinetics, as introduced in section 2.2.1. Based on this formalism, we then specify on the microscopic model introduced in section 2.3, as we consider the dynamics of the intrinsic apoptotic signalling pathway by both accounting for the Bcl-2 reaction kinetics and mitochondrial dynamics. To this end, we specify also on the effective population balance equation Eq. 2.55 in section 2.4.

3.3.1. Modelling the Bcl2 reaction network

In this section, we focus on models for the kinetics of the Bcl-2 protein signalling pathway reaction network. We propose a simple model of how Bcl-2 protein interactions mediate the release of Cyt c and set this in relation to the current literature. We then place this model into the context of the population balance equation and specify the qualitative form of deterministic drift vector $F_{\eta(t)}(\vec{c})$ and reaction binding noise diffusion matrix $\mathbf{D}_{\eta(t)}(\vec{c})$ in Eq. (2.55).

The temporal progression of mitochondrial outer membrane permeabilisation (MOMP), the dynamics of Bax pore formation mechanism, and the details of the Bcl-2 interaction network are today still subjects of active research [150]. Several models have been proposed to capture the qualitative dynamics of the apoptotic signalling pathway, which mainly focus on the interaction between proteins in the Bcl-2 family [129, 150, 156]. Central to these models is the link between increased concentrations of Bax-Bax and Bak-Bak homo-dimers and increased pore-formation [58, 157]. Here, we briefly study the simplest of such models, which accounts for the auto-catalytic self-activation of Bax by Bax-Bax homo-dimers, and the role of anti-apoptotic proteins and pro-apoptotic BH3-only proteins, as shown in Fig. 3.3. We do not distinguish between various pro-apoptotic BH3-only proteins and anti-apoptotic proteins, and collectively refer to the concentration of pro-apoptotic BH3-only proteins as [Act], and to the concentration of anti-apoptotic proteins as [Inhib]. For the sake of simplification, we exclusively focus on Bax proteins and do not consider Bak proteins explicitly. Inactive, cytosolic Bax_c is activated, and is transformed to active, membrane-bound Bax_m , which then forms membrane-bound homo-dimers Bax_D :



where $[X]$ refers to concentrations and we assume well-mixed conditions. Accounting for the conservation of mass for Bax with $[\text{Bax}_{\text{tot}}] = [\text{Bax}_c] + [\text{Bax}_m] + 2[\text{Bax}_D]$, the steady state solution in the thermodynamic limit yields

$$0 = k_1[\text{Act}] \left([\text{Bax}_{\text{tot}}] - [\text{Bax}_m] - \frac{2k_4}{k_5} [\text{Bax}_m]^2 \right) + \frac{k_2k_5}{k_4} [\text{Bax}_m]^2 \left([\text{Bax}_{\text{tot}}] - [\text{Bax}_m] - \frac{2k_4}{k_5} [\text{Bax}_m]^2 \right) - k_3[\text{Inhib}][\text{Bax}_m], \quad (3.2)$$

which is for given k_1, k_2, k_3, k_4, k_5 , and $[\text{Bax}_{\text{tot}}]$ a quartic equation in $[\text{Bax}_m]$. Notably, this quartic equation admits analytic solutions. Yet, as the analytic solution is convoluted, we here restrict to investigating a graphical analysis to emphasize the general features of the solution.

We normalise the concentrations to $[\text{Bax}_{\text{tot}}] \equiv 1 [\text{conc.}]$, where [conc.] refers to a rescaled concentration unit. τ refers to a time unit. Fixing the reaction rates $k_4/k_5 = 0.1 [\text{conc.}]^{-1} \tau^{-1}$, $k_2 = 80 \tau^{-1}$ and $k_1 = k_3 = 1 \tau^{-1}$, we find regions of bistability, as we vary the concentration of pro-apoptotic and anti-apoptotic proteins, see Fig. 3.4. For this effective one-dimensional dynamics, we interpret the temporal evolutions of Bax_m as an effective gradient dynamics $\partial_t [\text{Bax}_m] = -\nabla_{\text{Bax}_m} V([\text{Bax}_m])$. This interpretation allows for an intuitive approach to the kinetics of the membrane-bound Bax concentration $[\text{Bax}_m]$. We find that $[\text{Bax}_m]$ effectively evolves in a bistable potential, in which the concentration

3. Application to multi-scale fluctuations in the regulation of cell death

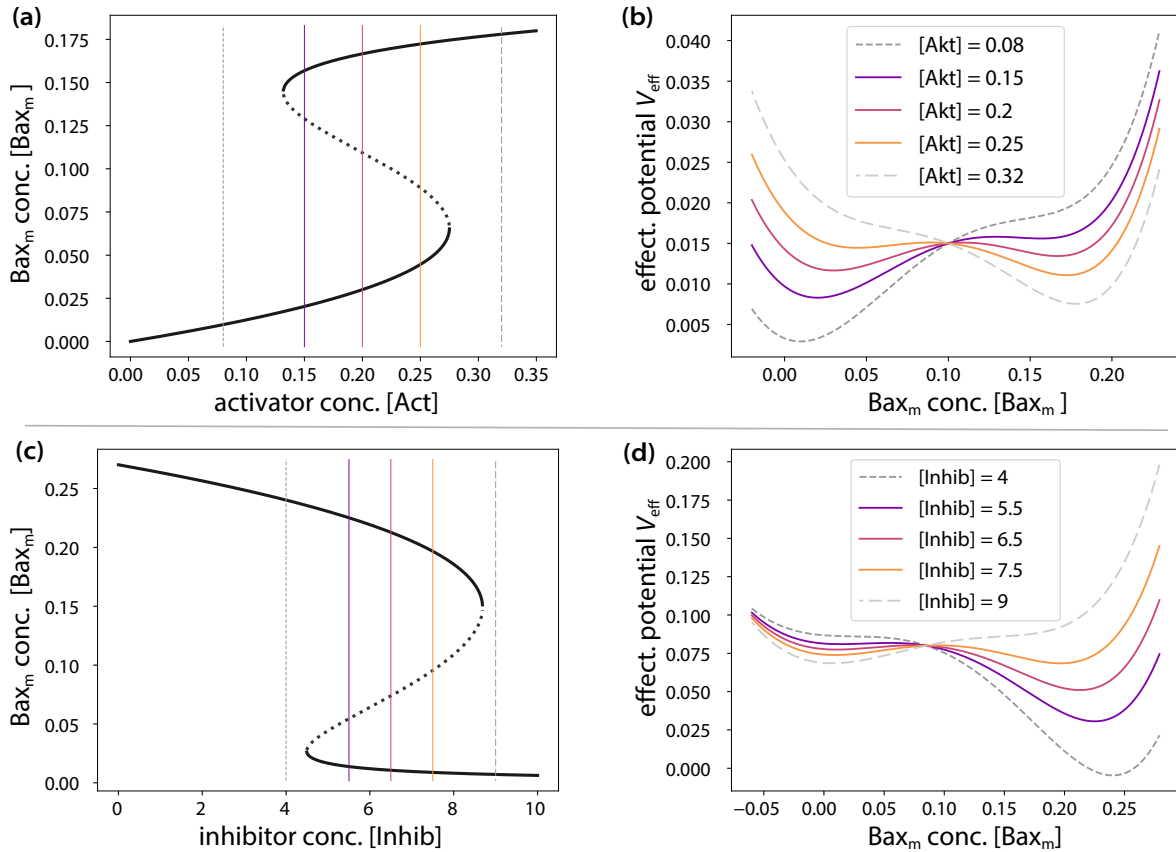


Fig. 3.4.: The Bax accumulation dynamics are effectively captured by a bistable potential. For the parameters specified in section 3.3.1, we systematically vary the concentration of activator (a,b) and inhibitor concentration (c,d). In (a) and (c), we find that the bifurcation diagram shows a cusp-bifurcation. Stable fixed points are indicated by a bold line, while the unstable fixed points are represented by a dashed line. The one-dimensional effective dynamics in $[Bax_m]$ allows for tracking the dynamics as gradient dynamics. With $d_t[Bax_m] = -d_c V_{\text{eff}}([Bax_m])$, the effective potential is plotted in (b) and (d). We find that the effective potential is a bistable potential. Changing the activator and the inhibitor concentration changes the skew of the potential. Different colours correspond to different activator and inhibitor concentrations, accordingly indicated also in (a) and (c). All concentrations are in the effective units $[conc.]$, and V_{eff} in $[conc.]^2/\tau$, as introduced in section 3.3.1.

of pro-apoptotic and anti-apoptotic proteins sets the skew of the potential. We link the two wells of the bistable potential with two different steady-states of the kinetics, which describe two different functional operating states of the signalling pathway. We refer to the state with low $[Bax_m]$ concentration as *physiological* Bax concentration state, while we term the high concentration state as apoptotic state. We associate the apoptotic state with the increased formation of pores in the mitochondrial membrane and the release of Cyt c. In the context of apoptotic decision-making, we are interested in the transition from the physiological to the apoptotic state. This translates in the picture of the effective bistable potential to a transition from the low-concentration well to the high concentrations state.

Extensive apoptotic models that take into account varying affinities of different pro-apoptotic and anti-apoptotic proteins have qualitatively agreed with the finding of a bistability for membrane-bound Bax [129, 141, 156]. This qualitative result is also robust when

subjected to a refined analysis considering the preferential spatial location of proteins of the Bcl-2 family in either the cytosol or the mitochondrial outer membrane. A precise measurement of reaction rates and total concentrations is experimentally challenging and prone to error. Order of magnitude estimates demonstrated that bistability can occur for a physiologically plausible parameter choice [129, 141], and footage of bistability for membrane-bound Bax was observed in experiments [141, 156]. Furthermore, the concentrations of Bcl-2 proteins estimated on individual mitochondria is approximately ~ 20 nM [158] for the physiological state, which is in agreement with measured estimates of a few hundred Bax proteins per mitochondrion [159]. These estimates suggest that the apoptosis reaction pathway should be treated in a stochastic framework, as introduced in section 2.2.1, compare also to [70]. This formally sets the basis for the estimation of the drift term $F_{\eta(t)}(\vec{c})$ and the diffusion term $\mathbf{D}_{\eta(t)}(\vec{c})$ within the context of the population balance equation in Eq. (2.55).

Estimating the membrane diffusion of proteins of size ~ 25 kDa with $\sim 10 \mu\text{m}^2 \text{s}^{-1}$ [160], results in a membrane mixing on the order of seconds. This leads us to consider mitochondria as a well-mixed reaction compartment. We assume fast diffusion of the cytosolic Bcl-2 family proteins with higher molecular copy numbers than on individual mitochondria and model them as a fluctuating signal $\eta(t)$. We neglect spatial correlation between organelles through diffusion of the cytosolic Bcl-2 proteins and consider independent realisations of stochastic apoptotic dynamics on separated, not-fused mitochondria. Molecular binding noise induces stochastic transitions of individual mitochondria from the low to the high membrane-bound Bax concentration state. Conversely, the transition from the high to the low concentration state is inhibited by the occurrence of MOMP and the subsequent lysis and degradation of mitochondria. Although we can formally extract estimates for the drift term $F_{\eta(t)}(\vec{c})$ and the diffusion term $\mathbf{D}_{\eta(t)}(\vec{c})$ from reaction network models, this requires the precise estimation of reaction rates and physiological concentrations of Bcl-2 family proteins by experimental measurements. Alternatively, a qualitative discussion of the signalling pathway kinetics can be used to estimate how different model refinements qualitatively affect the kinetics. We will investigate this in the next section.

3.3.2. Effective model of the apoptotic signalling pathway

We are interested in investigating how mitochondrial dynamics qualitatively affect the kinetics of the Bcl-2 signalling pathway. Quantitative analysis of apoptosis quickly becomes analytically intractable, is highly specific for given cell types and can be prone to errors due to the estimation of a large number of reaction rates and physiological concentrations, compare for example with [159]. In contrast, a qualitative analysis allows us to evaluate the influence of various parameters and the general effects of mitochondrial dynamics on apoptotic signalling. Therefore, we introduce an effective model for the temporal evolution of the concentration of membrane-bound Bax on each mitochondrion. Our motivation for using an effective model is to enable analytic tractability, which allows us to estimate how model refinements qualitatively affect our findings, as we will show in section 3.4. To ensure plausible results, we estimate the parameters of the effective model by comparison with experiments

In the effective model, each mitochondrion is characterised by the membrane-bound Bax concentration $[\text{Bax}_m] \equiv \tilde{c}$ and its size s , where we introduced \tilde{c} for notational simplicity. Recall, that the membrane-bound Bax concentration \tilde{c} evolves stochastically in a bistable potential, where the skew of the potential is set by the level of stress metabolites in the cell

3. Application to multi-scale fluctuations in the regulation of cell death

cytosol, as discussed in section 3.3.1. Consistent with the picture of a bistable potential, two attractive fixed points of the kinetics for \tilde{c} can be distinguished: a low and a high potential well. These concentrations fixed points represent two different equilibrium states of the signalling pathway and are denoted by \tilde{c}_l^* and \tilde{c}_h^* , respectively. The potential well with the higher Bax concentration, $\tilde{c}_h^* > \tilde{c}_l^*$, corresponds to the release of Cyt c from the mitochondrion. We define the effective potential

$$V_{\text{eff}}(\tilde{c}) = a(\tilde{c} - \tilde{c}_0)^4 - b(\tilde{c} - \tilde{c})^2 + \alpha(\tilde{c} - \tilde{c}_0), \quad (3.3)$$

where we used a constant \tilde{c}_0 to centre the potential around the origin for notational simplicity. $a, b \in \mathbb{R}^+$ are positive real-valued parameters of the bistable potential. $\alpha \in \mathbb{R}$ refers to the initial skew of the potential, which is the initial apoptotic priming.

The exact functional form of $D(\tilde{c})$ requires precise estimation of molecular concentration and chemical reaction rates in the Bcl-2 signalling pathway, making estimates of $D(\tilde{c})$ highly prone to errors and sensitive to model details. Here, we make use of a strong approximation of $D(\tilde{c})$, which grants analytical tractability and allows us to study how variations in $D(\tilde{c})$ can affect the findings qualitatively. As \tilde{c}_h^* is associated with the release of Cyt c, we are mainly interested in fluctuations around \tilde{c}_l^* and the *escape* into the high concentration state. Consequently, we approximate $D(\tilde{c})$ around \tilde{c}_l^* . As a rule of thumb, the diffusion coefficient is proportional to the total amount of proteins, such that $D(\tilde{c}) \sim \tilde{c}$. Assuming that the low concentration well and the barrier of the potential, $\tilde{c}_l^* \sim \tilde{c}_b^*$, are on the same order of magnitude, we approximate to zeroth order $D(\tilde{c}) \approx D(\tilde{c}_l^*) \equiv D$. Note that generalisations to higher orders can be incorporated into further analysis. The effects of multiplicative noise will be discussed at the end of section 3.4. Additionally, we account for external signals $\eta(t)$, in which we incorporate changes in pro-apoptotic and anti-apoptotic proteins with. Together, the effective model shows as

$$\boxed{\partial_t \tilde{c} = -\partial_{\tilde{c}} V_{\text{eff}}(\tilde{c}) + \frac{D}{\sqrt{v}} \xi(t) + \eta(t)}, \quad (3.4)$$

where $\xi(t)$ refers to white Gaussian noise and we correct for the size of mitochondria by \sqrt{v} in agreement with the approximation presented in section 2.2.1. We discuss how modifications of the potential or the noise affect our qualitative findings in section 3.4. For fixed $\eta(t) = \eta$, we rescale the potential, such that the low concentration state is $c_l^* \equiv 0$ and $c_h^* \equiv 1$. In the notation of Eq. (3.4), we define weak as stimuli $\eta(t)$ which let the system predominantly remain in a bistable configuration. Conversely, we define strong apoptotic stimuli as stimuli in which the high concentration state c_h^* is the only stable fixed point of the system. In particular, we only speak of apoptotic decision-making in the context of weak apoptotic stimuli, as the system necessarily evolves quickly into the high Bax-concentration state for strong apoptotic stimuli.

To include also on the mitochondrial dynamics, we adapt the notion of hybrid systems as we numerically implement a trajectory version of the multi-scale dynamics. To this end, we define the state of the system analogous to Eq. (2.19) in section 2.3, as

$$\mathbb{S} = \begin{bmatrix} \vdots \\ [c_i, v_i] \\ \vdots \end{bmatrix}. \quad (3.5)$$

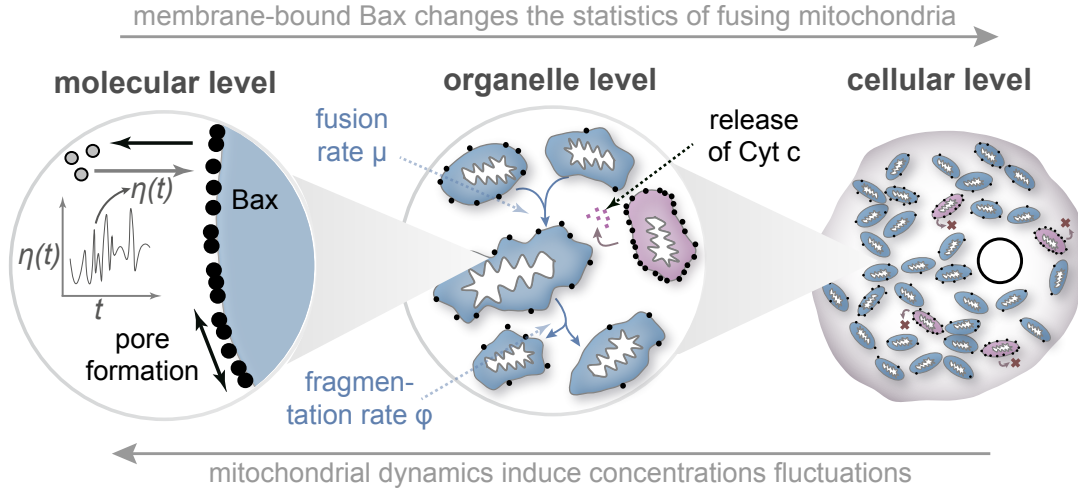


Fig. 3.5.: Effective model of the intrinsic apoptotic signalling pathway. We investigate the response kinetics of the intrinsic apoptotic signalling pathway to fluctuating stress stimuli $\eta(t)$ by explicitly accounting for the Bax binding dynamics and mitochondrial fusion and fragmentation. Increased stress levels translate into an increased binding of Bax to the mitochondrial membrane. Mitochondrial fusion and fragmentation dynamics result in the steady redistribution of proteins among mitochondria. By this mitochondrial dynamics induce concentration fluctuations in membrane-bound Bax. Conversely, mitochondrial binding and unbinding dynamics induce concentration differences between mitochondria. By this, Bax dynamics affect the statistics of fusing mitochondria, with regard to what the concentrations of the two fusing mitochondria are. Moreover, the accumulation of Bax results in the formation of pores on the mitochondria membrane, the release of toxin Cyt c and the subsequent lysis of cells. By this, Bax dynamics directly affect the statistics of mitochondria with regard to their membrane-bound Bax concentration at the population level.

We define that mitochondria are fully described by their size v_i and the Bax concentration c_i on their membranes. Symbolically, we define stochastic trajectories of the system as

$$\frac{d}{dt}\mathbb{S}(t) = \mathcal{L}_{\text{Bax}}[\mathbb{S}(t)] + \mathcal{F}_{\text{fus+frag}}[\mathbb{S}(t)]. \quad (3.6)$$

Here, $\mathcal{L}_{\text{Bax}}[\mathbb{S}(t)]$ refers to the stochastic dynamics in Eq. (3.4) that happen in parallel and independently on the different mitochondria. $\mathcal{F}_{\text{fus+frag}}[\mathbb{S}(t)]$ refers to stochastic, time-discrete events of mitochondrial fusion and fragmentation that alter the system. For the stochastic compartment fusion and fragmentation dynamics, we consider the stochastic rates defined in the context of Smoluchowski aggregation-fragmentation dynamics defined in section 2.2.3. We consider this model for the numerical simulation of the system, in line with the numerical routine described in section B.1. [100, 147] have demonstrated that the Smoluchowski aggregation-fragmentation dynamics adequately capture the mitochondrial size distribution, as size-independent fusion kernels and fission kernels proportional to the mitochondrial size are considered. We assume that mitochondrial dynamics happen on the timescales of minutes, as measured in [61, 62, 145, 148]. With this model, we want to investigate if we can also identify in the context of apoptosis the predicted quasi-particle kinetics discussed in chapter 2. Moreover, we want to assess how mitochondrial dynamics qualitatively affect the response kinetics of the apoptotic signalling pathway and possibly assess the biological functions of mitochondrial dynamics.

3. Application to multi-scale fluctuations in the regulation of cell death

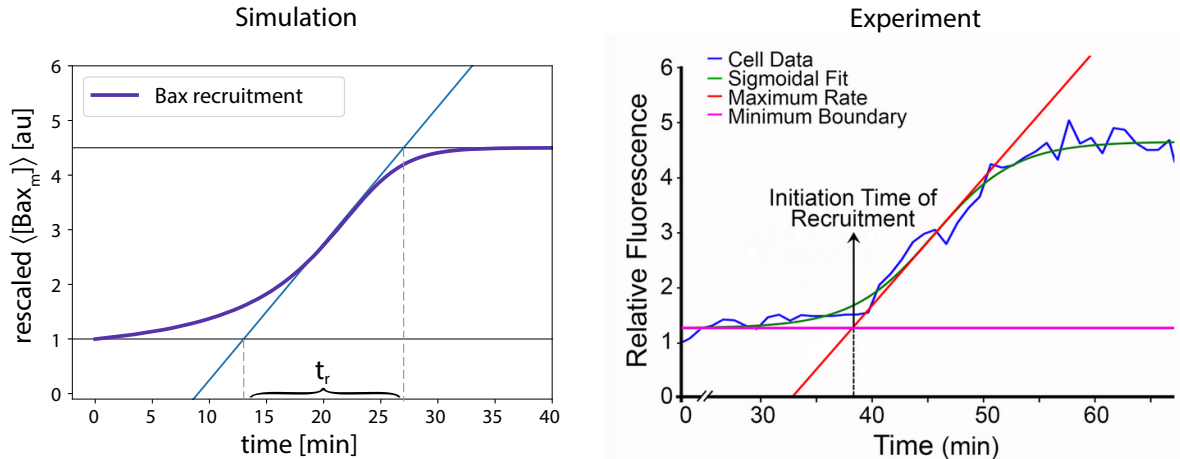


Fig. 3.6.: Comparison of Bcl-2 reaction kinetics between simulated and experimental timescales. By comparing with experimental data, we adjust the timescale for the translocation from the low to high Bax concentration state on the mitochondrial membrane. (a) Shows the collective translocation from the low to the high Bax concentration state in simulations of the effective model Eq. (3.4) in response to a strong apoptotic stimulus. Plotted is the mean Bax concentration on the mitochondrial membrane $\langle [Bax_m] \rangle$, where the average is drawn over the ensemble of mitochondria. (b) is a Figure presented in [161] in Fig. 2E. Here, they track the Bax accumulation dynamics with fluorescent microscopy of individual mitochondria. The presented line represents an ensemble average. We rescaled (a) to visually fit to (b). By comparison, we estimate the characteristic timescale $t_r = 15$ min as the translocation timescale. We fix all other physiological timescales of the effective model accordingly.

For a qualitative analysis, we are interested in order-of-magnitude estimates of the parameters in Eq. (3.4), which we find by comparison with experiments. We adjust a and b according to the time-scale of Bax accumulation on the mitochondrial membrane upon a strong apoptotic stimulus. [161] measured the duration of the transition from the low to the high Bax-membrane concentration state in response to the poisoning of the cell with apoptosis-inducing drug STS and found an estimate of $\delta t \sim 15$ min, as illustrated in Fig. 3.6. By this, we also define the characteristic timescale of our system as $t_r = 15$ min. This timescale gives an order of magnitude estimate for the movement c_l^* to c_h^* if the bistability is demolished by a negative skew $\alpha \ll 0$. This timescale coincides roughly with the measurement that Bax translocates to mitochondria at a rate of $4.7 \pm 0.2 \times 10^{-3} \text{ s}^{-1}$, as obtained by fluorescent recovery after photo-bleaching (FRAP) experiments [162]. This is consistent with an equilibrium between the on and off rates of Bax.

While an estimate of D based on molecular concentrations and reaction rates is error-prone, we estimate the order of magnitude of this parameter by the escape rate of individual mitochondria from c_l^* to c_h^* in the presence of weak apoptotic stimuli, as done in experiments by [153, 155]. In particular, [155] showed that over a time span of 4 h only a subset of $< 10\%$ mitochondrial mass underwent mitochondrial outer membrane permeabilisation in response to weak apoptotic stimuli, which gives an order of magnitude for D for a given potential $V_{\text{eff}}(c)$.

In the following section, we compare numerical modelling with the qualitative predictions of quasi-particle kinetics, see section 2.5, in the context of apoptosis. For the numerical simulations, we employ the kinetics of the effective model in Eq. (3.4). Addi-

tionally, we consider a finite set of organelles of different sizes v_i , which undergo discrete events of organelle fusion and fragmentation. As investigated in section 2.4.5, the effects of organelle fusion and fragmentation are likely to dominate the effects of organelle dynamics, if we consider homeostatic conditions in the absence of apoptotic stimuli and no explicit dependence of the organelle dynamics on the Bax concentration c . Furthermore, we assume that the kinetics of the signalling pathway are fast compared to the lysis of mitochondria. In section 3.4, we will relax on this assumption and explore how the inclusion of the lysis of mitochondria due to pore formation on the mitochondrial membrane affects our qualitative findings.

3.4. Quasi-particle kinetics in the regulation of cell death

In section 2.6, we elucidated on how the dynamics of compartmentalised stochastic reaction systems can be captured by simple equations of motion for a quasi-particle. To apply this to the specific organelle-associated signalling pathway of cell death decision-making, we discussed the specifics of mitochondrial dynamics in section 3.2.3.1, the kinetics of the Bcl-2 reaction network in section 3.2.3.2, and an effective model in Section 3.3.2. Based on the effective model, Eq. (3.6), we qualitatively study the effects of mitochondrial fusion and fragmentation on the response kinetics of the apoptotic signalling pathway to apoptotic stimuli. In this section, we display the benefit of the effective equation of motion Eq. (2.73) for an intuitive approach to the kinetics of a compartmentalised stochastic system, as we perform a graphical analysis of Eq. (2.73). Subsequently, we compare numerical simulations with semi-analytic solutions of the effective equations of motion, as we consider physiologically plausible parameter estimates. We focus on fixed apoptotic stimuli $\eta(t) = \eta$ in this section and generalise our findings to fluctuating stimuli in the subsequent section 3.5

In section 3.3.1, we discussed how the membrane-bound Bax concentration c is qualitatively described by stochastic movement in a bistable potential. We use c following a gradient dynamics to increase our understanding of the effective kinetics of c . We consider fixed apoptotic stimuli $\eta(t) = \eta$ and a time-invariant effective potential $V_{\text{eff}}(t) = V_{\text{eff}}$. In the absence of apoptotic signals, the potential is skewed to a stable fixed point at low Bax membrane concentrations, c_l^* . An apoptotic stimulus will drive it into the bistable region, where both the high and low concentration states, c_h^* and c_l^* , are stable fixed points. Recall, that we refer to weak and strong apoptotic stimuli depending on whether the potential is skewed towards the bistable or monostable region, respectively. Of particular interest in the context of apoptotic decision-making are weak apoptotic stimuli, where deregulation of the apoptotic signalling pathway can lead to abnormal cell death or carcinogenic effects.

We start our qualitative analysis by examining numerical simulations of the compartmentalised stochastic reaction kinetics system. In accordance with the model outlined in section 3.3, we observe that following the application of a weak apoptotic stimulus, two qualitatively distinct distributions emerge, as depicted in Fig. 3.7. Fig. 3.7 illustrates schematically the dispersion of the mitochondrial ensemble in the concentration phase space, with and without mitochondrial fusion and fragmentation. At the bottom of Fig. 3.7, we provide an illustration of the distributions in the concentration phase space, with mitochondria of varying concentrations depicted in different colours. Notably, when fusion and fragmentation processes are absent, the mitochondrial ensemble dispersed throughout the concentration phase space, with organelles occupying both the

3. Application to multi-scale fluctuations in the regulation of cell death

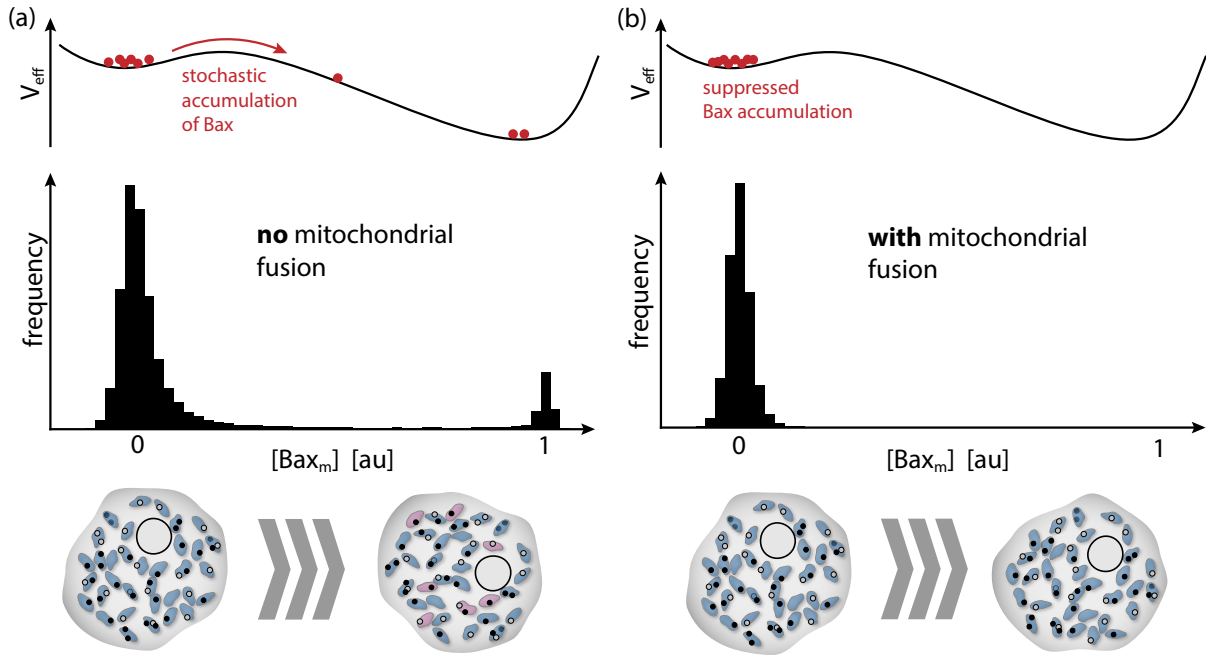


Fig. 3.7.: Mitochondrial dynamics give rise to a localisation of the apoptotic signalling pathway in the concentration phase space. We conduct numerical simulations to assess qualitatively the effect of mitochondrial fusion and fragmentation of the simulation. For this we choose physiological parameter conditions, as we match the translocation time-scale to $t_r = 15$ min and set the rate of mitochondrial fusion and fragment to $\mu t_r = 3.3$. We adjusted the effective (molecular) diffusion coefficient to $Dt_r = 6 \times 10^3$ in rescaled concentration units, which results in the absence of mitochondrial fusion and fragmentation to the stochastic switching of a subset $< 10\%$ from the low to the high concentration state, in line with the observation in [155]. In the top plot, we have an illustration of the effective potential, where individual mitochondria are represented as red dots. In the middle, a histogram illustrates the frequency statistics of the mitochondrial ensemble in one-dimensional $[Bax_m]$ concentration space. The bottom illustrates that ensemble statistics in the concentration phase space and the real space are distinctly different. The identical mitochondrial size distributions are considered in (a) and (b). While we see the random accumulation of Bax on mitochondria in ensembles with no mitochondrial fusion and fragmentation dynamics in (a), we find in (b) that mitochondrial fusion and fragmentation dynamics give rise to a localisation of the mitochondrial ensemble in the concentration phase space. The stochastic accumulation of Bax and the subsequent release of the toxin Cyt c is suppressed.

high and low Bax concentration states. Conversely, when mitochondria fusion and fragmentation are present, the ensemble of mitochondria remains as a collective in the low concentration state, consistent with experimental evidence of limited mitochondrial outer membrane permeabilisation (MOMP) [153–155].

Next, we perform a graphical analysis of the effective equations of motion, Eq. (2.73). For weak apoptotic stimuli, we are interested in the transition from the low Bax concentration state c_l^* to the high Bax concentration state c_h^* . In order to qualitatively examine this, we illustrate the kinetics of the quasi-particle in a bistable potential. We do not specify the details of the potential, as this analysis is purely qualitative. Our findings will be refined by considering physiologically plausible parameter estimates after study-

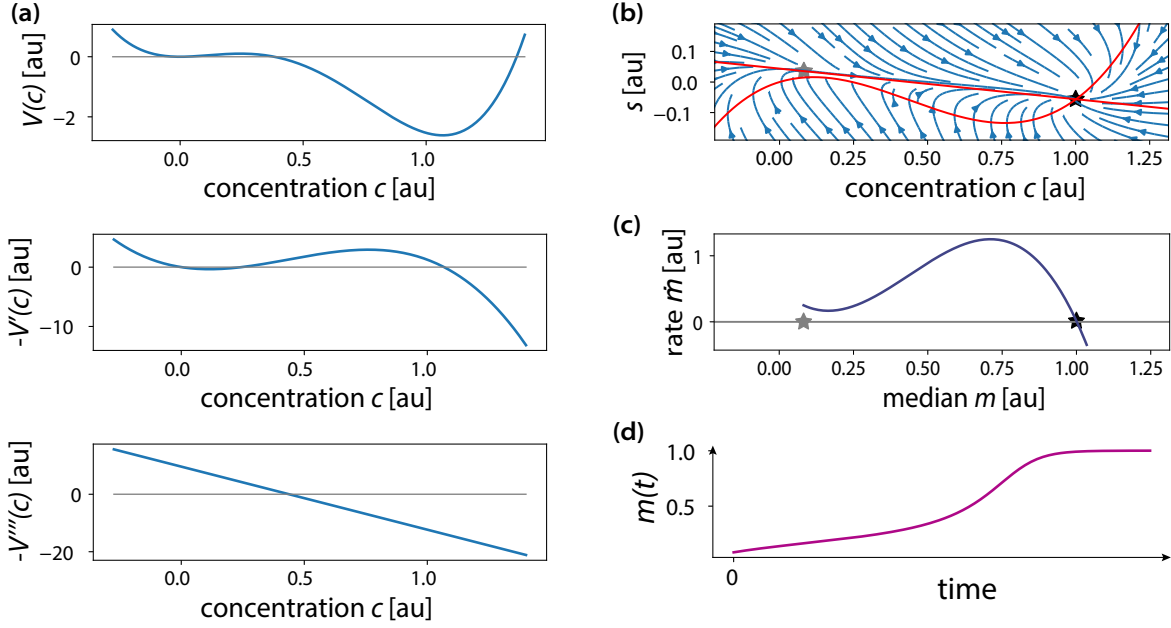


Fig. 3.8.: Graphical analysis of the equations of motion for the quasi-particle in the context of apoptotic decision-making. The simple equations of motion in Eq. (2.73) allow for graphical analysis, which we applied to the simple qualitative model in Eq. (3.4). From this, we can directly read off the qualitative response kinetics of the apoptotic signalling pathway to fixed, weak apoptotic stimuli. Here, we present a qualitative analysis with parameter choices in arbitrary units. (a) Plotted are the effective potential, its gradient and its third derivative. (b) phase-portrait of n Eq. (2.73) in a bistable potential. Red lines are the nullclines of the dynamics. The stable fixed point is indicated by a black star. the grey start refers to the ensemble mean at time $t = 0$. (c) Eq. (2.65) gives an estimate for the dynamics along the central manifold. (d) Graphical integration of the rates in (c) predicts sigmoidal response kinetics of the localised mitochondrial ensemble in the concentration phase space. There here presented analysis only has a qualitative character and emphasises that our analysis allows us to qualitatively assess the kinetics of the multi-scale system sketched in section 2.3 by a simple graphical analysis.

ing the dynamics qualitatively. In Fig. 3.8 (a), the bistable potential subjected to a weak apoptotic stimulus is shown, along with its gradient and third derivative. The grey line indicates zero-crossings, which correspond to the fixed points of the kinetics for point particles in the case where $\gamma = 0$. The third derivative of the potential in the example shown is a linear function. The third derivative $\gamma/2 \cdot V'''(c)$ reduces the barrier between the two stable fixed points for the quasi-particle kinetics, and thus acts like a perturbation. Note, that the strength of the perturbation is proportional to the variance over all mitochondrial compartments. This effectively reduces the region of attraction of the fixed point at low Bax concentrations for the quasi-particle.

Fig. 3.8 (b) displays the phase portrait of the equations in Eq. (2.73). The red lines represent the nullclines, where both differential equations independently vanish. The crossings of the nullclines indicate fixed points. For finite dispersion above a critical value ($\gamma > \gamma^*$), only the high concentration state (c_h^*) remains as a stable fixed point, even though the potential $V_{\text{eff}}(c)$ is still in the bistable region. The stable fixed point is indicated by a black star, and the position of the mitochondrial ensemble in the low-concentration

3. Application to multi-scale fluctuations in the regulation of cell death

state is indicated by a grey star. Blue arrows show the flow in the concentration phase space. We observe the emergence of a slow centre manifold, which the flows rapidly decay towards. The centre manifold is well approximated by the nullcline where $\partial_t s = 0$. Consequently, the dynamics of m along the centre manifold are well approximated by Eq. (2.74). In Fig. 3.8 (c), we sketch Eq. (2.74) from the grey star to the black star. We observe that the rate increases as the position of the mitochondrial ensemble m approaches the stable steady state. By performing a graphical integration, we find that the quasi-particle relaxes to the stable steady state following a sigmoidal relaxation, as shown in Fig. 3.8 (d). The transition into the high Bax concentration state is initially suppressed on short timescales and facilitated on long timescales after the ensemble has crossed the potential barrier between the two states. Note, however, that this qualitative analysis does not enable us to further assess the timescales which would correspond to *short* and *long* timescales. We elaborate on these timescales by a semi-analytic approach after we study the qualitative differences we expect in the response kinetics due to mitochondrial fusion and fragmentation.

As demonstrated in section 2.7, we expect altered fixed points for the quasi-particle in contrast to a hyper-fused mitochondrial network or mitochondria with no fusion and fragmentation. To this end, we compare four different hypothetical mitochondrial ensembles, which differ in their dynamics. First, we consider an ensemble with mitochondrial fusion and fragmentation, which exhibits the emergent collective, quasi-particle degree of freedom. Second, we consider an ensemble with no mitochondrial fusion and fragmentation, which has the same mitochondrial size distribution as the ensemble with fusion and fragmentation. We consider as a third ensemble, an organelle ensemble with no fusion and fragmentation, again the same size distribution, but with a rescaled diffusivity, $D_{rs} < D$. Here, we rescale the diffusivity such that both the organelle ensemble with fusion and fragmentation and this organelle ensemble show the same variance in dispersion in the absence of apoptotic stimuli. As a fourth model, we consider an ensemble where all mitochondria are hyper-fused to build a big, percolated mitochondrial network. We formally set $s \rightarrow \infty$, and hence $D \rightarrow 0$. We refer to this ensemble as a *point particle* in analogy to the *quasi-particle*. For the case of vanishing diffusivity ($D \rightarrow 0$), both states c_h^* and c_l^* are stable fixed points, and transition between the two states is only achieved when the bistable region is left in response to strong apoptotic stimuli. In contrast, when diffusivity is finite, $D > 0$, an ensemble of mitochondria with absent fusion and fragmentation, mitochondria are expected to randomly switch between the high and low concentration states.

We next compare our qualitative predictions of the response kinetics with numerical simulations, as shown in Fig. 3.9. For this, we again consider the four hypothetical mitochondrial ensembles. Here, we compare the changes in the mean amount of membrane-bound Bax over the mitochondrial ensemble ($\langle c \rangle$) in response to apoptotic stimuli and turn to physiologically plausible parameter choices. Note, that we obtained the physiologically plausible parameter choices by comparing with experimentally measured timescales of the systems, as outlined above. Specifically, we find that the response kinetics for the four different ensembles are qualitatively similar for strong apoptotic stimuli, Fig. 3.9 (a), but differ for weak apoptotic stimuli, Fig. 3.9 (b). While the ensemble with no mitochondrial fusion and fragmentation and vanishing diffusivity is stable in low-concentration states, the two ensembles with finite diffusivity show an approximately exponential relaxation. Notably, even on short timescales, a small proportion of mitochondria switch into the high-concentration state in response to weak apoptotic stimuli. This is in contrast to the

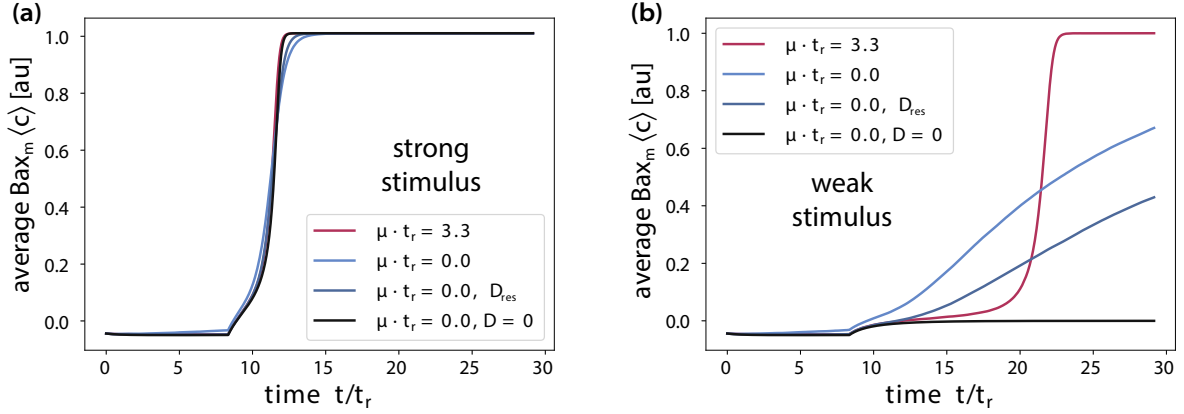


Fig. 3.9.: Accounting for mitochondrial dynamics results in qualitative different response kinetics in full stochastic simulations. In full stochastic simulations following the model in Eq. 3.6 are evaluated to show the response kinetics to a strong (a) and weak (b) apoptotic stimulus. The physiological plausible simulation parameters for (b) are identical to Fig. 3.7. For (a) the skew of the potential is chosen, such that the bistable region is left. the stimulus is applied at time $t = 9/t_r$. The mean Bax concentration $\langle c \rangle$ is tracked, where the mean is computed over the finite-sized mitochondrial ensemble. Four different ensembles are distinguished, where all ensembles show identical mitochondrial size distribution. Besides an ensemble with and an ensemble without fusion and fragmentation dynamics, we also consider mitochondrial ensemble without fusion and fragmentation dynamics and rescaled (molecular) diffusion constant. See section 3.4 for details. While we find that all ensembles show the same response kinetics for the strong apoptotic stimulus. For weak apoptotic stimuli, we find that the response kinetics are distinctly different. Moreover, we find the full stochastic simulations of the system and the sigmoidal response kinetics, which we predicted by the graphical analysis in Fig. 3.8.

response of the quasi-particle, where the response to the apoptotic stimulus is suppressed on short timescales and facilitated on long timescales. This is in qualitative agreement with our graphical analysis presented in Fig. 3.8. In particular, the response is initially inhibited compared to the ensemble with matched ensemble variance and facilitated on long timescales compared to the ensemble in the absence of mitochondrial fusion and fragmentation. On short timescales, the steady fusion and fragmentation dynamics impede the stochastic escape of individual mitochondria to the high-concentration state. On long timescales, after the mean and the median of the ensemble have crossed the potential barrier, mitochondrial fusion and fragmentation facilitate the crossing of the barrier for individual mitochondria.

Further corroborating our qualitative findings, we next examine how well we can capture the qualitative dynamics by solving the effective equations of motion in Eq. (2.65). semi-analytically by numerical integration. For this, we compare the result of Eq. (2.65) with the full stochastic simulations following Eq. (3.6). We test our results with different parametrisations of the potential and different estimates of system parameters. Additionally, we consider a finite ensemble of mitochondria with different sizes, which undergo stochastic, time-discrete events of fusion and fragmentation.

The effective equation Eq. (2.74) has one free parameter γ , which is linked to the variance over the mitochondrial compartment ensemble. We fix this parameter by a single, independent simulation, from which we assess the ensemble variance in the absence of an

3. Application to multi-scale fluctuations in the regulation of cell death

apoptotic stimulus. Our semi-analytic prediction is thus parameter-free. As Eq. (2.74) is a non-linear differential equation, we solve it by direct numerical integration using `odeint` in `python`. The theoretical prediction for the ensemble dynamics, in the absence of mitochondrial fusion and fragmentation, follows Kramer’s escape problem for mitochondria of different sizes, see appendix A.6. Assuming that mean and median are close in the ensemble of interacting mitochondria, we map out the average Bax concentration $\langle c \rangle$ and consider Eq. (2.74) as an approximation of the mean Bax concentration.

Figures 3.10 (a) and (b) compare the ensemble response for two different potential parametrisations with and without mitochondrial fusion and fragmentation. Physiologically plausible parameter choices were made, with the timescale of macroscopic concentration changes linked to experimentally observed timescale, Fig. 3.6, and the time-scale of mitochondrial fusion and fragmentation set on a timescale of minutes. Time was rescaled consistently with the timescale of macroscopic concentration changes $t_r = 15$ min. A qualitative agreement is observed between the theoretical prediction and the numerical simulations, with the sigmoidal response kinetics correctly predicted by the full stochastic simulations and the numerical integration of Equation (2.74).

By systematically altering the simulation parameters, we investigate how the results are qualitatively affected. In Fig. 3.10 (c), we systematically increase the rate of mitochondrial fusion and fragmentation, while by keeping the size distribution fixed. We predict that the variance over the mitochondrial compartment ensemble will be inversely proportional to the rate of mitochondrial fusion, $\gamma \propto \mu^{-1}$. Our simulation and the semi-analytic solution confirm that a decrease in the fusion rate leads to a decrease in the sigmoidal shape. However, we find that the simulation and the semi-analytic solution begin to deviate at small fusion rates, thus necessitating refinement of Eq. (2.74). We improve the quality of the semi-analytic solution again by decreasing the diffusivity D , which strengthens the sigmoidal shape and delays the shift from the low concentration state to the high concentration state, see Fig. 3.10 (d). Lastly, we consider the cases of changing the skew of the potential in Fig. 3.10 (e) and reducing the strength of the potential globally in Fig. 3.10 (f). Our findings indicate that lower potential barriers correspond to weaker sigmoidal shapes with a faster transition between the low and the high concentration states, whilst increased potential barriers have the opposite effect. Note, that for all different setups, Eq. (2.74) yields reasonable good estimates. Further recall, that the semi-analytic prediction admits no free fit-parameters!

This systematic scan of parameters enables us to generalise our qualitative insight into the sigmoidal translocation dynamics in steady state to general bistable potentials. We find that the qualitative insight for suppressing a response to weak apoptotic stimuli on short timescales and facilitating the response on long timescales is not a result of specifics of the $V_{\text{eff}}(c)$, but is a general feature of the switching between two stable steady states. Additionally, it should be noted that the sigmoidal response is only invoked above a critical value of stimulus strength, as the sigmoidal response requires the vanishing of the fixed point at low Bax membrane concentrations, see Fig. 3.8 (b). Furthermore, we conclude that the exact time-point of the transition between low and high-concentration states depends on the specifics of the potential, and a quantitative prediction of the transition time requires a precise estimate of the physiological reaction rates and concentrations, which cannot be obtained from the effective model. Nonetheless, we can make a rough estimate of the order of magnitude of the timescales on which the response is suppressed. Linking the timescale of suppression with the timescale of escaping from the lower potential well, we expect this timescale to be of the same order of magnitude, yet several times larger

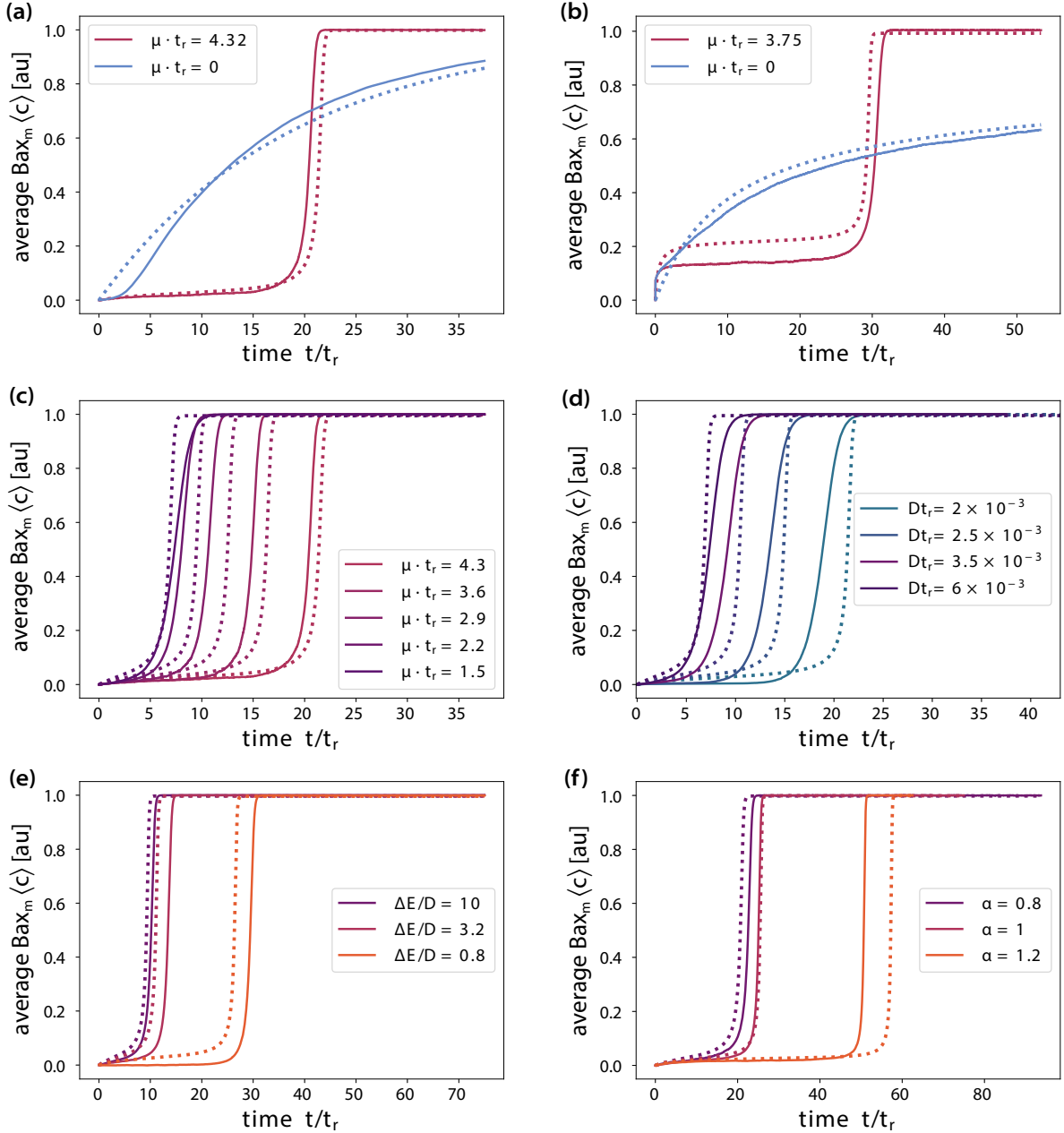


Fig. 3.10.: The equations of motion for the quasi-particle agrees with full stochastic simulations. We compare the equations of motion in Eq. (2.65) with full stochastic simulations (solid lines) and find quantitative good agreement. We obtain the solution of Eq. (2.65) by numerical integration. A single fit parameter is fixed by independent measurement of the ensemble variance in the absence of apoptotic stimuli. The other parameters are read off from the simulation. Both the simulation (solid line) and the semi-analytic result (dotted line) are rescaled by t_r . Two different potential parametrisations are considered in (a) with $V'(c)t_r = 0.01(c(2.5 - 3.6c + 0.25c^2))$ and in (b) with $V'(c)t_r = 0.1(c(5 - 1.5c + 0.1c^2))$. For (a), the molecular diffusivity is $Dt_r = 6 \times 10^{-3}$ and (b) is $Dt_r = 2 \times 10^{-2}$. All simulation parameters are in units of the rescaled concentration. Find the model for $\mu = 0$ in appendix A.6. The simulation parameters in (a) are the same as in Fig. 3.7 and 3.9. The average mitochondrial size is $\langle v \rangle = 2$. For(c-f) identical parameters to (a). (c) With reducing mitochondrial fusion and fragmentation rate μ the sigmoidal shape gets less distinct. (d) For $\mu t_r = 1.5$ the sigmoidalness is more emphasised for lower molecular diffusion constant. (e,f) Increasing the potential barrier gives more distinct sigmoidal responses. For (e) a skew is applied. For (f) the potential is multiplied with the strength parameter α .

3. Application to multi-scale fluctuations in the regulation of cell death

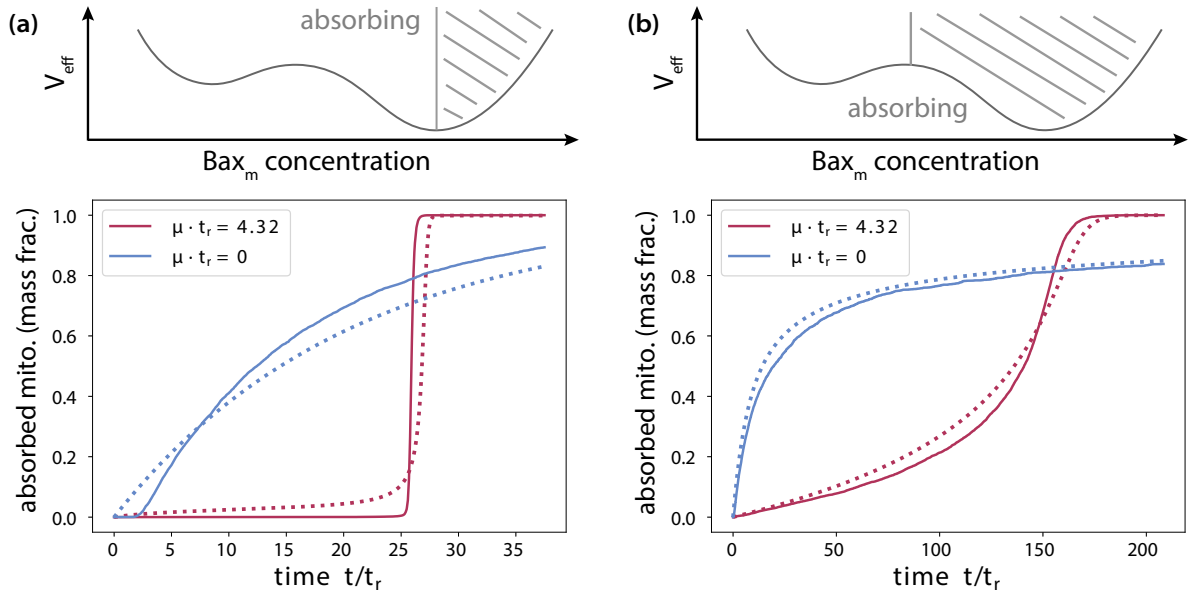


Fig. 3.11.: The sigmoidal relaxation dynamics are robust if additionally the degradation of mitochondria in response to Bax accumulation are considered. Absorbing boundaries are considered as specified by the sketches. Plotted is one the y -axis the mass fraction of absorbed mitochondria. Numerical simulations are shown in dotted lines, the theoretical predictions are shown in solid lines. For (a) the identical simulation parameters as in Fig. 3.10 (a) are considered. Also (b) the same potential parametrisation is chosen, but $Dt_r = 9 \times 10^{-4}$ and $\mu tr = 4$ is chosen. While we used the effective equations of motion in Eq. (2.65) for (a) and find still a good agreement. For (b) we used the model in appendix A.5. This model admits one free fit parameter, that we determined by visual inspection. We find that the sigmoidal relaxation dynamics are robust additionally the degradation of mitochondria is considered. Furthermore, our theory yields well qualitative agreement.

than the translocation time t_r , see Fig. 3.10.

For the analysis in Fig. 3.10, we neglected the lysis of mitochondria as they reach the high concentration state. We now relax this assumption by investigating two different scenarios to account for our current ignorance of the exact temporal dynamics of cytochrome c release and its effects on mitochondrial dynamics [41]. In the first scenario, we assume that mitochondria stop undergoing fusion and fission dynamics and release cytochrome c as they reach the high concentration state c_h^* . In the second scenario, we assume that mitochondria release cytochrome c after crossing the potential barrier and cease their fusion and fission activities. For both scenarios, we model the lysis of mitochondria as an absorbing boundary condition in our system. Instead of tracking the mean amount of membrane-bound Bax, we directly quantify the mass fraction of Cyt c releasing mitochondria m_c . Recall that the effective attraction to the mean in the approximation Eq. (2.56) formally requires us to exclude absorbed mitochondria from the computation of the mean.

In accordance with the framework of Smoluchowski aggregation-fragmentation dynamics, see section 2.2.3, we set the rate of mitochondrial fusion proportional to the mass of mitochondria not releasing Cyt c , $\mu \propto m_0 - m_c$. This can be made intuitive by assuming that, with a reduced number of mitochondria, the mitochondrial density and the rate at

which two mitochondria meet decrease. In the case of absorption in the high concentration state, Fig. 3.11 (a), we find a qualitative agreement with the semi-analytic solution of Eq. (2.74) and observe that the absorbing boundary condition only marginally alters the dynamics compared to Fig. (3.10). When absorption is considered at the barrier of the potential, the ensemble mean excluding the fraction of absorbed mitochondria is by construction stable in the low concentration state and the approximations for Eq. (2.74) fails. Returning to Eq. (2.55), we can treat the problem as a modified Kramer's escape problem, which also allows for a semi-analytic treatment with one free fit parameter, see appendix A.5. We find well qualitative and quantitative agreement between the simulations and the theory that admits one free fit parameter in Fig. 3.11 (b). Furthermore, in both the simulation and the semi-analytical prediction, we observe a sigmoidal response dynamics to a weak apoptotic stimulus when the absorbing boundary condition is placed at the potential barrier; however, the sigmoidal shape is less pronounced and the dynamics occur on longer timescales.

Intuitively, we can understand the sigmoidal response dynamics by tracking the dynamics from the perspective of individual mitochondria. Initially, the stochastic escape is suppressed as mitochondria are effectively pulled back to the low-concentration state on short timescales. As the mean and median of the distribution have crossed the potential, the dynamics shift and mitochondria remaining in the low concentration state are now actively pulled across the potential barrier by mitochondria compartment fusion and subsequent fragmentation. Also in the case of an absorbing boundary condition at the potential barrier, the stochastic escape is initially suppressed on short timescales, yet the active pulling over the barrier is absent on long timescales. Instead, the sigmoidal shape results from the steady decrease of the mitochondrial fusion rate μ as the mitochondrial mass are reduced. Consequently, the suppression of the stochastic escape vanishes as the mitochondrial compartments get absorbed.

As previously demonstrated, the sigmoidal response dynamics is a general feature of compartmentalised stochastic reaction kinetics systems when subjected to dynamics in bistable potentials. Our qualitative findings are not affected by the details of the parametrisation of the model in Eq. (3.4). We now conclude this chapter by discussing the effects of multiplicative noise. In the case of absorption at the potential barrier, corrections due to multiplicative noise [163, 164] can be straightforwardly accounted for as corrections of the Kramer's escape rate. We do not anticipate that multiplicative noise will qualitatively impact the sigmoidal relaxation. In the absence of absorption, a more refined analysis can formally account for multiplicative noise in Eq. (2.72). Nevertheless, we expect that multiplicative noise will have qualitative effects similar to those of an additional drift on the system. For the quasi-particle, the assumption of fixed dispersion should be carefully re-evaluated, as the variance should reflect the multiplicative character of the noise. While multiplicative noise complicates the analysis, we anticipate that the sigmoidal response dynamics will remain in the presence of multiplicative noise.

Concluding, we find that a sigmoidal response is a qualitative characteristic of compartmentalised stochastic reaction kinetics systems if the transition between two stable states is evoked by an external stimulus. In the case of apoptotic decision-making, this results in the initially suppressed response to weak apoptotic stimuli on a short timescale. Yet, conversely, on longer timescales, compartment fusion and fragmentation help to facilitate the response to the kinetics on longer timescales. This section has focused on the response to constant, non-fluctuating external stimuli. The next section will generalise the qualitative insights gained to general, fluctuating signals $\eta(t)$

3.5. Fluctuating stimuli and the emergence of a kinetic low-pass filter

In section 3.4, we studied the response dynamics of compartmentalised stochastic reaction kinetics systems applied to the context of apoptotic decision-making for constant apoptotic stimuli. While the response dynamics for strong apoptotic stimuli are only slightly affected by mitochondrial (compartment) dynamics, the kinetics differ strongly when considering mitochondrial dynamics in the context of weak apoptotic stimuli. We depicted the collective ensemble dynamics in the presence of mitochondrial fusion and fragmentation with a quasi-particle-like ensemble configuration and observed sigmoidal relaxation dynamics to the high Bax concentration state in response to weak apoptotic stimuli. We further established that the shape and timing of the transition between low and high Bax concentration states depend on the reaction network kinetics and require detailed quantification of reaction rates and concentrations under physiological conditions.

Considering that the interior of cells constitutes a highly stochastic environment, where proteins are continually synthesised and degraded, we generalise in this section to fluctuating stimuli and show that the interplay of protein complex dynamics and mitochondrial fusion and fragmentation act as a kinetic low-pass filter. This allows cells to suppress responses to fast noise fluctuations while allowing for responses to slow, biologically relevant changes in their environment. We examine the implications of this for the quality of apoptotic decision-making in the following section 3.6.

At the molecular level, the reaction network among proteins in the Bcl-2 family mediates the release of the toxin Cyt c for individual mitochondria. As discussed in section 3.2.3.2, this family includes a variety of pro-apoptotic and anti-apoptotic species, which collectively constitute the cell's stress level and set the strength of an apoptotic stimulus. This, in particular, enables the cell to respond to a wide range of different stress triggers, such as oxidative stress, radiation stress, metabolic stress, toxin-induced stress and DNA damage. Recognising the interior of the cell as a highly stochastic environment, we anticipate that the level of pro- and anti-apoptotic species will vary over time.

To investigate the effects of fluctuating stimuli, we consider that the collective stress level $\eta(t)$ follows a Gaussian stochastic process. We set $\eta(t)$ to follow an Ornstein-Uhlenbeck process, $d\eta = \theta_{OU}(\eta_0 - \eta)dt + \sqrt{D_{OU}}dW$, where W is a standard Wiener process. We scale $\theta_{OU} \propto \tau^{-1}$ and $D_{OU} \propto \tau^{-1}$, with τ the timescale of the Ornstein-Uhlenbeck process. This scaling allows us to systematically vary *how fast* $\eta(t)$ fluctuates while keeping the amplitude of the fluctuations constant, as $\lim_{t \rightarrow \infty} \text{Var}(\eta(t)_\tau) = \text{const.}$. We assume that the average of $\eta(t)$ is at the level of a weak-apoptotic stimulus and $\sqrt{\text{Var}_t(\eta(t))} + \langle \eta(t) \rangle_t < \eta_s$ so that the amplitude of $\eta(t)$ remains in the region of weak apoptotic stimuli in a σ -environment. Nevertheless, this allows for the stochastic occurrence of stress levels η which correspond to strong apoptotic stimuli.

In Fig. 3.12 (a), we qualitatively compare the responses of two ensembles with and without fusion and fragmentation dynamics to a fluctuating stimulus $\eta(t)$. The parameter choice here is identical to that in Fig. 3.12 (b), but $\eta(t)$ follows an Ornstein-Uhlenbeck-process. For technical reasons, we neglect the lysis of mitochondria subsequent to the accumulation of membrane-bound Bax. Experimentally, this can be achieved by inhibiting Bax homo-oligomerisation [149]. We study the relaxation of this assumption later in this section. The realisation of the fluctuating stress level $\eta(t)$ is presented as a grey profile line. For the ensemble with no fusion and fragmentation, we find that the mean Bax-membrane concentration in the ensemble $\langle c \rangle$ closely follows the fluctuations of the

3.5. Fluctuating stimuli and the emergence of a kinetic low-pass filter

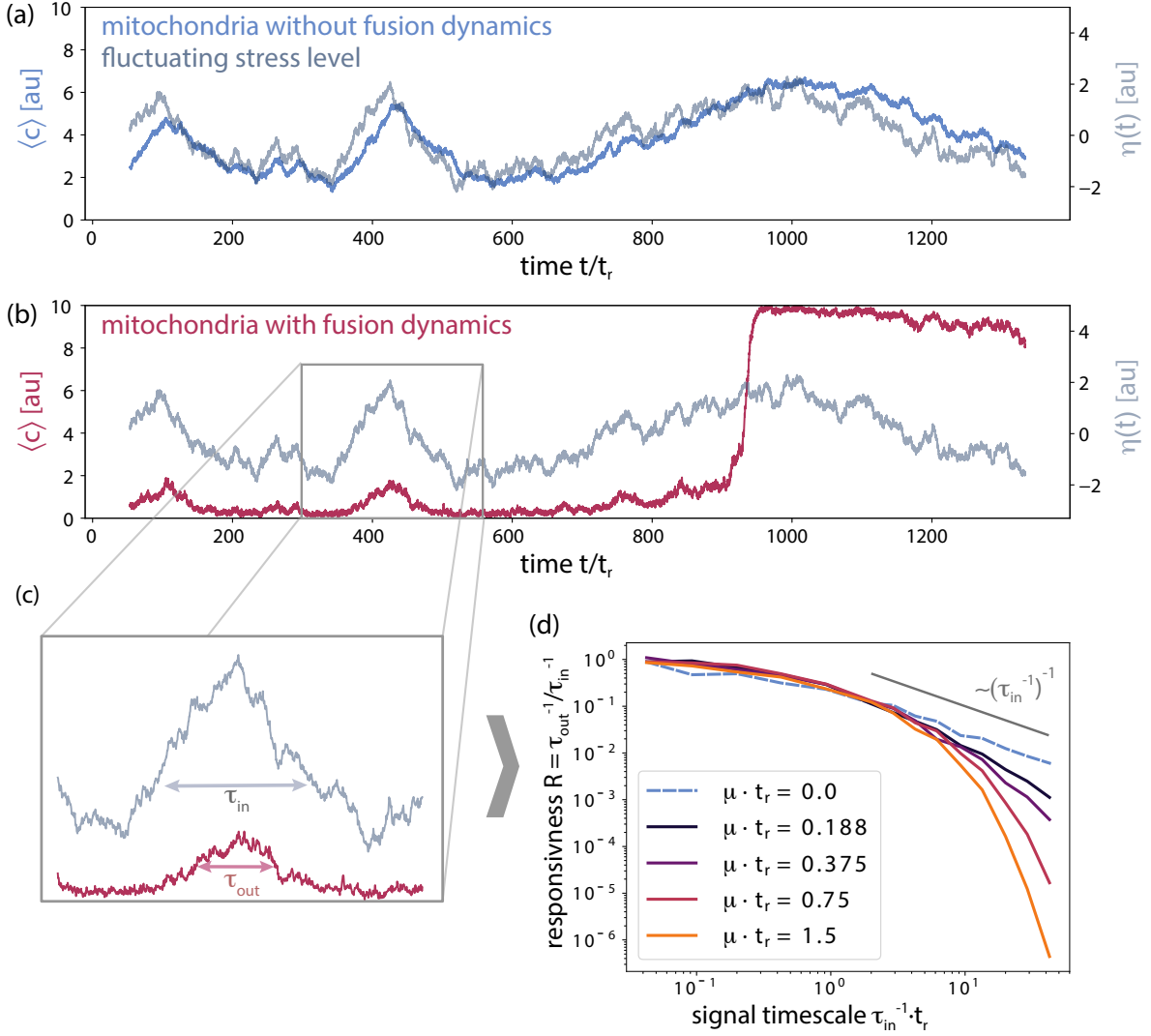


Fig. 3.12.: Sigmoidal relaxation kinetics give rise to a kinetic low-pass filter. We perform full stochastic simulations to investigate the response to fluctuating stimuli $\eta(t)$. We use the same simulation parameter as in Fig. 3.10 b for $\eta(t) = 0$ and consider the noise as linear skew on the potential. We consider as noise amplitude a variation of $\sigma_\eta = 0.25\Delta E$ of the barrier height. (a) The mean of the mitochondrial ensemble without mitochondrial dynamics closely follows every fluctuation in stress level $\eta(t)$. This is in contrast to the mitochondrial ensemble with mitochondrial fusion and fragmentation dynamics. Here, we see that the response is suppressed for fast fluctuations and facilitated for persistent stress levels. This generalises the sigmoidal response kinetics. (c) Schematic to illustrate how the time-scale of the stress level (τ_{in}) and the systems response (τ_{out}) is computed. (d) Systematically varying the timescale τ_{in} we check for the ratio of $\tau_{out}^{-1}/\tau_{in}^{-1}$ to quantify how frequently fluctuations in the stress level are translated into a systems' response. We find that the fast noise fluctuations are filtered out by orders of magnitude, while still allowing the system to respond to slow biological relevant changes in the stress level. Mitochondrial dynamics give rise to a kinetic low-pass filter. We expect the quantitative features of the filter to depend on specifics of the potential and the strength of the noise amplitude.

3. Application to multi-scale fluctuations in the regulation of cell death

stress level. This corresponds to an intermediate level of mitochondria in the high Bax concentration state. The situation is different for an ensemble with mitochondrial fusion and fragmentation, where we observe that the Bax concentration predominantly resides in the low Bax membrane concentration state, with only a small subset of mitochondria in the Bax concentration state. When the stress level $\eta(t)$ is persistent on an increased level, we find an abrupt change from the low to the high Bax concentration state and a strong response of the system. This qualitatively generalises the idea of sigmoidal response kinetics for fixed apoptotic stimuli, as demonstrated in section 3.4.

Next, we formalise the observations by systematically varying the timescale of the fluctuating apoptotic stimulus and setting it in relation to the timescale of the ensemble response. We determine the timescale by measuring the auto-correlation time of both the stimulus $\eta(t)$ and the fluctuating mean Bax concentration $\langle c(t) \rangle$. Specifically, the autocorrelation with a lag Δt is

$$\rho_{\Delta t} = \frac{\text{Cov}[X_t, X_{t+\Delta t}]}{\text{Var}[X_t]} \quad (3.7)$$

and we define the auto-correlation time τ by approximating $\rho_{\Delta t} \approx \exp(-\Delta t/\tau^{-1})$, this is illustrated in Fig. 3.12 (b). Here, we use the same definition to determine both the auto-correlation time of the stimulus τ_η and the ensemble response τ_c . Note that macroscopic changes in the time signal dominate the auto-correlation time, which renders it particularly suitable for the detection of an ensemble transition from the low to the high concentration state. We interpret the ratio $R = \tau_\eta/\tau_c$ as a measure of the responsiveness of the system. If fluctuations in the stimulus $\eta(t)$ are readily translated into a response of the ensemble $\langle c(t) \rangle$, both the stimulus and the ensemble show macroscopic changes on the same timescale, with the ratio close to unity, $R \approx 1$. Conversely, for $R \ll 1$, the timescale of macroscopic concentration changes in the ensemble is much larger than macroscopic changes in the stimulus, implying that fluctuations in the stimulus $\eta(t)$ are translated into a system's response only with a low frequency. In this case, the fluctuations are filtered out, as they are suppressed by the ensemble dynamics. For the case $R \gg 1$, macroscopic concentration changes in the ensemble happen more frequently compared to the changes in the stimulus. In this case, the stimulus has only a marginal effect on the progression of apoptosis. Note that we expect to occlude the last case by construction². By construction, the timescale of the stimulus $\eta(t)$ is given by $\tau_\eta = \theta_{\text{OU}}^{-1}$. By rescaling the diffusivity in the Ornstein-Uhlenbeck process accordingly to receive a constant variance scaling, we guarantee that changes in the auto-correlation τ_c are purely evoked by *how fast* the stimulus is fluctuating.

In Fig. 3.12 (c), we systematically map the responsiveness R over the inverse timescale of the fluctuating stimulus $\eta(t)$ for different rates of mitochondrial fusion and fragmentation μ . Here, we keep the size distribution of mitochondria fixed for all different mitochondrial fusion rates μ . Fast noise fluctuations in $\eta(t)$ correspond to low values of τ and are shown on right side of the x-axis, while slow changes in $\eta(t)$ are shown on the left side. We find that for all mitochondrial fusion and fragmentation rates considered here, the responsiveness approaches $R = 1$ for slowly varying stimuli $\eta(t)$. In contrast, a mitochondrial ensemble with higher fusion and fragmentation rates approaches lower values in the responsiveness $R_\mu \ll R_{\mu'}$ for higher fusion rates $\mu > \mu'$. We find that mitochondrial dynamics facilitate the suppression of fast noise fluctuations of the stimulus with an

²In experimental setups, $R \gg 1$ hints towards the fact that the wrong stimulus was measured.

order-of-magnitude effect.

Qualitatively, this is in line with the visual observation we made on the trajectory pictures, as the response to stimulus $\eta(t)$ is suppressed on short timescales and facilitated on long timescales. In agreement with the observation that faster rates of mitochondrial fusion correspond to stronger suppression of the response, we find that $R_\mu < R_{\mu'}$ for $\mu < \mu'$ on all timescales τ_η . As demonstrated for the response to fixed apoptotic stimuli, the filtering capacity of the system should be viewed as a qualitative result, as the quantitative values are strongly dependent on the specifics of the Bcl-2 reaction network. Additionally, the transition from the responsive dynamics $R(\tau_\eta) \approx 1$ to $R(\tau'_\eta) \ll 1$ is sensitive to the strength of fluctuations $\text{Var}_t(\eta(t))$. An order of magnitude estimate suggests that the transition τ_η^* lies on the order of magnitude of the Bax translocation time t_r , as illustrated in Fig. 3.12 (c). We conclude that mitochondrial dynamics give rise to a kinetic low-pass filter, allowing cells to repress the response to short, transient stress fluctuations.

For the analysis presented here, we considered the absence of mitochondrial lysis following the release of Cyt c, and allowed for the recovery of individual mitochondria from the high Bax concentration state back to the low Bax concentration state. This formally prevents apoptosis in cells, enabling us to create a large dataset on how Bax accumulation dynamics are affected by mitochondrial fusion and fragmentation. Note that the auto-correlation time is sensitive to macroscopic concentration changes. As such, the kinetic low pass filter quantifies both the accumulation and retro-translocation dynamics of Bax. If mitochondrial lysis is included, only the accumulation dynamics of Bax are quantifiable; however, as discussed in Fig. 3.11, we anticipate that this will still yield a sigmoidal response kinetics. Consequently, we expect the qualitative finding of mitochondrial fusion and fragmentation giving rise to a kinetic low-pass filter to be robust in the presence of the progression of the mitochondrial signalling pathway. Next, we interpret this finding in the context of apoptotic decision-making, focusing on the sensitivity and specificity of the response dynamics.

3.6. Improvement of the sensitivity and specificity of apoptotic decision-making

Having investigated in sections 3.4 and 3.5 how the fusion and fragmentation of mitochondrial compartments suppress the response to apoptotic stimuli on short timescales and facilitate the response to apoptotic stimuli on long timescales, we now interpret these findings in the context of the quality of apoptotic decision-making. To this end, we focus on the sensitivity and specificity of the ensemble responses, which quantify the degree of facilitation and suppression of the system's response. By doing so, we can draw conclusions on the qualitative responses of how apoptotic signalling is affected by mitochondrial dynamics.

In a physiological context, we are interested in the decision-making process of apoptosis in the context of a binary decision: whether cells undergo apoptosis in response to a stress stimulus, or whether they suppress the response. Misregulation of this apoptotic pathway can lead to severe diseases, which present two different scenarios. If it induces cells to more frequently conduct apoptosis in response to weak or transient stimuli, this results in increased cell death rates, potentially damaging organs and impeding their functionality. In layman's terms, cells are dying when they should not be. We refer to this misregulation as an increased rate of false positives. Conversely, misregulation of the apoptosis pathway

3. Application to multi-scale fluctuations in the regulation of cell death

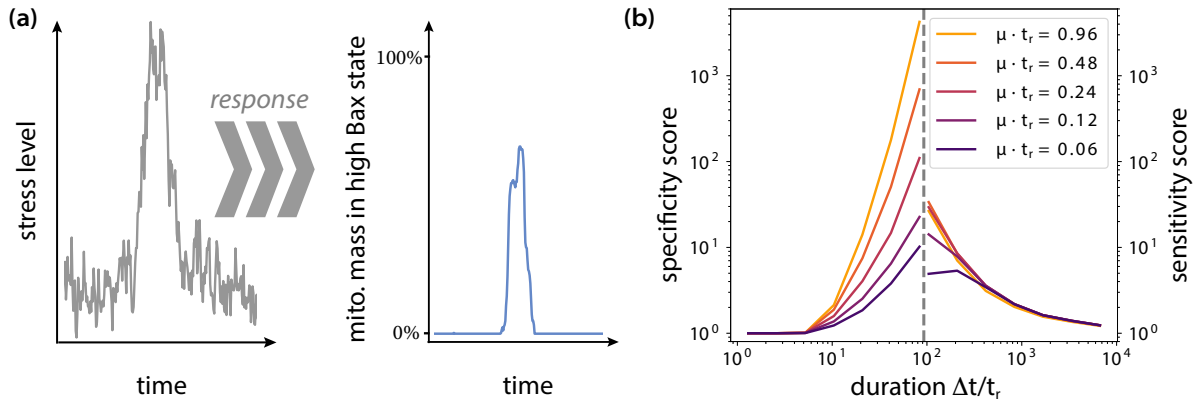


Fig. 3.13.: Mitochondrial dynamics improve the quality of apoptotic decision-making. We perform full stochastic simulations to investigate the quality of apoptotic decision-making. We use the same simulation parameter as in Fig. 3.10 b for $\eta(t) = 0$ and consider the noise as linear skew on the potential. We specify the noise as outlined in section 3.6. (a) Illustrates the noisy, transient fluctuation upon which the response of the system is evaluated. As we do not consider absorbing boundary conditions and track the mass fraction of mitochondria in high Bax concentration state. We next consider the maximum of this mass fraction as the response value of the system. (b) We compute the specificity and sensitivity as outlined in section 3.6. In particular, we assess the sensitivity and the specificity scores as fold-increases in contrast to the ensemble with no fusion and fragmentation dynamics. We set the decision time to where the ensemble with no fusion and fragmentation yields on average an ensemble response of 50% mitochondria in the high-concentration state. We find that mitochondrial dynamics increase the sensitivity and specificity score by orders of magnitude. Notably, the sensitivity score decreases for large μ , reflecting the suppression of responses by mitochondrial fusion and fragmentation.

which impedes apoptosis leads to the accumulation of cells, a hallmark of cancer. Here, cells are not dying when they should be, and we refer to this as false negatives. To assess the quality of decision-making, we quantify the rate of false positives and false negatives in terms of the sensitivity and specificity of a response.

We assess how mitochondrial dynamics affect the quality of decision-making by comparing mitochondrial ensembles undergoing fusion and fragmentation dynamics, with an ensemble without mitochondrial dynamics. We will, in particular, consider the ensemble with no mitochondrial dynamics as the ground truth of our assessment.

In accordance with the investigation of the kinetic low-pass filter in section 3.5, we are interested in how the timescale of stimuli affects the sensitivity and specificity of the response. To model the occurrence of a transient weak apoptotic signal, we refine the apoptotic signal $\eta(t)$ by superimposing a bell-shaped curve, as illustrated in Fig. 3.13 (a). We set the transient to reach 75% of the bistable region and the σ -environment to cover 25% of the width of the bistable region. As the timescale of the system is altered, both the timescale of the transient and the timescale of the fluctuations are rescaled. The response is measured by the maximum of the mitochondria mass fraction accumulated in the high-concentration state over the course of the stimulus.

Conceptually, we evaluate how the sensitivity and specificity change in comparison to the mitochondrial ensemble in the absence of mitochondrial fusion and fragmentation. We consider this ensemble as the ground truth of our investigations. We set the timescale

3.7. Testing for the predicted quasi-particle kinetics in experiments

separating the regime of preferential suppression and preferential conductance of apoptosis at the time point, where the mitochondrial ensemble in the absence of mitochondrial fusion and fragmentation shows on average maximally half of its mitochondrial mass switched to the high Bax concentration state. We refer to this time point as τ^* . We quantify with the specificity the absence of false positives, and hence the effective repression of the response for timescales $\tau < \tau^*$. We quantify a specificity score s_μ with the probability of a response smaller than 5%. Analogously, we consider for the sensitivity the rate of true positives as a measure for the facilitation of a response on timescales $\tau > \tau^*$. We quantify a sensitivity score n_μ with the probability of a response larger than 95%. We assess the probability of true and false positives by computing 10^5 independent simulation runs for each time point.

In Fig. 3.13 (b), we map out the specificity and sensitivity scores as fold-increases compared to the organelle ensemble with no mitochondrial fusion and fragmentation, s_μ/s_0 and n_μ/n_0 respectively. We find that mitochondrial fusion and fragmentation lead to orders of magnitude increases in both sensitivity and specificity. For the specificity, we observe a steady increase with an increasing rate of mitochondrial fusion and fragmentation. In contrast, sensitivity is maximal for intermediate fusion and fragmentation rates and decreases for higher rates. These findings are consistent with the observation that mitochondrial fusion and fragmentation suppress the response on short timescales but facilitate the response on long timescales. Moreover, specificity and sensitivity also quantify the localisation of the mitochondrial ensemble in the concentration phase space, which effectively reduces the probability of finding mitochondrial ensembles intermixed in the high and the low Bax concentration state. It follows also that the sensitivity score decreases for high mitochondrial fusion and fragmentation rates, in line with the qualitative observation that the response is strongly suppressed for larger rates of mitochondrial fusion and fragmentation, as for example illustrated in Fig. 3.10 (b).

With this, we conclude our qualitative analysis of how mitochondrial fusion and fragmentation affect the response kinetics of apoptotic signalling. Our findings demonstrate that if the dynamics of mitochondria is accounted for, the response on short timescales is suppressed and the response on long timescales is facilitated. This provides a kinetic low-pass filter, which allows cells to suppress the response to short, transient fluctuations in their stress level, see Fig. 3.12 (c). We quantified the quality of decision-making in terms of the specificity and the sensitivity of the result and found an order-of-magnitude increase for both. We considered physiological plausible parameters and performed a qualitative analysis, which allowed us to discuss model refinements and the qualitative effect of various model parameters. Furthermore, our findings suggest that organelle fusion and fragmentation can lead to measurable predictions in cell-culture experiments.

3.7. Testing for the predicted quasi-particle kinetics in experiments

In sections 3.4, 3.5 and 3.6, we have examined, in a theoretical context, how organelle dynamics can qualitatively affect the kinetics of organelle-associated signalling pathways. Specifically, we have analysed how mitochondrial fusion and fragmentation can homogenise the concentration of Bax across the mitochondrial ensemble, thus reducing the variance among individual mitochondria. This homogenisation results in collective responses of the organelle ensemble to fixed, weak apoptotic stimuli: these responses are

3. Application to multi-scale fluctuations in the regulation of cell death

suppressed on short timescales and facilitated on long timescales for the effective ensemble dynamics, compared to an ensemble of mitochondria without fusion and fragmentation dynamics. We then generalised this insight to fluctuating, weak apoptotic stimuli and deduced that mitochondrial fusion and fragmentation can give rise to a kinetic low-pass filter and increase the sensitivity and specificity of apoptotic decision-making by orders of magnitude. Thus far, we have only studied these findings theoretically and through numerical simulations. In this section, we consider how our theoretical considerations can be tested experimentally. Doing so, we emphasise the experimental challenges to manipulate the mitochondrial dynamics and to precisely measure low protein concentrations without interfering with the system.

Mitochondrial dynamics can be impaired by either the treatment with chemical substance or by using genetic knockout strains [59, 60, 140]. In both cases, either the fusion or the fragmentation dynamics of mitochondria are impeded to alter the mitochondrial dynamics. The effect on mitochondrial dynamics is often quantified by the change in the mitochondrial size distribution instead of direct quantification of the fusion rate [59, 154, 155]. As a consequence, the effects of altered mitochondrial dynamics and altered mitochondrial size distribution are experimentally often intermingled. To disentangle the effects of mitochondrial fusion and fragmentation dynamics from the effects of altered mitochondrial size distributions, formally perturbations both on the fusion and on the fragmentation rate need to be performed, which result in size distributions with decreased and increased average mitochondrial size respectively. Yet, the perturbation of mitochondrial dynamics is not equally possible for all cell types. Either two different knock-out lineages need to be grown, or chemicals are not readily available or have additional side effects influencing and weakening the observation. Here, theoretical considerations can assist the interpretation by considering the additional effects of altered mitochondrial size distributions.

Besides manipulating mitochondrial dynamics, also the measuring of membrane protein concentrations without interfering with the dynamics is a challenge for experiments. As the direct observation of protein kinetics is prevented by the resolution limit of optical microscopy³, only indirect measurements using fluorescent protein analogues or chemical dyes can be performed [161, 165, 166]. Yet, careful cross-validation of additional measurements is required to ensure that the kinetics of the fluorescent proteins and dyes accurately reflect the physiological operations of the cells. Furthermore, the determination of concentration through quantification of fluorescence is generally subject to error due to the need for precise calibration, photo-bleaching effects, and the inability to reflect absolute concentration values [161]. In our discussion of experimental setups and comparison of our theoretical predictions with findings in the literature, we will critically assess the extent to which the experiments have validating character.

In section 3.5, we argued that apoptotic stimuli $\eta(t)$ can only be considered fixed in well-controlled laboratory conditions, while physiological stimuli are stochastically fluctuating. Experimentally, the exact strength of apoptotic stimuli is difficult to precisely control. Prominent choices include the tumour necrosis factor alpha (TNF- α), staurosporine (STS), actinomycin D (Act D) or the chemical ABT-737 [167–169]. TNF- α activates caspases [41] and thus potentially allows for the precise control of perturbations; however,

³Though the resolution limit can be lowered by reducing the wavelength of the illumination source by, for example, considering electron transmission microscopy, these measurements yield a strong physiological perturbation on the cell and measurement of reaction dynamics cannot be claimed to reflect physiological conditions.

it may also activate the extrinsic apoptotic signalling pathway, which renders TNF- α an unsuitable inducer of apoptosis in this context. STS and Act D are specific inducers of the intrinsic apoptotic signalling pathway but do not act directly on the Bcl-2 interaction network. Therefore, the level of apoptotic signalling can only be discussed on the basis of qualitative comparisons of different toxin concentrations. Furthermore, the degree of fluctuations in the signalling can only be determined through additional measurements. ABT-737 is a biomimetic molecule which mimics the effects of pro-apoptotic BH3-only proteins. This chemical is still experimental [153, 169]. Yet, ABT-737 it offers the possibility to precisely perturb the apoptotic signalling bath by interfering with the Bcl-2 reaction network in a controlled manner. As our analysis remains qualitatively valid both for static and fluctuating apoptotic stimuli, see sections 3.4 and 3.5, we consider STS, Act D, and ABT-737 suitable apoptosis inducers in experimental setups.

From a theoretical perspective, we can make various qualitative predictions regarding the effects of mitochondrial fusion and fragmentation dynamics on the kinetics of apoptotic signalling. These predictions range from statistical to qualitative changes in the temporal evolution and response kinetics, as well as how parameter changes can qualitatively affect the dynamics of cell death. However, the challenge of experimentally testing our findings in this context lies in the difficulty of applying precise system perturbations and measuring without interfering with the system. As the dynamics at a subcellular scale cannot be directly inferred from microscopy videos with arbitrary spatial and temporal resolution, it is not possible to conduct experiments in direct analogy to the simulations in the sections 3.4, 3.5 and 3.6, see also [161, 166]. Therefore, in this section we will go through the different theoretical predictions individually and discuss possible experimental setups to test them. We will refer to the relevant experimental observations in the literature that have motivated our modelling choices in section 3.3, and discuss which experimental setups would be conclusive for verifying the collective organelle dynamics.

3.7.1. Test for the localisation of mitochondria in the concentration phase space

Our central prediction regarding the effects of mitochondrial fusion and fragmentation on apoptotic decision-making is that they result in a homogenisation of the mitochondrial ensemble with respect to the variance in Bcl-2 concentrations. Specifically, we predict that the variance in mitochondrial outer membrane concentration is reduced in the presence of mitochondrial fusion and fragmentation, even in the absence of apoptotic stimuli. To test this prediction, it is necessary to impair mitochondrial dynamics and determine the concentration of membrane proteins.

Weaver et al., [146], investigated the effect of mitochondrial fusion and fragmentation on the variability of mitochondrial outer membrane protein concentrations. To do so, they compared fibroblast cell lines with a genetic knock-out of the mitochondrial fusion proteins MFN 1/2. The variance in the mitochondrial membrane concentration was assessed by measuring the release of fluorescent Cyt c from mitochondria in response to a strong apoptotic stimulus. It was argued that the variability in mitochondrial outer membrane protein concentrations directly impacts the variability of individual mitochondria at the time point of Cyt c release. Indeed, the authors observe a significant decrease in steepness and an increase in variance when mitochondrial dynamics were impaired.

Our observations are in agreement with the theoretical predictions regarding the effects of mitochondrial fusion and fragmentation on protein concentration variance. The

3. Application to multi-scale fluctuations in the regulation of cell death

authors of the study suggest that the variance reduction in cells with functional Mnf1/2 may be due to protein exchange among mitochondria. To verify this conclusion, further quantification of the altered mitochondrial size distribution and additional measurements with different size alterations would be necessary. Additional clarity could be achieved by comparing the observation to the predicted effects from equation Eq. (2.55), provided the size distribution had been experimentally obtained. Therefore, the experiments in [146] provide evidence of the potential for collective ensemble dynamic. From a different perspective, these experiments effectively illustrate the need for a stochastic framework when modelling apoptotic signalling due to the chemical binding noise at low protein copy numbers. Moreover, they effectively demonstrate that, at the very least, the heterogeneity of the mitochondrial size distribution, if not mitochondrial dynamics, must be taken into consideration when studying the kinetics of the apoptotic signalling pathway.

In this study, Cao et al., [155], investigated the effects of mitochondrial fusion and fragmentation on the random switching of individual mitochondria to the high Bax concentration state in response to weak apoptotic stimuli. To do so, mouse embryonic fibroblast cells were used, with knockout strains created for both MNF 1/2, impeding mitochondrial fusion, and DRP1, impeding mitochondrial fragmentation. Weak, sublethal apoptotic stimuli were applied and the amount of lysed mitochondria measured by initially dyeing the mitochondrial membrane space and then quantifying the number that had lost their fluorescent signal. Qualitative analysis revealed strongly altered mitochondrial size distributions; those with impaired mitochondrial fusion had an increased number of small, fragmented mitochondria, while those with impaired mitochondrial fission had elongated mitochondria. This was in line with Smoluchowski aggregation dynamics, see 2.2.3. Furthermore, the authors observed that predominantly small, fragmented mitochondria were prone to stochastic lysis in response to weak apoptotic stimuli, which was also consistent with modelling predictions and numerical observation, see e.g. Fig. 3.9. Notably, only an increase in the number of stochastically lysed mitochondria was observed when mitochondrial fusion was impaired, but not when mitochondrial fission was impaired. This is also in line with our theoretical findings, as also an increase in mitochondrial size reduces the level of stochastically dedicative mitochondria. Also here, the authors argue that mitochondrial fusion and fragmentation dynamics induce the observed effects due to the intermixing of mitochondrial outer membrane proteins. Yet, to make this statement conclusive, additional experiments would be necessary to exclude that the effect is only due to a change in mitochondrial sizes.

Fig. 3.9 showed that stochastic deactivation is also suppressed in organelle ensembles with reduced molecular noise D_{res} . However, the suppression is weaker than in an organelle ensemble with mitochondrial fusion and fragmentation dynamics. To corroborate the results presented in [155], we suggest measurements with longer intoxication times for DRP1 knockout cell lines, which are likely to show qualitative differences in the suppression kinetics. A quantitative analysis of the mitochondrial size distribution could also serve to corroborate their conclusion. Therefore, we summarise that the results of [155] support the plausibility of the qualitative results of the effective model introduced in section 3.3, while they are not conclusive on our theoretical prediction of *quasi-particle* kinetics. While in this section we focused on static properties, we consider possible experimental setups to measure the temporal kinetics of apoptotic decision-making in the next section.

3.7.2. Observing sigmoidal response kinetics of the quasi-particle in experiments

In section 3.4, we further investigated this by comparing the effective equations of motion with numerical simulations and found that sigmoidal response kinetics is a qualitative feature of the time-evolution of the apoptotic signalling pathway when mitochondrial fusion and fragmentation are taken into account. To directly observe the quasi-particle-like, collective ensemble kinetics, one would need to track the evolution of the distribution over time and measure observables in a manner analogous to the analysis presented in section 3.4. However, this is challenging to accomplish experimentally for various reasons.

To investigate the temporal evolution of Bax concentration changes in individual mitochondria within the same cell, we must utilise fluorescent microscopy techniques. However, continuous time-lapse observation can be impeded by photo-toxicity [161, 166]. Decreasing the temporal resolution reduces photo-toxic effects but worsens the tracking of individual mitochondria as they move actively within the cytosol. Moreover, the movement of individual mitochondria out of the focal plane can also impede tracking. The apoptotic dynamics themselves present a challenge on experimental timescales. We predict that the sigmoidal dynamics will proceed with little change until an abrupt switch from low to high Bax concentration state occurs [165]. In this situation, increased temporal resolution for the brief interval of transition dynamics would be desirable, but this would necessitate self-adaptation of the microscopy process and parallel evaluation of microscopy data to the measurement process.

Furthermore, it is difficult to detect the stochastic switching of individual mitochondria, due to the rapid lysis and degradation of those in the high Bax concentration state. This means that the observation of these mitochondria effectively involves detecting ‘holes’ in the mitochondrial ensemble. There are very few experimental observations which indicate that the ‘pulling of mitochondria across the potential barrier’, and therefore the sigmoidal dynamics, may be observable, see for example the supplemental videos in [161]. However, this evidence is not statistically conclusive. Comparing the time traces of different cells is difficult as they present as different stochastic realisations and so, to gain further insight into the temporal evolution, it is necessary to analyse ensembles of cells.

3.7.3. Testing for the sigmoidal progression of apoptosis in cell culture experiments

The central qualitative prediction we make in this chapter is that mitochondrial fusion and fragmentation dynamics will generate a kinetic low-pass filter in apoptotic decision-making. However, measuring this prediction experimentally presents a conceptual challenge. As discussed previously, obtaining statistically significant results from tracking individual cells is a difficult undertaking. On the other hand, observing the dynamics on the molecular level for a large cell culture is not feasible, so we would prefer to measure the effects of apoptotic decision-making, i.e. measuring the percentage of apoptotic cells. Furthermore, we cannot directly determine the filtering capacity in experiments, as we cannot precisely control the fluctuating stimuli and test for different timescales in experiments.

To circumvent these problems, we notice that the sigmoidal relaxation dynamics are a hallmark of the quasi-particle kinetics we expect to find in the apoptotic signalling pathway. Furthermore, we interpret these sigmoidal relaxation dynamics as the mechanistic

3. Application to multi-scale fluctuations in the regulation of cell death

basis of the kinetic low-pass filter. In order to assess the validity of the quasi-particle kinetics concept experimentally, we make use of the characteristic finding that the sigmoidal relaxation dynamics are more accentuated for *weak* apoptotic stimuli, while we expect the sigmoidal shape to shift towards exponential-like relaxations for strong apoptotic stimuli. Compare for this for example with Fig. 3.9, Fig. 3.10, and Fig. 3.14 (d). In the absence of mitochondrial fusion and fragmentation dynamics, we would anticipate a scaling and *stretching* of the response. As such, when we assess different stimuli with various duration and strength, we anticipate to find sigmoidal relaxation kinetics. This prediction, however, is formally based on Cyt c release and assumes that the stimulus is applied directly and accurately. This consequently sets the challenge to consider pre- and post-modifications in the apoptotic signalling pathway from a theoretical standpoint.

While both STS and Act D are specific inducers of apoptosis via the intrinsic pathway, they do not directly act on the Bcl-2 protein network. By changing the duration that cells are exposed to varying concentrations of Act D or STS, we can control the strength and duration of an apoptotic stimulus. However, this additionally leads to stochastic variations in the apoptotic stimulus $\eta(t)$ for different cells in the same cell culture, resulting in increased apoptotic variability and varying release times of Cyt c. Note, that we have also not specified the progression of apoptosis after the release of Cyt c. However, because the release of Cyt c is a bottleneck in the apoptotic pathway, we expect that the effects of sigmoidal relaxation dynamics will translate to the entire pathway, including the disappearance of sigmoidals when the stimulus is increased. To corroborate our qualitative argument, we conduct stochastic models and find that the sigmoidal relaxation is indeed robust towards variation in the time-point of apoptosis stimulus application, variability in the bistable potential, and post-modifications by assuming threshold values of released Cyt c for the induction of apoptosis. These results are presented in Fig. 3.14 (e,f) and detailed out in the appendix A.7.

While other sigmoidal processes are commonly observed in biological systems, we argue that the change in functional shape from sigmoidal to exponential dynamics is a characteristic of quasi-particle kinetics. Note that, for example, Hill functions used to describe gene activation have a sigmoidal dependence on concentration, but not temporal dependence. On the other hand, sigmoidal relaxation dynamics demand autocatalytic mechanisms, which are usually fixed in their functional shape and thus do not permit a shift to exponential-like relaxation dynamics. Note that our theory predicts a significant inhibition of the response to weak apoptotic stimuli on short timescales, yet allows for responses on later timescales. This presents a qualitative difference which can be used to evaluate the quasi-particle kinetics experimentally; see Fig. 3.14 (e,f) and the black arrows.

Experiments tracking the predicted sigmoidal dynamics were performed in the group of Philipp Mergenthaler at the Charité research hospital in Berlin by Lina Hellwig. To this end, Lina Hellwig developed an apoptosis assay, which allows subjecting cell cultures to varying apoptosis inducer concentrations for varying time periods. For this, Lina Hellwig grew neural stem cell cultures (NSC) and induced pluripotent stem cells cultures (iPSC), subjected them to varying Act D concentrations, and evaluated the progression of apoptosis in the cell culture by flow cytometry (FACS). To specify for apoptotic cell death, cells are died with Annexin V and DAPI, which allows distinguishing in experiments apoptosis from unspecific cell death. NSC cell cultures were grown for 3 days before inducing apoptosis, while iPSC cell cultures were grown for 2 days. Before evaluation by flow cytometry, the cells are washed, fixed, and dyed. Thus, by design, the progression

3.7. Testing for the predicted quasi-particle kinetics in experiments

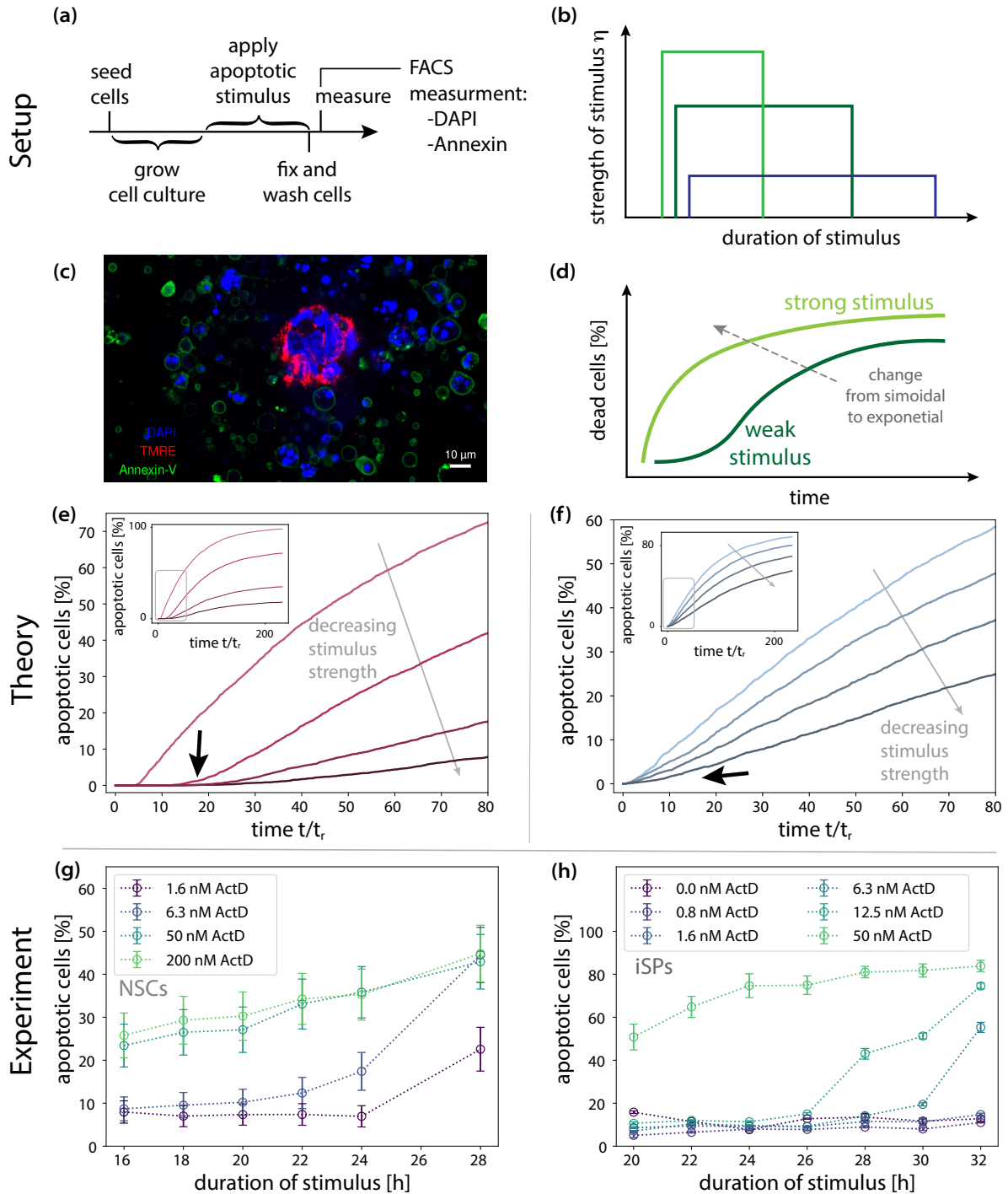


Fig. 3.14.: Observing the sigmoidal progression of apoptosis in cell culture experiments. (a) Schematic representation of the experimental setup. (b) To test for the sigmoidal progression, the strength and duration of apoptotic stimuli are systematically varied. (c) Microscopy image of apoptotic hiPSCs. Image courtesy Lina Hellwig and Philipp Mergenthaler. (d) We qualitatively predict a characteristic shift from sigmoidal to exponential progression statistics as the strength of the apoptotic stimulus is increased. (e,f) We corroborate our qualitative argument by numerical simulations, see appendix A.7 for details. The suppression of apoptosis for weak stimuli at low concentrations is qualitative characteristic, for which we test in experiments. (g,h) Experiments performed by Lina Hellwig in the group of Philipp Mergenthaler on NSC can iPSC cell cultures. Errorbars show the standard deviation over three technical replicates.

3. Application to multi-scale fluctuations in the regulation of cell death

of apoptosis needs to be evaluated by comparing different replicas, as the cell culture sample is destroyed in the measurement processes. For each measurement point, three technical replicas are considered. Two experiments are presented in Fig. 3.14 (g,h). Here, Lina Hellwig and Philipp Mergenthaler find the characteristic suppression of apoptosis for low Act D concentrations, resulting in a sigmoidal progression of apoptosis, and thus in line with our theoretical prediction. Note that here we only performed a qualitative comparison, as we did not fit the experimental data.

Note, that the results strongly hint towards our theory of effective ensemble kinetics. However, they remain so far inconclusive, as a sigmoidal progression of apoptosis may also be attributable to pre- or post-modifications in the signalling pathway that has not been taken into consideration theoretically. We currently plan to corroborate our findings by experimentally interfering with the mitochondrial dynamics.

3.8. Discussion of applying quasi-particle kinetics to apoptotic decision-making

In this section, we reconcile our model assumptions and findings by critically assessing the plausibility of separating timescales when discussing organelle-associated signalling pathways. Specifically, we consider the extent to which mitochondrial dynamics could affect the kinetics of the signalling pathway as mitochondrial fusion and fragmentation often occur within minutes. Following this discussion, we consider the potential relevance of our findings for therapeutic approaches to mitigate or facilitate cell death in medical applications.

3.8.1. Is a separation of timescales a plausible choice for organelle-associated signalling pathways?

One central objection that may be raised against the theory presented in this chapter is, that the dynamics at the chemical reaction level occur on a much faster timescale than the dynamics of organelle fusion and fragmentation. While this objection is in general valid, it does not imply that organelle dynamics play a negligible role in the kinetics of organelle-associated signalling pathways. Indeed, the extent to which organelle dynamics fundamentally alter response kinetics depends on the specific research question being asked. Note, that the effective ensemble dynamics derived in Eq. (2.55) were obtained without assuming fast organelle dynamics, but by considering a continuum limit in the number of organelles. This formally limits our analysis to large organelle ensembles, yet it also allows us to examine the effect of arbitrarily slow interaction rates. Notably, we find that the additional *interaction potential*, which serves as a perturbation on the deterministic dynamics dictated by molecular reactions, becomes weaker as the rate of mitochondrial interaction decreases. Depending on the system parameters and the research question at hand, this additional interaction potential may be treated as a negligible perturbation on the kinetics of the signalling pathway. However, it is important to emphasise that our analysis enables us to assess the strength of this effect *a posteriori*, thereby allowing us to determine in which contexts organelle dynamics are central to the kinetics with strong qualitative effects. Before discussing potential objections to not performing a separation of timescales, note that we have already used physiologically plausible parameter choices

3.8. Discussion of applying quasi-particle kinetics to apoptotic decision-making

In sections 3.4, 3.5 and 3.6, where we observed qualitatively strong effects. Here, we will now discuss why we consider strong effects plausible.

In the beginning of section 3.4, we discussed the significant impact organelle fusion and fragmentation have on the kinetics of signalling pathways in a static picture. While the dynamics a priori allow the exploration of the full phase space; organelle fusion and fragmentation counteract this dispersion and result in localisation in the concentration phase space. This *qualitative* result is independent of the timescale and is corroborated by the experimental findings of [146]. Yet, the qualitative effects vanish if the kinetics of the reaction network is already characterised by a single, stable fixed point in the concentration phase space, as this formally already represents a localisation in the concentration phase space. However, it should be noted that, in general, signalling pathways with non-linear reactions cannot be characterised by a single stable fixed point in the concentration phase space. This is consistent with the altered fixed points observed in section 2.7.2 and Fig. 2.9.

We find that there are certain parameter regimes in which organelle fusion and fragmentation have, admittedly, little effect on the kinetics of the response. We also discuss the plausibility of such a parameter regime in the context of apoptotic signalling, as we discuss, in particular, the response to strong apoptotic stimuli shown in Fig. 3.9 (a). On a heuristic level, we suggest that organelle dynamics can significantly impact the kinetics of signalling pathways when macroscopic concentration changes occur on a timescale similar to or longer than organelle dynamics. This in particular the case as we consider weak, sub-lethal apoptotic stimuli [153, 155]. To further understand the influence of timescales on chemical reactions, it is instructive to consider the effective Bax model with an absorbing boundary condition at the potential barrier. In this context, macroscopic concentration changes correspond to the stochastic escape rate from the potential well, as depicted in Fig. 3.11 (b). As demonstrated in appendix A.5, the interaction potential can be directly related to a modification of the effective potential barrier. This allows us to evaluate the strength of the interaction potential as a perturbation on the stochastic escape rate.

As rule of thumb, we find that organelle dynamics can qualitatively suppress the stochastic response when the rate of organelle fusion and fragmentation is faster than the rate of escape from the potential well. In this context, it is instructive to consider organelle fusion and fragmentation as perturbations that reset organelles back to the bottom of the potential well and thus inhibit escape events. Although the molecular dynamics of relaxation within the potential well may be fast compared to the rate of organelle fusion and fragmentation, the relevant timescale for chemical reactions is Kramer's escape rate, which may be slower than organelle dynamics and thus let organelle dynamics play a significant role in the response.

The parameter regimes for the application of the effective equation of motion for collective organelle dynamics in Eq. (2.73) are restricted by the explicit assumption that s in Eq. (2.73) is small compared to macroscopic concentration changes. This effectively sets the timescale of macroscopic concentration changes and the effective interaction potential at the same order of magnitude, $\vec{F}_{\eta(t)} \sim \phi[f(\vec{c}, t)]$. However, note that this choice of parameters reflects a physiological situation. Note that the time-scale or experimental concentration changes is estimated on the timescale of ~ 10 min [161, 162] with mitochondrial fusion and fission dynamics happening on timescales $\sim 2-20$ min [61, 62, 148]. While this may seem like a slow timescale for chemical reactions, note that the binding process requires the insertion of the protein's transmembrane domain into the lipid bilayer of the outer mitochondrial membrane; A molecular process that involves crossing potential bar-

3. Application to multi-scale fluctuations in the regulation of cell death

riers at the molecular scale. This heuristic explanation for the observed slow timescales further suggests that our analysis may be well-suited for the study of organelle-associated signalling pathways in which translocation and binding to a membrane-enclosed organelle are central steps in the pathway.

Additionally, the experimental evidence presented in sections 3.7 supports the idea that mitochondrial dynamics can affect the kinetics of the apoptotic signalling pathway. Based on this, we conclude that it is plausible that a separation of timescales may not be generally applicable when analysing the kinetics of organelle-associated signalling pathways. However, it is important to bear in mind that we made certain assumptions in deriving the effective model and that it is always necessary to carefully verify that these assumptions are satisfied when applying the model to specific systems. It may also be necessary to refine the modelling assumptions in certain cases. In section 3.9, we will next discuss the extent to which the qualitative findings we made in the context of apoptotic signalling may be instructive for other organelle-associated signalling pathways. Before doing so, we will briefly discuss the potential therapeutic implications of our qualitative findings.

3.8.2. Potential therapeutic strategies for facilitating and mitigating apoptosis by mitochondrial dynamics

The control of apoptosis is of fundamental therapeutic importance in cases ranging from treating genetic dispositions resulting in the misregulation of the apoptotic signalling pathway, the mitigating of strokes, and in increasing the efficiency and mitigating of the side effects of cancer treatments [170, 171]. Here, we discussed mitochondrial morphology and mitochondrial dynamics as potential control parameters to suppress or facilitate cell death. As notably the mitochondrial morphology and dynamics are strongly affected by the metabolic environment of cells [172], manipulation of mitochondrial dynamics represents a potential orthogonal target for biochemical drugs that may increase the efficiency, sensitivity, and specificity of treatments. In the following, we briefly speculate on potential implications for therapeutic application.

The connection between the mutation of mitochondrial proteins, their functional importance, and the symptoms they cause in the context of genetic diseases affecting mitochondria is often phenomenological in nature [173]. To investigate links between mutations and their functional effects, and to target mitigating the symptoms of mitochondrial diseases, the investigation of mitochondrial dynamics may provide an invaluable means of elucidating such correlations. In the context of stroke, altering mitochondrial dynamics to increase fusion is a potential strategy to limit the regions affected by stroke [174]. This approach may be especially advantageous, as the vascular system in the brain restructures its transport dynamics in response to ischaemia, whereby strokes transiently stress cells in a wider neighbourhood. Furthermore, in regards to cancer therapies, the analysis of mitochondrial dynamics may offer a target for the analysis of personalised treatments [175]. In such cases, the measurement of mitochondrial dynamics could provide instructive insights into how cancer treatments could be metabolically supplemented to improve their efficacy and reduce their side effects. While the therapeutic applications based on qualitative findings remain purely speculative, we conclude that organelle dynamics, in general, are a highly promising research area with as-yet-unappreciated potential. Consequently, we suggest that further experimental and modelling efforts should be undertaken to translate conceptual insights into practical applications.

3.9. Discussion on quasi-particle kinetics in signalling pathways beyond apoptosis

In a previous section, we illustrated how organelle dynamics influence the kinetics of organelle-associated signalling pathways in the context of the intrinsic apoptotic pathway involving Bcl-2 proteins. In this section, we will explore selected examples of how the kinetics deviate from the dynamics of the intrinsic apoptotic signalling pathway. Specifically, we will examine the metabolic regulation of oxidative species by the oxidative phosphorylation pathway (OXPHOS), the metabolic regulation of the activity of the mammalian target of rapamycin complex 1 (mTORC1) on lysosomes, the organization of Rab proteins on endosomes, and the regulation of cellular anti-viral inflammation responses by the pathway centred around mitochondrial anti-viral signalling proteins (MAVS).

3.9.1. Application to the regulation of oxidative phosphorylation

Oxidative phosphorylation is one of the two main metabolic pathways in eukaryotes, with the other pathway being glycolysis [176]. Energy is produced through the oxidation of nutrients by respiratory enzymes of the eukaryotic electron transport chain located on the inner membrane of mitochondria. The process of respiratory energy production is referred to as oxidative phosphorylation (OXPHOS) [64]. In addition to the synthesis of adenosine triphosphate (ATP), oxidative phosphorylation produces reactive oxygen species (ROS), such as superoxide or hydrogen peroxide, which act as free radicals and cause cellular damage through their non-specific reactions with other biomolecules. The central challenge for oxidative phosphorylation is balancing ATP synthesis with the production of ROS. To this end, the respiratory chain consists of a series of complexes that allow for the consumption of synthesized ATP to reduce the amount of ROS produced. [64, 65, 177] demonstrated that the reaction network centred around complex III of the respiratory chain can operate in two different modes, which differ in whether ATP is consumed and ROS production is reduced or the yield of ATP synthesis is increased. In particular, the concentration of succinate in mitochondria was shown to be a bifurcation parameter, and bistable regions and hysteresis were experimentally measured. This suggests a qualitative similarity to the apoptotic signalling pathway discussed in section 3.4.

Similar to the apoptotic signalling pathway, the oxidative phosphorylation pathway is located in mitochondria that are subject to ongoing fusion and fragmentation dynamics. Note that we presented the effective bistability of Bax membrane concentration on mitochondria as a central prerequisite for sigmoidal response kinetics. Based on this, we would expect to see analogous kinetics in the metabolic regulation of oxidative phosphorylation. In particular, we expect that mitochondria will synchronize their metabolic function in response to altered environmental conditions that demand increased ATP synthesis. We expect that an orchestrated response can increase the efficiency of intracellular energy production. To date, the role of mitochondrial fusion and fission in the adaptability of aerobic metabolism has not been experimentally examined. Based on our theoretical investigations, we suggest that focusing on mitochondrial dynamics may be a potential target for the treatment of metabolic misregulation and aberrant ROS production, with potential applications ranging from the control of ageing to the reduction of carcinogenic potential.

3.9.2. Application to the regulation of protein synthesis (mTORC1 pathway)

The mammalian target of rapamycin complex 1 (mTORC1) is a central regulator of cellular protein homeostasis, growth, and proliferation through its mediation of protein translation [66]. As such, the regulation of the activation and deactivation of mTORC1 is crucial for the proliferative fate of cells. A key step in the activation of mTORC1 is its translocation to lysosomes and its complex formation with the protein Rheb, which also localises on the lysosomal membrane [67, 178].

Similar to mitochondria, lysosomes are intracellular, membrane-enclosed organelles that organize central metabolic processes within their interior and serve as signalling platforms on their membrane. In layman's terms, the interior of lysosomes is associated with the cellular waste disposal system, as it is enriched with hydrolytic enzymes that break down and degrade a wide variety of biomolecules. Similar to mitochondria, lysosomes are constantly undergoing cycles of fusion and fragmentation [179] and are therefore highly dynamic organelles. On their membrane, lysosomes serve as the signalling hub for the mTORC1 pathway. In particular, the translocation of inactive mTORC1 from the cytosol to the lysosomal membrane is a well-accepted prerequisite for the activation of mTORC1 [67, 178]. On the lysosomal membrane, the complex formation with the GTP-binding protein Rheb is the central step in mTORC1 activation. The concentration of monomeric Rheb proteins, in turn, is controlled by the localization of the Tuberous sclerosis complex (TSC) on the lysosomal membrane [178, 180, 181]. The formation and translocation of the TSC complex is controlled by a variety of different cellular signals, including growth factor availability, amino acid abundance, oxidative stress prevalence, and the prevalence of stress granules [181]. The dynamics controlling TSC complex formation and membrane translocation kinetics is subject to current research and have not yet been conclusively elucidated by experiments. Note that the existence of positive feedback loops has been speculated on by independent studies [181–183]. A positive feedback loop would be the prerequisite for bistability in the binding dynamics [184].

Yet, a bistable switching mechanism analogous to the accumulation of Bax on mitochondrial membranes has not been investigated in the context TSC accumulation on lysosomal membranes so far. We thus can not conclusively predict analogous response kinetics in the context of the regulation of the mTorc1 pathway. Furthermore, the role of lysosomal dynamics has not been discussed for the regulation of mTorc1 activity, yet. Our theoretical investigations suggest that lysosomal dynamics might be a central element to affect mTorc1 regulation and we suggest experimental investigations.

3.9.3. Application to endosomal maturation

Endosomes are part of the endocytic membrane transport pathway that enables the transport of molecules from the plasma membrane or the trans-Golgi network to lysosomes [185]. Like lysosomes, endosomes are organelles enclosed by a single membrane and undergo frequent dynamics of fusion and maturation. The maturation of endosomes is particularly associated with a switch from the accumulation of Rab5 proteins on early endosomes to Rab7 protein accumulation on late endosomes [73, 186]. In addition, feedback between the Rab concentration composition on endosomes and their fusion dynamics has been suggested [186]. While the transition from Rab5 accumulation to Rab7 accumulation has been discussed in the context of a bistable situation, the feedback of the Rab membrane concentration with endosomal dynamics is expected to introduce additional

dynamic effects compared to the response kinetics observed in the context of apoptotic signalling. A further central difference to mitochondrial dynamics is the central importance of endosomal synthesis and degradation/fusion with lysosomal vesicles. This demands the explicit accounting for birth and death terms in the context of the population balance equation in Eq. (2.55). The specific boundary conditions and feedback with the endosomal maturation process might lead to the suppression of the ensemble localisation in phase space. As consequence, we do not expect to find the analogous response kinetics for the endosomal maturation pathway as we presented for the apoptotic signalling pathway. Nonetheless, we speculate, that a profound analysis of the endosomal dynamics in the framework of Eq. (2.55) with an explicit accounting for the fusion flux approximation in equation (2.56) might provide new insight in endosomal signalling dynamics.

3.9.4. Application to cellular innate immune signalling (MAVS pathway)

In section 3.2.3.1, we have extensively discussed the outer mitochondrial membrane as a hub for the signalling pathway involved in apoptosis. In addition to its role in apoptosis and metabolic regulation, the outer mitochondrial membrane is also a central hub for immune signalling [57]. The Rig-I signalling pathway detects double-stranded viral mRNA in the cytosol of cells and ultimately leads to the synthesis of NF- κ B, a transcription factor that initiates cellular inflammation responses [187]. Central to the Rig-I signalling pathway is the accumulation of mitochondrial anti-viral signalling proteins (MAVS) on the outer mitochondrial membrane into large aggregates, which serve as platforms for the IKK complex that synthesizes NF- κ B [188]. In contrast to the accumulation of Bax proteins into homo-oligomers during apoptotic signalling, MAVS complexes are estimated to be much larger [189, 190] and no translocation of MAVS to the mitochondrial membrane has been observed experimentally. Unlike Bax, MAVS is considered to only exist in an active form that is steadily localised on the mitochondrial membrane [191, 192]. It is speculated that the aggregation dynamics of MAVS are catalyzed by Rig-I bound to viral RNA [187]. No bistability for the MAVS membrane concentration has been observed, yet.

A central aspect of the molecular dynamics considered in Eq. (2.55) is the mapping of the chemical reaction dynamics of the signalling pathway onto a set of effective coupled stochastic differential equations. This formalism is particularly suited for describing chemical reaction dynamics that are subject to steady binding and unbinding from a membrane, such as the translocation dynamics of Bax to the mitochondrial membrane. In contrast, the central dynamics of MAVS complex formation are the intricate reversible aggregation dynamics, which require the careful treatment of correlated noise in the framework introduced in section 2.2.1, while tracking the dynamics in the high-dimensional aggregate size distribution space. As introduced in section 1.3, this suggests the treatment of MAVS signalling in the context of closed systems rather than effective dynamics in open systems, as presented here in chapter 3 for the apoptotic signalling pathway and Bax translocation kinetics. As a result, we expect different kinetics for the signalling pathway. We will extensively study the dynamics of the MAVS signalling pathway in chapter 5 after generally discussing an effective description of the effects of compartment dynamics in closed systems in chapter 4.

3.10. Conclusion

In this chapter, we have explored the application of the quasi-particle described in chapter 2 to organelle-associated signalling pathways. We focused particularly on the intrinsic apoptotic signalling pathway within cell death decision-making. We found that mitochondrial fusion and fragmentation can suppress the system's response to weak, transient stress perturbations, yet facilitate the response to persistent stress perturbations, see section 3.4. By this, the mitochondrial dynamics act as a kinetic low-pass filter on stress fluctuations, see section 3.5, and lead to improved quality of apoptotic decision-making, see section 3.6. Although we cannot track the motion of the quasi-particle experimentally, we argued in section 3.7.3 that the sigmoidal response kinetics are unaffected by pre- and post-modifications in the apoptotic signalling pathway. Our predictions were corroborated by experiments performed by our experimental collaborators Philipp Mergenthaler and Lina Hellwig. Our findings suggest that the rate of mitochondrial fusion and fragmentation allows cells to regulate to what degree stress fluctuations are suppressed. In this context, it is interesting to note that the timescale of mitochondrial dynamics has been observed to depend on the metabolic conditions of the cell [60, 138, 172]. It is interesting to speculate that by this cells could adjust their proneness to cell death to the availability of nutrients.

We have previously discussed the plausibility of our findings in this chapter in section 3.8, with particular emphasis on the timescale of the Bcl-2 reaction kinetics and the timescale of mitochondrial dynamics. In addition, we have considered the potential implications of our findings on therapeutic approaches. In section 3.7, we have presented cumulative evidence that suggests our theory correctly predicts quasi-particle kinetics in organelle-associated signalling pathways, though the experimental evidence is yet inconclusive. In this context, we suggest that experimentally manipulating mitochondrial dynamics could serve to verify our predictions. Moreover, in section 3.9, we have discussed the direct translation of our findings of the intrinsic apoptotic signalling pathway to other signalling pathways.

In this chapter, we did not attempt to model the dynamics of organelle-associated signalling pathways but have instead sought to determine the effects of organelle dynamics on the response kinetics, with a particular emphasis on the qualitative effects of organelle fusion and fragmentation. We highlighted the importance of considering both the timescale of organelle dynamics and the timescale of macroscopic concentration changes when it comes to signalling pathways. Furthermore, we suggest that strong, orchestrated responses may be of biological relevance, and that organelle dynamics should be considered as a central factor in understanding the kinetics of organelle-associated signalling pathways. We acknowledge that organelle dynamics have further levels of regulation, which we did not account for in our theoretical approach. Yet, we argue that our findings nonetheless have a significant impact on the dynamics of organelle-associated signalling pathways and we propose organelle dynamics as central players to understand the kinetics of organelle-associated signalling pathways. We propose that future experimental research focused on assessing the biological function of organelle dynamics may provide a fruitful avenue for identifying novel therapeutic strategies.

4. Towards a thermodynamics of closed compartmentalised systems

4.1. Introduction

The Encyclopedia Britannica defines thermodynamics as the "science of the relationship between heat, work, temperature, and energy" [193]. Thermodynamics was initially developed to study the performance of steam engines and is thus primarily concerned with macroscopic observables [21]. Yet, in order to determine the general applicability of the concepts of work, temperature, and energy to other systems, it became necessary to understand the relationship between thermodynamics and the microscopic dynamics of the constituting elements that form a physical system. This, however, constitutes a significant challenge, as the analysis of systems with many interacting constituents becomes impractical due to the large number of terms generated by interactions among individual constituents. Statistical physics was instrumental in providing a bridge between macroscopic thermodynamics and microscopic dynamics, particularly through the analysis of the thermodynamics of gases using statistical methods [6]. Besides contributing to the development of more efficient engines, thermodynamics has been applied to the analysis and optimization of chemical reactions and is now a fundamental aspect of physical chemistry [194]. In the 20th century, the concept of thermodynamics was expanded to include the relationship between entropy and information content [195]. Based on this concept, and motivated by the goal of estimating the energy budgeting of engines, thermodynamic theories experienced a renaissance in the field of biological physics as biological systems, particularly cells, were interpreted as *biological engines*. This yielded the question if the energy consumed by living systems can be linked to the work they perform, including both mechanical work and information processing. As biological systems inherently operate out of equilibrium, theories need to be extended to capture non-equilibrium thermodynamics. Undoubtedly, deriving a general theory of non-equilibrium thermodynamics in the context of biological systems is a challenging task. However, the analysis of biologically inspired systems from the perspective of statistical physics offers a promising approach to expanding our understanding of non-equilibrium thermodynamics.

In the chapters 2 and 3, we have demonstrated the emergence of a collective degree of freedom in *open* compartmentalised stochastic systems arising from the interplay between stochastic particle dynamics and compartment fusion and fragmentation. The ensuing dynamic degree of freedom is reminiscent of quasi-particles and it gives rise to a kinetic low-pass filter on cellular stress fluctuations in the context of apoptotic decision-making. The phenomenology of *closed* compartmentalised systems, in which we impose mass conservation both on the level of the stochastic many-body dynamics as well as on the level of the compartment mass, differs fundamentally from the dynamics of open compartmentalised systems. In chapter 2 we found that the emergence of the quasi-particle resides on compartment fusion and fragmentation dynamics that effectively counteract the dispersive dynamics in the concentration phase space induced by the contact to a particle bath.

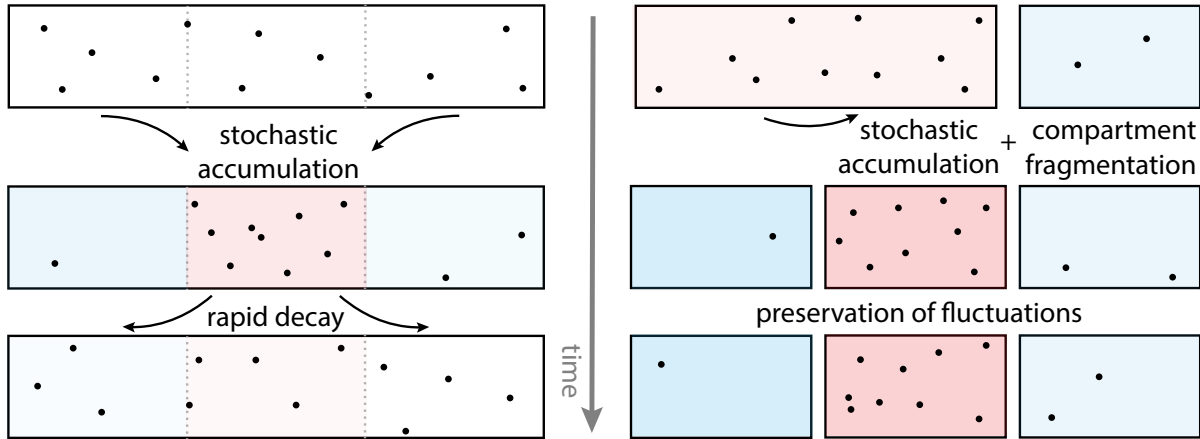


Fig. 4.1.: Schematic of how dynamic compartmentalisation gives rise to the creation and preservation density fluctuation A fully-connected system (left) is contrasted with a system subject to compartment fusion and fragmentation dynamics (right). The fluctuations between compartments are illustrated by density fluctuations, with areas of above-average density being coloured red and below-average density being coloured blue. These fluctuations arise spontaneously as a result of the stochastic movement of particles. In a fully-connected compartment system, density fluctuations rapidly dissipate. However, in a system subject to compartment fragmentation, density fluctuations are preserved until the next compartment fusion event occurs. Do compartment fusion and fragmentation by this change the statistics of the realised system states?

As we prohibit contact with a particle bath, fluctuations between compartments are fully dictated by the compartment dynamics. As detailed out in section 2.4.3, the fluctuations induced by compartment fragmentation play a dominating role in the dynamics of closed compartmentalised systems. We will demonstrate in this chapter, that the effects of compartment dynamics on macroscopic properties thus depend on the kinetic details of the stochastic many-body dynamics. Thermodynamics provides a general set of observables, such as work and entropy, that elucidate the macroscopic properties of both equilibrium and non-equilibrium systems. For example, in chapter 2 the characterising phenomenology was a localisation of probability distributions in phase-space. The concept of entropy provides a general quantification of the effect that dynamic compartmentalisation has on the microscopic degrees of freedom.

Focusing on closed compartmentalised systems we evoke a central difference regarding the statistics of fluctuations among the *open* and *closed* compartmentalised system: In *closed* compartmentalised systems, compartment fusion and fragmentation give rise to the creation and preservation of fluctuations among the compartments. This is exemplified for density fluctuations in Fig. 4.1. In this example, the stochastic spatial dynamics of particles give rise to the spontaneous accumulation of particles, which manifests in density fluctuations. While density fluctuations rapidly decay in connected systems, the fragmentation of compartments preserves the density fluctuations until the next compartment fusion event occurs. The new constraints within a compartment cause the enclosed dynamics to relax into a new steady state, which in turn affects the statistics of density fluctuations. In this chapter, we investigate how this mechanism alters the statistics of the realised system states and thus the total entropy of the system. Specifically, we examine

whether we can assign a notion of work to processes of compartment fusion and fragmentation. In the following chapter 5, we will further explore how our findings contribute to our understanding of cellular immune responses to RNA virus infections.

We start this chapter by providing a brief literature review on the statistical physics of dynamic compartmentalisation, with a specific focus on the insertion and removal of partitions in isolated systems. We then introduce a scheme that we term *Gergesian demons*, which enables us to study a wide range of stochastic microscopic dynamics enclosed in dynamic compartments, and allows us to deepen and challenge our understanding of the thermodynamics of multi-scale systems. As a next step, we specify the enclosed microscopic dynamics as a stochastic version of the ideal gas to gain intuitive mechanistic insight. Based on our findings, we ask how widely applicable insight gained from studying the ideal gas is to arbitrary stochastic many-body dynamics enclosed in dynamic compartments. To generalise to stochastic many-body dynamics, we utilise the powerful formalism of the Second quantisation. We demonstrate that a simple operator condition can be used to assess the strength by which compartment fusion and fragmentation affect the total entropy. Specifically, this allows for the assessment of whether compartment fusion and fragmentation affect the total entropy by performing a simple algebraic calculation, without the need to analytically solve or numerically simulate the system. We discuss our findings in the context of the scheme of "Gergesian demons" and exorcise thermodynamic inconsistencies by identifying the subtle notion of how compartment fusion and fragmentation performs work on systems. We conclude the chapter by discussing the technological and biological relevance of our findings. This work was developed in collaboration with Rushikesh Shinde, whose Master's thesis I co-supervised. Rushikesh Shinde particularly worked on how an ideal gas is affected by dynamic compartmentalisation.

4.2. Literature review on the thermodynamics of compartmentalisation

In this section, we introduce several thermodynamic concepts that we will frequently employ in this chapter. We maintain a close connection with the historic foundations of thermodynamics to provide guidance on the thermodynamic properties of multi-scale systems that we wish to investigate. Inspired by organelles, we focus on compartments enclosing internal dynamics and consider the thermodynamic implications of modifying these compartments, with a particular focus on compartment fusion and fragmentation.

As mentioned in the previous section, the development of statistical physics and thermodynamics is closely tied to the study of gases enclosed in compartments. Since the early days of thermodynamics, operations manipulating compartments show as conceptual challenges and led to a number of significant insights that deepened our understanding of thermodynamics. To gain insight into the thermodynamics of dynamic compartmentalisation, we revisit the historic advances that were achieved by externally modifying compartments through the insertion and removal of partitions. Next, we discuss the concepts of entropy and reversibility, Gibbs' paradox, and Maxwell's demon.

4.2.1. The definition of entropy

Compartment fusion and fragmentation result in the creation and preservation of density and energy fluctuations among compartments. As the stochastic many-body dynamics

4. Towards a thermodynamics of closed compartmentalised systems

enclosed in the compartments relax to new steady states, we expect compartment dynamics to directly affect the statistics of the realised system states. In this subsection, we review some definitions of entropy to the extent necessary to investigate the thermodynamics of systems subject to dynamic compartmentalisation. Despite its importance to thermodynamics and statistical physics, entropy is an abstract quantity. This has led to debates about the correct definition of entropy in the early days of thermodynamics, which continue to this day for specific systems [196–198]. After providing a formal definition of entropy, we demonstrate, using a small example system, how the Gibbs-Shannon entropy is particularly well-suited for assessing dynamic compartmentalisation systems.

The Encyclopedia Britannica defines entropy as "the measure of a system's thermal energy per unit temperature that is unavailable for doing useful work" [199]. While this definition does not provide a formal, mathematical definition of entropy, it highlights the practical purpose of entropy in the context of steam engines. This definition is also useful in the motivation to study the thermodynamics of biological systems, as we are interested in the functioning of *biological engines*. Conceptually, this definition lays the groundwork for a fundamental definition of entropy through the second law of thermodynamics, which, in Planck's version, reads [200]:

Every process occurring in nature proceeds in the sense in which the sum of the entropies of all bodies taking part in the process is increased. In the limit, i.e. for reversible processes, the sum of the entropies remains unchanged.

This statement formally defines entropy by its functional purpose. The second law states that not all conceivable processes are realisable in physical systems. For example, heat will only flow from a hot to a cold object. The change in entropy is the quantity that determines whether a process can only occur in a forward temporal direction (irreversible) or in both forward and backward directions (reversible). While the total entropy of all bodies involved in a process increases for irreversible processes, the entropy of individual bodies (subsystems) is allowed to decrease. This implies that bringing a system back to its initial state - i.e., the state before the process started - requires the exertion of work on the system for irreversible processes. As a small corollary, this also implies that cyclic processes must show no change in entropy between the different states of the cycle.

While this verbatim definition of entropy gives precise information about the desired function of entropy, it does not provide information on how entropy is connected to the dynamics of systems. There are several competing formulations of entropy, which can be evaluated for their thermodynamic consistency through reconciliation with the laws of thermodynamics, particularly the second law. Here, we focus on the formulations of Ludwig Boltzmann and Josiah Gibbs, who made significant contributions to the development of general laws linking statistical physics with the desired function of entropy in a thermodynamic context. It is worth noting that both definitions result in different entropies for small systems, which we will discuss in more detail after formally defining the Boltzmann and Gibbs entropies.

To define the Boltzmann and Gibbs entropies, we introduce the concept of microstates and macrostates of statistical ensembles, cf., for example, [201]. A microstate is a specific microscopic configuration of a thermodynamic system, while the macrostate of a system refers to the macroscopic observables of an ensemble. Several microstates belong to the same macrostate if they yield identical macroscopic observable values upon measurement. We postulate that the microstates belonging to a macrostate are indistinguishable. Let A be the set of different macrostates $a \in A$. The macrostate a can be in $W(a)$ possible configurations, denoted by $i_a = 1, \dots, W(a)$. We call $W(a)$ the multiplicity of the macrostate

4.2. Literature review on the thermodynamics of compartmentalisation

a. We postulate that all configurations i_a have the same probability $p_{i_a} = p(a)$. Therefore, the probability of a macrostate is given by $P(a) = W(a)p(a)$. The Boltzmann entropy of a macrostate is

$$S_B = \log(W(a)), \quad (4.1)$$

while the equivalent definition for the system's entropy is the average Boltzmann entropy [21, 201]

$$\bar{S}_B = \sum_a P(a) \log(W(a)). \quad (4.2)$$

In contrast, Gibbs' definition of entropy is given on the basis of probability distribution of microstates [21, 201]

$$S_G = - \sum_i^n p_i \log(p_i), \quad (4.3)$$

where the index i runs over all microstates of the system and p_i as defined above¹. As Gibbs' definition of entropy shares the same functional form as Shannon's definition of the information content of a message, the definition of the entropy above is often referred to as Gibbs-Shannon entropy. Notably, the Gibbs-Shannon entropy demands knowledge about the microscopic dynamics and measurements of microstates. However, precise measurements of the microstates cannot be accessed for all systems.

While both the Gibbs entropy and the average Boltzmann entropy give estimates of the entropy of the system, the definitions are not equivalent. [201] showed that Gibbs-Shannon entropy can be recovered from the averaged Boltzmann entropy by account for the *entropy of fluctuations of the macrostates* :

$$S_G = \bar{S}_B - \sum_{a \in A} P(a) \log(P(a)). \quad (4.4)$$

Note, that this equality resides on the assumption that microstates summarised into a macrostate in the averaged Boltzmann entropy have the identical probability of occurring and hence the same weight in the Gibbs-Shannon entropy. We next illustrate with a simple example the difference between the averaged Boltzmann entropy and the Gibbs-Shannon entropy and learn important lessons on the choice of macro-states when turning to dynamic compartmentalisation later in this chapter.

Consider a simple system with total volume $V = 4V_0$ in which a single particle is enclosed. We now consider a cyclic process where we insert and remove partitions on two different positions. Specifically, we consider

- configuration *C1*: All compartments are connected
- configuration *C2*: A partition is inserted between compartments 2 and 3
- configuration *C3*: The partition is removed and all compartments are connected
- configuration *C4*: A partition is inserted between compartments 3 and 4,

¹Note, that in this formulation we can relax on the assumption $p_{i_a} = p(a)$.

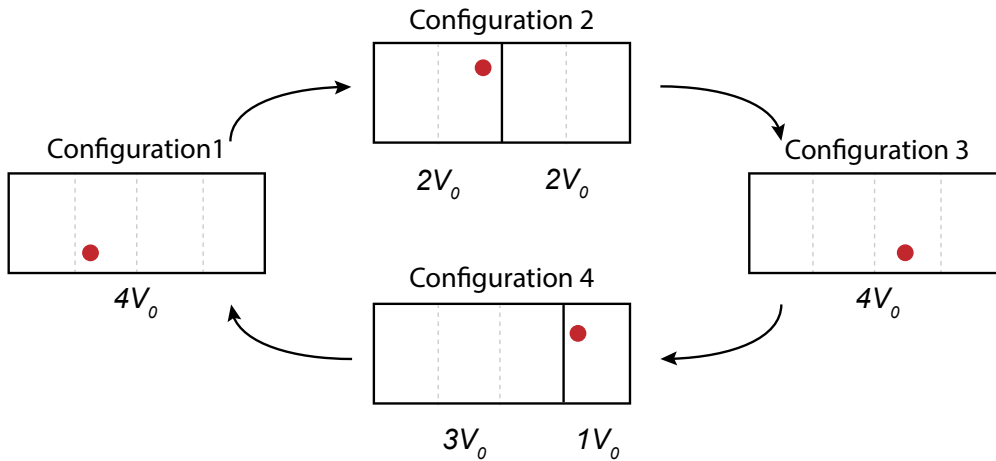


Fig. 4.2.: A single particle system subject to a cyclic process. By inserting and removing a partition in different places of an isolated system, a cyclic process is created. The insertion and removal of the partition performs no work on the system.

see also the illustration in Fig. 4.2. We now calculate the averaged Boltzmann entropy and the Gibbs-Shannon entropy in every state. Starting with the averaged Boltzmann entropy, we find

- $C1$: We only have one compartment with a multiplicity $W(a) = 4$. Hence, we have $\bar{S}_B = 1 \cdot \log(4)$.
- $C2$: We have two compartment with each a multiplicity $W(a_i) = 2$. Hence, we have $\bar{S}_B = 1/2 \log(2) + 1/2 \log(2) = \log(2)$
- $C3$: We only have one compartment with a multiplicity $W(a) = 4$. Hence, we have $\bar{S}_B = 1 \cdot \log(4)$
- $C4$: We have one compartment with a multiplicity $W(a_1) = 3$ and one compartment with $W(a_2) = 1$. Hence we have $\bar{S}_B = 3/4 \cdot \log(3) + 1/4 \cdot \log(1)$.

Note, that the average Boltzmann entropy is different for each state. This contradicts the definition of entropy as we have a cyclic process in which no work is performed on the system. However, we have considered different macrostates over the course of the cycle by considering different compartment volume distributions. The average Boltzmann entropy is sensitive to these inconsistencies in observable macrostates. If we calculate the Gibbs-Shannon entropy instead, we obtain the summation of the microstate probability: $S_G = -\sum_i^4 1/4 \cdot \log(1/4) = \log(4)$ for all states $C1, C2, C3, C4$. It is only by accounting for the entropy of fluctuations of the macrostates that we find that the average Boltzmann entropy is consistent with the second law. Importantly, the inconsistency in the average Boltzmann entropy in the above example arose due to switching the definition of macrostates between different configurations, as a result of varying volume distributions. This is a general pitfall to be aware of when studying entropy in the context of dynamic compartmentalisation. When we consider dynamic compartmentalisation later in this chapter, we will pay special attention to being consistent in the definition of macrostates by only comparing identical volume distributions.

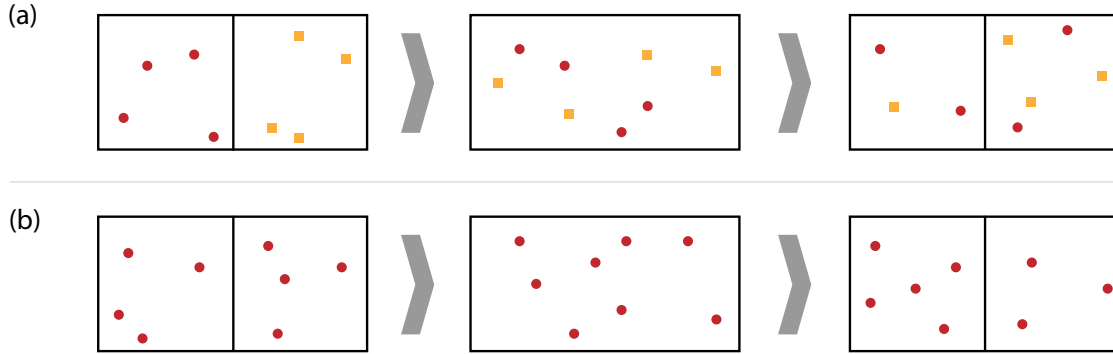


Fig. 4.3.: Illustration of Gibbs' paradox (a) Two distinguishable gases are separated in two subsystems. After removing a partition between the two compartments, the gases mix. Reinserting the barrier results in the creation of two indistinguishable subsystems. (b) Two indistinguishable gases undergo the same processes as in (a). While for (a) the initial and the final configuration differ, the initial and the final configuration appears identical for (b), though the same processes occurring for both (a) and (b).

4.2.2. Gibbs' paradox

The central motif of dynamic compartmentalisation is the separation and fusion of subsystems, as the thermodynamics of setting subsystems into contact and releasing them out of contact again is historically discussed in the context of Gibbs' paradox. Examining Gibbs' paradox provides us with direct insight on the thermodynamics of binary compartment fusion and fragmentation.

To understand Gibbs' paradox [202], we consider two isolated compartments, A and B, separated by an isolating partition. Both compartments contain an ideal gas, which is defined as a gas that exhibits no chemical reactions with itself, the other gas, or the walls of the compartments. The volume, pressure, and temperature of the gases in both compartments are identical. We refer to the two compartments as subsystems A and B, enclosing gas A and gas B respectively. As the partition between the two compartments is removed and the gases are allowed to mix, we will find that, in the thermodynamic limit, half of gas A will move to subvolume B and half of gas B will move to subvolume A. After this process, we can re-insert the partition, creating two separated subsystems once again. This process is illustrated in Fig. 4.3. If gas A from gas B can initially be distinguished, we will find that the two compartments are in a different configuration after the mixing process than they were before the partition was removed. The system's entropy has increased due to the mixing of the gases. However, if we cannot distinguish gas A from gas B, the two subsystems will appear unchanged from the initial configuration, and the system's entropy will not have changed, despite the fact that a mixing of the gases has occurred. This paradox is deeply connected to entropy being subjective to an observer. One observer might detect a change in entropy, while another observer finds no change, despite the fact that entropy is a state function of the system.

From a semantic perspective, Gibbs' paradox arises from a non-rigorous treatment of the concepts of reversibility and recoverability, and a flawed application of the concepts of macrostates. It is important to recall that macrostates are defined as containing several indistinguishable microstates. A vanishing mixing entropy for two indistinguishable gases

4. Towards a thermodynamics of closed compartmentalised systems

A and B does not imply that gas A and gas B are separated again in the two subsystems after the partition is re-inserted, as the concept of reversibility might suggest. As gas A and gas B are indistinguishable, the observer cannot assess if gas A and gas B are separated or mixed after the system is separated again. Both the initial state and the state after partition re-insertion are different *microstate*, but belong to the same *macrostate* for an observer who cannot distinguish gas A and gas B. A vanishing mixing entropy allows the system to visit different microstates, but only if all of these microstates belong to the same macrostate. It is possible that two different observers might consider different macrostates of the system and, as a result, measure the system's entropy differently. However, there is no paradoxical notion involved if the same measurement abilities are consistently applied and not intermixed when formulating the problem, as noted by [200, 203].

A more subtle understanding of the paradox emerges when considering Gibbs' thought experiment at a scale below the thermodynamic limit and taking into account the stochastic dynamics of a finite system, as noted by [21]. In this context, subsystems A and B differ after the partition is re-inserted. For the purpose of clarifying how Gibbs' paradox can be generalised to finite stochastic dynamics, we focus here on the configurational entropy, that is the distribution of indistinguishable gas particles between two subsystems A and B, while ignoring their energies. It is straightforward to extend this analysis to include energies as well. We assign two volumes, V_A and V_B , to the two subsystems and consider a total of N particles. We assume that the momentum and position of each particle are statistically independent and that the positions of any two particles, i and j , are also statistically independent. This implies that the probability of finding a particle in subvolume A is $p_A = V_A/(V_A + V_B)$. We define the number of particles in volume V_A as a macrostate describing the state of the system. The probability of finding the system in a specified state is given by

$$P(N_A, N - N_A) = \frac{N!}{N_A!(N - N_A)!} \left(\frac{V_A}{V_A + V_B} \right)^{N_A} \left(\frac{V_B}{V_A + V_B} \right)^{N - N_A}. \quad (4.5)$$

Note, that this binomial distribution fully defines the statistics of the system. Based on these statistics, we define an entropy, which takes above probability distribution as an argument to compute the entropy of the system, see for further explanations section 4.2.1. If we insert a partition between the two subsystems, we prevent the exchange of particles between them. However, as we are unaware of the state that the system is in when we insert the partition, the newly isolated system is also described by a probability distribution. In fact, the probability distribution for this case is equal to the probability distribution describing the system in the absence of the partition, as given by Eq. (4.5). As a result, both systems have the same entropy. [21] provides a further generalization of this argument, taking into account the energy of the particles as well. In the same work, he also presents a generalization to multiple compartments, where the binomial probability distribution is replaced by the multinomial distribution.

In summary, we find that inserting a partition into a system of non-interacting particles leaves the system's entropy unchanged, as the macrostate statistics are unchanged. However, it is important to note that the reverse process, namely bringing two systems into contact by removing a partition, generally increases the entropy. If we start from a specified initial configuration, the initial probability distribution is not given by a binomial distribution, as given by Eq. (4.5), but rather by a delta distribution. In this case, the macrostate statistics change, and the entropy increases.

For dynamic compartmentalisation systems, we conclude that we in general expect

changes in the systems' entropy when we allow for the fusing of compartments. We only expect the fusion of two compartments not to cause an increase in entropy, if the two fusing compartments are characterised before fusion with statistics that are identical to the compartments after the binary fragmentation of the compartments. We conclude that assessing the statistics of fragmented compartments is a central task when quantifying how compartment fusion and fragmentation *perform work* on dynamic compartmentalisation systems.

4.2.3. Maxwell's demon

Maxwell's demon is a striking example of a thought experiment that has troubled the scientific community over decades² [204]. James Clerk Maxwell formulated this thought experiment to challenge the concept of entropy. He considered two isolated compartments, both filled with an ideal gas at the same temperature, separated by an isolating wall with a small trapdoor built into it. When the trapdoor is closed, the wall is perfectly isolating. When it is open, it allows for the passage of individual particles. It is important to note that opening and closing the trapdoor performs no volume work on the system by definition.

Maxwell introduced an intelligent being that can observe and measure the velocity of every particle and is in control of the trapdoor [204]. This being allows the passage of particles that are faster than average from the left compartment to the right, and slower than average from the right to the left. In doing so, the being sorts the particles such that the right compartment increases in terms of the enclosed energy and therefore temperature, while the left compartment cools down, see Fig. 4.4 for an illustration. This results in a heat flux against the temperature gradient. Furthermore, the final configuration is different from the initial configuration. However, if the partition is removed and re-inserted in the final state, the system returns to its initial state while increasing the entropy, as discussed in the context of Gibbs' paradox. The sorted state hence shows a *decreased* entropy, while no *volume* work was performed on the system.

Maxwell constructed with his thought experiment a seemingly microcanonical system in which the entropy is increased without performing volume work on the system. This, however, contradicts the second law. Depending on one's point of view, Maxwell's thought experiment disproved the second law or hints towards an incomplete definition of entropy. Setting aside the question of the realisability of such a demonic system, the conceptual possibility of such a system exposed a major caveat in the connection between the statistical physics of gases and thermodynamics. Notably, the seminal work of Leo Szillard [205] and later Landauer [206, 207] *exorcised the demon*, [208, 209]. To this end, they linked the *lost* change in entropy to an increase of entropy of the demon as it performs measurements and creates memory when operating the trapdoor. By exorcising Maxwell's demon, they introduced the notion of information processing into the realm of thermodynamic theories.

Szillard's demon is a simplification of Maxwell's demon, as it involves a gas composed of a single particle [204, 205]. By inserting a partition in the middle of a compartment, the system is split into two asymmetric subsystems: one subsystem contains the particle, while the other subsystem is empty. Allowing the partition to move freely, the subsystem containing the particle expands while the empty subsystem shrinks until the empty

²Maxwell originally coined the term of an intelligent being. Yet, since *Maxwell's intelligent being* challenged the scientific community, Lord Kelvin coined the term of *Maxwell's demon* [204].

4. Towards a thermodynamics of closed compartmentalised systems

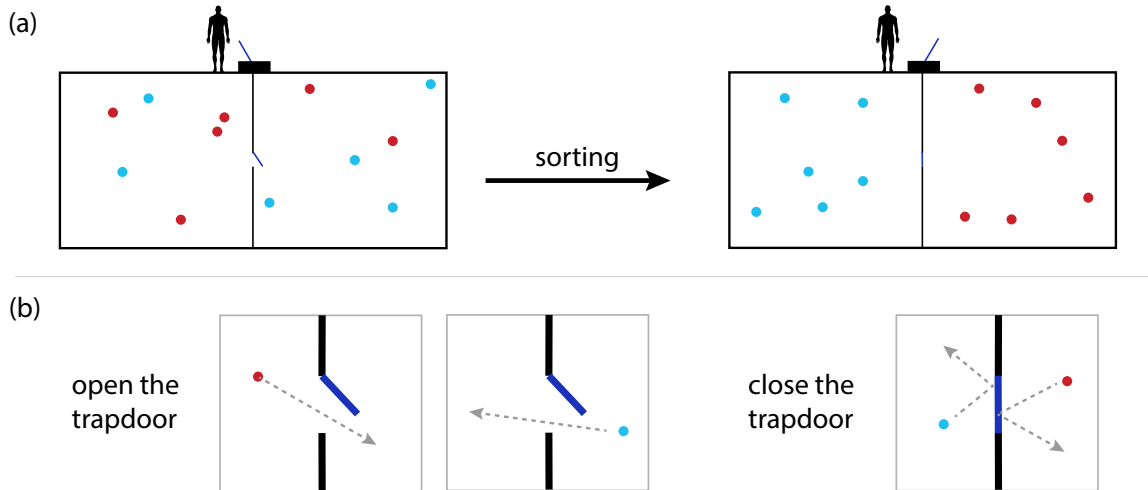


Fig. 4.4.: Schematic of Maxwell's demon. (a) Maxwell's demon performs sorting of hot and cold particles into separate subsystems by controlling a trapdoor. (b) Illustration of the trapdoor opening and closing policy.

subsystem disappears. At this point, the partition is moved to the walls of the formerly empty compartment. While the partition is moving, a weight attached to it can extract work from the system. However, in order to extract work, we need to know in which direction the partition will be moving so that the weight can be attached to the correct side of the partition. This requires measuring the system after inserting the partition and memorizing this measurement. This suggests a strong connection between the information gained from the system and the extractable work. The key insight that "exorcises the demon" is that the system is not in the same position at the end of the "cycle" as it was at the beginning: the memory created in the measurement process still exists. Landauer's erasure principle states that every bit of information erasure costs $-k_B T \log(2)$ [206, 207], which is equal to the amount of work extractable from one cycle.

By now, several generalisations of Szilard's demon has been studied including extensions to N -particle systems and q partitions [210]. Notably, these generalisations only consider particle number fluctuations and demand the intermediate contact to heat baths as well as the synchronous insertion of partitions. In more general terms, in the recent literature several types of thermodynamic demons are distinguished, such as Maxwell's demon [211], Szilard's demon [210], or gambling demons [212]. We refrain from a detailed discussion of thermodynamic demons but instead refer to a vast literature on these systems [204, 210–214].

In summary, the study of demons³ can be useful in challenging our understanding of thermodynamics. To this end, it is helpful to consider a conceptual definition of demons: thermodynamic demons appear as paradoxical outcomes of protocols applied to systems that seemingly contradict the second law of thermodynamics. These paradoxes highlight limitations in our thermodynamic and statistical physics theories, challenge our intuition about thermodynamic systems and reveal imprecise and superficial formulations in our theories. As a result, studying thermodynamic demons can deepen our understanding of the physical laws and symmetries that shape our reality.

³It should be emphasised again that the author of this thesis does not believe in the existence of either supernatural or thermodynamic demons.

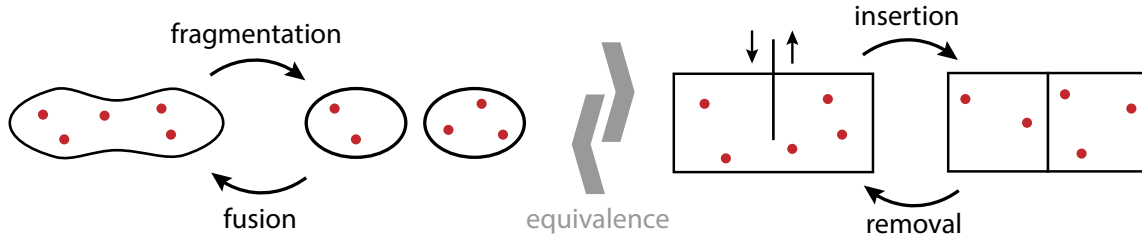


Fig. 4.5.: Schematic illustration of the equivalence of dynamic compartmentalisation and partition insertion and removal

4.3. Model definition: How compartment dynamics induce temporal ordering

Building upon the concepts introduced in the literature review in section 4.2, we aim to describe the thermodynamics of compartmentalised systems. In this section, we will establish the formal basis for this investigation. We begin by investigating the link between dynamic compartmentalisation and modifications of system boundaries, focusing on how compartment fusion and fragmentation can be linked to the insertion and removal of partitions. Next, we will use this analogy to investigate how dynamic compartmentalisation introduces a notion of temporal order in multi-scale systems. Specifically, we will consider a simple scheme that allows us to rigorously determine the extent to which we need to adjust our thermodynamic concepts when studying multi-scale systems subject to dynamic compartmentalisation. There, we also explicitly state the research question we investigate in this chapter 4.

4.3.1. The connection between dynamic compartmentalisation and the modification of system constraints

As discussed in section 1.3, dynamic compartmentalisation is inherently a multi-scale setup, as it involves dynamics on two different spatial scales. On a mesoscopic level, we define compartments that change over time, enclosing microscopic dynamics that stochastically evolve inside them. Most generally, we consider stochastic many-body dynamics as being enclosed in dynamic compartments. The two central assumptions of our approach are that the microscopic dynamics in separated compartments evolve independently of each other and that the microscopic dynamics are independent of the spatial coordinates of the compartment. We next study the compartment dynamics in the context of a thermodynamic framework.

From the perspective of an individual compartment, changing the compartment changes the constraints placed on the microscopic dynamics enclosed within it. This can be best illustrated by assuming that each compartment is a perfectly isolating box enclosing a gas, such that each compartment is a microcanonical ensemble characterized by the compartment volume, number of gas particles, and total energy of the gas particles. Some compartment dynamics, such as compartment growth, change the volume. It is clear that this process performs volume work on the enclosed microscopic dynamics. As discussed in section 2.2.2, there are many different compartment processes, including compartment growth and shrinkage, changes in compartment shape, compartment creation and annihilation, and compartment fusion and fragmentation.

4. Towards a thermodynamics of closed compartmentalised systems

While the thermodynamic implications of processes such as compartment volume changes and compartment creation and degradation can be directly assessed in terms of work performed or energy injected into the system, the processes of compartment fusion and fragmentation require more careful consideration. To this end, we make a conceptual link between compartment fusion and fragmentation and the removal and insertion of partitions into a system, as illustrated in Fig 4.5. Both compartment fusion and fragmentation, as well as partition insertion and removal, are binary processes involving two compartments. For both compartment fusion and partition removal, two previously separated compartments are brought into contact, allowing particles of the enclosed microscopic dynamics to freely interact with each other and be exchanged between the two compartments. Conversely, for compartment fragmentation and partition insertion, two compartments previously in contact are separated, such that the enclosed microscopic dynamics evolve independently of each other upon separation.

Here, we assume that both the fusion and fragmentation of compartments are instantaneous processes, as well as the insertion and removal of partitions. A notable difference is that partition insertion maintains the spatial position of compartments, which is not necessarily the case for compartment fragmentation. However, the microscopic dynamics are independent of the spatial coordinates of the compartment. The compartments can be separated by partition insertion and subsequently spatially separated with no effect on the enclosed microscopic dynamics within the partition. The compartments can also be spatially moved after partition insertion, similar to compartment fragmentation. However, the spatial position of compartments becomes important in the context of which compartments are allowed to fuse. In the remainder of this chapter, we make the approximation that compartment fusion and fragmentation is equivalent to partition insertion and removal.

As discussed in the context of Gibbs' paradox, the insertion and removal of partitions demand careful thermodynamic analysis. While in the context of Gibbs' paradox, a binary situation with two compartments is discussed, we want to study an arbitrary number of compartments in the context of dynamic compartmentalisation. When we study the thermodynamic effects of dynamic compartmentalisation in the remainder of this chapter, we put an exclusive focus on compartment fusion and fragmentation, which we consider the hallmarks of dynamic compartmentalisation. We will briefly touch on other compartment dynamics again in section 4.6.4.

4.3.2. Temporal order induced by compartment fragmentation

In the study of dynamic compartmentalisation systems, we examine composite systems that typically have multiple compartments. While the analysis of a binary system with two compartments was the focus of Gibbs' paradox, the generalization to systems with more compartments allows for additional degrees of freedom when examining the insertion and removal of partitions. For systems with $N \geq 2$ compartments, it is necessary to consider the temporal order in which partitions are inserted and removed. Here, we will delve into how this impacts the enclosed microscopic dynamics.

We define our compartment system in analogy to Eq. (2.20) in section 2.3 as a full stochastic system on the basis of a transition rate matrices in the formalism of Master

4.3. Model definition: How compartment dynamics induce temporal ordering

Equations. To this end, we define the compartmentalised system as

$$\mathbb{S} = \begin{bmatrix} \vdots \\ [\vec{n}_i, v_i] \\ \vdots \end{bmatrix}. \quad (4.6)$$

We consider the system to be described by a list of compartments, each specified by the state of the internal stochastic many-body system and compartment properties, as in chapter 2. We specify on the compartment properties to be fully described by the compartment volumes v_i . For notational simplicity later in this chapter, we define the state of the enclosed dynamics in terms of the occupation number vector \vec{n}_i , which counts how many particles are in specified states x_i . With $N(\mathbb{S})$ we refer to the total number of compartments in a given realisation of the system \mathbb{S} .

In a semi-symbolic notation, the dynamics of the system are given in the Master-Equation framework by

$$\begin{aligned} \frac{d}{dt}P(\mathbb{S}) = & \sum_i^{N(\mathbb{S})} \left(\sum_{\vec{n}'_i \neq \vec{n}_i} Q_i(\vec{n}'_i \rightarrow \vec{n}_i, v_i) P \left(\begin{bmatrix} \vdots \\ [\vec{n}'_i, v_i] \\ \vdots \end{bmatrix} \right) \right) \\ & - P(\mathbb{S}) \sum_i^{N(\mathbb{S})} \left(\sum_{\vec{n}'_i \neq \vec{n}_i} Q_i(\vec{n}_i \rightarrow \vec{n}'_i, v_i) \right) + \mathcal{R}_{(t)}[P(\mathbb{S})]. \end{aligned} \quad (4.7)$$

We refer to the transition rates of the enclosed stochastic many-body dynamics in compartment i with $Q_i(\vec{n}'_i \rightarrow \vec{n}_i, v_i)$ and to the compartment dynamics with the symbolic operator $\mathcal{R}_{(t)}[P(\mathbb{S})]$. Note, that whether a system is considered closed or open, as introduced in section 1.3, is specified by the details of enclosed dynamics and the compartment dynamics. We specify the microscopic dynamics in section 4.4.1 and section 4.5.1, and focus in further of this section on the compartment dynamics.

The multi-scale nature of dynamic compartmentalisation systems makes the analysis of their dynamics complex, both in terms of analytical tractability and numerical feasibility. In order to gain an understanding of the thermodynamic effects of dynamic compartmentalisation, we simplify the dynamics in this study to a minimal example. This allows us to investigate how the creation and preservation of fluctuations among compartments affect the statistics of realised system states. In similarity to Maxwell's demon, we next introduce a simple scheme that provides insight into the thermodynamic effects of dynamic compartmentalisation. Using this scheme, we then address the general research question we investigate in this chapter 4.

We consider a chain of N compartments, $C = c_i | i = 1, \dots, N$, each with equal volume v , that encloses stochastic many-body dynamics. Between each pair of compartments, c_i, c_{i+1} , an immobile partition may be inserted or removed. These partitions are in one of two states, $\mathcal{P}_i \in 0, 1$, which denote the absence or presence of the partition, respectively. The set of all partition configurations is defined as $\mathcal{P} = \mathcal{P}_i | i = 1, \dots, N - 1$. Inspired by Maxwell's demon, we assume that each partition is controlled by a "dumb" demonic being that has access to an external time protocol but cannot observe the system itself. This time protocol dictates when the demon should connect or separate two compartments, regardless of the microscopic dynamics within the compartments. We consider a micro-canonical setup in which all walls and partitions are isolating, and assume that partitions

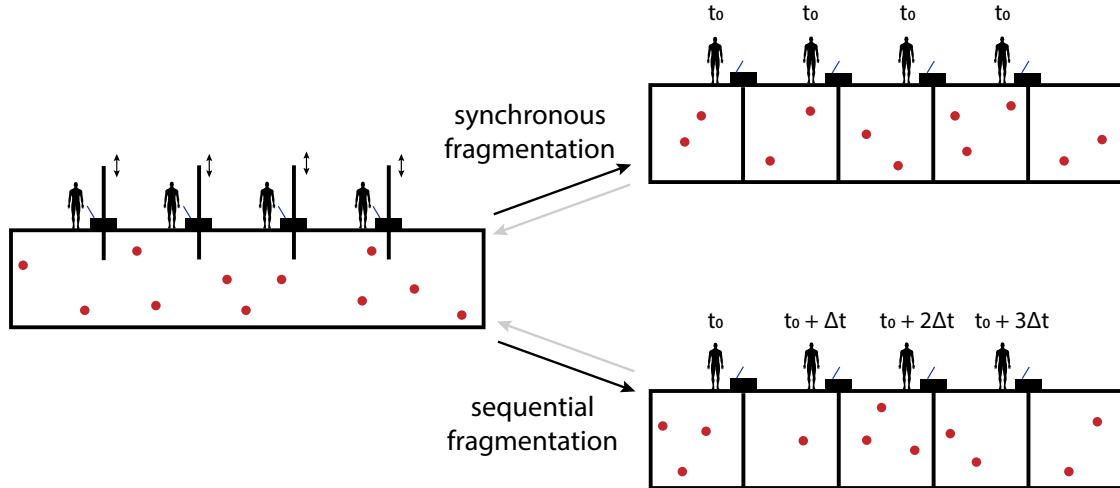


Fig. 4.6.: **Introducing Gergesian demons: Does an external time protocol of partition insertion and removal affect the macrostate statistics of the system?** We consider a system with a fixed number of compartments that are individually inserted and removed according to an external time protocol. In particular, we define the process of synchronous fragmentation, where all partitions are inserted at the same point in time. In contrast, partitions are inserted one after the other for sequential fragmentation. Both synchronous and sequential fragmentation results in the same distribution of compartment volumes. By removing all partitions, transitions from the synchronous to the sequentially fragmented state and vice versa are possible without performing volume work on the system. For which conditions do the synchronous to the sequentially fragmented state show identical macrostate statistics?

are inserted and removed without performing work on the system. Will different time protocols result in different macrostate statistics and hence different system entropies? As in this setup every partition is individually controlled, we term the legion of demons in this setup *Gergesian demons*, as they are many.

In the following, we focus on two specific time protocols, which we term synchronous and sequential fragmentation. We define an initial state $\mathcal{P}^0 = \{\mathcal{P}_i = 0 | i = 1, \dots, N-1\}$ and we assume that the microscopic dynamics enclosed in the system relaxed to an equilibrium state. We define a time protocol of partition insertion and removal as a sequence $(\vec{s}_t)_{t \in T}$, where $\vec{s}_t \in \{0, 1\}^{N-1}$ indicates for $s_t^i = 1$ a change in the configuration of the i th partition from its current configuration to the other configuration and no change for $s_t^i = 0$ at time t . T is the list of time points at which barrier modifications happen. Starting from \mathcal{P}^0 at a time t_0 , we define the synchronous fragmentation time protocol

$$s_{\text{syn}} = (\vec{s}_0), \quad \vec{s}_0 = (1, \dots, 1)^\top, \quad T = \{0\} \quad (4.8)$$

as a process where all partitions are inserted in the system at the same time. This formally agrees with a generalisation of Gibbs paradox as discussed by [21], see also section 4.2, if the stochastic many-dynamics is an ideal gas. For the second compartmentalisation process, we define a time interval $\Delta t \gg \tau$ which is greater than the internal relaxation time of the stochastic many-body dynamics enclosed in the system. We define sequential

4.3. Model definition: How compartment dynamics induce temporal ordering

fragmentation as

$$s_{\text{seq}} = (\vec{s}_0, \dots, \vec{s}_{N-1}), \quad \vec{s}_i = (0, \dots, \underbrace{i}_{i\text{th index}}, \dots, 0)^\top, \quad T = \{t_0, t_0 + \Delta t, \dots, t_0 + (N - 2)\Delta t\}. \quad (4.9)$$

In this process, partitions are inserted one after each other with a time difference Δt , such that in every step a small compartment of volume v is separated from the remaining system. By construction, we allow the system in this process to relax to a new equilibrium state after splitting a small part from the system. Both synchronous fragmentation and sequential fragmentation yield the same final distribution of compartment volumes. We thus consider the same macrostates, if we evaluate the enclosed dynamics per compartment, as we for example track the energy per compartment. We conclude, that different compartment content statistics imply different total system entropies. Note, that while synchronous fragmentation is an instantaneous process, sequential fragmentation has the notion of an *arrow of time*. For s_{seq} the compartments in the final configuration are created at different instances in time, with a clear correlation between the creation time and position in the system. This is illustrated in Fig. 4.6.

As we consider finite system sizes and stochastic dynamics for the many-body dynamics enclosed in the compartments, after applying a fragmentation time protocol, we find a stochastic realisation of the system. Here, we are not interested in specific realisations of macrostates but in the statistics of the macrostates after executing a time protocol. For the synchronous fragmentation protocol, we expect all compartments to have the same statistics, as we have by definition no dependency on space in our system. The situation is a priori different for sequential fragmentation. After inserting a barrier, the system evolves in time and fluctuations from the partitioning process potentially add up over time.

We formally define the macrostate statistics of the system in the initial configuration \mathcal{P}^0 as $P(\mathcal{S}_0)$. We define the macrostate statistics obtained by synchronous fragmentation as $P(\mathcal{S}_{\text{syn}})$ and by sequential fragmentation as $P(\mathcal{S}_{\text{seq}})$. Recall, that we allow for both the insertion and removal of partitions such that we can cyclically interchange between state $\mathcal{S}_0 \rightarrow \mathcal{S}_{\text{seq}} \rightarrow \mathcal{S}_0 \rightarrow \mathcal{S}_{\text{syn}} \rightarrow \mathcal{S}_0$. If we consider the compartmentalised system as isolated system, and $P(\mathcal{S}_{\text{seq}}) \neq P(\mathcal{S}_{\text{syn}})$, the second law of thermodynamics allows us to assess the work performed by compartment fusion and fragmentation.

Comparing synchronous and sequential fragmentation constitutes a minimal model to assess the effects of compartment fusion and fragmentation dynamics on statistics of the realised system states. The sequential fragmentation protocol manifests the heuristic idea of creating and preserving density fluctuations, while the synchronous fragmentation protocol constitutes a benchmark. The synchronous fragmentation protocol results in a compartment configuration with identical size distribution as for synchronous fragmentation, but, by construction, all compartments show identical statistics. Notably, this minimal system allows for analytical tractability. In the following chapter 4, we investigate how creating and preserving fluctuations due to compartment fragmentation and fusion change the system statistics. We in particular approach this problem from a thermodynamic perspective, and assess the changes in the system entropy induced by compartment fusion and fragmentation. Based on this, we interpret the notion of work performed on the system by compartment dynamics. In order to investigate this system, we will first study the ideal gas subject to synchronous and sequential fragmentation processes in section 4.4 and then turn to a generalisation by making use of the formalism of

the Second quantisation in section 4.5. We next briefly elucidate compartment dynamics beyond the synchronous and sequential fragmentation processes.

4.3.3. Compartment fusion and fragmentation dynamics

In section 4.3.2, we introduced two specific compartment dynamic protocols: synchronous and sequential fragmentation. There are infinitely many other time protocols that could be constructed to investigate dynamic compartmentalisation. Additionally, in Fig. 4.6, we have assumed a preserved spatial setting. Relaxing this constraint allows for further compartment dynamics as the connectivity between compartments is allowed to vary over time, potentially resulting in macrostate statistics that are different from those achievable through fragmentation processes.

Although there is a wide range of processes to investigate, we have chosen to focus on two simple, analytically tractable compartment dynamic processes, which give insight on compartment fusion and fragmentation dynamics. If synchronous and sequential fragmentation show different macrostate statistics, we conclude that compartment fusion and fragmentation dynamics in general alter the macrostate statistics. On the other hand, if both synchronous and sequential fragmentation produce identical macrostate statistics, we conclude that there exist no compartment fusion and fragmentation protocols that induce different macrostate statistics. We will provide a proof of this in section 4.4.4, when we study the ideal gas subject to synchronous and sequential compartment fragmentation. In the following, when we refer to dynamic compartmentalisation, we compare the synchronous and sequential fragmentation protocol.

4.4. The ideal gas subject to dynamic compartmentalisation

In section 4.2, we briefly reviewed a historic perspective on the insertion and removal of partitions, which set the foundation to analyse binary merging and binary fragmentation of compartments. In this context, we built a lot of our physics intuition of thermodynamics and statistical physics on the behaviour of the ideal gas. In this section, we take the ideal gas a paradigmatic model system to study the thermodynamics of dynamic compartmentalisation by analysing the setup of *Gergesian demons* introduced in section 4.3.2. Notably, in this chapter, we present an analytical proof structure, which allows for direct generalisation to arbitrary stochastic many-body dynamics. We investigate here the ideal gas to exemplify the structure of the proof. At the end of this subchapter, in section 4.4.5, we will discuss the generalisability of the ideal gas as a model system.

4.4.1. Understanding the ideal gas as stochastic many-body dynamics

Before we investigate the ideal gas under dynamic compartmentalisation, we need to precisely define the model under consideration. To this end, we refine the model presented in section 4.3.2, where we introduced the scheme of *Gergesian demons*. While the compartment dynamics are fully defined by the two fragmentation processes s_{seq} and s_{syn} , we need to further specify the microscopic enclosed many-particle dynamics, which we here set to be the ideal gas.

We are considering a microcanonical system in which no fluxes of energy or particles are allowed through the system's boundaries or partitions. Each gas particle i is characterised by a position vector and a momentum vector, (\vec{r}_i, \vec{p}_i) . When particles collide, they exchange momentum in a stochastic manner. We assume that the position and momentum of the particles are independent variables and that the momentums of two colliding particles are statistically independent, which corresponds to the molecular chaos hypothesis [215]. For simplicity, we consider particles of the same mass, m . Instead of analysing the momentum vector, we focus on the kinetic energy per particle, $E_i = \vec{p}_i^2/2m$. We consider a finite number of particles, \mathcal{N} , enclosed in our system. As we assume the particles to be randomly and uniformly distributed in space, we neglect the position dependence and define the full state of the system as the vector $\vec{E} = E_1, E_2, \dots, E_{\mathcal{N}}$. Note that, as we defined a microcanonical setup, the total sum of $E = \sum_i E_i$ is a conserved quantity. In this setup, inserting a single partition corresponds to a binomial splitting of the particles into the two newly created subsystems, with the probability of being assigned to each subsystem equal to its volume fraction.

Recall that the compartment configuration resulting from either sequential or synchronous fragmentation is identical. In the final configuration, each compartment is described by a tuple $(\vec{\mathcal{E}}, \vec{\mathcal{N}})$, where $\vec{\mathcal{E}} = \mathcal{E}_1, \dots, \mathcal{E}_N$ is the vector of total energies and $\vec{\mathcal{N}} = \mathcal{N}_1, \dots, \mathcal{N}_N$ is the number of particles per compartment. Similar to \vec{E} , the total energy is conserved, such that $E = \sum_i \mathcal{E}_i$. Similarly, the total number of particles is also conserved, as $\mathcal{N} = \sum_i \mathcal{N}_i$. Note that every compartment in the final configuration is itself a microcanonical ensemble, each characterised by $(\mathcal{E}_i, \mathcal{N}_i, v)$.

The dynamics of the ideal gas are defined by how momentum is exchanged upon particle collision. Here, we approximate the ideal gas as a hard sphere gas and invoke the molecular chaos hypothesis. Given that particles i and j collided with energies E_i and E_j , the probability for new energies E'_i and E'_j is

$$p(E'_i, E'_j | E_i, E_j) = \frac{1}{E_i + E_j} \quad (4.10)$$

for a two-dimensional system. The dynamics of such a gas are thoroughly explained in various textbooks, such as [6, 21]. A simple numerical exercise is to implement the dynamics of a hard sphere gas in simulations. However, we are not interested in a qualitative description of the ideal gas dynamics here. Instead, we seek efficient implementations that allow for fast computations and analytical treatment. For this reason, we will study the ideal gas as a multivariate random variable in the next section.

4.4.2. Finite-sized ideal gas ensembles as a multi-variate random variables

For further analysis, it is necessary to know about fluctuations and the full ensemble probability distribution in order to correctly assess the effect of dynamic compartmentalisation. To this end, we turn to a statistical description of the ideal gas, treating the state of the system \vec{E} as a multivariate random variable and deriving the probability distribution $p_E(\vec{E})$. In this section, we closely follow [216] to demonstrate that Dirichlet distributions are suitable to describe the ensemble statistics of an ideal gas.

Let an ideal gas be defined by N particles confined in a volume V in d dimensions with identical mass m . Let \vec{r}_i be the position of the particle i and \vec{p}_i its momentum. We

4. Towards a thermodynamics of closed compartmentalised systems

consider only full elastic collisions among the particles and with the walls of the volume. Furthermore, we consider the walls to be isolating, such that

$$E = \frac{1}{2m} \sum_i \vec{p}_i^2, \quad (4.11)$$

the total energy is conserved. With this, the microscopic state of the system is fully defined. For simplicity, we change from momentum coordinates to velocity coordinates $\vec{p}_i = m\vec{v}_i$. Let \vec{v} the composite vector over all velocity vectors \vec{v}_i . The velocity vector \vec{v} is constrained on the hypersphere with radius $R = \sqrt{2E/m}$. The total phase space hence has a dimension of $g = 2dN - 1$. We introduce the notation \vec{v} and \vec{r} as vectors over all particle velocities and positions, respectively.

Here, we do not derive the statistics from the collision dynamics solving Boltzmann's kinetic equations but assume molecular chaos, such that every accessible state in the g -dimensional phase has equal probability.⁴ We find that the total volume of the accessible phase space is given by

$$\Omega = V^N \frac{2\pi^{dN/2}}{\Gamma(dN/2)} R^{dN-1}, \quad (4.12)$$

where we made use of the Gamma-function Γ . This phase space volume is typically the starting point to define the Boltzmann entropy. Here, we take a different route, as we need a description in terms of probability distributions. In particular, making use of the molecular chaos hypothesis, we find the probability distribution

$$f_{\vec{r},\vec{v}}(\vec{x}, \vec{y}) = \frac{1}{\Omega} \mathbf{1}_V(\vec{x}) \mathbf{1}_{y=R}(\vec{y}) \quad (4.13)$$

for the system to be in any accessible state of the phase space. Here, we made use of indicator functions $\mathbf{1}_A(\vec{x})$, which counts whether a state $\vec{x} \in A$ in a set A . The first indicator function checks whether the state is inside the confined volume, while the second term checks if the total energy is conserved. We integrate out the positional degrees of freedom and show that the probability to find a specified velocity vector for our system \vec{v} is uniformly distributed on the hypersphere with radius R defined above.

Next, we apply two variable transformations. In a first step, we normalise to dimensionless variables $u_{i,\alpha} = v_{i,\alpha}/R$, which yields

$$f_{\vec{u}}(\vec{x}) = \frac{\Gamma(dN/2)}{2\pi^{dN/2}} \mathbf{1}_{x=1}(\vec{x}). \quad (4.14)$$

Next, we shift to the squared version $w_{i,\alpha} = u_{i,\alpha}^2$ such that the constraint on the sum simplifies to $\sum_i^N \sum_\alpha^d w_{i,\alpha} = 1$. The Jacobian of this transformation is given by

$$\left| \frac{\partial \vec{u}}{\partial \vec{w}} \right| = \frac{1}{2^{dN}} \prod_{i=1}^N \prod_{\alpha=1}^d w_{i,\alpha}^{-1/2}. \quad (4.15)$$

⁴Indeed, while this assumption is central in statistical physics, it is not rigorously proven [6, 7, 216]. However, note that this assumption is also the basis for the Boltzmann entropy on which a large portion of the statistical physics of gases is built [21].

4.4. The ideal gas subject to dynamic compartmentalisation

Note that for $w_{i,\alpha}$ the accessible space in the phase space is given by the unit simplex

$$S = \left\{ \vec{x} \in \mathbb{R}^n : \forall i x_i \geq 0 \wedge \sum_i x_i = 1 \right\}. \quad (4.16)$$

With this, the probability distribution reads

$$f_{\vec{w}}(\vec{x}) = \frac{\Gamma(dN/2)}{[\Gamma(1/2)]^{dN}} \prod_{i=1}^N \prod_{\alpha=1}^d x_{i,\alpha}^{1/2-1}, \quad (4.17)$$

which is a symmetric Dirichlet distribution. In a final step, we define the normalised energy per particle

$$\varepsilon_i = \frac{E_i}{E} = \sum_{\alpha} \frac{v_{i,\alpha}^2}{R^2} = \sum_{\alpha} w_{i,\alpha}, \quad (4.18)$$

and make use of the aggregation law of Dirichlet distribution, to find the symmetric Dirichlet distribution of the energy per particle vector

$$f_{\vec{\varepsilon}}(\vec{x}) = \frac{\Gamma(dN/2)}{[\Gamma(1/2)]^{dN}} \prod_{i=1}^N \prod_{\alpha=1}^d x_{i,\alpha}^{d/2-1}. \quad (4.19)$$

Note, that this distribution reduces to a uniform distribution for $d = 2$, but does not reduce to a uniform distribution for general dimensions $d > 2$. While this result is typically not discussed in standard textbooks, indeed the well-known statistical distributions of the ideal gas can be extracted from the Dirichlet distribution, such as the gamma distribution for the energy and the Maxwell-Boltzmann distribution for the particle velocity as marginalised distributions in the thermodynamic limit, see for example [216]. Note, that the Dirichlet distribution has several specific statistical characteristics, which set this multi-variate distribution special. Most notably, the Dirichlet distribution is characterised as only continuous multi-variate probability distribution yielding complete neutrality.

We define a random vector $\vec{x} = (x_1, x_2, \dots, x_N)$ on the unit simplex S defined above. Recall that the elements of the vector are globally coupled by the constraint $\sum_i x_i = 1$. Formally, x_1 is termed *neutral* if and only if x_1 is statistically independent from the rescaled vector

$$x_{1*} = \left(\frac{x_2}{1-x_1}, \frac{x_3}{1-x_1}, \dots, \frac{x_N}{1-x_1} \right). \quad (4.20)$$

In turn, x_2 is termed neutral if and only if x_2 is statistically independent of the rescaled vector

$$x_{2*} = \left(\frac{x_3}{1-x_1-x_2}, \frac{x_4}{1-x_1-x_2}, \dots, \frac{x_N}{1-x_1-x_2} \right), \quad (4.21)$$

and so on. If all x_i are neutral, then the vector is termed completely neutral. A distribution that only yields completely neutral vectors is called completely neutral. Applying this concept to the ideal gas, we find an exotic type of statistical dependence. Formally, all particles are globally coupled due to the global constraint of energy conservation. If we sample and extract an arbitrary number of particles from the ideal gas and measure the total energy of this sample, then add this energy back to the remaining particles in the

ideal gas to create a second sample, complete neutrality predicts that both samples are now statistically independent. In layman's terms, we can *scale the global coupling away* for the ideal gas. This gives us a hint of what to expect for the thermodynamics of the ideal gas under dynamic compartmentalisation, which we will investigate after presenting evidence from numerical experiments.

4.4.3. Simulation of the ideal gas subject to sequential and synchronous compartment fragmentation

In our numerical routines, outlined in appendix B.3, we in particular make use of describing a finite-sized ideal gas ensemble by a Dirichlet distributed random variable. Note that also in the following chapter 4.4.4 we will make use of the Dirichlet distributed random variables. Using the numerical routine, we can effectively sample systems of arbitrary size. However, we focus on small systems in this case, as we need both a lower number of repetitions to find reliable statistics and a decrease in simulation time. It is important to note that we are interested in precise statistics, as we cannot yet estimate the strength of the effects induced by compartment dynamics. In this section, we consider statistics derived from 2×10^6 independent runs.

First, we directly contrast synchronous fragmentation with sequential fragmentation. We consider an ensemble of 30 ideal gas particles with an initial energy of $\tilde{\mathcal{E}}$ enclosed in a 5-compartment system. Here, we normalize the energy scale such that the average energy per particle is $\tilde{\mathcal{E}}/\mathcal{N} = 1$. For the evaluation of the statistics, we consider the total enclosed energy per compartment \mathcal{E}_i . For an ideal gas in two dimensions (2Dd), we find that all compartments show the same distribution $p^{\text{syn}}\mathcal{E}_i(\varepsilon)$ of energy per compartment after synchronous fragmentation, as shown in Fig.4.7 (a). This result is expected, as by construction all compartments are indistinguishable.

For sequential fragmentation, we also find that all compartments show the same distribution $p_{\mathcal{E}_i}^{\text{seq}}(\varepsilon)$ of energy per compartment, see Fig. 4.7 (b). As the first compartment created by either synchronous or sequential fragmentation has the same distribution $p_{\mathcal{E}_1}^{\text{syn}}(\varepsilon) = p_{\mathcal{E}_1}^{\text{seq}}(\varepsilon)$, we find that both synchronous and sequential fragmentation show the same statistics $p_{\mathcal{E}_i}^{\text{syn}}(\varepsilon) = p_{\mathcal{E}_i}^{\text{seq}}(\varepsilon)$ for the 2d ideal gas. The analogous analysis for a three-dimensional ideal gas (3d), see Fig. 4.7 (c) and (d), shows the same result of synchronous and sequential fragmentation being equivalent, as both processes result in the same macrostate statistics. Note that due to equivalence of $p_{\mathcal{E}_1}^{\text{syn}}(\varepsilon) = p_{\mathcal{E}_1}^{\text{seq}}(\varepsilon)$, it is sufficient to only investigate the sequential fragmentation process to assess an equivalence of synchronous and sequential fragmentation. If sequential and synchronous are not equivalent, this implies that the compartments resulting from sequential fragmentation show different macrostate statistics.

Next, we test whether we started our numerical investigations in a parameter regime where differences for the sequential fragmentation are vanishingly small and thus were undetectable by our numerical simulations. We thus want to systematically check for other system sizes. To begin with, we investigate whether the initial number of particles in the system has any impact on possible deviations between compartments when subjected to a sequential fragmentation process. In Fig. 4.8, we systematically vary the initial number of particles in a 3-compartment system from $\mathcal{N} = 10$ to $\mathcal{N} = 200$. All compartments show the same macrostate statistics.

Finally, we consider systems with a varying number of compartments. It is possible that fluctuations may accumulate over the course of sequential fragmentation, resulting in more

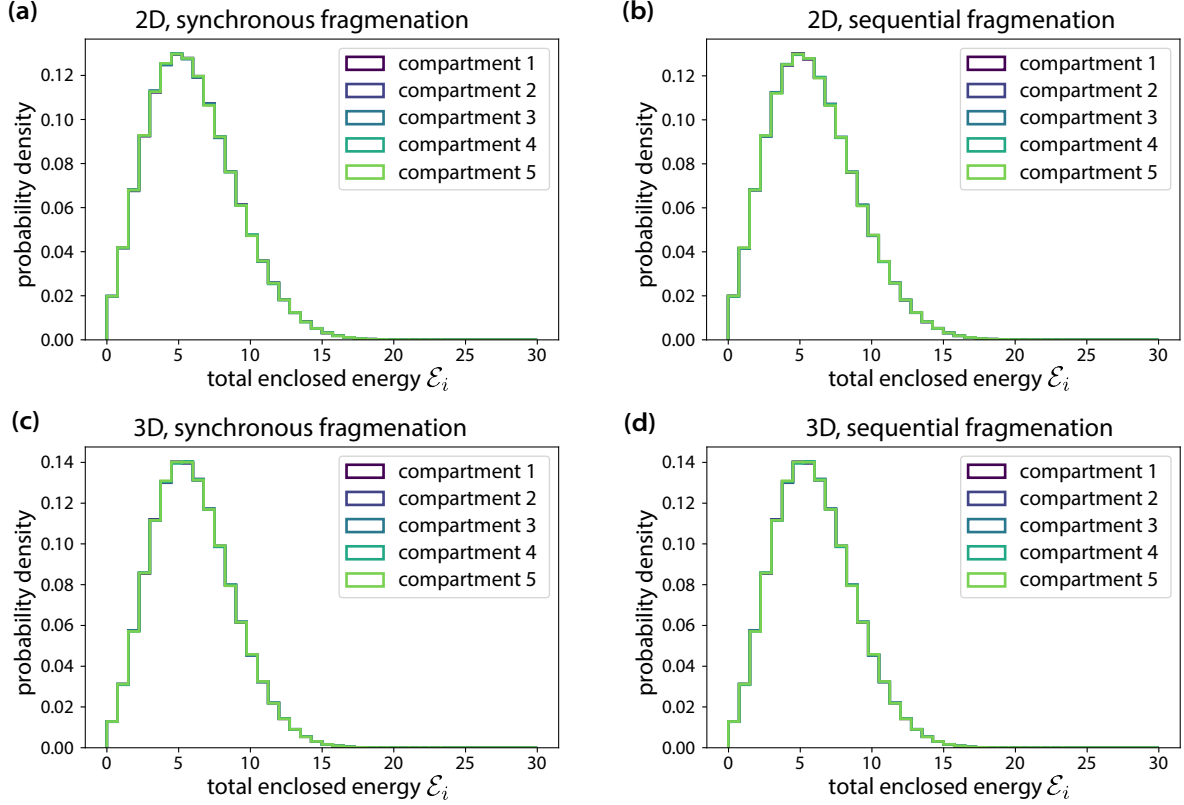


Fig. 4.7.: Comparing synchronous and sequential fragmentation for an ideal gas enclosed in a 5-compartment system in two and three dimensions. An ensemble of ideal gas particles with initial size $\mathcal{N} = 30$ and initial energy $\tilde{\mathcal{E}}$ is enclosed in a 5-compartment system. Shown is the statistics over the total energy enclosed per compartment \mathcal{E}_i . The energy is measured in units of the average energy per particle, $\mathcal{E} = 30\tilde{\mathcal{E}}/\mathcal{N}$. The 5-compartment system is fragmented by both a sequential and a synchronous fragmentation process. Ideal gas dynamics in two and three dimensions are both investigated. Ideal gas dynamics are simulated following Algorithm 2 and Algorithm 1. A total number of 2×10^6 independent runs were performed to create the statistics. As by construction, the statistics of the total enclosed energy \mathcal{E}_i per compartment is identical for all compartments for synchronous fragmentation in both 2d, (a), and 3d, (c). Also for sequential fragmentation, all compartments show the same statistics for \mathcal{E}_i in both 2d, (b), and 3d, (d). As the statistics of the first compartment are identical for both synchronous and sequential fragmentation by construction, synchronous and sequential fragmentation yield identical statistics in both 2d and 3d.

4. Towards a thermodynamics of closed compartmentalised systems

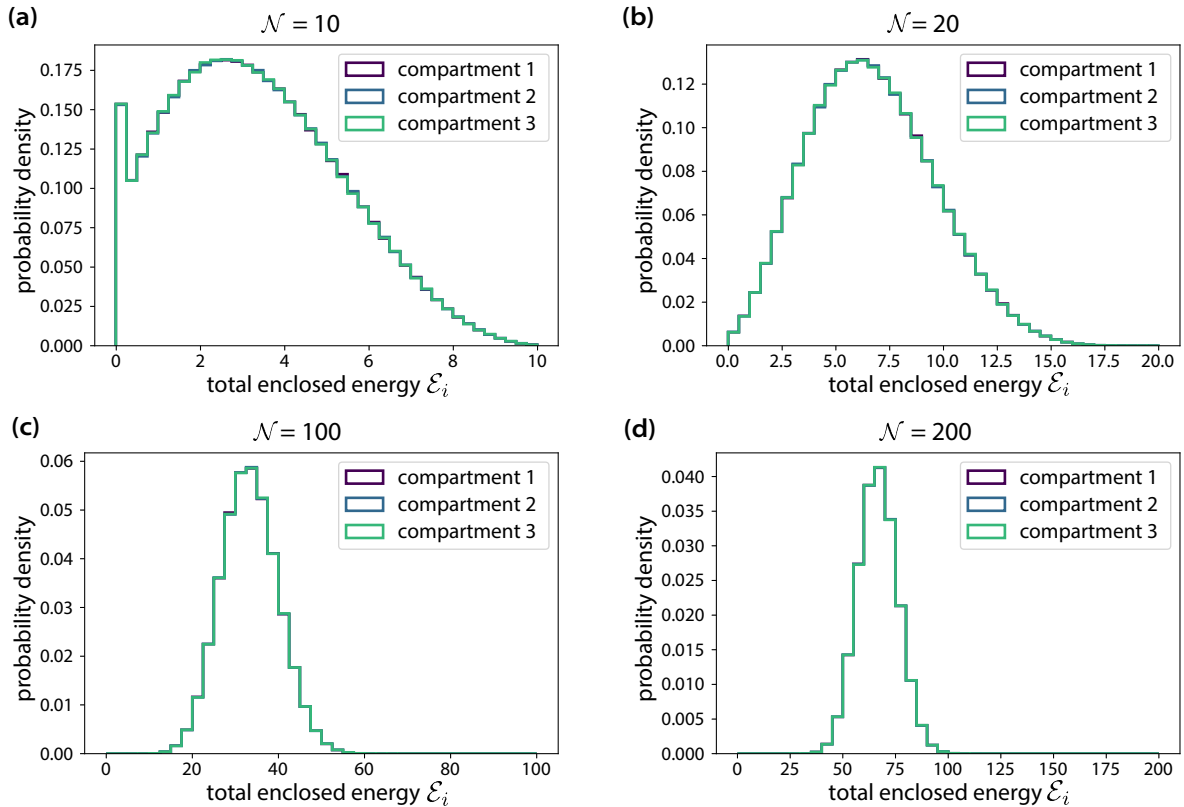


Fig. 4.8.: Sequential fragmentation of an ideal gas with varying total particle number. An ideal gas in 2d enclosed in a 3-compartment system is subjected to sequential fragmentation. Shown is the statistics over the total energy enclosed per compartment \mathcal{E}_i . The total number of enclosed particles is systematically increased from (a) $\mathcal{N} = 10$, (a) $\mathcal{N} = 20$, (a) $\mathcal{N} = 100$, to (a) $\mathcal{N} = 200$. The enclosed energy is measured in units of the average energy per particle. A total number of 2×10^6 independent runs were performed to create the statistics. Sequential fragmentation shows no differences in the statistics of the total enclosed energy \mathcal{E}_i independent of the total number of enclosed particles \mathcal{N} .

pronounced differences in macrostate statistics when more compartments are present. In Fig.4.9, we systematically increase the number of compartments while keeping the initial number of particles fixed at $\mathcal{N} = 30$. Again, we find that the macrostate statistics are unchanged by sequential fragmentation, as all compartments display identical macrostate statistics regardless of when they are created. These numerical results suggest that the ideal gas in a microcanonical setup is unaffected by dynamic compartmentalisation. To corroborate our findings, we next present an analytical argument, where we prove that dynamic compartmentalisation shows no effect on the ideal gas.

4.4.4. Proof of entropic neutrality under dynamic compartmentalisation

The numerical experiments presented in the previous section suggest that the ideal gas is unaffected by the timing of partition insertion. In this section, we provide an analytical proof of this observation using specific properties of the Dirichlet distribution. This proof was initially presented in the Master's thesis of Rushikesh Shinde. This work formally

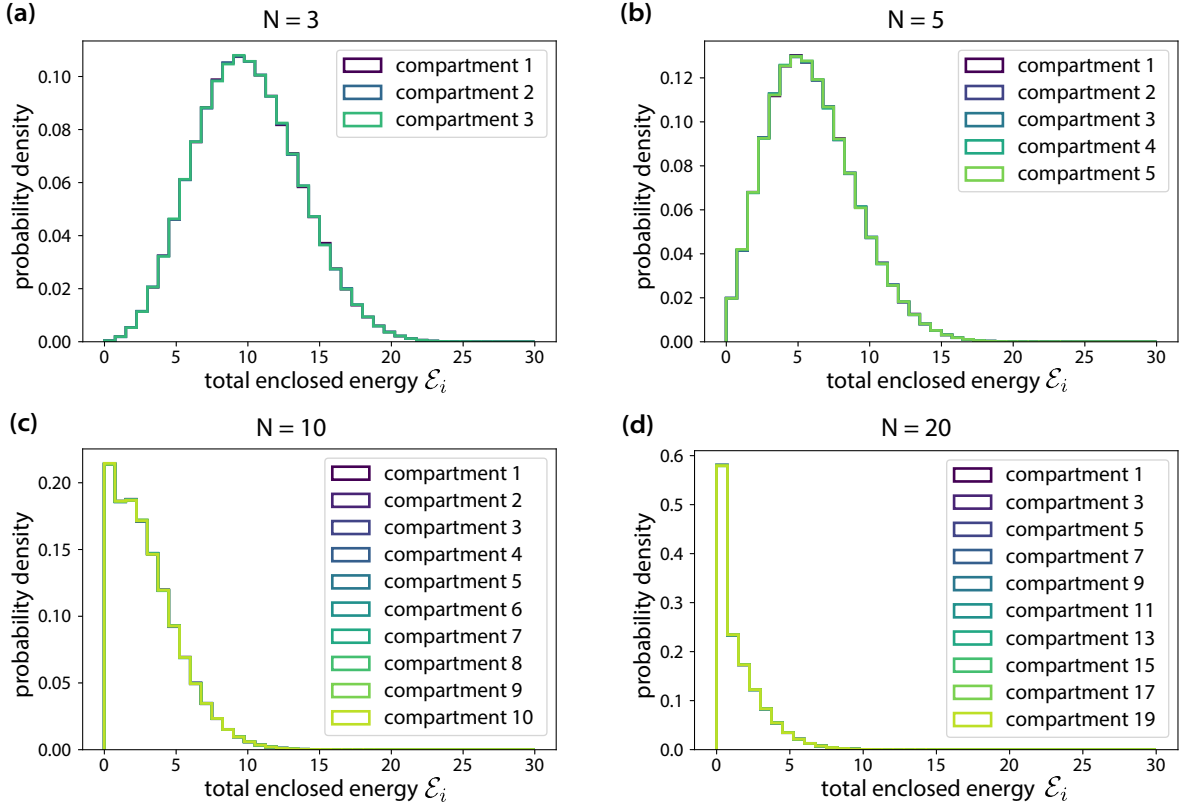


Fig. 4.9.: Sequential fragmentation of an ideal gas in systems with varying total compartment number An ideal gas in 2d enclosed with an initial number of $\mathcal{N} = 30$ particles is subjected to sequential fragmentation. Shown is the statistics over the total energy enclosed per compartment \mathcal{E}_i . The total number of considered compartments is systematically increased from (a) $N = 3$, (a) $N = 5$, (a) $N = 10$, to (a) $N = 20$. The enclosed energy is measured in units of the average energy per particle. A total number of 2×10^6 independent runs were performed to create the statistics. Sequential fragmentation shows no differences in the statistics of the total enclosed energy \mathcal{E}_i independent of the total number of considered compartments $N = 20$.

shows an extension to the Gibbs paradox, as we consider multiple compartments and discuss the notion of time in this context. While investigating an ideal gas subject to dynamic compartmentalisation is a constructed example with little practical relevance, we introduce with the following proof a structure which allows for a direct generalisation to arbitrary stochastic many-body dynamics, that we will employ again in section 4.5.

In section 4.4.2, we demonstrated how an ideal gas ensemble can be described as a multivariate random variable following a Dirichlet distribution and briefly mentioned special statistical properties of this distribution. In this section, we provide a formal proof of the invariance of the ideal gas under dynamic compartmentalisation. To do so, we first review the identities between the Dirichlet, Gamma, and Beta distributions. Using these relationships, we consider the specific case of sampling a subset from an ensemble and removing it, followed by allowing the remaining ensemble to relax to a new equilibrium and comparing the statistics of the new equilibrium to those of the extracted sample. From this, we generalize to the cases of synchronous versus sequential fragmentation, and subsequently to general compartment fusion and fragmentation processes.

4. Towards a thermodynamics of closed compartmentalised systems

Sampling a Dirichlet distribution Let $\vec{X} \in \mathbb{R}_+^n$ be a random vector on the unit simplex $\sum_i^n X_i = 1$ whose distribution is given by

$$f(\vec{X}|\vec{\alpha}) = \frac{\Gamma(\sum_i^n \alpha_i)}{\prod_i^n \Gamma(\alpha_i)} \prod_i^n x_i^{\alpha_i-1}, \quad (4.22)$$

where $\vec{\alpha} \in \mathbb{R}_+^n$. Then $\vec{X} \sim \text{Dir}(\vec{\alpha})$ is distributed according to a Dirichlet distribution with parameter vector $\vec{\alpha}$ [217]. If $\alpha_i = \alpha \forall i$, then the Dirichlet distribution is a symmetric Dirichlet distribution. A Dirichlet distributed random vector of size n can be obtained by sampling n independent Gamma variables. Let $Y_i \sim \text{Gamma}(\alpha_i, \theta)$, $i = 1, \dots, n$ be independent Gamma distributed random variables with different shape parameter α_i and identical scale parameter θ . Defining the sum $Z = \sum_i^n Y_i$, the normalised vector

$$\vec{Y}' = \left(\frac{Y_1}{Z}, \frac{Y_2}{Z}, \dots, \frac{Y_n}{Z} \right) \sim \text{Dir}(\vec{\alpha}) \quad (4.23)$$

follows a Dirichlet distribution [217].

Relations between the Beta and the Gamma distribution Let $X \sim \text{Gamma}(\alpha, \theta)$ and $Y \sim \text{Gamma}(\beta, \theta)$ be two independent Gamma distributed random variables. Then the sum $Z_1 = X + Y$ is also given by a Gamma distribution [217]

$$Z_1 \sim \text{Gamma}(\alpha + \beta, \theta). \quad (4.24)$$

On similar terms, the quotient $Z_2 = X/(X + Y)$ is distributed like a Beta distribution [217]

$$Z_2 \sim \text{Beta}(\alpha, \beta). \quad (4.25)$$

Let now $X \sim \text{Gamma}(\alpha + \beta, \theta)$ and $Y \sim \text{Beta}(\alpha, \beta)$ be two independent random variables. Then the product $Z = XY$ is distributed like a Gamma distribution

$$Z \sim \text{Gamma}(\alpha, \theta). \quad (4.26)$$

In the following, we will make use of these identities to prove the invariance of the ideal gas under dynamic compartmentalisation.

Proof of entropic neutrality We now proceed to prove that partial sample removal and subsequent resampling leave the Dirichlet distribution invariant. To this end, we prove that the sum of energy extracted by a n particle sampling in two time-separated steps follows the same distribution. Following this proof, we demonstrate how this binary sampling implies invariance under dynamic compartmentalisation using a proof by induction.

We begin by defining a random vector of size N sampled from a symmetric Dirichlet distribution

$$\vec{X} \sim \text{Dir}(\vec{\alpha}), \quad \alpha_i = \frac{d}{2} \quad \forall i = 1, 2, \dots, N. \quad (4.27)$$

Next, we extract a sample from \vec{X} . To this end, we first define the set $\mathbf{N} = \{1, 2, \dots, N\}$.

4.4. The ideal gas subject to dynamic compartmentalisation

We randomly sample $n \leq N/2$ elements from the random vector \vec{X} . We define the index set \mathbf{I}_1 with total size $\#\mathbf{I}_1 = n$ and $i \in \mathbf{I}_1$ unique, which encodes the extracted sample. With this, we define the sum

$$\sigma_1 = \sum_{i \in \mathbf{I}_1} X_i \quad (4.28)$$

over the sample. We define the subset $\mathbf{I}_1^{-1} = \mathbf{N} \setminus \mathbf{I}_1$ as the remainder of the sampling. The size of the set is $\#\mathbf{I}_1^{-1} = N - n$ and the sum over its elements is given by $\sum_{i \in \mathbf{I}_1^{-1}} X_i = 1 - \sigma_1$. Next, we draw a new random vector from a Dirichlet distribution $\vec{Y}' \sim \text{Dir}(\alpha)$ of size $N - n$ and normalize $\vec{Y} = \vec{Y}'(1 - \sigma_1)$, such that $\sum_i^{N-n} Y_i = 1 - \sigma_1$. Note, that \vec{Y}' is independent of \vec{X} . We define a new random subset $\mathbf{I}_2 = n$ and define the sum $\sigma_2 = \sum_{i \in \mathbf{I}_2} Y_i$. In the following, we will prove that

$$\sigma_1 \sim \sigma_2 \quad (4.29)$$

are identically distributed random variables.

To prove the above statement, we begin by constructing \vec{X} by N independent Gamma variables $U_i \sim \text{Gamma}(\alpha, \theta)$:

$$X_i = \frac{U_i}{\sum_i^N U_i}. \quad (4.30)$$

Using this construction, the sum σ_1 is given by

$$\sigma_1 = \frac{\sum_{i \in \mathbf{I}_1} U_i}{\sum_j^N U_j}. \quad (4.31)$$

Analogously, we make use of $N - n$ additional independent Gamma variables $U'_i \sim \text{Gamma}(\alpha, \theta)$ to define σ_2 :

$$\sigma_2 = \frac{\sum_{i \in \mathbf{I}_2} U'_i}{\sum_j^{N-n} U'_j} \left(1 - \frac{\sum_{i \in \mathbf{I}_1} U_i}{\sum_j^N U_j} \right) = \frac{\sum_{i \in \mathbf{I}_2} U'_i}{\sum_j^{N-n} U'_j} \left(\frac{\sum_{i \in \mathbf{I}_1^{-1}} U_i}{\sum_j^N U_j} \right). \quad (4.32)$$

We realise that both σ_1 and σ_2 share the identical denominator $\sum_j^N U_j$. We simplify to

$$\sigma'_1 = \sum_{i \in \mathbf{I}_1} U_i \quad (4.33)$$

$$\sigma'_2 = \frac{\sum_{i \in \mathbf{I}_2} U'_i}{\sum_j^{N-n} U'_j} \left(\sum_{i \in \mathbf{I}_1^{-1}} U_i \right). \quad (4.34)$$

From this definition, we can directly read off

$$\sigma'_1 \sim \text{Gamma}(nd/2, \theta). \quad (4.35)$$

4. Towards a thermodynamics of closed compartmentalised systems

For readability, we define $Z_1 = \sum_{i \in \mathbf{I}_2} U_i'$ and $Z_2 = \sum_{i \in \mathbf{I}_2^{-1}} U_i'$, such that

$$\sigma_2' = \frac{Z_1}{Z_1 + Z_2} \left(\sum_{i \in \mathbf{I}_1^{-1}} U_i \right) = Z \left(\sum_{i \in \mathbf{I}_1^{-1}} U_i \right). \quad (4.36)$$

We can directly read off, that $Z \sim \text{Beta}(nd/2, (N - 2n)d/2)$. As the sum in the brackets is distributed like $\text{Gamma}((N - n)d/2, \theta)$, we find that

$$\sigma_2' \sim \text{Gamma}(nd/2, \theta). \quad (4.37)$$

As σ_1' and σ_2' are identically distributed, we also find that σ_1 and σ_2 are identically distributed. Note, that the two samples σ_1 and σ_2 are only identically distributed if both samples are of the same size.

After having provided a mathematical proof of the invariance of the Dirichlet distribution under random sample extraction, we consider the implications of this proof for the thermodynamics of ideal gases, before turning to generalisations of the proof account for random sample sizes. As previously established in section 4.4.2, starting with a Dirichlet distributed random vector corresponds to considering an ensemble of an ideal gas in an isolated compartment at equilibrium. There is a formal equality between the Dirichlet random vector \vec{X} and the state vector \vec{E} describing the energy per particle, as we normalize the ensemble energy $E = 1$ through initial rescaling. The creation of a sub-sample \mathbf{I}_1 corresponds to randomly moving a subset of gas particles to a new isolated compartment. Summing over this sub-sample corresponds to measuring the macrostate of the newly created subsystem in terms of the number of particles $\mathcal{N}_1 = n$ and total energy $\mathcal{E}_1 = \sigma_1$ it contains. This also determines the macrostate of the other subsystem as $\mathcal{N}_2' = N - n$ and $\mathcal{E}_2' = 1 - \sigma_1$. Sequential and synchronous fragmentation differ in the timing between the insertion of subsequent partitions. For sequential fragmentation, we let a time difference $\Delta t \gg \tau$ pass. Yet, importantly, we find that both newly created subsystems are directly at time $\Delta t = 0$ already in a new equilibrium, characterised by $(\mathcal{E}_2', \mathcal{N}_2')$ and $(\mathcal{E}_1, \mathcal{N}_1)$. This is due to the special property of the Dirichlet distribution. From subsystem $(\mathcal{E}_2', \mathcal{N}_2')$ we extract a new sample with $(\mathcal{E}_2, \mathcal{N}_2)$. In the proof above we demonstrated that both newly created subsystems 1 and 2 with an ideal gas have identical statistical properties if $\vec{N}_2 = \vec{N}_1$.

When creating subsystems by inserting partitions, the sample size is a random variable following a binomial distribution. By construction of the binomial splitting, the first and second separated compartments have the same particle distribution $\mathcal{N}_1 \sim \mathcal{N}_2$ if the compartment volumes $v_1 = v_2$ are identical. Using this and the results above, we find that the macrostate statistics in both compartments 1 and 2 are identically distributed if they are created by partition insertion. Following the same line of argument, separating off a third compartment also yields identical macrostate statistics, if $v_1 = v_2 = v_3$. By induction, we find that this holds true for all further compartments of identical volume size. Note, that these findings are based on the special statistical properties of the Dirichlet distribution.

Focusing next on synchronous fragmentation, there is no step of resampling and the samples are drawn from the same random vector \vec{X} . Hence σ_1 and σ_2 are trivially identically distributed due to the construction of \vec{X} by $u_i \sim \text{Gamma}(\alpha, \theta)$. Hence, also if separated by synchronous fragmentation, all compartments show identical macrostate statistics. Indeed, we already expected the later result by following the arguments given

by [21] in chapter 6.

Note, that by construction, the set \mathbf{I}_1^{-1} forms a Dirichlet distributed random vector with the constraints $\sigma_2 = 1 - \sigma_1$. As a consequence, the sub-set \mathbf{I}_1^{-1} is already in equilibrium. As a consequence, the equilibration time is formally vanishing, $\tau = 0$. This implies that all fragmentation time protocols that result in the same compartment volume distribution will show identical macrostate statistics.

Next, we extend our findings to time protocols that involve removing partitions, i.e. fusion of compartments. In the first step, we argue that we can reverse any time protocol without changing the macrostate statistics of the system and then turn to the general removal of compartments. Without loss of generality, we consider a system consisting of two compartments in contact, i.e., with no partition separating them. Following the construction of the Dirichlet distribution, we find that splitting the Dirichlet distributed random vector results in two random vectors that are themselves distributed like a Dirichlet distribution rescaled by the sum of their components. The two newly created subsystems are already in steady-state configurations. Note, that the conjecture of the two Dirichlet distributions in the subsystems describes again a Dirichlet distribution. Analogous to the argument given in section 4.2.2, both the system with the partition removed and the partition inserted are described by the same statistics.

By tracking transitions between the system's microstates, we find that all transitions created by resampling the two random vectors in the subsystems are also allowed transitions in the system without the partition inserted. It is important to note that this is a special property of the Dirichlet distribution, as the splitting of a Dirichlet-distributed random vector results in two rescaled Dirichlet-distributed random vectors. Conversely, not all transitions between microstates possible in the system without a partition can be realised in the system with the partition inserted. However, if the two subsystems are randomly distributed with macrostate statistics identical to those created by a partition insertion, their conjecture gives the same probability distribution of the system's microstates as for the system with no partition inserted. Generalizing to an arbitrary number of compartments, this implies that we can revert any partition insertion and thus we can invert any fragmentation protocol.

Note, however, that for dynamic compartmentalisation, we are particularly interested in fusion processes of compartments, which are not simply the reversal of fragmentation protocols. To make this final generalization, we make use of the formal equivalence of sequential and synchronous fragmentation. For synchronous fragmentation, all compartments have the same macrostate statistics by construction. In particular, we cannot distinguish any order of the compartments. This implies that we can rearrange the compartments in an arbitrary order. For sequential fragmentation, we have demonstrated that we can in particular revert the division of the last two connected compartments by binary fusion. We refer to these two fused compartments as *the last fused compartment*. As synchronous fragmentation and sequential fragmentation yield the same macrostate statistics, we can also rearrange the compartments created by sequential fragmentation. The fusion of any two compartments recreates the statistics of *the last fused compartment*.

In a final step, we now make use of the equivalence of synchronous and sequential fragmentation to conclude on arbitrary compartment fusion and fragmentation dynamics: If synchronous and sequential fragmentation show the same macrostate statistics and hence the dynamics are entropically neutral, then any compartment fusion and fragmentation process is entropically neutral. With this, we conclude a formal extension of Gibbs' paradox, as we have extended the vanishing system entropy to an arbitrary number of

partitions and arbitrary partition insertion and removal protocols, and more importantly to any aggregation fragmentation process when investigating the ideal gas.

4.4.5. The ideal gas as a special case?

In section 4.4.4, we proved that the system's entropy of an ideal gas is not affected by dynamic compartmentalisation. From this, we gain first insight into the general thermodynamics of dynamic compartmentalisation, as the random insertion and removal of partitions do not affect the internal dynamics enclosed in the compartments. We proved that the heuristic idea of creating and preserving density fluctuations averages out and hence has no effect if the stochastic many-body dynamics is specified to be an ideal gas.

We have seen that this *entropic neutrality under compartment fusion and fragmentation* relies fundamentally on the statistics of the Dirichlet distribution, which captures the ensemble statistics of the ideal gas. This raises the question of how special the ideal gas is in this respect. Our initial inspiration for studying the thermodynamics of dynamic compartmentalisation came from living matter and specifically from organelle dynamics. In this context, the study of low number gases in compartments is a rather artificial example. This leaves the question of how applicable the ideal gas is as a model for gaining general thermodynamic understanding unanswered.

A straightforward extension of our findings to a larger class of stochastic many-particle dynamics is given directly by the Dirichlet distribution: if the equilibrium distribution of the statistics is described by a Dirichlet distribution, then the dynamics - and more generally the system's entropy - is unaffected by dynamic compartmentalisation. However, this raises the question of which processes, aside from the ideal gas, are described by a Dirichlet distribution. We gain insight into this by recalling the derivation of the Dirichlet distribution in the context of the ideal gas in section 4.4.2. There, the fundamental assumption yielding the Dirichlet distribution is the assumption of a uniform distribution of states in the phase space as a result of the molecular chaos hypothesis. Consequently, we find that our intuitive understanding of "*entropic neutrality under compartment fusion and fragmentation*" so far is based on an assumption. While the assumption of molecular chaos is well-suited to capturing the dynamics of the ideal gas, a generalization to stochastic many-body dynamics is not straightforward. In particular, it is preferable to connect the finding of *entropic neutrality under compartment fusion and fragmentation* directly to microscopic interaction rules, rather than basing it on an assumption about the distribution of realised microstates in the phase space. In the following section 4.5, we give a formal generalization to stochastic many-body dynamics based on Master equations. For this, we follow the structure of the proof presented in section 4.4.4.

4.5. Stochastic many-body dynamics subject to dynamic compartmentalisation

In Section 4.4, we demonstrated that the entropy of an ideal gas system is invariant under dynamic compartmentalisation: partitions can be inserted and removed in an arbitrary order without affecting the macrostate statistics of the ideal gas. By proving this property analytically, we showed that this *entropic neutrality under compartment fusion and fragmentation* is deeply connected to special statistical identities of the Dirichlet distribution. We chose to focus on the ideal gas to develop an intuition for how compartment

fusion and fragmentation affect stochastic many-body dynamics enclosed in the dynamic compartments. However, we have yet to determine the extent to which this insight gained by studying the ideal gas is generalizable, as we proved its *entropic neutrality* to be rooted in the special statistical properties of the Dirichlet distribution.

Our main motivation for studying this topic stems from the study of biological matter. In this context, we are interested in exploring general many-body dynamics that include chemical reactions, rather than just studying the ideal gas. In this chapter, we present a general framework based on the formalism of Master Equations, which allows studying dynamical systems from a kinetic perspective [17]. We extend the formalism of Master Equations to be applicable to dynamic compartmentalisation. Specifically, we start by refining the model definition previously given in section 4.3.2 by specifying how we account for arbitrary stochastic many-body dynamics describable by Master Equation. Next, we introduce the formalism of Second quantisation, which enables us to describe the ensemble statistics of stochastic many-body dynamics with Master Equations in a convenient manner. Based on this, we quantify the extent to which compartment dynamics perform a generalised form of work on the system. We illustrate this concept with two case examples and conclude by investigating general properties of stochastic many-body dynamics that are necessary for *entropic neutrality under compartment fusion and fragmentation*.

4.5.1. Refinement on boundary conditions

When studying the ideal gas under dynamic compartmentalisation, we investigated micro-canonical (N, V, E) -ensembles and in particular reduced the description of the system's state to an energy vector \vec{E} . As we turn to a generalisation of the dynamics, we need to extend on this definition. In particular, we want to investigate the general properties of the particles that extend beyond the notion of energy. The most placative extension in the context of biological systems is to study the chemical states of particles, e.g. changes from monomeric to dimeric and to oligomeric states. In more general terms, we consider agents that distribute an abstract quantity among themselves. We generalise our definition from N particles enclosed in the system each with a specified energy E_i to a total mass of N monomeric particles in the system and state that every particle complex is described by an element $\xi \in \Xi$, where Ξ is a countable set. An example of this generalisation is to consider the total size of homo-oligomeric complexes in units of monomers. The condition of forming a countable set will allow us to apply the formalism of the Second quantisation later in this chapter. Due to this condition, we are formally restricted to discrete dynamics. Note, however, that taking suited continuity limits offers a route for generalisations to continuous dynamics.

As we have generalised the notion of energy above, we need to refine the boundary conditions of the system with respect to external energy fluxes. With the formalism of the Master Equation, both equilibrium and non-equilibrium dynamics can be described. As the Master Equation is based on kinetic rules, the steady states of the Master Equation are not necessarily equilibrium solutions. Yet, non-equilibrium steady states demand a steady flux of energy to obtain the dynamics. As a consequence, when we prohibit energy and heat fluxes into the system and impose that no work is performed on the system, not all conceivable dynamics in terms of kinetic rules are physically realisable. Here we focus in particular on kinetic rules that fulfil detailed balance in steady states, i.e. equilibrium dynamics. This restriction allows us to precisely disentangle different contributions of work that we perform on the system.

4.5.2. Describing compartment dynamics in the formalism of the Second quantisation

Describing particle interaction models based on kinetic interaction rules offers an intuitive approach to understanding complex stochastic many-body dynamics. These models can be directly translated into algorithmic rules for numerical simulations. However, we aim to corroborate the findings of these numerical experiments with analytic proofs. This formally requires connecting the particle interaction rules to the resulting ensemble statistics.

In this section, we demonstrate that the formalism of the Second quantisation provides a powerful framework for describing particle interaction dynamics in the context of dynamic compartmentalisation. Specifically, we show that the Second quantisation allows us to prove the presence or absence of *entropic neutrality* under dynamic compartmentalisation directly from the imposed kinetic rules of particle interaction, without having to explicitly compute the ensemble statistics.

The central gist of the Second quantisation is to track the statistics of the ensemble dynamics in the Fock space. For this, we set the indistinguishability between particles, as we count how many particles are in a designated particle state $|n_i\rangle$. A realisation of a system's state is given by $|n_0, n_1, \dots, n_{N_s}\rangle = |\vec{n}\rangle$, which describes for the whole ensemble how many particles are in which particle state. Here, N_s is the number of particle states. Each realisation is associated with a realisation probability $P(n_0, n_1, \dots, n_{N_s}; t)$. We define the state vector of the system with

$$|\psi(t)\rangle = \sum_{\vec{n}} P(\vec{n}; t) |\vec{n}\rangle, \quad (4.38)$$

summarizing the probability distribution over different realisations. We define the linear map $\langle \vec{n} |$, such that $\langle n'_0, n'_1, \dots, n'_N | n_0, n_1, \dots, n_N \rangle = \prod_i \delta_{n'_i, n_i}$. We define a contraction vector $\langle \vec{n}_0 | = \sum_j \langle \vec{n}_j |$ as a sum over the set of normalised orthogonal basis vectors. Note, that the state $|\psi(t)\rangle$ is properly normalised $\langle \vec{n}_0 | \psi(t) \rangle = 1$, as the probabilities $P(\vec{n}_j; t)$ are normalised. We describe the particle interactions in terms of transition rates between realisations $\mathcal{T}_{\vec{n} \rightarrow \vec{n}'}$. This allows translating the dynamics of particle interactions to a Master Equation formalism, as detailed in the appendix A.1.

Specifically, the Master equation is defined as

$$\frac{d}{dt} P(\vec{n}, t) = \sum_{\vec{n}'} [\mathcal{T}_{\vec{n}' \rightarrow \vec{n}} P(\vec{n}', t) - \mathcal{T}_{\vec{n} \rightarrow \vec{n}'} P(\vec{n}, t)]. \quad (4.39)$$

Using the state vector $|\vec{n}\rangle$, we recast the Master Equation in the form of a Hamiltonian

$$\frac{d}{dt} |\psi(t)\rangle = \hat{\mathcal{H}} |\psi(t)\rangle. \quad (4.40)$$

With this, we find the symbolic solution of the differential equation as

$$|\psi(t)\rangle = e^{t\hat{\mathcal{H}}} |\psi_0\rangle, \quad (4.41)$$

where $|\psi_0\rangle$ denotes the initial conditions. We identify $e^{t\hat{\mathcal{H}}}$ as the time-evolution operator. The Hamiltonian $\hat{\mathcal{H}}$ entails all transition rates \mathcal{T} . We find that the steady states of the

dynamics

$$0 |\psi_{\text{ss}}(t)\rangle = \frac{d}{dt} |\psi_{\text{ss}}(t)\rangle = \hat{\mathcal{H}} |\psi_{\text{ss}}(t)\rangle \quad (4.42)$$

are the kernel of the Hamiltonian. In the next step, we expand the Hamiltonian in terms of annihilation and creation operators, which will become useful in further analysis.

We define the annihilation operator \hat{a}_i , which acts on the i -th element of the Fock space and describes the annihilation of a particle in state x_i following $\hat{a}_i |\dots, n_i, \dots\rangle = n_i |\dots, n_i - 1, \dots\rangle$. The creation operator $\hat{a}_i^\dagger |\dots, n_i, \dots\rangle = |\dots, n_i + 1, \dots\rangle$ is the complex conjugate of the annihilation operator. Combining these two operators, we define the number operator

$$\hat{n}_i |\dots, n_i, \dots\rangle = \hat{a}_i^\dagger \hat{a}_i |\dots, n_i, \dots\rangle = n_i |\dots, n_i, \dots\rangle \quad (4.43)$$

as the product of creation and annihilation operator. This operator gives the occupation number of the i -th element of the Fock space for a given realisation $|\vec{n}\rangle$. Additionally, we define the normalisation operator $\hat{\mathcal{R}}$, such that

$$\hat{\mathcal{R}} |\dots, n_i, \dots\rangle = \frac{1}{\sum_i^{N_s} w_i n_i} |\dots, n_i, \dots\rangle = \frac{1}{\mathcal{N}} |\dots, n_i, \dots\rangle, \quad (4.44)$$

where we define $\hat{\mathcal{R}} |\vec{0}\rangle = 1 |\vec{0}\rangle$. We define with w_i the weight of the state i . In absence of aggregation dynamics, all particle states have the same weight $w_i = 1$. In the case of aggregation dynamics, a dimer state would, for example, have a weight $w_2 = 2$. \mathcal{N} is the total number of particles in the system. The commutator of two operators is defined as $[\hat{p}, \hat{q}] = \hat{p}\hat{q} - \hat{q}\hat{p}$. In general, operators do not commute. The commutator for the annihilation and creation operators is given by $[\hat{a}_i, \hat{a}_j^\dagger] = \delta_{i,j}$. Here, we express the commutation relation of the normalisation operator $\hat{\mathcal{R}}$ with the annihilation and creation operator in a multiplicative form as $\hat{\mathcal{R}}\hat{a}_i = \frac{\mathcal{N}}{\mathcal{N}-1}\hat{a}_i\hat{\mathcal{R}}$ and $\hat{\mathcal{R}}\hat{a}_i^\dagger = \frac{\mathcal{N}}{\mathcal{N}+1}\hat{a}_i^\dagger\hat{\mathcal{R}}$, which will be useful in the further analysis. Following this general definition of operators, we next study the thermodynamics of dynamic compartmentalisation by first focussing on the fragmentation of compartments.

4.5.2.1. Fragmentation of compartments in the framework of the Second quantisation

In analogy to the proof given in section 4.4.4, we are interested in how the temporal evolution of the ensemble is affected by sample extraction. Note, that with this we formally investigate how the stochastic many-body dynamic enclosed in the compartment responds to the perturbation of sample extraction. First, we focus on the special case of a sample extraction of size $n = 1$ and subsequently conclude on arbitrary sample extraction sizes. To this end, we define the probability of finding a single particle in a particle state x_i as p_i . We next make use of the closed compartmentalised system being mass conserving. In the absence of aggregation dynamics, all realisations $|\vec{n}_j\rangle$ of a system with fixed constraints have the same number of particles. We directly extract the probability vector \vec{p} for sampling a single random particle from the system in state $|\psi(t)\rangle$ using

$$\vec{p}(t) = \langle \vec{n}_0 | \left(\sum_i \vec{e}_i \hat{n}_i \right) \hat{\mathcal{R}} |\psi(t)\rangle = \frac{1}{\mathcal{N}} \langle \vec{n}_0 | \sum_i \vec{e}_i \hat{n}_i |\psi(t)\rangle. \quad (4.45)$$

4. Towards a thermodynamics of closed compartmentalised systems

Using this, we define the sample extraction operator $\hat{\mathcal{S}}$ making use

$$\hat{\mathcal{S}} = \left(\sum_i \hat{a}_i \right) \hat{\mathcal{R}} = \hat{\mathcal{Q}} \hat{\mathcal{R}}, \quad (4.46)$$

where a single particle in state x_i is removed. Note that by construction a particle in state x_i is removed with a probability $p_i = n_i/\mathcal{N}$. For abbreviation purpose, we defined $\hat{\mathcal{Q}} = \sum_i \hat{a}_i$.

We are interested in the difference of two samples taken subsequently with a time difference $\Delta t = t - t_0$ between the two sample extractions. We define the statistics of the first sampling as \vec{p}_1

$$\vec{p}_1 = \langle \vec{n}_0 | \left(\sum_i \vec{e}_i \hat{n}_i \right) \hat{\mathcal{R}} | \psi_{\text{ss}}(t_0) \rangle = \frac{1}{\mathcal{N}} \langle \vec{n}_0 | \sum_i \vec{e}_i \hat{n}_i | \psi_{\text{ss}}(t_0) \rangle \quad (4.47)$$

as the sample extraction from the steady state vector. By construction, the sample extraction perturbs the state such that $\hat{\mathcal{S}} | \psi_{\text{ss}}(t) \rangle \neq | \psi_{\text{ss}}(t) \rangle$. Next, we let the system evolve for a sufficient time to reach the new equilibrium and we extract the second sample

$$\vec{p}'_2 = \langle \vec{n}_0 | \left(\sum_i \vec{e}_i \hat{n}_i \right) \hat{\mathcal{R}} e^{t\hat{\mathcal{H}}} \hat{\mathcal{S}} | \psi_{\text{ss}}(t_0) \rangle, \quad (4.48)$$

similar to the idea of sequential fragmentation defined in section 4.3.2. Note, that we define the probability vector \vec{p}_2 using the proper normalisation $\vec{p}_2 = \vec{p}'_2 \cdot \mathcal{N}/(\mathcal{N} - 1)$. This yields

$$\vec{0} = \vec{p}_1 - \frac{1}{\gamma} \vec{p}_2 = \langle \vec{n}_0 | \left(\sum_i \vec{e}_i \hat{n}_i \right) \hat{\mathcal{R}} \left(\mathbb{1} - \frac{1}{\gamma} e^{t\hat{\mathcal{H}}} \hat{\mathcal{S}} \right) | \psi_{\text{ss}}(t_0) \rangle \quad (4.49)$$

with $\gamma = \mathcal{N}/(\mathcal{N} - 1) \in \mathbb{R}$ a real number and $\mathbb{1}$ the identity operator. This implies

$$\left(\mathbb{1} - \frac{1}{\gamma} e^{t\hat{\mathcal{H}}} \hat{\mathcal{S}} \right) | \psi_{\text{ss}}(t) \rangle = 0 | \psi_{\text{ss}}(t) \rangle = 0, \quad (4.50)$$

Notably, we find an intrinsic symmetry of the system's states $|\psi(t)\rangle$, which constitutes as self-similarity of sample extraction probabilities \vec{p} differing only by a rescaling. Note, that due to this self-similarity, the argument of removing a randomly sampled single particle can be iteratively applied. This allows a straightforward generalisation to arbitrary sample sizes. We emphasize, that proofing the equivalence of $\vec{p}_2 = \vec{p}_1$ follows the analogous proof structure as presented in the proof of entropic neutrality of the ideal gas in section 4.4.4.

Note, that by using the framework of the Second quantisation, there is no need to compute specific statical distributions and identities between distributions. Using the formalism of the Second quantisation, the whole proof boils down to the computation of the commutator of the sampling operator $\hat{\mathcal{S}}$ and the time evolution operator $e^{t\hat{\mathcal{H}}}$. Yet, since the Hamiltonian is usually a sum of non-commuting products of operators, the direct computation of the commutator with the exponential of the Hamiltonian is of major complicatedness. To circumvent this computation, we take the derivative of the

time evolution operator

$$0 = \frac{d}{dt} |\psi_{\text{ss}}(t)\rangle = \frac{1}{\gamma} e^{t\hat{\mathcal{H}}} \hat{\mathcal{H}} \hat{\mathcal{S}} |\psi_{\text{ss}}(t)\rangle. \quad (4.51)$$

As $\hat{\mathcal{H}} |\psi_{\text{ss}}(t)\rangle = 0 |\psi_{\text{ss}}(t)\rangle$ for steady states by definition, we find that $\vec{p}_2 = \vec{p}_1$ iff $[\hat{\mathcal{H}}, \hat{\mathcal{S}}] |\psi_{\text{ss}}(t)\rangle = 0 |\psi_{\text{ss}}(t)\rangle$, which we denote as $[\hat{\mathcal{H}}, \hat{\mathcal{S}}]_{\text{ss}} = 0$ to stress the dependence on the evaluation of steady-state solutions. This additional simplification allows us to predict entropic neutrality under dynamic compartmentalisation by performing the simple calculation of a commutator relation between the sampling operator and the Hamiltonian of the dynamics.

In a final step, we now extend the formalism from one particle sample extraction to extracting a random number of particles. To this end, we introduce the simplified notation of state $|\psi(t)\rangle = \sum_j b_j |\vec{n}_j(t)\rangle$, where the index j runs over all possible system realizations $|\vec{n}_j(t)\rangle$ and b_j is an abbreviation for the probability to find the system in state $|\vec{n}_j(t)\rangle$. We further abbreviate the binomial probability

$$p_n(k) = \binom{n}{k} p^k (1-p)^{n-k}, \quad (4.52)$$

with the success probability for a particle to be extracted. Finally, we introduce the generalised normalisation operator

$$\hat{\mathcal{R}}(k) = \frac{1}{\prod_{l=1}^k (\mathcal{N} - (l-1))}, \quad (4.53)$$

where we made use of the mass conservation property of closed compartmentalised systems.

A sample extraction due to the insertion of a partition corresponds to $\hat{\mathcal{K}}$, with

$$\hat{\mathcal{K}} |\psi(t)\rangle = \sum_j b_j \sum_k^{\mathcal{N}_j} \hat{\mathcal{Q}}^k \hat{\mathcal{R}}(k) p_{\mathcal{N}_j}(k) |\vec{n}_j(t)\rangle, \quad (4.54)$$

where \mathcal{N}_j is the number of particles in state $|\vec{n}_j(t)\rangle$. The sampling success probability is given by the volume ratio separated from the system by partition insertion, with $p = v_s/v_0$. As we are interested in the commutator relation of $\hat{\mathcal{K}}$ with \mathcal{H} , we are interested in commuting the relation $\hat{\mathcal{H}} \hat{\mathcal{Q}}^k$. We here restrict ourselves to only consider dynamics where transitions between states originate from either two-body or one-body particle interaction, like the exchange of energy quanta, the binary aggregation of complexes, or the fragmentation of complexes. However, note that a generalisation to arbitrary dynamics entailing multi-body interactions is straightforward. We formally define the commutator $[\hat{\mathcal{H}}, \hat{\mathcal{Q}}] = \hat{\mathcal{H}}_1$ and $[\hat{\mathcal{H}}_1, \hat{\mathcal{Q}}] = \hat{\mathcal{H}}_2$. Note that due to restriction to at maximal

4. Towards a thermodynamics of closed compartmentalised systems

two-body interaction $[\hat{\mathcal{H}}_2, \hat{\mathcal{Q}}] = 0$ Then commuting $\hat{\mathcal{H}}$ and $\hat{\mathcal{Q}}^k$ results in the hierarchy

$$\begin{aligned}\hat{\mathcal{H}}\hat{\mathcal{Q}}^0 &= \hat{\mathcal{H}} \\ \hat{\mathcal{H}}\hat{\mathcal{Q}}^1 &= \hat{\mathcal{Q}}\hat{\mathcal{H}} + \hat{\mathcal{H}}_1 \\ \hat{\mathcal{H}}\hat{\mathcal{Q}}^2 &= \hat{\mathcal{Q}}^2\hat{\mathcal{H}} + 2\hat{\mathcal{Q}}\hat{\mathcal{H}}_1 + \hat{\mathcal{H}}_2 \\ &\dots \\ \hat{\mathcal{H}}\hat{\mathcal{Q}}^k &= \hat{\mathcal{Q}}^k\hat{\mathcal{H}} + k\hat{\mathcal{Q}}^{k-1}\hat{\mathcal{H}}_1 + T_{k-1}\hat{\mathcal{Q}}^{k-2}\hat{\mathcal{H}}_2, \quad \forall k > 2,\end{aligned}\tag{4.55}$$

where T_k is the k -th triangular number. For the dynamics to be entropically neutral under the random insertions of partitions, the application of the random sampling operator $\hat{\mathcal{K}}$ and subsequently the Hamiltonian $\hat{\mathcal{H}}$ must vanish in steady state,

$$\boxed{\hat{\mathcal{H}}\hat{\mathcal{K}}|\psi_s(0)\rangle = 0|\psi_s(0)\rangle}.\tag{4.56}$$

Note, that if we have proven the equivalence of \vec{p}_1 and \vec{p}_2 after random sampling due to particle insertion, we follow the identical proof structure as given in section 4.4.4 for the ideal gas to show that synchronous and sequential fragmentation yield the identical macrostate statistics. Next, we focus on the fusion of two compartments to assess if the dynamics are entropically neutral under dynamic compartmentalisation. Following this, we discuss our findings in the context of a generalised notion of work in section 4.5.2.3.

4.5.2.2. Fusion of compartments in the framework of the Second quantisation

In section 4.5.2.1, we have demonstrated how the formalism of Second quantisation can be utilised to describe the impact of compartment fragmentation on the statistical properties of enclosed stochastic many-body dynamics. Specifically, we have shown that fragmentation of compartments is represented by a fragmentation operator $\hat{\mathcal{K}}$ that acts on the system state $|\psi\rangle$. We have considered the fragmentation of a compartment as a perturbation to the state $|\psi\rangle$. In section 4.5.2.3, we discuss this perturbation in the context of a generalised notion of work performed on the system by fragmentation. In this subsection, we will now proceed to explain how compartment fusion can be represented within the framework of Second quantisation. As in the case of compartment fragmentation, we regard compartment fusion as a perturbation to a given compartment.

The central difference between compartment fragmentation and compartment fusion is that the latter is a two-body process: Whereas the statistics of fragmenting a compartment are fully defined by the statistics of the compartment subject to fragmentation, the statistics of fusion depend on the statistics of the two fusing compartments. To this end, we consider one compartment to be *perturbed* and the other compartment to supply the fusion statistics. This approach is analogous to considering only one of the two daughter compartments in the perturbation approach of the fragmentation operator presented in section 4.5.2.1. We define the fusion statistics as $|\psi'\rangle = \sum_l b_l |\vec{n}_l\rangle$ and the fusion operator

$$\hat{\mathcal{J}}_{|\psi'\rangle}|\psi\rangle = \sum_l b_l \prod_j^{N_s} (\hat{a}^\dagger)^{n_{l;j}} |\psi\rangle, a\tag{4.57}$$

where we made use of the product over all components of the \vec{n}_j vector.

The argument for investigating whether compartment fusion affects the dynamics follows the same structure as that for compartment fragmentation presented in section 4.5.2.1.

Specifically, we use the same reasoning and make use of the sample extraction vectors \vec{p}_1 and \vec{p}_2 . We conclude that compartment fusion does not affect the macro-state statistics of the system only if the single-particle sampling shows the same statistics. Following the arguments presented in section 4.5.2.1, we find the analogous condition

$$\boxed{\hat{\mathcal{H}}\hat{\mathcal{J}}_{|\psi'\rangle}|\psi_s(0)\rangle = 0|\psi_s(0)\rangle} \quad (4.58)$$

for fusion not to affect the statistics of the system.

Note, that in contrast to compartment fragmentation, we in general expect the fusion of the compartment to change the statistics of the system. As previously discussed in the literature review of Gibbs' paradox in section 4.2.2, the fusion of compartments typically leads to a non-vanishing mixing entropy. However, there is a special case where the statistics of the system do not change: That is when the two compartments being fused have the same statistics as if they were created by a previous fragmentation process. As we demonstrated in section 4.4.4 while studying the ideal gas, we expect that compartment fusion vanishes in Eq. (4.58), if the two fusing compartments are created by the fragmentation process of a larger system that is in a steady state. A mathematical proof based on the operators still needs to be provided. However, it is worth noting that the fusion operator $\hat{\mathcal{J}}_{|\psi'\rangle}$ is not the inverse of the fragmentation operator $\hat{\mathcal{K}}$, as reversing a fragmentation process requires keeping track of the correlation between $|\psi\rangle$ and $|\psi'\rangle$. In the next section, we interpret the processes of compartment fusion and fragmentation in terms of a generalised notion of work.

4.5.2.3. Entropy changes induced by compartment fusion and fragmentation

In sections 4.5.2.1 and 4.5.2.2, we derived the fragmentation operator $\hat{\mathcal{K}}$ and the fusion operator $\hat{\mathcal{J}}_{|\psi'\rangle}$ applied to a specified compartment state $|\psi\rangle$ to formalize the processes of compartment fragmentation and fusion within the framework of Second quantisation. Specifically, we have linked the vanishing of the iterative application of the fusion and fragmentation followed by the Hamiltonian $\hat{\mathcal{H}}$ operator with compartment fusion and fragmentation not affecting the macrostate statistics of the system. In this section, we will quantify the perturbation of $\hat{\mathcal{J}}_{|\psi'\rangle}$ and $\hat{\mathcal{K}}$ performed on states $|\psi\rangle$.

When we fuse or fragment a compartment, we alter the constraints on the stochastic dynamics enclosed within the compartment. Let $|\vec{n}_j\rangle$ refer to possible realizations of microscopic dynamics in a compartment before a compartment process, and $|\vec{m}_j\rangle$ refer to possible realizations of microscopic dynamics in the compartment after fusing or fragmenting the compartment. $|\vec{n}_j\rangle$ and $|\vec{m}_j\rangle$ form non-overlapping sets in a common phase space. As a consequence, the phase space of $|\psi_n\rangle$ and $|\psi_m\rangle$, which describe system states before and after a compartment process, are not overlapping in phase space. We thus understand the operators $\hat{\mathcal{J}}_{|\psi'\rangle}$ and $\hat{\mathcal{K}}$ as maps between different regions in phase space.

When we test for the vanishing relations in Eq. (4.56,4.58) we inquire whether $\hat{\mathcal{J}}_{|\psi'\rangle}$ and $\hat{\mathcal{K}}$ map steady states of $|\psi_{n,ss}\rangle$ to steady states of $|\psi_{m,ss}\rangle$. If the relation in Eq. (4.56) and Eq. (4.58) is not vanishing, we find that the system relaxes to a steady state after the compartment process. In this case, compartment fusion or fragmentation alter the statistics of the system. We state that compartment fusion or fragmentation has not been *perturbed*, if the $\hat{\mathcal{J}}_{|\psi'\rangle}$ and $\hat{\mathcal{K}}$ map steady states of $|\psi_{n,ss}\rangle$ to steady states of $|\psi_{m,ss}\rangle$. Conversely, if the relation in Eq. (4.56) and Eq. (4.58) is not vanishing, we state that compartment fusion or fragmentation has *perturbed* the system.

4. Towards a thermodynamics of closed compartmentalised systems

We next quantify to what extent the statistics of the system are altered in response to a compartment process. We propose to quantify the strength of the perturbation by $\langle \vec{n}_0 | \hat{\mathcal{H}} \hat{\mathcal{J}}_{|\psi\rangle} | \psi_n \rangle = W_a$ and $\langle \vec{n}_0 | \hat{\mathcal{H}} \hat{\mathcal{K}} | \psi_n \rangle = W_f$. Due to the mapping to a different region in the phase space, we additionally consider the normalisation as we consider the commutator

$$\langle \vec{n}_0 | [\hat{\mathcal{H}}, \hat{\mathcal{J}}_{|\psi\rangle}] | \psi_n \rangle = \Delta W_a \quad (4.59a)$$

$$\langle \vec{n}_0 | [\hat{\mathcal{H}}, \hat{\mathcal{K}}] | \psi_n \rangle = \Delta W_f. \quad (4.59b)$$

Note that the additional normalisation is by construction vanishing as the steady states are considered. ΔW_a has the same units as the eigenvalues of the Hamiltonian $\hat{\mathcal{H}}$ of the system. We link the non-vanishing commutator relation to changes in entropy, as the perturbed system is relaxing to a new steady state.

Recalling Maxwell's demon, we find that the demon was formally performing work on the system, as the entropy was altered. We suggest interpreting ΔW_a and ΔW_f as generalised notions of work. Furthermore, if the relations Eq. (4.56) and Eq. (4.58) are vanishing in steady state, we also find $\Delta W_a = 0$ and $\Delta W_f = 0$, and we find that compartment fusion and fragmentation does not affect the system's statistics. This further argues towards a connection between ΔW_a and work performed on the system.

Note, however, that we have employed a kinetic perspective in this discussion, as we defined the dynamics of the stochastic many-body dynamics based on transition rates, without formally stating the thermodynamic ensemble of the dynamics. As a consequence, the eigenvalues of $\hat{\mathcal{H}}$ are not necessarily in units of energy, which dilutes the notion of work for ΔW_f . Furthermore, it should be noted that work is precisely defined by the first and second laws of thermodynamics. To further consolidate ΔW_a and ΔW_f as in a generalised notion of work performed on the system, additional proofs are necessary. Next, we investigate two case examples which allow us to further illuminate the general question of under which conditions the statistics of stochastic many-body dynamics are unaffected by dynamic compartmentalisation.

4.5.3. Quantised gases subject to sequential compartment fragmentation

Before delving into the application of the formalism of Second quantisation to a quantised version of the ideal gas in this subsection, we revisit the dynamics of quantised ideal gases from a kinetic perspective. In this context, an isolated compartment containing a quantised gas is described by a state vector $\varepsilon = (\varepsilon_1, \varepsilon_2, \dots, \varepsilon_{\mathcal{N}})$, where \mathcal{N} denotes the total number of particles and $\varepsilon_i \in \mathbb{N}_0$ represents energy on particles in state i . We consider quantised energies, such that $\varepsilon_j = j\varepsilon_1$. We adhere to the methodology previously employed in section 4.4.1 for the ideal gas and neglect the spatial positions of each particle, assuming that particles collide with equal probability regardless of their state, i.e., the number of energy quanta carried by each particle. This corresponds to the molecular chaos hypothesis.

The collision of particles results in the redistribution of energy quanta among the two colliding particles. The particle redistribution dynamics are characterised by rates $f((\varepsilon_i, \varepsilon_j) \rightarrow (\varepsilon'_i, \varepsilon'_j))$, which describe that particle i and j carrying the energy ε_i and ε_j collide and after the collision carry ε'_i and ε'_j with $\varepsilon_i + \varepsilon_j = \varepsilon'_i + \varepsilon'_j$. Specifically, we refine

the collision rates

$$f((\varepsilon_i, \varepsilon_j) \rightarrow (\varepsilon'_i, \varepsilon'_j)) = f_{\text{I}}(\varepsilon_i, \varepsilon_j) p_{\text{E}}(\varepsilon'_i, \varepsilon'_j | \varepsilon_i + \varepsilon_j). \quad (4.60)$$

Here, we utilise a combination of an interaction rate f_{I} and an exchange probability p_{E} . In the case of the quantised analogue of the ideal gas, the interaction probability is unbiased, $f_{\text{I}}(\varepsilon_i, \varepsilon_j) = \text{const.}$, such that the probability for any two particles to interact is equally likely and independent of the particle state. For the exchange probability, we consider symmetric probability distributions centred around $(\varepsilon_i + \varepsilon_j)/2$ on the finite support $[0, \varepsilon_i + \varepsilon_j]$, $p_{\text{E}}(\varepsilon'_i, \varepsilon'_j | \varepsilon_i + \varepsilon_j) = g_{[0, \varepsilon_i + \varepsilon_j]}(\varepsilon'_i)$. In particular, we consider $g_{[0, \varepsilon_i + \varepsilon_j]}((\varepsilon_i + \varepsilon_j)/2 - y) = g_{[0, \varepsilon_i + \varepsilon_j]}((\varepsilon_i + \varepsilon_j)/2 + y)$, $\forall y \leq (\varepsilon_i + \varepsilon_j)/2$ and $g_{[0, 1]}(\varepsilon) = g_{[0, a]}(a\varepsilon)$, $\forall a \in \mathbb{R}^+$. Here, we find for the quantised version of the ideal gas in two dimensions, that $p_{\text{E}}(\varepsilon'_i, \varepsilon'_j | \varepsilon_i + \varepsilon_j) = 1/(\varepsilon_i + \varepsilon_j) \delta((\varepsilon'_i + \varepsilon'_j) - (\varepsilon_i + \varepsilon_j))$ as the exchange probability is uniformly distributed. Distinguishing between the interaction and the exchange probability allows for simple generalisations of the ideal gas with an intuitive understanding of the implication for its dynamics.

To derive the Hamiltonian for the quantised ideal gas, we first note that all transitions follow the same functional form. As introduced in section 4.5.2, we translate the dynamics to the Fock space, where the index i refers to the energy levels rather than individual particles. Notably, n_i now refers to the number of particles with energy level i . State transitions in $|\vec{n}\rangle$ are caused by two-particle interactions. In line with the kinetic perspective on the particle dynamics, we find the transition rates

$$\mathcal{T}_{(i,j) \rightarrow (i',j')} = n_i n_j f((i, j) \rightarrow (i', j')), \quad (4.61)$$

$$\mathcal{T}_{(i,j) \rightarrow (i',j')} = f((i, j) \rightarrow (i', j')) \hat{a}_{j+l}^\dagger \hat{a}_{i-l}^\dagger \hat{a}_j \hat{a}_i, \quad (4.62)$$

The rate $f((i, j) \rightarrow (i', j'))$ encodes both the interaction rates as well as the exchange probabilities. In particular, if $f((i, j) \rightarrow (i', j')) = f((j, i) \rightarrow (i', j'))$ and the exchange probability $p_{\text{E}}(\varepsilon'_i, \varepsilon'_j | \varepsilon_i + \varepsilon_j)$ following the definitions above, the dynamics fulfil detailed balance by construction. This implies, that the dynamics of the quantised version of the ideal gas presented here are physically realisable in a micro-canonical setup⁵.

In the remainder of this section, we leave $f((i, j) \rightarrow (i', j'))$ unspecified, which corresponds to probing models for arbitrary interaction rates and exchange probabilities fulfilling the detailed balance condition. We introduce the abbreviated notation $f((i, j) \rightarrow (i', j')) \equiv f_{i,j,i',j'}$. The Hamiltonian is given by the sum over all particles i, j ,

$$\hat{\mathcal{H}}_{\text{qg}} = \sum_{i,j,i',j'} f_{i,j,i',j'} (\hat{a}_{j'}^\dagger \hat{a}_{i'}^\dagger - \hat{a}_j^\dagger \hat{a}_i^\dagger) \hat{a}_j \hat{a}_i, \quad (4.63)$$

see also appendix A.1. The subscript "qg" is an abbreviation for "quantised gas". We probe the commutator relation of this Hamiltonian $\hat{\mathcal{H}}_{\text{qg}}$ with the sampling operator $\hat{\mathcal{S}}$. This yields

$$[\hat{\mathcal{H}}_{\text{qg}}, \hat{\mathcal{S}}] |\psi_{\text{s}}(t)\rangle = (\hat{\mathcal{H}}_{\text{qg}} \hat{\mathcal{S}} - \hat{\mathcal{S}} \hat{\mathcal{H}}_{\text{qg}}) |\psi_{\text{s}}(t)\rangle = \hat{\mathcal{H}}_{\text{qg}} \hat{\mathcal{S}} |\psi_{\text{s}}(t)\rangle, \quad (4.64)$$

where the second term in the second equation vanishes by definition of the steady state $|\psi_{\text{s}}(t)\rangle$. Both $\hat{\mathcal{H}}_{\text{qg}}$ and $\hat{\mathcal{S}}$ are sums of products of annihilation, creation, and normalisation

⁵Here, we go with the notion of physically realisable systems, as "not being in contradiction with fundamental laws of physics".

4. Towards a thermodynamics of closed compartmentalised systems

operators, for which the commutator relations are known. We find

$$\left(\sum_{i,j,i',j'} f_{i,j,i',j'} (\hat{a}_{j'}^\dagger \hat{a}_{i'}^\dagger - \hat{a}_j^\dagger \hat{a}_i^\dagger) \hat{a}_j \hat{a}_i \right) \left(\sum_i \hat{a}_i \right) \hat{\mathcal{R}} |\psi_s(t)\rangle = \hat{\mathcal{L}} \hat{\mathcal{R}} |\psi_s(t)\rangle \quad (4.65)$$

and see that we need to commute both $\sum_i \hat{a}_i$ and $\hat{\mathcal{R}}$ through the Hamiltonian. In a first step, we first neglect $\hat{\mathcal{R}}$ and find

$$\hat{\mathcal{L}} = \left(\sum_i \hat{a}_i \right) \hat{\mathcal{H}}_{\text{qg}} - \sum_{i,j,i',j'} f_{i,j,i',j'} (\hat{a}_{j'}^\dagger + \hat{a}_{i'}^\dagger - \hat{a}_j^\dagger - \hat{a}_i^\dagger) \hat{a}_j \hat{a}_i. \quad (4.66)$$

Note, that the second term refers to the commutator $[\hat{\mathcal{H}}_{\text{qg}}, \hat{\mathcal{Q}}] = \hat{\mathcal{H}}_{\text{qg},1}$, as

$$\hat{\mathcal{H}}_{\text{qg},1} = \sum_{i,j,i',j'} f_{i,j,i',j'} (\hat{a}_{j'}^\dagger + \hat{a}_{i'}^\dagger - \hat{a}_j^\dagger - \hat{a}_i^\dagger) \hat{a}_j \hat{a}_i. \quad (4.67)$$

Furthermore, $[\hat{\mathcal{H}}_{\text{qg},1}, \hat{\mathcal{Q}}] = 0$ vanishes by construction of $\hat{\mathcal{H}}_{\text{qg}}$. Commuting the normalisation operator $\hat{\mathcal{R}}$ and $\hat{\mathcal{L}}$ in a next step, we find

$$\hat{\mathcal{L}} \hat{\mathcal{R}} = \left(\sum_i \hat{a}_i \right) \hat{\mathcal{R}} \hat{\mathcal{H}}_{\text{qg}} - \frac{\mathcal{N} - 1}{\mathcal{N}} \hat{\mathcal{R}} \hat{\mathcal{H}}_{\text{qg},1}. \quad (4.68)$$

The first term on the right-hand side vanishes by definition. The second term cannot be reduced to the Hamiltonian $\hat{\mathcal{H}}_{\text{qg}}$, as $\hat{\mathcal{H}}_{\text{qg}}$ and $\hat{\mathcal{H}}_{\text{qg},1}$ are distinctly different. However, note that for the state $|\psi_s(t)\rangle$ detailed balance holds, as $|\psi_s(t)\rangle$ is an equilibrium state. Detailed balance implies that two realisations $|\vec{n}_i\rangle$ and $|\vec{n}_j\rangle$ connected by a balanced transition with respect to their rates $P(\vec{n}_i) \mathcal{T}_{\vec{n}_i \rightarrow \vec{n}_j} = P(\vec{n}_j) \mathcal{T}_{\vec{n}_j \rightarrow \vec{n}_i}$. Note, that by the construction of the Hamiltonian, each realisation $|\vec{n}_i\rangle$, which is mapped with a rate $\mathcal{T}_{\vec{n}_i \rightarrow \vec{n}_j}$ to state $|\vec{n}_j\rangle$, is also mapped with the same rate and a negative sign to itself. If detailed balance holds, $\hat{\mathcal{H}}_{\text{qg}}$ maps $|\vec{n}_i\rangle$ at the same rate to $|\vec{n}_j\rangle$ as $|\vec{n}_j\rangle$ is mapped to itself with negative sign. This is the mechanism by which $|\psi_s(t)\rangle$ is mapped to the kernel of $\hat{\mathcal{H}}_{\text{qg}}$. Careful inspection shows that if detailed balance is fulfilled for $\hat{\mathcal{H}}_{\text{qg}}$ with a state $|\psi_s(t)\rangle$, then $|\psi_s(t)\rangle$ is also in the kernel of $\hat{\mathcal{H}}_{\text{qg},1}$. Thus, the second term vanishes due to the fulfilled detailed balance condition. This can be proven by lengthy calculations, or directly spotted by a reader with a trained eye. Concluding, we proved

$$\boxed{[\hat{\mathcal{H}}_{\text{qg}}, \hat{\mathcal{S}}] |\psi_s(t)\rangle = 0 |\psi_s(t)\rangle}, \quad (4.69)$$

implying that indeed the sample extraction operator and time evolution operator commute for the quantised gas, if the system is initially in equilibrium and detailed balance is fulfilled. Note, that this in particular also implies that $[\hat{\mathcal{H}}_{\text{qg}}, \hat{\mathcal{S}}^k] |\psi_s(t)\rangle = 0 |\psi_s(t)\rangle \forall k > 0$. We want to emphasize, that the commutator only vanishes if $|\psi(t)\rangle$ has already relaxed to equilibrium. This condition is in general not true for arbitrarily prepared initial states of the system!

In the final step, we generalise to the sampling of a random number of particles by investigating if also $\hat{\mathcal{K}}$ and $\hat{\mathcal{H}}_{\text{qg}}$ commute when applied to the equilibrium state $|\psi_s(t)\rangle$. We note, that the dynamics preserve the particle number such that every realisation $|\vec{n}_j\rangle$

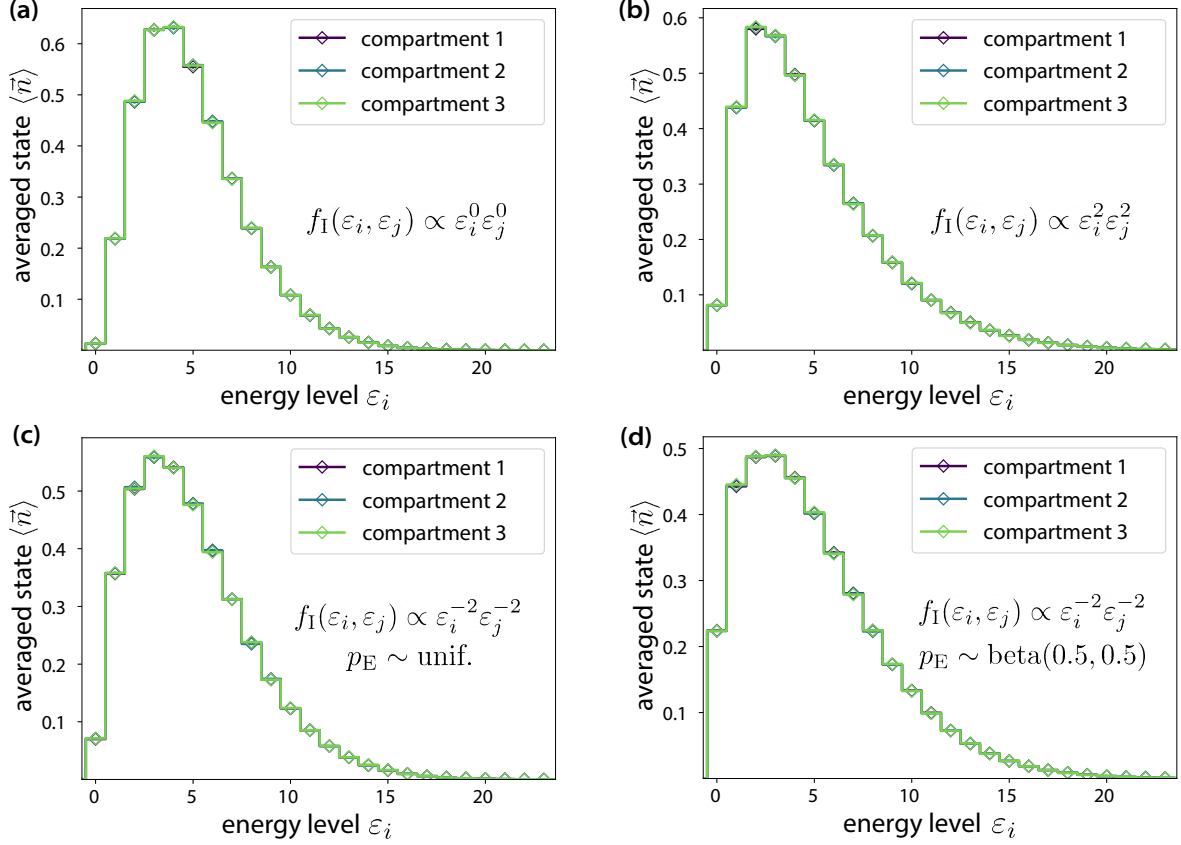


Fig. 4.10.: Quantised gases with two body interaction rules respecting detailed balance are unaffected by sequential fragmentation Quantised gas models as introduced in section 4.5.3 are enclosed in a 3-compartment system subject to sequential fragmentation. Four different interaction rules are implemented in (a)-(d). The interaction rates f_I are proportional to $f_I \propto \varepsilon_i^\alpha, \varepsilon_j^\alpha$, where $\varepsilon_i, \varepsilon_j$ are the energies of the two interacting particles i and j . The exchange probability is a discretised version of the beta distribution, where $\text{beta}(3, 3)$ is used for (a) and (b), while $\text{beta}(0, 0)$ is used for (c) and (d). These dynamics preserve detailed balance in their steady state by construction. The total number of independent iteration runs is 5×10^5 for each simulation (a)-(d). The simulation time was chosen long enough to grant relaxation to equilibrium. The total number of particles is $\mathcal{N} = 12$ with an initial total energy $\mathcal{E} = 60\varepsilon$ in discretised simulation units ε . The average state $\langle \bar{n} \rangle$ describes an average number of particles with energy level ε_i in a specified compartment. The error bars indicate a 5σ environment. The effects of dynamic compartmentalisation vanish for all dynamics (a)-(d) in agreement with our theoretical prediction, see also section 4.5.3 .

4. Towards a thermodynamics of closed compartmentalised systems

has the same total number of particles \mathcal{N} . Hence, we simplify

$$\hat{\mathcal{K}} |\psi(t)\rangle = \sum_j b_j \sum_k^{\mathcal{N}_j} \hat{\mathcal{Q}}^k \hat{\mathcal{R}}(k) p_{\mathcal{N}_j}(k) |\vec{n}_j(t)\rangle = \sum_k^{\mathcal{N}_j} \hat{\mathcal{Q}}^k \hat{\mathcal{R}}(k) p_{\mathcal{N}_j}(k) |\psi(t)\rangle. \quad (4.70)$$

Next, we notice that $\hat{\mathcal{K}} \hat{\mathcal{H}}_{\text{qg}} |\psi_s(t)\rangle = 0 |\psi_s(t)\rangle$ vanishes by construction. For $\hat{\mathcal{H}}_{\text{qg}} \hat{\mathcal{K}} |\psi_s(t)\rangle$, we need to commute $\hat{\mathcal{H}}_{\text{qg}}$ through every summand. Noting that $\hat{\mathcal{R}}(k)$ commutes up to a rescaling factor with $\hat{\mathcal{H}}_{\text{qg}}$, and since $[\hat{\mathcal{H}}_{\text{qg}}, \hat{\mathcal{Q}}^k] |\psi_s(t)\rangle = 0 |\psi_s(t)\rangle \forall k > 0$, we find that $[\hat{\mathcal{K}}, \hat{\mathcal{H}}_{\text{qg}}]_s = 0$. In analogy to the line of argument in section 4.4 for the classical ideal gas, we conclude that also the removal of partitions, and thus the fusion of compartments, thus not affect the statistics of the system. We conclude that stochastic gases that fulfil detailed balance are entropically neutral under dynamic compartmentalisation.

We corroborate this theoretical prediction by numerical simulations. We insert quantised gases with different interaction rules into 3-compartment systems and perform sequential fragmentation processes. To analyze the dynamics of the system, we compute statistics from 5×10^5 independent runs. For this, we compute the averaged state vectors $\langle \vec{n}_i \rangle$ per compartment i and plot histograms of single-particle sampling experiments for each compartment. We consider small systems with initially $\mathcal{N} = 12$ particles, as we expect to find differences between compartments stronger pronounced in the statistics for smaller systems. We start with an initial configuration where all 12 particles are in the 5th energy level $|\psi_0\rangle = |0, 0, 0, 0, 12, 0, 0, \dots\rangle$. Before fragmenting the system, we give sufficient time for the system to relax into equilibrium. We estimate the relaxation time τ_{rel} with approximately 2000 two-particle interactions to have happened. In Fig. 4.10 (a) we consider that collision rate is independent of the particle states, $f_{\text{I}} = \text{const.}$. For the exchange probability, we consider a discretised version of the beta distribution $p_{\text{E}}(i'|i+j) = \text{int}(u \cdot (i+j))$, where $f(x)$ is the function rounding x to the nearest integer and u beta(3, 3) is a beta distributed random variable. We find no difference in the statistics of the averaged state vectors $\langle \vec{n}_1 \rangle = \langle \vec{n}_2 \rangle = \langle \vec{n}_3 \rangle$ between the compartments. This indicates that this model of a quantised gas is entropically neutral under dynamic compartmentalisation.

In Fig. 4.10 (b)-(d), we check other quantised gas models with simulation parameters analogous to Fig. 4.10 (a). For (b), we consider the collision rate to be proportional to the squares energy levels, as $f_{\text{I}}(\varepsilon_i, \varepsilon_j) \propto \varepsilon_i^2 \varepsilon_j^2$. For (c) and (d), we consider that the collision rate is inversely proportional to the squares energy levels, as $f_{\text{I}}(\varepsilon_i, \varepsilon_j) \propto \varepsilon_i^{-2} \varepsilon_j^{-2}$. For (c), we consider a discretised beta distribution with u beta(1, 1), which corresponds to a uniform distribution. For (d), we consider a discretised beta distribution with u beta(0.5, 0.5). For all Fig. 4.10 (b)-(d), we find that the statistics of the averaged state vectors $\langle \vec{n}_1 \rangle = \langle \vec{n}_2 \rangle = \langle \vec{n}_3 \rangle$ between the compartments are identical. Hence, we find in accordance with our theoretical predictions that all quantised gas models are unaffected by sequential compartmentalisation.

As the numerical simulations are in full agreement with our analytical predictions, we conclude that all stochastic gas models, that are based on two-particle interactions and fulfil detailed balance are entropically neutral under dynamic compartmentalisation. Next, we turn to a second case example, as we focus on reversible polymerisation dynamics.

4.5.4. Reversible polymerisation dynamics subject to sequential compartment fragmentation

Having studied the quantised version of the ideal gas in section 4.5.3, we now turn away from stochastic gases and study processes closer to biology by focussing on chemical reactions. Specifically, we start by studying the paradigmatic example of reversible dimerisation



where A_1 refers to a monomeric building blocks and A_2 to dimer configuration. After we study this specific model under dynamic compartmentalisation, we will generalise to general dynamics entailing chemical reactions in a next step.

For reversible dimerisation, we are interested in the amount of monomers and dimers in the system. A realisation of the systems dynamic in a compartment is given by $|n_1, n_2\rangle$, with the total number of monomers and dimers respectively. In analogy to the energy conservation in the case of the ideal gas, the total mass over all particles is conserved to $n_1 + 2n_2 = \mathcal{N}$. We define a constant aggregation rate k and dimer-dissociation rate k^{-1} . The Hamiltonian is given by

$$\hat{\mathcal{H}}_{\text{di}} = k \cdot (\hat{a}_2^\dagger - \hat{a}_1^\dagger \hat{a}_1^\dagger) \hat{a}_1 \hat{a}_1 + k^{-1} \cdot (\hat{a}_1^\dagger \hat{a}_1^\dagger - \hat{a}_2^\dagger) \hat{a}_2. \quad (4.72)$$

Analogous to the example of the quantised ideal gas, we compute the commutator with the sampling operator $\hat{\mathcal{S}}$. To this end, we perform the same separation $\hat{\mathcal{L}} = \hat{\mathcal{H}}_{\text{di}}(\hat{a}_1 + \hat{a}_2)$ and initially neglect $\hat{\mathcal{R}}$ as

$$\hat{\mathcal{L}} = (\hat{a}_1 + \hat{a}_2) \hat{\mathcal{H}}_{\text{di}} - k \cdot (1 - \hat{a}_1^\dagger - \hat{a}_1^\dagger) \hat{a}_1 \hat{a}_1 - k^{-1} \cdot (\hat{a}_1^\dagger + \hat{a}_1^\dagger - 1) \hat{a}_2, \quad (4.73)$$

$$\hat{\mathcal{H}}_{\text{di},1} = +k \cdot (1 - \hat{a}_1^\dagger - \hat{a}_1^\dagger) \hat{a}_1 \hat{a}_1 + k^{-1} \cdot (\hat{a}_1^\dagger + \hat{a}_1^\dagger - 1) \hat{a}_2. \quad (4.74)$$

Notably, we find that $[\hat{\mathcal{H}}_{\text{di},1}, \hat{\mathcal{Q}}] = \hat{\mathcal{H}}_{\text{di},2}$ is not vanishing

$$\hat{\mathcal{H}}_{\text{di},2} = -2k \hat{a}_1 \hat{a}_1 + k^{-1} \hat{a}_2. \quad (4.75)$$

Next commuting the normalisation operator $\hat{\mathcal{R}}$ through $\hat{\mathcal{L}}$, we find

$$\begin{aligned} [\hat{\mathcal{H}}_{\text{di}}, \hat{\mathcal{S}}] |\vec{n}_j\rangle &= (\hat{a}_1 + \hat{a}_2) \hat{\mathcal{R}} \left(k \cdot \left(\frac{\mathcal{N} - 1}{\mathcal{N}} \hat{a}_2^\dagger - \hat{a}_1^\dagger \hat{a}_1^\dagger \right) \hat{a}_1 \hat{a}_1 + k^{-1} \cdot \left(\frac{\mathcal{N} + 1}{\mathcal{N}} \hat{a}_1^\dagger \hat{a}_1^\dagger - \hat{a}_2^\dagger \right) \hat{a}_2 \right) \\ &\quad - \hat{\mathcal{R}} \frac{\mathcal{N} - 1}{\mathcal{N}} \left(k \cdot \left(\frac{\mathcal{N} - 2}{\mathcal{N} - 1} - 2\hat{a}_1^\dagger \right) \hat{a}_1 \hat{a}_1 + k^{-1} \cdot \left(2\hat{a}_1^\dagger \frac{\mathcal{N}}{\mathcal{N} - 1} - 1 \right) \hat{a}_2 \right) |\vec{n}_j\rangle. \end{aligned} \quad (4.76)$$

We find that transition rates are altered with respect to the Hamiltonian $\hat{\mathcal{H}}_{\text{di}}$. As a consequence, terms that have vanished in the Hamiltonian due to detailed balance, do not vanish for $[\hat{\mathcal{H}}_{\text{di}}, \hat{\mathcal{S}}]_{\text{ss}} \neq 0$. Hence, we expect dimerisation reactions with fixed reaction rates k to show effects under dynamic compartmentalisation.

Before we check our theoretical prediction with numerical experiments, we first generalise to arbitrary chemical reaction networks. Recall, that the state of such networks can be represented in terms of the system realizations $|\vec{n}_j\rangle$, where the particle state x_i refers

4. Towards a thermodynamics of closed compartmentalised systems

to a specific chemical species, and n_i denotes the total number of particles in state x_i present in the system. Some reactions between chemical species result in the formation of a new species, thereby rendering the total number of chemical objects not conserved. However, we maintain the conservation of total mass in the system by ensuring that the number of monomeric building blocks remains constant. We now proceed to formalise chemical reaction networks, in order to simplify the notation in the framework of the Second quantisation.

To this end, we distinguish three classes of chemical reactions. First, we consider reactions that alter the configuration of chemical species, such as $A \rightleftharpoons B$. This conserves the total number of chemical objects in the system. Second, we examine aggregation reactions, in which two chemical species merge, for example, $A + B \rightarrow C$. This results in a decrease of the total number of chemical objects in the system. Last, we consider dissociation reactions, in which a single chemical species split into two species, for example, $C \rightarrow A + B$, which leads to an increase in the total number of chemical objects in the system. A generalisation to include chemical reactions of higher order or the dissociation into multiple chemical species is straightforward. Here, we refer to these three classes as *I*, *II*, and *III*, respectively. For a given reaction network, we define a set of index lists, which encode the chemical species involved in each reaction, i.e. $C_I = \{(i; j)\}$, $C_{II} = \{(i, j; k)\}$, and $C_{III} = \{(k; i, j)\}$. We restrict our consideration to chemical reaction networks in which all reactions are reversible, meaning that there is a one-to-one correspondence between every reaction in C_{II} and C_{III} . Specifically, we refer to reactions in C_{II} with $k_{i,j;k}$ and C_{III} with $k_{i,j;k}^{-1}$. With this naming convention, the Hamiltonian is

$$\begin{aligned} \hat{\mathcal{H}}_{\text{CRN}} = & \sum_{(i,j) \in C_I} k_{i,j} (\hat{a}_j^\dagger - \hat{a}_i^\dagger) \hat{a}_i + k_{i,j}^{-1} (\hat{a}_i^\dagger - \hat{a}_j^\dagger) \hat{a}_j \\ & + \sum_{(i,j;k) \in C_{II}} k_{i,j;k} (\hat{a}_k^\dagger - \hat{a}_j^\dagger \hat{a}_i^\dagger) \hat{a}_j \hat{a}_i + \sum_{(k;i,j) \in C_{III}} k_{i,j;k}^{-1} (\hat{a}_j^\dagger \hat{a}_i^\dagger - \hat{a}_k^\dagger) \hat{a}_k. \end{aligned} \quad (4.77)$$

For this Hamiltonian, we can directly compute its commutators $[\hat{\mathcal{H}}_{\text{CRN}}, \hat{\mathcal{Q}}] = \hat{\mathcal{H}}_{\text{CRN},1}$ and $[\hat{\mathcal{H}}_{\text{CRN},1}, \hat{\mathcal{Q}}] = \hat{\mathcal{H}}_{\text{CRN},2}$

$$\hat{\mathcal{H}}_{\text{CRN},1} = \sum_{(i,j;k) \in C_{II}} k_{i,j;k} (1 - \hat{a}_j^\dagger + \hat{a}_i^\dagger) \hat{a}_j \hat{a}_i + \sum_{(k;i,j) \in C_{III}} k_{i,j;k}^{-1} (\hat{a}_j^\dagger + \hat{a}_i^\dagger - 1) \hat{a}_k, \quad (4.78)$$

$$\hat{\mathcal{H}}_{\text{CRN},2} = -2 \sum_{(i,j;k) \in C_{II}} k_{i,j;k} \hat{a}_j \hat{a}_i + 2 \sum_{(k;i,j) \in C_{III}} k_{i,j;k}^{-1} \hat{a}_k. \quad (4.79)$$

Analogous to the case of the dimers, we find that aggregation rates from reactions of class C_{II} and dissociation rates from reactions in class C_{III} do not commute with $\hat{\mathcal{R}}$, as commuting with $\hat{\mathcal{R}}$ leaves a numeric prefactor before the rates that breaks detailed balance. This implies that also $[\hat{\mathcal{H}}_{\text{CRN}}, \hat{\mathcal{K}}]_{\text{ss}} \neq 0$ is not vanishing. Hence, we expect chemical reaction networks entailing aggregation and dissociation reactions to be affected by dynamic compartmentalisation.

We corroborate our theoretical prediction by simulating chemical reaction networks in 3-compartment systems subject to sequential fragmentation, see Fig. 4.11. Here, we do not simulate the chemical reactions by molecular dynamics simulations, but directly by simulating the rates of the Master Equation. To this end, we consider 4 different models, that are specified in Tab. 4.1, which all fulfil detailed balance. The fulfilment of detailed balance refers here both to the chemical reaction network in the thermodynamic limit, as well as to the Markov chain transition network that results from considering the chemi-

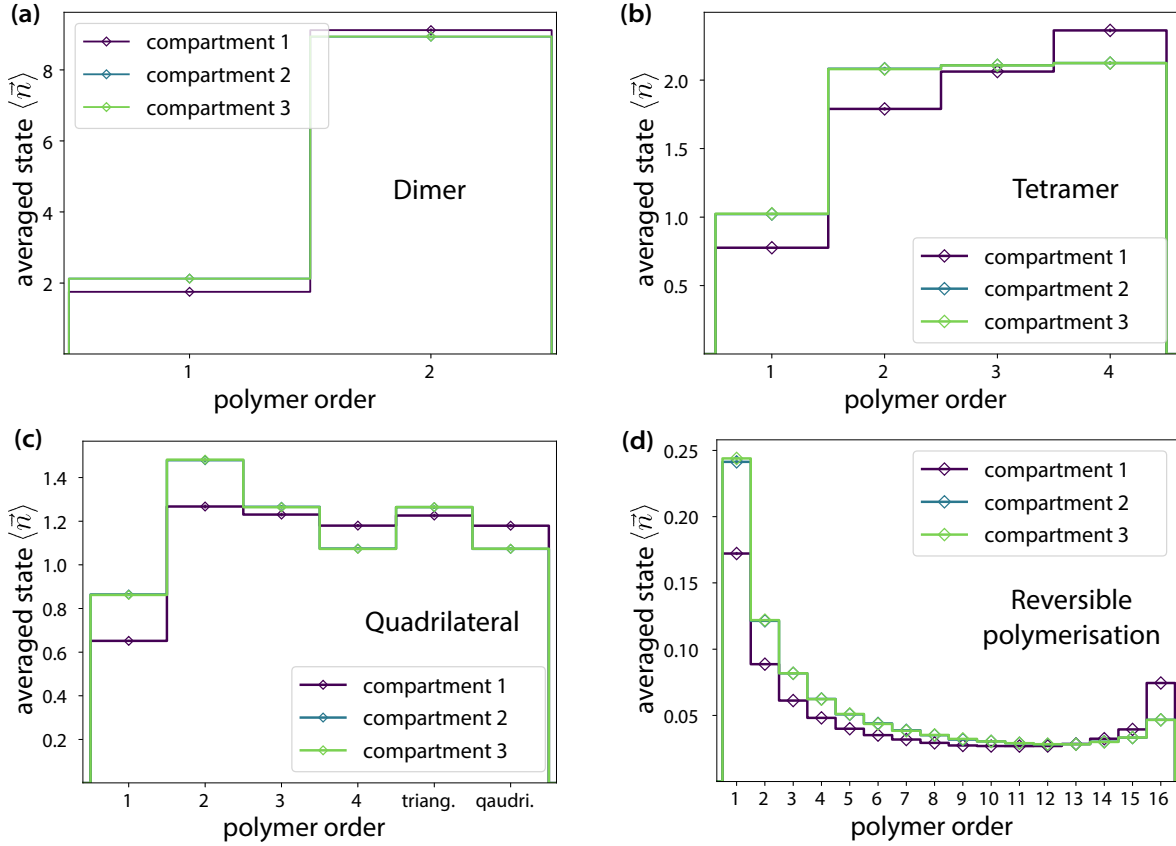


Fig. 4.11.: Sequential fragmentation affects chemical reaction systems with reaction rates independent of the fragmentation process. Four different chemical reaction systems entailing reversible aggregation dynamics are enclosed in a three-compartment system subject to sequential fragmentation. (a) shows a dimerisation system, (b) Tetramer complex formation kinetics, (c) quadrilateral complex formation, (d) reversible polymerisation up to order 16. The reaction rates are detailed in tab 4.1. All reaction schemes fulfil detailed balance in their steady-state configurations. In agreement with the theoretical prediction in section 4.5.4, the statistics of polymers of different order in the first versus the second and third compartment differs. The total number of independent iteration runs is 5×10^5 for each simulation (a)-(d). The simulation time was chosen long enough to grant relaxation to equilibrium with $t = 40\tau$, τ the simulation timescale. The total number of initial monomers is $\mathcal{N} = 60$ for (a)-(c) and $\mathcal{N} = 16$ for (d). Polymer order refers to the length of the build polymer, with monomers being of order 1 and dimers of order 2. 'triang.' and 'quadri.' refer to triangular and quadrilateral complexes, respectively. The averaged state $\langle \bar{n} \rangle$ describes the average amount of polymers of expected in a compartment.

4. Towards a thermodynamics of closed compartmentalised systems

Dimer model		
$A_1 + A_1 \xrightleftharpoons[k_{1,1}^{-1}]{k_{1,1}} A_2$	$k_{1,1} = 1$	$k_{1,1}^{-1} = 1$
Tetramer model		
$A_1 + A_1 \xrightleftharpoons[k_{1,1}^{-1}]{k_{1,1}} A_2$	$k_{1,1} = 1$	$k_{1,1}^{-1} = 1$
$A_1 + A_2 \xrightleftharpoons[k_{1,2}^{-1}]{k_{1,2}} A_3$	$k_{1,2} = 1$	$k_{1,2}^{-1} = 2$
$A_1 + A_3 \xrightleftharpoons[k_{1,3}^{-1}]{k_{1,3}} A_4$	$k_{1,3} = 1$	$k_{1,3}^{-1} = 2$
$A_2 + A_2 \xrightleftharpoons[k_{2,2}^{-1}]{k_{2,2}} A_4$	$k_{2,2} = 1$	$k_{2,2}^{-1} = 4$
Quadrilateral model		
$A_1 + A_1 \xrightleftharpoons[k_{1,1}^{-1}]{k_{1,1}} A_2$	$k_{1,1} = 1$	$k_{1,1}^{-1} = 1$
$A_1 + A_2 \xrightleftharpoons[k_{1,2}^{-1}]{k_{1,2}} A_3$	$k_{1,2} = 1$	$k_{1,2}^{-1} = 2$
$A_1 + A_3 \xrightleftharpoons[k_{1,3}^{-1}]{k_{1,3}} A_4$	$k_{1,3} = 1$	$k_{1,3}^{-1} = 2$
$A_2 + A_2 \xrightleftharpoons[k_{2,2}^{-1}]{k_{2,2}} A_4$	$k_{2,2} = 1$	$k_{2,2}^{-1} = 4$
$A_3 \xrightleftharpoons[k_{\text{Tri}}^{-1}]{k_{\text{Tri}}} \text{Tri.}$	$k_{\text{Tri}} = 2$	$k_{\text{Tri}}^{-1} = 2$
$A_4 \xrightleftharpoons[k_{\text{Quad}}^{-1}]{k_{\text{Quad}}} \text{Quad.}$	$k_{\text{Quad}} = 2$	$k_{\text{Quad}}^{-1} = 2$
Reversible polymerisation		
$A_i + A_j \xrightleftharpoons[k_{i,j}^{-1}]{k_{i,j}} A_{i+j}$	$k_{i,j} = ij$	$k_{i,j}^{-1} = i + j$

Table 4.1.: List of reactions and rate constants used for the chemical models fulfilling detailed balance. All reaction rates are in units of $[k] = 1/\tau$, where τ is the simulation timescale. For the quadrilateral model, trimers can react to a triangle complex configuration (Tri.), which is resistant to decay and inert to further aggregation. Analogous, tetramers react to a quadrilateral complex configuration (Quad.), which is inert. All reaction schemes fulfil detailed balance.

cal reaction network with a finite number of species. For the statistics, we consider for each model 5^5 independent runs. For the statistics, we evaluate the averaged state vector $\langle \vec{n} \rangle$. For the simulations, we grant sufficiently long simulation times between compartment fragmentation events, to grant relaxation into equilibrium states, as we allow for a temporal evolution of $t = 40\tau$, τ the simulation timescale, between subsequent compartment events. This grants for more than 1×10^4 chemical reaction events per model. We consider initially $\mathcal{N} = 60$ monomers for Fig. 4.11 (a)-(c) and $\mathcal{N} = 16$ for (d). In agreement with our theory, we find that the second and third compartments show the same statistics $\langle \vec{n}_2 \rangle = \langle \vec{n}_3 \rangle$ for all considered reaction models (a)-(d). In contrast to this, but also in agreement with our theoretical prediction, we find that the first fragmented compartment shows different statistics $\langle \vec{n}_1 \rangle \neq \langle \vec{n}_{2,3} \rangle$. We conclude that despite the chemical reaction network fulfilling detailed balance, the microscopic dynamics are affected by dynamic compartmentalisation. In particular, this implies that the external protocol of partition insertion and removal evokes a change in the system entropy of the 3-compartment system. Recall in this context the introduction of the concept of *Gergesian demons* in section 4.3.2. It is not clear to what extent we performed work on the chemical reaction network system, as we insert partition, just from the inspection of the microscopic interaction rules in the Hamiltonian. In the next section, we will discuss the exorcism of *Gergesian demons* in the context of chemical reaction networks.

We corroborate our theoretical prediction by simulating chemical reaction networks in 3-compartment systems subject to sequential fragmentation, see Fig. 4.11. Rather than simulating the chemical reactions using molecular dynamics simulations, we directly simulated the system based on stochastic transition rates. Here, we examine four different models, which are detailed out in Tab. 4.1, all of which satisfy the principle of detailed balance. The satisfaction of detailed balance refers here both to the chemical reaction network in the thermodynamic limit and to the Markov chain transition network that arises from considering the chemical reaction network with a finite number of species. For each model, we conduct 5×10^5 independent runs for statistical analysis. We evaluate the average state vector $\langle \vec{n} \rangle$, and simulate for sufficiently long periods between compartment fragmentation events to allow for relaxation into the equilibrium states. We consider a runtime of $t = 40\tau$, where τ is the simulation timescale, between subsequent compartment fragmentation events. This corresponds to more than 1×10^4 chemical reaction events between fragmentation events.

We consider initially $\mathcal{N} = 60$ monomers for Fig. 4.11 (a)-(c) and $\mathcal{N} = 16$ for (d). In agreement with our theory, we find that the second and third compartments show the same statistics $\langle \vec{n}_2 \rangle = \langle \vec{n}_3 \rangle$ for all considered reaction models (a)-(d). In contrast to this, but also in agreement with our theoretical prediction, we find that the first fragmented compartment shows different statistics $\langle \vec{n}_1 \rangle \neq \langle \vec{n}_{2,3} \rangle$. We conclude that despite the chemical reaction network fulfilling detailed balance, the microscopic dynamics are affected by dynamic compartmentalisation. In particular, this implies that the external protocol of partition insertion and removal alters the system's entropy of the 3-compartment system. Recall in this context the introduction of the concept of *Gergesian demons* in section 4.3.2. It is not clear from inspection of the microscopic interaction rules in the Hamiltonian alone to what extent work is performed on the chemical reaction network system as we insert the partition. In the next section, we will discuss the exorcism of *Gergesian demons* in the context of chemical reaction networks.

4.6. Effects of dynamic compartmentalisation on the total system's entropy

In sections 4.5.3 and 4.5.4, we examined the examples of quantised stochastic gases and reversible polymerisation dynamics under sequential fragmentation. We found that quantised stochastic gases exhibit entropic neutrality under dynamic compartmentalisation, while reversible polymerisation dynamics result in different macrostate statistics per compartment when subjected to a sequential fragmentation process. By explicitly calculating the commutator relation between the sampling operator and the Hamiltonian $[\hat{\mathcal{K}}, \hat{\mathcal{H}}]_s$, we were able to predict the behaviour of model dynamics under dynamic compartmentalisation dynamics; which we then validated through numerical experiments by simulating the dynamics. However, the dependence of the macrostate statistics of chemical reaction networks on the specific compartment dynamics raises issues of thermodynamic consistency, as discussed in the context of Gergesian demons in section 4.3.2. In the following, we address this issue by discussing ways to *exorcise the Gergesian demons*. Following this discussion, we provide a general overview of how to deviate from entropic neutrality and connect the notion of entropic neutrality directly to symmetries in the microscopic interaction rules. This connection will enable us to investigate general routes to non-equilibrium thermodynamics in the context of compartmentalised multi-scale systems. Concluding this section, we briefly examine the entropic effects of compartment dynamics beyond compartment fusion and fission.

4.6.1. Discussing thermodynamic inconsistencies

Our analysis and simulations have demonstrated that the statistics of chemical reaction kinetics are affected when subjected to dynamic compartmentalisation, implying that the system's entropy varies depending on whether the system was subjected to synchronous or sequential fragmentation. However, we can revert between these states by removing all partitions and subsequently inserting them following the alternate fragmentation protocol. This thermodynamic inconsistency, referred to as *Gergesian demons* in section 4.3.2, can be addressed by considering the type of work performed on the system. To this end, we adopt a mathematical approach, examining whether entropic neutrality can be achieved by modifying the transition rates in the Hamiltonian after a fragmentation event. We also discuss the physical implications of modifying or not modifying the Hamiltonian.

We now ask whether we can find a simple rule on how to modify $\hat{\mathcal{H}}_{\text{CRN}}$ in such that the steady states of $\hat{\mathcal{H}}_{\text{CRN}} |\psi_{\text{ss}}(t)\rangle = 0 |\psi_{\text{ss}}(t)\rangle$ are in the kernel of $\hat{\mathcal{H}}'_{\text{CRN}} \hat{\mathcal{K}} |\psi_{\text{ss}}(t)\rangle = 0 |\psi_{\text{ss}}(t)\rangle$. To this end, we make use of the abbreviated notion of $|\psi_{\text{ss}}(t)\rangle$ and find

$$\hat{\mathcal{H}}'_{\text{CRN}} \hat{\mathcal{K}} |\psi(t)\rangle = \sum_j b_j \sum_m^{\mathcal{N}_j} (\hat{\mathcal{H}}'_{\text{CRN}} \hat{\mathcal{Q}}^m) \hat{\mathcal{R}}(m) p_{\mathcal{N}_j}(m) |\vec{n}_j(t)\rangle. \quad (4.80)$$

Note, that we changed the index in the second sum from k to m in order to avoid confusion with the notation when considering systems involving chemical reactions. In the analysis of the quantised gases, we were able to simplify this expression by noting that all states $|\vec{n}_j\rangle$ had the same number of particles, $\mathcal{N} = \text{const}$. However, as we showed in section 4.5.4, we cannot use the same simplification for chemical reaction networks, as the number of particles in different realisations is not a conserved quantity. On the other hand, the varying number of particles per state $|\vec{n}_j\rangle$ was the mathematical reason that the sampling

4.6. Effects of dynamic compartmentalisation on the total system's entropy

operator $\hat{\mathcal{S}}$ and the Hamiltonian $\hat{\mathcal{H}}_{\text{CRN}}$ do not commute, resulting in a dependence of the dynamics on the specifics of the compartment dynamics. By examining $\hat{\mathcal{H}}'_{\text{CRN}}\hat{\mathcal{Q}}^m$, we find that the individual orders of m need to vanish, as $\hat{\mathcal{Q}}^m$ maps to states with a reduced number of monomeric building blocks. Therefore, we next seek modifications of $\hat{\mathcal{H}}'_{\text{CRN}}$ that result in the individual vanishing of the summands in the hierarchy in Eq. (4.55).

To this end, we first simplify the relation of $\hat{\mathcal{R}}(k)$ and $p_{\mathcal{N}_j}(k)$. We find

$$\hat{\mathcal{R}}(m)p_{\mathcal{N}_j}(m)|\vec{n}_j\rangle = \frac{(\mathcal{N}-m)!}{\mathcal{N}!} \frac{\mathcal{N}!}{(\mathcal{N}-m)!k!} p^m(1-p)^{\mathcal{N}-m} |\vec{n}_j\rangle = \alpha_m \beta_{\mathcal{N},m} |\vec{n}_j\rangle \quad (4.81)$$

Recall, that we are interested in the vanishing of summands with the same order of m . We find, that each realisation $|\vec{n}_j\rangle$ is multiplied with two factors, one solemnly depending on m and one depending on both the total number of particles \mathcal{N} and m . As we demand each order in m to vanish individually, we note that each realisation $|\vec{n}_j\rangle$ is multiplied by the same α_m but different $\beta_{\mathcal{N},m}|\vec{n}_j\rangle$. Note, that the multiplication with $\beta_{\mathcal{N},m}$ causes the breakdown of detailed balance.

To fix this breakdown, we consider two realisations $|\vec{n}_v\rangle$ and $|\vec{n}_w\rangle$ linked by a reversible aggregation reaction. Without loss of generality, we consider that $|\vec{n}_v\rangle$ transitions to $|\vec{n}_w\rangle$ via an aggregation reaction with rate $ki, j; k$, while $|\vec{n}_w\rangle$ transitions to $|\vec{n}_v\rangle$ through a dissociation reaction with the rate $ki, j; k^{-1}$. Note that the total number of particles in $|\vec{n}_v\rangle$ is one greater than in $|\vec{n}_w\rangle$, with $\mathcal{N}_v = \mathcal{N}_w + 1$ by construction. For the state $|\psi_{\text{ss}}(t)\rangle$ to be in detailed balance, we must have $b_v k_{i,j;k} \hat{a}_k^\dagger \hat{a}_j \hat{a}_i |\vec{n}_v\rangle = b_w k_{i,j;k^{-1}} \hat{a}^\dagger k \hat{a} k |\vec{n}_w\rangle$. However, upon accounting for $\beta_{\mathcal{N},m}$, it becomes apparent that this equality no longer holds: $b_v k_{i,j;k} \beta_{\mathcal{N}_v,m} \hat{a}_k^\dagger \hat{a}_j \hat{a}_i |\vec{n}_v\rangle \neq b_w k_{i,j;k^{-1}} \beta_{\mathcal{N}_w,m} \hat{a}^\dagger k \hat{a} k |\vec{n}_w\rangle$. Note that the ratio $\beta_{\mathcal{N}_v,m}/\beta_{\mathcal{N}_w,m} = (1-p)$ is connected to the success probability of sampling. As such, by rescaling all aggregation rates to $ki, j; k \rightarrow k_{i,j;k}/(1-p) = k'_{i,j;k}$, detailed balance can be re-established. As a result, all summands in the hierarchy created by $[\hat{\mathcal{H}}_{\text{CRN}}, \hat{\mathcal{Q}}^m]$ vanish individually, and

$$\boxed{\hat{\mathcal{H}}'_{\text{CRN}} \hat{\mathcal{K}} |\psi_{\text{ss}}(t)\rangle = 0 |\psi_{\text{ss}}(t)\rangle.} \quad (4.82)$$

Hence, rescaling all aggregation reaction rates $k'_{i,j;k}$ after a compartment fragmentation according to the sampling success probability p yields entropic neutrality. Before we next discuss the physical implication of considering rescaled Hamiltonians after compartment fusion, we first turn to numerical simulations to corroborate our theoretical prediction.

We set up the simulations analogous to the simulations of the chemical reaction networks subject to dynamic compartmentalisation without rescaling the aggregation rate, as detailed out in Fig. 4.11. In Fig. 4.12 we considered the same chemical reaction network models, using the same simulation parameters. In this particular case, we examined a three-compartment system, in which the success probability of being sampled in the first room is $p = 1/3$. As per our theoretical predictions, we rescaled the aggregation rates for the dynamics within the still connected compartments 2, 3 to $k_{i,j;k} \rightarrow k_{i,j;k} \cdot 3/2$. Our results indicate that, in accordance with our theoretical predictions, all compartments exhibit identical averaged state vectors, with $\langle \vec{n}_1 \rangle = \langle \vec{n}_2 \rangle = \langle \vec{n}_3 \rangle$.

We find that if there would a physical reason to consider a rescaled Hamiltonian, we would exorcise thermodynamic inconsistencies and find that compartment fragmentation performs no work on the system. To make physical sense of rescaling the Hamiltonian, we argue for an intrinsic connection between the volume of the fragmented compartment

4. Towards a thermodynamics of closed compartmentalised systems

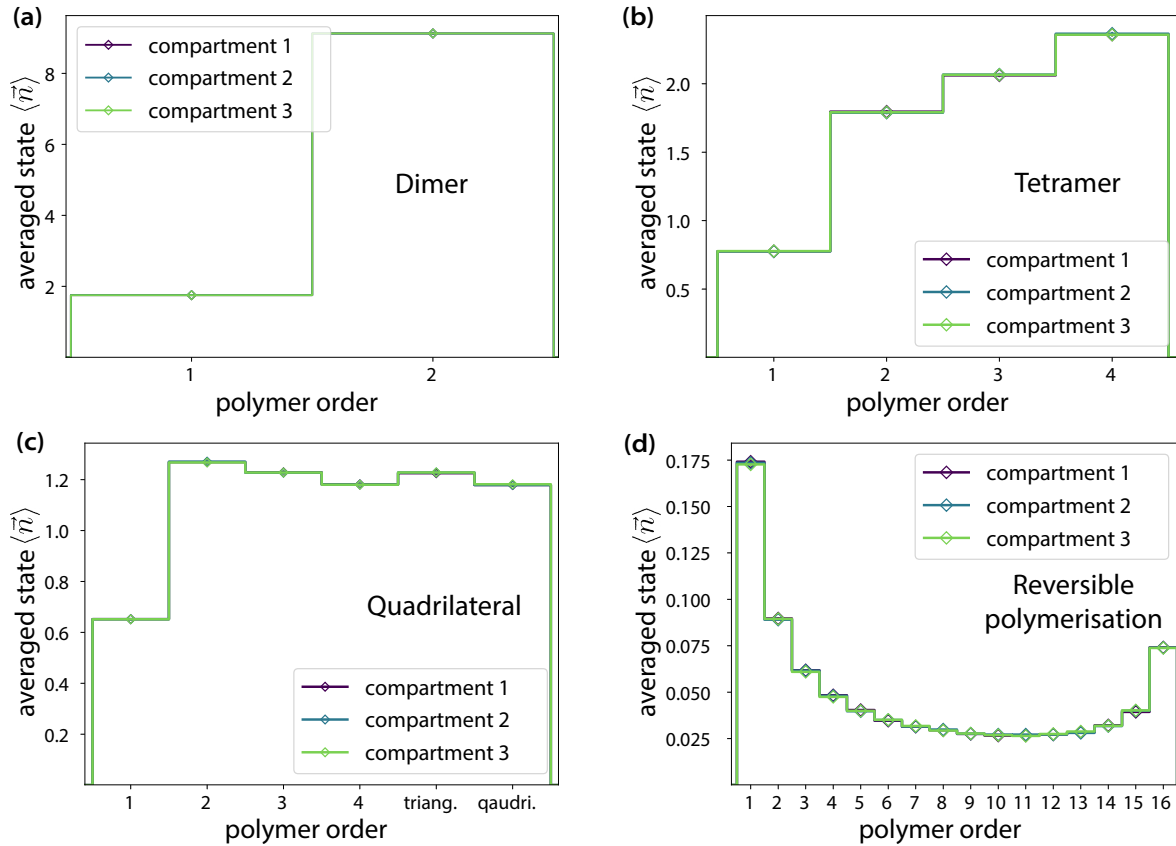


Fig. 4.12.: The effects of sequential fragmentation on chemical reaction systems vanishes for rescaled aggregation rates. The system and simulation parameters are identical to the simulations presented in Fig 4.12, the difference that the aggregation rates are rescaled after the fragmentation of the first compartment by $v_0/v_{2+3} = 3/2$. As a consequence, the effects of sequential fragmentation is vanishing, in agreement with our analytical findings presented in section 4.6.1.

and the success probability p . Without loss of generality, consider a composite system of two compartments with volume v_1 and v_2 . Starting in a configuration with no partition inserted, we find that the dynamics are spread over the full volume $v_0 = v_1 + v_2$. As we insert a partition, there is a probability $p = v_1/v_0$ that a particle resides in compartment 1 after partition insertion. Rescaling the aggregation rates in compartment 2 with $k_{i,j;k}/(1-p) = k_{i,j;k} \cdot v_0/v_2$ corresponds to rescaling the aggregation rates with the new volume available for the dynamics in compartment 2. This suggests a density dependence of the aggregation reactions.

Heuristically, a volume dependence of the aggregation reactions can be derived by considering dynamics within a physical space. In contrast to chemical reactions in category C_I or C_{III} , as introduced in Section 4.5.4, aggregation reactions result from two-body interactions. In order for an aggregation reaction to occur, two chemical entities must collide in physical space. As the accessible volume within a compartment is increased, the average distance between chemical entities also increases, thus reducing the rate of collisions between them. We find that if the dynamics contain reaction from all types C_I , C_{II} , and C_{III} , the rescaling the aggregation rates is a non-uniform rescaling of the Hamiltonian. Recall that for the case of the quantised gas, this rescaling would be uniform.

Notably, in our calculations, we do not need to rely on a heuristic explanation for

the volume rescaling. In particular, as we induce fluctuations in the number of particles due to partition insertion, it is not a priori clear how density fluctuations should be correctly accounted for. However, if we postulate that any dependence of the chemical reactions on the compartment dynamics should vanish in a micro-canonical setup, in order to exorcise the Gergesian demons, then the volume dependence of the aggregation reaction rates drops out as a consequence. This is insightful, as we find the volume rescaling as a thermodynamic consequence without the need of justification from actual physical microscopic models of chemical reactions. From this perspective, not rescaling the aggregation rates corresponds to first restricting the volume by partition insertion and subsequently expanding the volume to regain the initially available volume. Note that the volume work does not originate from microscopic models, but rather as a consequence of thermodynamic consistency.

As a corollary, this analysis also reveals subtle differences between the procedures of sample extraction by removal of chemical objects from the system and sample extraction by separation of subsystems. While for the former, we consider the extraction of a fixed number of chemical objects, for the latter we consider the extraction of a random number of chemical objects. Note that in the case of sample extraction by removal, the Hamiltonian cannot be rescaled by a volume notion. This implies that sample extraction by removal performs work on chemical reaction network systems that entail aggregation reactions. In the next section, we delve deeper into these discussions by exploring how entropic neutrality under dynamic compartmentalisation can be broken. This will give us insight into how work can be performed on compartmentalised multi-scale systems.

4.6.2. Linking microscopic interaction rules with entropic neutrality under dynamic compartmentalisation

The fact, that the microscopic interaction rules dictate whether compartment fusion and fission effects the macrostate statistics teaches us valuable lessons about the thermodynamics of multi-scale systems. We made use of the concept of *Gergesian demons* in section 4.3.2 to introduce a notion of temporal order into our system. Recall, that in the scheme implemented here no notion of a measurement of the system was considered. Naïvely, however, one could wonder if a measurement of time, which is needed to implement an external time protocol, would be imprinted in the statistics of the system. While this idea might sound superficially intriguing, the fact that different microscopic interaction rules set different behaviours under dynamic compartmentalisation hints towards a different direction.

In section 4.5.2.3, we discussed how the commutator relations in Eq. (4.59) can be linked to assess the strength of perturbation of compartment fusion and fragmentation on the systems dynamics and interpreted this in the context of a generalised notion of work. In particular, if we set the system dynamics to happen in an isolated system, steady states of the Hamiltonian $\hat{\mathcal{H}}$ are equilibrium states. Formally, we then tested whether the sampled state $|\psi'\rangle \hat{\mathcal{S}} |\psi_{ss}\rangle$ is in the kernel of the Hamiltonian and thus also an equilibrium state. Conversely, if the commutator relation is *not* vanishing, the new state $|\psi'\rangle$ is not an equilibrium state. In this case, the processes of the insertion of a partition and removal are genuine non-equilibrium processes. In this light, we indeed expect time protocols to affect the macro-state statistics.

4. Towards a thermodynamics of closed compartmentalised systems

Quadrilateral model		
$A_1 + A_1 \xrightleftharpoons[k_{1,1}^{-1}]{k_{1,1}} A_2$	$k_{1,1} = 1$	$k_{1,1}^{-1} = 1$
$A_1 + A_2 \xrightleftharpoons[k_{1,2}^{-1}]{k_{1,2}} A_3$	$k_{1,2} = 1$	$k_{1,2}^{-1} = 2$
$A_1 + A_3 \xrightleftharpoons[k_{1,3}^{-1}]{k_{1,3}} A_4$	$k_{1,3} = 1$	$k_{1,3}^{-1} = 0.01$ (sup.) $k_{1,3}^{-1} = 12$ (fac.)
$A_2 + A_2 \xrightleftharpoons[k_{2,2}^{-1}]{k_{2,2}} A_4$	$k_{2,2} = 1$	$k_{2,2}^{-1} = 4$
$A_3 \xrightleftharpoons[k_{\text{Tri}}^{-1}]{k_{\text{Tri}}} \text{Tri.}$	$k_{\text{Tri}} = 4$	$k_{\text{Tri}}^{-1} = 1$
$A_4 \xrightleftharpoons[k_{\text{Quad}}^{-1}]{k_{\text{Quad}}} \text{Quad.}$	$k_{\text{Quad}} = 4$	$k_{\text{Quad}}^{-1} = 1$
Reversible polymerisation		
$A_i + A_j \xrightleftharpoons[k_{i,j}^{-1}]{k_{i,j}} A_{i+j}$	$k_{i,j} = \lambda \cdot ij$	$k_{i,j}^{-1} = \frac{1}{(i+j)}$ (sup.) $k_{i,j}^{-1} = (i+j)^2$ (fac.)

Table 4.2.: List of reactions and rate constants used for the chemical models breaking detailed balance. All reaction rates are in units of $[k] = 1/\tau$, where τ is the simulation timescale. For the Quadrilateral model, detailed balance is broken by either suppressing or facilitating the dissociation of tetramers into a monomer and a trimer. For the reversible polymerisation model, stabilizing or facilitating the decay of larger oligomers breaks detailed balance. Changing the parameter λ does not affect the breaking of detailed balance. Here $\lambda = 0.02$ was chosen for the suppression of the polymer dissociation and $\lambda = 40$ in the model with facilitation.

4.6.3. Breaking entropic neutrality by performing work on the system

In section 4.6.1, we have exorcised the *Gergesian demons* from systems entailing reversible aggregation dynamics embedded in compartments subject to dynamic compartmentalisation by accounting for a rescaling of the reaction rates with the available compartment volume. In this section, we adopt a contrasting perspective and consider how entropic neutrality under dynamic compartmentalisation can be broken. In investigating this question, we do not evoke thermodynamic demons but instead, learn about how we can perform work on multi-scale systems. To this end, we will distinguish four different types of work contributions, which we directly link to the internal dynamics or the compartment dynamics.

While investigating the quantised gas and the chemical reaction systems, we have employed detailed balance to demonstrate entropic neutrality under dynamic compartmentalisation. Detailed balance is widely regarded as a signature of equilibrium, as it stipulates that each process is in equilibrium with its inverse process. Thus any trajectory of the system has an equal forward and backward probability, implying that entropy production is nullified [17]. The breaking of detailed balance implies that the system cannot be considered in a micro-canonical setup. As a result, the system's entropy is permitted to change in accordance with the time protocol used for dynamic compartmentalisation. Without detailed balance, there is no a priori reason to assume that sequential and synchronous fragmentation will yield identical macrostate statistics. In this context, it is

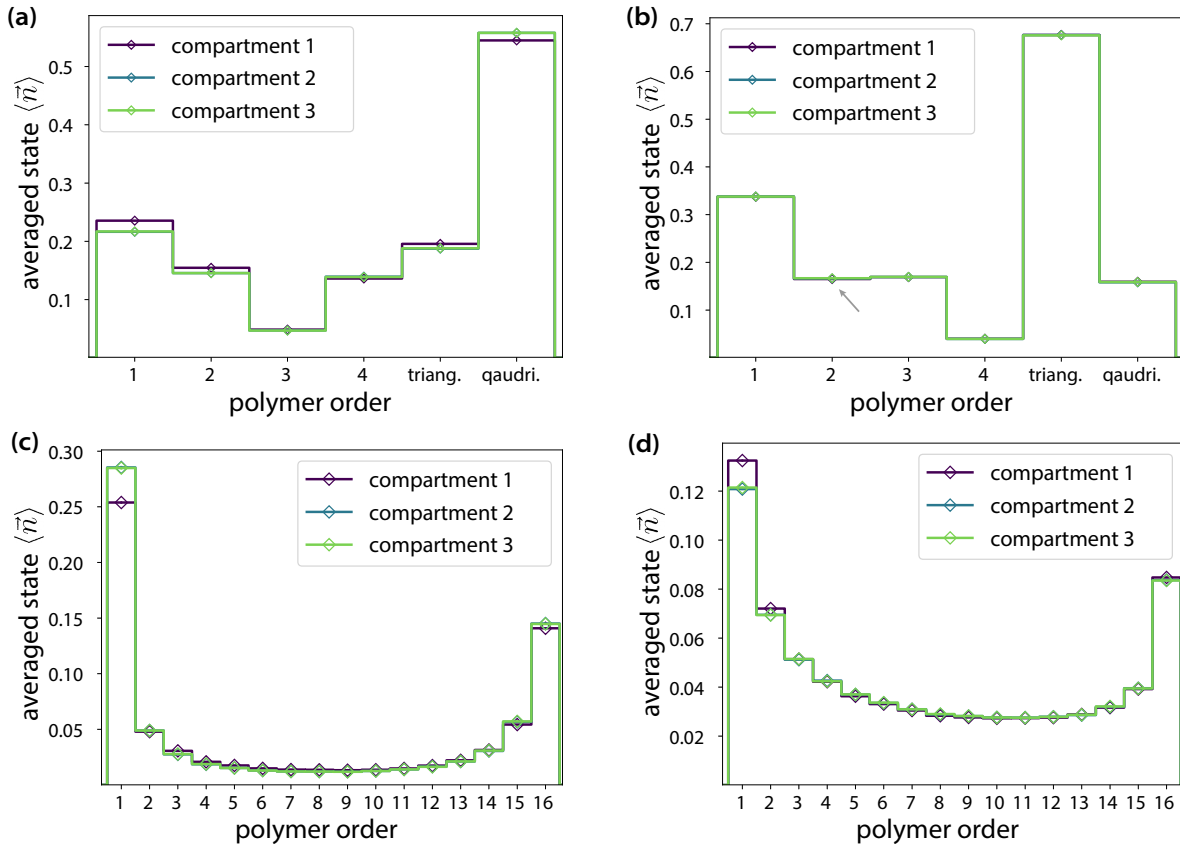


Fig. 4.13.: The effects of sequential fragmentation on chemical reaction systems with broken detailed balance do not vanish for rescaled aggregation rates. A three-compartment system is subject to a sequential fragmentation. Analogous to Fig. 4.12, the aggregation rates are rescaled after the fragmentation of the first compartment. The enclosed chemical reaction systems are deviations from Fig. 4.11 (c),(d) breaking detailed balance by changing rates. The specific reaction rates for the modified quadrilateral complex formation (a,b) and reversible polymerisation kinetics (c,d) are given in Tab. 4.2. The total number of independent iteration runs is 5×10^5 for both (a) and (b). The simulation time was chosen long enough to grant relaxation into a steady state with $t = 40\tau$, τ the simulation timescale. The total number of initial monomers is $\mathcal{N} = 12$ for (a,b) and $\mathcal{N} = 16$ for (c,d). While deviations in the statistics of the first compartment versus the second and third compartment is small for the quadrilateral system, it is not vanishing in contrast to Fig. 4.12 (c,d). The deviations are small in (b) and more pronounced for the reversible polymerisation system in (c,d).

worth recalling the calculations presented in sections 4.5.3 and 4.5.4.

An important way of breaking detailed balance is by externally fuelling chemical reactions. From the calculations presented in section 4.6.1, we expect that breaking detailed balance will break entropic neutrality under sequential fragmentation, even if we rescale the aggregation rates. We test this prediction in numerical simulations, see Fig. 4.13. Here, we consider variations of the chemical models used in Fig. 4.12 (c,d), namely a variation of the quadrilateral model and the reversible polymerisation. The new rates are detailed out in Tab. 4.2. For the quadrilateral model, we consider breaking detailed balance by manipulating a single reaction, namely either by suppressing the decay of tetramers into a monomer and a tetramer, Fig. 4.13 (a), or by facilitating this decay Fig. 4.13 (b).

4. Towards a thermodynamics of closed compartmentalised systems

For the reversible polymerisation model, we alter the kinetic rule for oligomer dissociation, which breaks detailed balance by construction. Also here, we consider a suppression of the dissociation, Fig. 4.13 (c), or a facilitation, Fig. 4.13 (d). We consider small systems of $\mathcal{N} = 12$ monomeric building blocks for the quadrilateral and $\mathcal{N} = 16$ monomeric building blocks for the reversible polymerisation simulations. The remaining simulation parameters are identical to the ones used in Fig. 4.12. For the evaluation we considered 2^6 independent simulation runs. We find that the macrostate statistics in the first compartment differ from the statistics in the second and third compartment, $\langle \vec{n}_1 \rangle \neq \langle \vec{n}_{2,3} \rangle$, which is in agreement with our theoretical predictions. We note, that the differences in the statistics are small in the case of quadrilateral model, in particular for Fig. 4.13 (b), but we find that the differences are not vanishing, see Fig. 4.13 (c). For Fig. 4.13 (c,d) the differences are more pronounced, particularly in the probability of sampling monomers.

Notably, we find that breaking detailed balance also affects the abundance of the largest aggregate. Suppressing the dissociation of tetramers results in an increase of the abundance of quadrilateral aggregates by 2% in the second and third compartments compared to the first compartment. Conversely, for the facilitation of the dissociation of tetramers, the abundance of quadrilaterals is reduced by 0.5%. For the reversible polymerisation dynamics, we also find that suppression of the dissociation reactions results in an increase in the abundance of the polymer of highest order, here the 16mer, by 4%. Conversely, for the facilitation of the dissociation reactions, we also find a decrease in 16mer abundance by 1.5%. While the effect in the here presented system is small, these findings suggest that dynamic compartmentalisation amplifies the effects of breaking detailed balance. We further explore this in chapter 5, where we study larger reversible polymerisation dynamics in larger systems. Note, the amplifying of detailed balance by compartment dynamics is currently a numerical observation that needs to be further corroborated by a proof in the framework of the Second quantisation.

Next, we ask to what extent the effect observed in Fig. 4.13 persists when we consider larger systems. In Fig. 4.14, we systematically increase the system size by increasing both the initial number of monomeric building blocks \mathcal{N} and the number of compartments N considered, such that the initial number of monomeric building blocks per compartment is constant, $\mathcal{N}/N = \text{const.}$. With otherwise identical simulation parameters as for Fig. 4.13, we find that the difference between the first and the last fragmented compartment increases with system size but levels off for large systems. We track how the number of expected monomers, Fig. 4.13 (a), and the number of expected quadrilateral aggregates, Fig. 4.13 (b), changes for sequentially fragmented compartments. Here, we see how the fluctuations created by fragmentation add up over time to yield a stronger effect for compartments that are separated later. Here, we see that the differences in statistics induced are small, as deviations are in the range of a few percent, but not vanishing.

While further investigations are required to examine how systems with broken detailed balance are affected by dynamic compartmentalisation, we here turn to a different approach to affect the statistics of realised system states through compartment fusion and fragmentation. To do this, we again consider the quantised gas models introduced in section 4.5.3. There, we considered stochastic dynamics dictated by transition rates. We next map these dynamics to Markov chain dynamics by converting from transition rates to transition probabilities. Note that these Markov chain dynamics also fulfil detailed balance by construction. Note that by using the Second quantisation formalism, we take a kinetic perspective on the dynamics of the system. The here presented formalism allows us to link the kinetic perspective with physical notions of performing work on the system

4.6. Effects of dynamic compartmentalisation on the total system's entropy

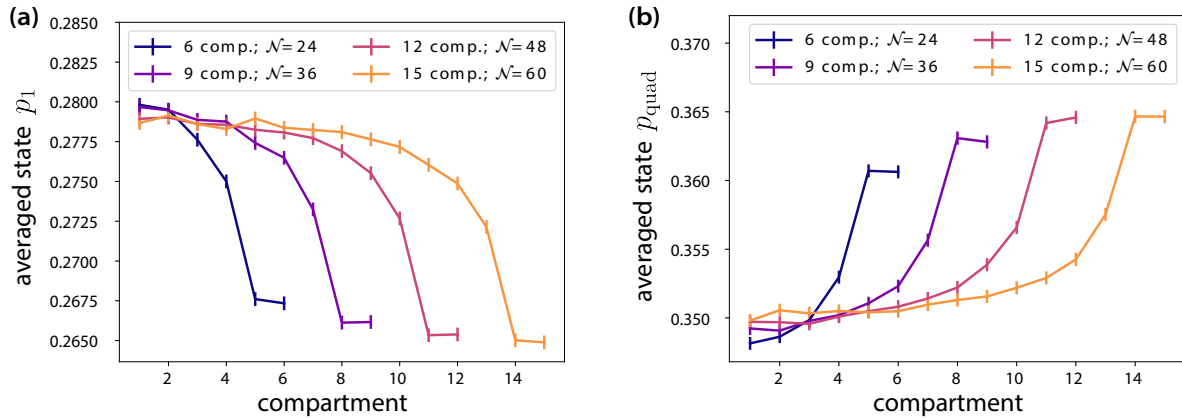


Fig. 4.14.: System size dependence of the effect of sequential fragmentation on chemical reaction systems with broken detailed balance The number of compartments considered in a sequential fragmentation protocol is increased from 6 compartments to 15 compartments while keeping the average number of initial monomer mass over the initial volume constant. The investigated enclosed dynamics is the quadrilateral complex formation with one broken detailed balance reaction as shown in Fig. 4.13 (a). The total number of independent iteration runs is 6×10^6 . (a) Shown is the average state of p_1 of monomers in different compartments created by sequential fragmentation. Analogously, (b) shows the average state of p_{quad} of quadrilateral aggregates. The compartment number gives the order at which the respective compartment was separated from the system. Error bars indicate a 2σ environment. The simulations suggest that the effect of dynamic compartmentalisation converges with increasing system size.

Numerically, this mapping is achieved by evaluating the dynamics after a fixed number of evolution steps instead of a fixed evolution time. Mathematically, this mapping demands the rescaling of each two-particle transition rate by all possible rates of leaving a realisation $|\vec{n}_i\rangle$ to any other system realisation $|\vec{n}_j\rangle$. An additional system state normalisation operator in the Hamiltonian $\hat{\mathcal{H}}_{\text{qg}}$ breaks the commutator relation $[\hat{\mathcal{H}}_{\text{qg}}, \hat{\mathcal{K}}]_{\text{ss}} = 0$. Note that here we are not just changing timescales, but fundamentally changing the transition rates between realisations. Testing this prediction in simulations, we find in Fig. 4.15, that we break entropic neutrality with this mapping. For the simulation, we consider the same simulation parameters as in Fig. 4.10 as introduced in section 4.5.3, with the simulation evaluated after $s = 2000$ simulation steps instead of an evaluation after a fixed time. We notice no deviations in Fig. 4.15 (a) between the compartments, which is in agreement with our expectations, as Fig. 4.15 (a) and Fig. 4.10 (a) are by construction formally equivalent. We find differences in the averaged state vectors $\langle \vec{n}_1 \rangle \neq \langle \vec{n}_2 \rangle = \langle \vec{n}_3 \rangle$ for Fig. 4.15 (b-d). In Fig. 4.16 we show that the stochastic gas models Fig. 4.15 (c,d) also produce a visually identifiable difference in the macrostates statistics of the total enclosed energy per compartment. While the mean energy per compartment is constant, the variance of the energy enclosed in a compartment is increased in the second and third compartments.

For the simulations in Fig. 4.15, detailed balance is fulfilled and no volume work is performed on the system. The notion of work in this example arises from the normalisation of the rates. Translating the mapping back to an interpretation in terms of transition rates, the rate for two particles with energy levels ε_i and ε_j to interact was independent in the model in section 4.5.3. However, as we introduced the normalisation, the rate for

4. Towards a thermodynamics of closed compartmentalised systems

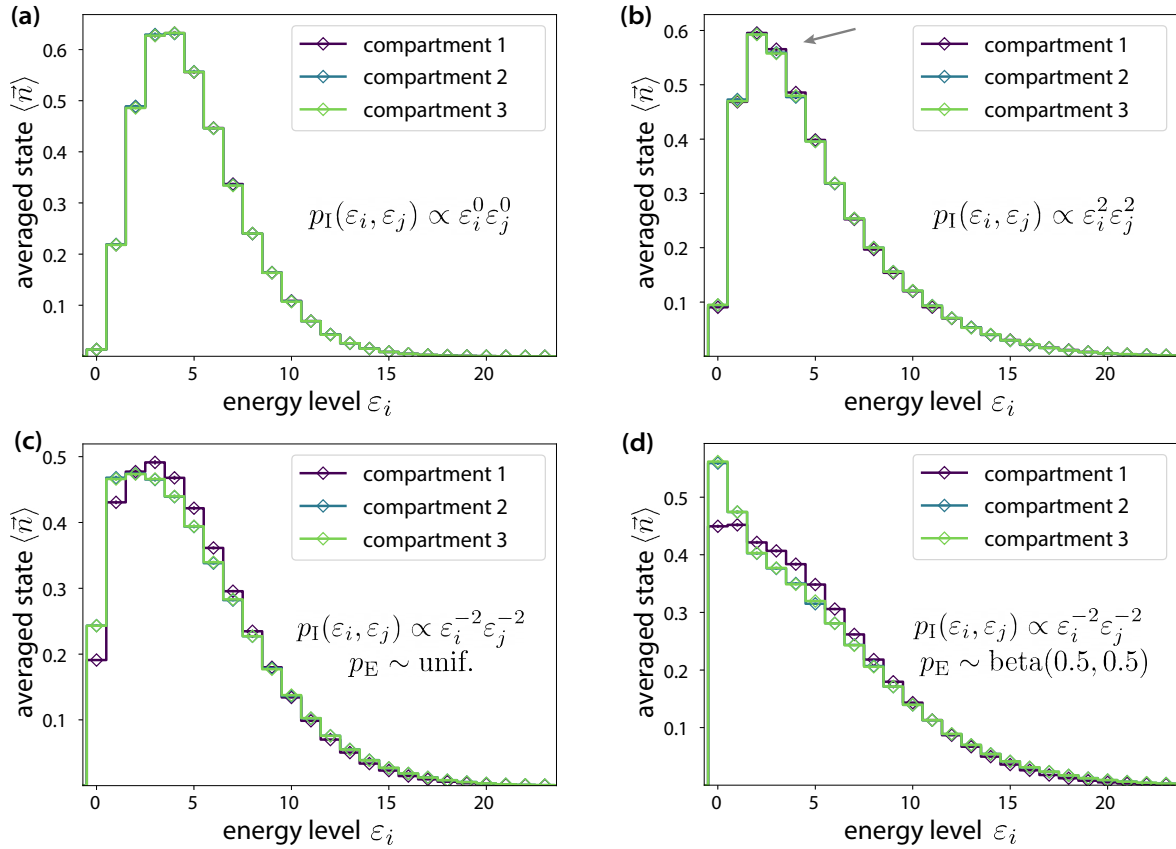


Fig. 4.15.: Quantised gases with globally coupled reaction rates are affected by sequential fragmentation processes The dynamics are analogous to Fig. 4.10, with transition rates rescaled with the total rate of escape from a specified state, which is formally analogous to a mapping to Markov chain dynamics, see also section 4.6.3. This implies a change from interaction rates f_I to interaction probabilities p_I . This mapping preserves the detailed balance conditions but induces a global coupling. The simulation parameters are identical to Fig. 4.10. The error bars indicate a 5σ environment. As Fig. 4.10 (a) and (a) in this figure are formally equivalent, the effect of sequential fragmentation vanishes in accordance with our theoretical prediction. In contrast, the sequential fragmentation process induces non-vanishing differences in the statistics for the first versus the second and third compartments for (b). Here, the arrow points to systematic deviations. These deviations are more pronounced for (c) and (d).

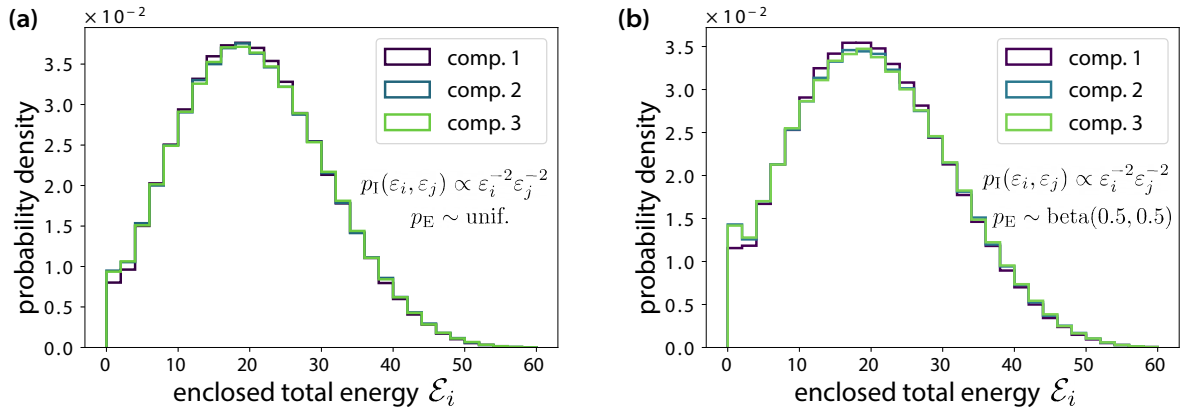


Fig. 4.16.: Sequential compartmentalisation affects the statistics of total energy per compartment. For Fig. 4.15 (c), (d) the total enclosed energy per compartment \mathcal{E}_i is computed. Difference in the averaged state $\langle \vec{n} \rangle$ translate into different statistics for \mathcal{E}_1 versus \mathcal{E}_2 and \mathcal{E}_3 . While all distributions $p(\mathcal{E}_i)$ show the same mean $\langle \mathcal{E}_1 \rangle = \langle \mathcal{E}_2 \rangle = \langle \mathcal{E}_3 \rangle$, for the specific examples presented here, the variance of the second and third room is increased.

two particles to interact is a function of the full current ensemble realisation $|\vec{n}_j\rangle$ and thus a global coupling between all particles was introduced. While we can argue from a mathematical perspective how this results in a non-vanishing commutator, we next interpret our results.

When a partition is inserted in this system, and two subsystems are separated, the global coupling is broken. While the normalisation of rates can be easily implemented numerically, the physical implications of these dynamics are obscured, and a realisation of the kinetic rules in a physical system is not straightforward. Setting aside the question of a possible realisation, we find that work is performed on the system by a partition insertion as correlations between particles are broken. By breaking the correlations, the internal energy of the system is modified. In models with a global coupling between the particles, the assumption that the insertion of a partition is done without performing work breaks down.

We touched on a fourth notion of work performed on the system already at the end of section 4.6.1. There, we discussed the subtle difference between extracting a random number of chemical objects and extracting a fixed number of chemical objects from a system with reversible aggregation reactions. If the compartment dynamics depend on the current realisation of the system, we break the assumption of randomly splitting particles between subsystems. This implies an implicit measurement of the system state and is thus connected to the thought experiment of Maxwell's demon. Additionally, by setting the fusion of compartments dependent on the enclosed macrostate, the condition that fused compartments show the same statistics as obtainable from a fragmentation process is broken. By setting the dynamics of the compartments in dependence on the current realisation of the system, the assumption of *dumb* demons made in section 4.3.2 is broken, opening the realm to discuss *true Gergesian demons* in the context of multi-scale systems. Note that for a careful analysis of such demonic systems, other notions of work must be carefully excluded.

In conclusion, in this section, we distinguished four different notions of how work is performed on systems subject to dynamic compartmentalisation, namely through volume work, the establishment or breaking of particle correlations due to global couplings, the

dependence of compartment dynamics on the current state of the system, or the breaking of detailed balance in the enclosed microscopic dynamics. These four different notions of work offer a range of opportunities to investigate non-equilibrium thermodynamics in the context of multi-scale systems. Notably, our approach allows assessing the notion of work by inspecting the definition of the microscopic dynamics in conjunction with the definition of the compartment dynamics. We will discuss the relevance of our findings for both technical and biological applications after briefly extending our discussion on the entropic effects of dynamic compartmentalisation by including compartment dynamics apart from compartment fusion and fission.

4.6.4. Effect of compartment dynamics beyond compartment fusion and fragmentation on the total entropy

In this chapter, we have set a predominant focus on the fusion and fission of compartments, and thus far we have neglected other compartment dynamics. However, the treatment of compartment growth and shrinkage, for instance, is less intricate and its thermodynamic implications are straightforward. The modification of the volume of a compartment performs volume work on the enclosed dynamics. These effects can be calculated using standard thermodynamic methods. Similarly, the erasure or creation of compartments are directly related to the thermodynamic costs of destroying or creating a micro-canonical ensemble from the void. We assume that the spatial positioning and shape of compartments do not affect the intrinsic dynamics and thus these compartment dynamics have no thermodynamic effect on the enclosed dynamics. To summarise, compartment dynamics provide a versatile toolbox to directly perform work on the dynamics enclosed in dynamic compartments, with compartment fusion and fragmentation being more subtle in their work contribution than other compartment dynamics. Notable, the careless application of compartment dynamics can lead to apparent thermodynamic inconsistencies. Thus, the study of dynamic compartmentalisation teaches us valuable lessons in the non-equilibrium physics of multi-scale systems.

4.7. Technical and biological relevance of dynamic compartmentalisation

In this chapter, we have presented a detailed analysis of the effects of compartment dynamics on the statistics of realised system states for closed compartmentalised stochastic systems. By considering equilibrium dynamics in micro-canonical setups, we have identified a system property that we term *entropic neutrality under dynamic compartmentalisation*, which refers to macrostate statistics being unaffected by the specifics of compartment dynamics. Through an examination of different models, including the ideal gas, quantised gas models, and chemical reaction networks, we have highlighted four distinct routes to investigate the non-equilibrium thermodynamics of compartmentalised multi-scale systems. In this section, we proposed a possible experimental setup in the context of microfluidics to verify our theoretical and numerical predictions and discuss the potential implications of dynamic compartmentalisation on sample preparation techniques and measurement procedures. This idea was developed in a discussion with Nico

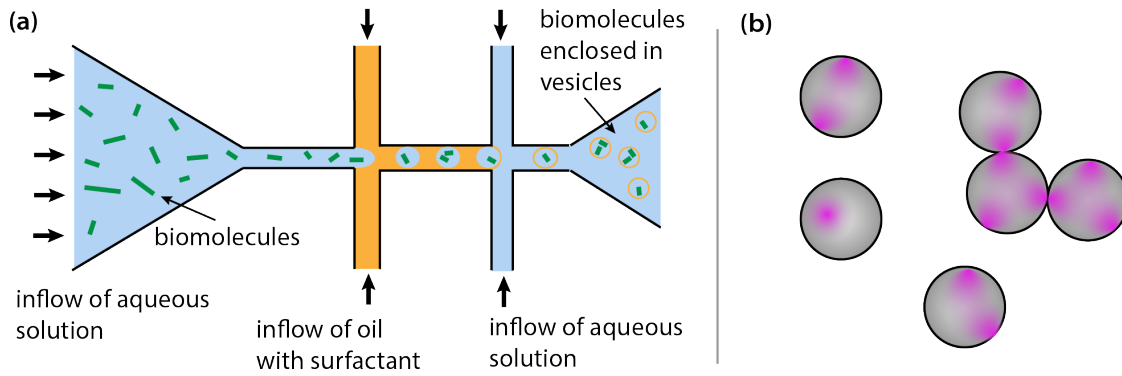


Fig. 4.17.: Experimental setups for investigating dynamic compartmentalisation (a) Experimental setup for the generation of lipid vesicles enclosing biomolecules as used in synthetic biology; The image is adapted from [218]. An aqueous solution is attributed with biomolecules and inserted into a microfluidic device. By adding oil enriched with a surfactant, and adding an additional aqueous solution, the biomolecules are compartmentalised into lipid vesicles. This corresponds to a sequential fragmentation procedure. (b) Schematic illustration of patchy colloids. Mesoscopic colloidal particles are physically or chemically patterned by a finite and small number of attractive sites arranged in precise geometries on the particle's surface. Allowing the tractability of dynamics with florescent microscopy, patchy colloids are used to study self-organisation dynamics [219]. A combination of both techniques might be suited to investigate the effects of sequential fragmentation on non-equilibrium chemical reaction systems.

Schrammar. Subsequent to discussing an experimental setup, we conclude by discussing the implications of dynamic compartmentalisation in biological systems.

In this chapter, we have placed a particular emphasis on the analysis of sequential compartment fragmentation processes. These processes are particularly amenable to both analytical and numerical study, and are also relatively straightforward to replicate experimentally. In designing experimental setups, it is crucial to be guided by numerical simulations, as these can provide estimates of the strength of effects and the statistics required to distinguish them from noise, particularly if there are no external sources of noise. Based on this, we find that experimental realisations demand the repetition of independent runs on the order of 10^4 to 10^5 . This, however, presents a significant constraint on experimental setup. It is worth noting that by carefully selecting dynamics, it may be possible to reduce the number necessary of runs to gain statistical significance by orders of magnitude. Besides a large number of runs, we find that low particle numbers are required for the system to show large statistical effects. The small system sizes should be easily observable in examples and the microscopic dynamics should be experimentally trackable. Given these constraints, we propose that microfluidic devices may be a suitable candidate for experimental realisation.

Microfluidic devices have been used in high-throughput experiments, where large sample sizes were evaluated quickly [220]. Furthermore, devices for sequential fragmentation dynamics for in vitro lipid vesicle production were designed, as illustrated schematically in Fig. 4.17 (a). This process involves coating an aqueous solution with oil and another aqueous solution to create small lipids. By this, the initial aqueous phase is fragmented into vesicles in a sequential fragmentation process. To realise the internal dynamics, patchy

4. Towards a thermodynamics of closed compartmentalised systems

colloids may be a suitable choice. These are mesoscopic colloidal particles with a finite and small number of attractive sites arranged in precise geometries on the surface, as shown in Fig. 4.17 (b). Patchy colloids are used to study self-organisation dynamics of reversible aggregation processes, as they are observable by fluorescent microscopy [219, 221]. By designing patchy colloids, different reaction dynamics can be realised, including the controllable implementation of reversible aggregation dynamics that break detailed balance. To verify our theoretical predictions experimentally, a careful design is required, along with close collaboration between theorists and experiments in order to avoid inconclusive statistics.

Experimental setup as Fig. 4.17 (a) are an experimental realisation of sequential fragmentation processes. We thus predict direct implications of our theory on the generation of lipid vesicles with such a setup. The *in vitro* creation of lipid vesicles is especially used in the context of synthetic biology [218, 222]. Here, biomolecules are separated into small compartments, to study their interplay in a restricted volume. This specifically serves as an experimental playground for the development of synthetic cells. Furthermore, in this context often fuelled chemical reactions are investigated, that break detailed balance, with the poster child example being the equipment of lipid vesicles with cytoskeleton fibres. For example, the synthesis and degradation of microtubules constantly consume energy in the form of GTP [223]. In such a setup we predict to have varying content distributions depending on the order the vesicles are created. How strong content statistics deviate between compartments needs to be assessed by modelling specific aggregation dynamics, which is beyond the work considered in this thesis. Yet, assessing effects in the context of building synthetic cells by sequential fragmentation offers a fruitful route for further investigations.

In addition to the microfluidic devices previously discussed, it is worth noting that sequential fragmentation processes are a common feature of measurement procedures. By extracting a subsystem for analysis, and subsequently repeating the process to increase sampling statistics, the measurement procedure becomes a realisation of a sequential fragmentation process. Furthermore, our study of reversible polymerisation dynamics has demonstrated that different sampling statistics may be observed depending on whether a subsystem or a defined number of objects is extracted from the system. This is particularly relevant when considering biological systems, where subsystems may be chemically modified or destroyed during the measurement procedure. It is thus crucial to verify that the enclosed dynamics are entropically neutral under dynamic compartmentalisation prior to conducting the measurement.

Notably, as demonstrated in Section 4.6.3, steady states are not sufficient to conclude on entropic neutrality under dynamics compartmentalisation. Sequential fragmentation processes can produce compartments with different macrostate statistics if the enclosed chemical reaction network dynamics break detailed balance. Furthermore, correlations between constituents can bias the measurement in a non-trivial manner. Additionally, the simple difference between extracting a random number or a fixed number of particles from the system can constitute performing work on the system. Consequently, caution is required when analysing sample statistics produced by iteratively sampling a system, where samples are discarded after measurement. This emphasises the need for a close interconnection between measurements and model development. While model development relies on measurements, a model can be used to assess systematic deviations in the sampling procedure, enabling refinement of the measurement, which in turn can lead to refined models. Note that a model is initially needed to assess the strength of deviations

potentially created by the measurement procedure.

Complementarily, the generation of distinct compartments could also be advantageous, depending on the nature of a task. We initiated this model with the aim of investigating dynamic compartmentalisation in the context of biological applications. As introduced in section 1.3, dynamic compartmentalisation is a common feature in biological systems. Exploring the thermodynamics of these systems could provide a productive approach to assessing the biological role of dynamic compartmentalisation in biological systems. Furthermore, dynamic compartmentalisation combined with detailed balance could be used to control the abundance of oligomer structures in the context of cell signalling. In Chapter 5, we will consider how dynamic compartmentalisation alters the abundance of MAVS aggregates, which are essential components in the innate immune response to viral infections in mammals. Generally, the analysis of broken detailed balance chemical reaction networks subject to dynamic compartmentalisation could enhance the signalling capabilities of cells, thus presenting a promising area for further investigation.

4.8. Discussion

In this chapter, we have considered the implications of compartment dynamics for closed compartmentalised systems from a thermodynamic perspective. We have paid particular attention to the issue of whether compartment fusion and fragmentation involve the performance of work on the system. We have compared two compartment protocols, which we have termed synchronous and sequential fragmentation, in order to determine whether compartment dynamics have an effect on the statistics of the realised system states, and therefore on the system's entropy. We have demonstrated that the ideal gas is *entropically neutral* under dynamic compartmentalisation, as compartment dynamics have no effect on the entropy of the system. Making use of the formalism of the Second quantisation, we have generalised our findings, proving a simple operator relation which allows the entropic neutrality to be determined by a simple algebraic condition. Along the same lines, we have proposed a generalised notion of work performed by compartment dynamics. We have discussed the thermodynamic consistency of our findings, demonstrating that our formalism is effective in detecting subtle notions of work performed on the system by compartment dynamics. We have concluded by discussing the biological and technical relevance of our findings. In the following chapter 5, we will consider our findings in the context of gelation and organelle-associated signalling pathways, with a particular focus on cellular immune responses to RNA-virus infections.

The motivation for our investigations in this chapter stems from the fact that the physics by which fluctuations are induced among compartments differs significantly between *open* and *closed* compartmentalised systems. Fluctuations in open compartments are induced by contact with an external reservoir, while in closed compartmentalised systems they are solely due to the creation and preservation of density fluctuations as a result of compartment fragmentation, as illustrated in Fig. 4.1. In this chapter, we have set out to investigate whether this mechanism could lead to a fundamental alteration of the statistics of realised system states. In section 4.3.2, we introduced the *Gergesian demons* scheme, which allows testing the extent to which the mechanism of preserved density fluctuations allows us to imprint a time-protocol on the system's statistics. In particular, as we impose isolated conditions on the compartments and demand that no work is performed by the demons as the partition is inserted, we expect that synchronous and sequential fragmentation will yield the same system state statistics. If this is not the case, we infer

4. Towards a thermodynamics of closed compartmentalised systems

that the Gergesian demons must have performed work on the system so as not to create thermodynamic inconsistencies. Thus, we find the scheme of Gergesian demons to be a useful framework for assessing work performed by compartment dynamics.

In agreement with our thermodynamic considerations, we observe that an ideal gas in isolated compartments is *entropically neutral* upon dynamic compartmentalisation. This is evidenced by numerical simulations in section 4.4.3, which are subsequently supported by a formal proof in section 4.4.4. Here, we find that the statistical property of the ideal gas responsible for entropic neutrality is closely related to describing the ensemble of the ideal gas using Dirichlet distributed random variables. We find that entropic neutrality of the ideal gas is fundamentally based on the assumption of the molecular chaos hypothesis and a uniform distribution of states in the momentum phase space, and not the energy phase space. This hints towards yet unappreciated special statistical properties and statistical identities of the ideal gas.

Having established a close connection between the entropic neutrality of the ideal gas and special statistical properties of the Dirichlet distribution in section 4.4, we sought in section 4.5 to extend our findings to other stochastic many-body dynamics subjected to dynamic compartmentalisation. We found that the Second quantisation framework provided a convenient tool for this purpose. By following the sketch of the proof in section 4.4.4, we reduced the analysis of the compartment fusion and fragmentation effect to calculating the commutator between the Hamiltonian and the fragmentation or fusion operator, as shown in Eq. (4.56) and Eq. (4.58), respectively. The Hamiltonian operator characterises the temporal evolution of the system. If the commutator is zero, we conclude that the compartment dynamics leave no imprint on the system's statistics. Consequently, we proposed that a non-vanishing commutator could be associated with a generalised notion of work performed on the system by the fusion or fragmentation of compartments. To confirm this proposition, it is necessary to formally prove that this connection is thermodynamically consistent in future research.

In sections 4.5.3 and 4.5.4, we studied a quantised version and chemical reactions within our derived formalism and demonstrated how our commutator relation can be used to detect subtle notions of work performed on the system. In section 4.6.3, we particularly examined the case of chemical reactions with broken detailed balance conditions, which are inconsistent with the assumption of isolated compartments. Thus, the fact that different system statistics are found for the synchronous and sequential fragmentation protocols does not imply thermodynamic inconsistencies. Nonetheless, the question of the type of work performed by the compartment fusion and fragmentation on the system remains unanswered. To gain insight into this relationship, an insightful approach could be to explicitly analyse the interplay between broken detailed balance and compartment fragmentation in a simple example.

We found that the effects of compartment dynamics are not vanishing but appeared to be small in the systems considered in this chapter. In the next chapter 5, we will explore whether the combined action of compartment fusion and fragmentation for systems larger by orders of magnitude can strengthen these effects. Furthermore, we will consider the implications of our findings in relation to cellular immune responses to RNA-virus infections.

In section 4.7, we discussed possible experimental setups and the technical relevance of our findings. Specifically, we suggested that micro-fluidic high-throughput measurements of patchy colloid dynamics could serve as a fruitful experimental setup for challenging our analytical predictions in experiments. We considered our findings to be particularly

relevant for the design of measurement procedures. We demonstrated that subtleties in the extraction of precise or average numbers can yield varying measurement results. We proposed that our theoretical findings may be applicable whenever measurements of interacting systems are performed iteratively by extracting constituents of the system and altering or destroying the sample in the measurement process. Furthermore, we suggested that our framework could be used to evaluate the thermodynamic consistency of coarse-grained lattice simulations, for example, those used to analyse the thermodynamics of phase separation.

From a conceptual standpoint, the analysis in this section allows for a new perspective on the fundamental statistical symmetries that shape our world. We deem our framework powerful to further investigate the (non)-equilibrium thermodynamics of compartmentalised systems. Through our analysis, we have demonstrated that compartmentalised systems are a class of systems that necessitates an extension of our thermodynamic considerations. We hypothesise that further analysis of the notion of work performed by compartment dynamics in a non-equilibrium context requires us to reconsider the current link between work and information processing in our thermodynamic frameworks.

5. Multi-scale fluctuations facilitate gelation in the innate immune response

5.1. Introduction

In 2020 the global COVID-19 pandemic had a disruptive impact on the global scale. The World Health Organisation’s 2019 report ‘World at Risk’ [224] had already highlighted the strategies necessary to counter pandemics. This illustrates the importance of accurately assessing the statistics of rare events. Extreme value theory is a branch of statistics which formalises the evaluation of extreme deviations from the median of probability distributions. A key result of extreme value theory is that the occurrence of extreme values follows different functional statistics, depending on whether the probability distributions of deviations display exponential or power-law tails [225]. As a general mathematical theory, extreme value statistics not only finds application when assessing economic risks but also predicts the occurrence of giant fluctuations in physical systems. As such, assessing if correlations in physical systems decay algebraically or exponentially is a central characteristic of how fluctuations propagate in the system. Classically, algebraic decays are associated with critical behaviour, long-ranged correlations, diverging system properties, and phase transitions [17].

In this chapter, we extend the findings of chapter 4 and investigate to what extent dynamic compartmentalisation influences the statistics of *extreme* fluctuations. This leads to the observation of statistical gelation in regimes that do not allow for gelation following classical criteria. We will investigate the biological relevance of our findings by applying them in the context of cellular immune responses to RNA-virus infections. Motivated by this biological example, we will focus on reversible polymerisation dynamics with broken detailed balance relations, as we have investigated in section 4.6.1. Doing so, we apply the insight we gained in the previous section in a biological context.

This chapter is structured as follows. We begin this chapter with a brief literature review of Smoluchowski aggregation-fragmentation dynamics, which is a convenient mathematical framework to study reversible polymerisation dynamics. Building on section 2.2.3, we examine physical models for the aggregation and fragmentation kernels. We also explore how the emergence of *giant* aggregates in reversible polymerisation is linked to the concept of *gelation*. Employing Smoluchowski aggregation-fragmentation dynamics, we refine the model system in section 5.3. As introduced in chapter 4, we consider *closed* compartmentalised systems, as the total aggregate mass and the total compartment mass conserved. We investigate general compartment fusion and fragmentation dynamics thereby restricted to mass-conserving dynamics. We then present our numerical investigations in section 5.4.

We will investigate a system with specified kernel choices for the reversible polymerisation kinetics in section 5.4.1. By doing so, we introduce the methodology we use to

investigate the phenomenology of the systems and establish how we assess the statistics of giant aggregates formation. Specifically, we find that steady compartment fusion and fragmentation dynamics facilitate the formation of aggregates larger than the average. Comparing compartments with one another, we find a power-law decay in density fluctuations. In section 5.4.2, we then generalise the reversible polymerisation dynamics. Here, we find that compartment fusion and fragmentation dynamics only facilitate aggregate formation if the kernels of the aggregation-fragmentation dynamics meet certain criteria that we specify in this section. We also elaborate on the mechanism by which the compartment dynamics give rise to giant aggregates and power-law statistics in the density fluctuations. For this, we reconcile with the idea of creating and preserving density fluctuations. In section 5.4.3, we then investigate the facilitation of the formation of large aggregates, as we systematically scale the system size. We examine a phenomenon that we term *multi-scale gelation*, as we find diverging moments in the aggregate size distribution of the system. We conclude this chapter by applying our findings to cellular immune responses to RNA-virus infections in section 5.5. For this, we focus on the organelle-signalling pathway around the protein MAVS, which we have briefly mentioned in section 3.9. This signalling pathway mediates inflammation responses when viral RNA is found in the cell cytosol. Our findings in this chapter highlight the importance of mitochondrial fusion and fragmentation dynamics for strong and efficient immune responses. The numerical routine used in this section was to a large extent developed in the Bachelor thesis project of Josef Kaenders, whose project I co-supervised.

5.2. Literature review on gelation in reversible polymerisation kinetics

In section 2.2.3, we introduced the concept of Smoluchowski aggregation-fragmentation dynamics in the context of population balance equations. We discussed its usefulness for modelling organelle fusion and fragmentation, and, in particular, the case of constant fusion and fragmentation kernels, which has been previously used in the literature [100, 147]. Additionally, we mentioned that Smoluchowski aggregation-fragmentation dynamics are also employed in the context of molecular reversible polymerisation reaction kinetics. In section 4.6.3, we investigated the case of reversible reaction kinetics and concluded that compartment dynamics can affect the statistics of the aggregate size distribution if detailed balance at the level of molecular reaction kinetics is broken.

In this section 5.2, we focus on Smoluchowski aggregation-fragmentation dynamics in more general terms and review specific kernel choices and their connection to physical models. We will then turn to the non-equilibrium formalism of *gelation* in Section 5.2.2. Gelation is, in particular, relevant to assess the statistics of *large* aggregates¹. We will exemplify in section 5.5 how the statistics of large aggregates play a central biological function in the cellular immune responses to RNA-virus infections.

¹We formally define large aggregates as aggregates larger than the mean aggregate size. Further note that here we refer to objects which are subject to Smoluchowski aggregation-fragmentation dynamics as *aggregates*.

5.2.1. Physical modelling of fusion and fragmentation kernels

Beginning with Smoluchowski's seminal work [88], the physics of the aggregation dynamics has been described by the specific aggregate size dependence of the aggregation and fragmentation kernels. Here, we review some of the specific choices for molecular aggregation and fragmentation kernels and put a special focus on kernel choices that admit solutions fulfilling detailed balance.

Different kernel choices are employed to investigate aggregation kinetics, depending on the governing physics. In engineering applications, a variety of aggregation kernels are used to examine aggregation dynamics from molecular aggregation [226–228] to aerosol coalescence [90]. Furthermore, in engineering contexts, aggregation-fragmentation dynamics are commonly analysed in terms of derived moment equations [72, 229, 230]. Homogeneity classes of kernels can provide direct information regarding the qualitative temporal evolution of the system [229]. The homogeneity class of the aggregation and the fragmentation kernel is defined by

$$K_{ai,aj} = a^{\alpha_a} K_{i,j} \quad \text{and} \quad F_{ai,aj} = a^{\alpha_f} F_{i,j}. \quad (5.1)$$

Based on the homogeneity classes of α_a and α_f different kernels are differently classified. We will regularly refer to the homogeneity classes of kernels when we next present a small subset of the popular aggregation kernel choices.

A prominent Kernel choice for aggregation dynamics was initially derived by Smoluchowski and is commonly referred as Brownian aggregation kernel [229, 231, 232],

$$K_{i,j} = D_{\text{eff}} \left(i^{1/3} + j^{1/3} \right) \left(i^{-1/3} j^{-1/3} \right) \quad (5.2)$$

which sets the aggregation rate of two aggregates of size i and j in the dependence of the collision rate of both aggregates assuming motion due to Brownian diffusion in 3 dimensions. D_{eff} refers to an effective spatial diffusion coefficient and is rescaled to set the correct physical units of the aggregation kernel. The first term of the Brownian aggregation kernel grows monotonically with increasing aggregate sizes of i and j , as the surface area, and thus the target area, of the aggregates increases. Note that this assumes the formation of spherical aggregates upon fusion, and that fusion occurs independent of the contact point of the two fusing aggregates. The second term is monotonically decreasing with the aggregate size, reflecting the fact that the diffusion coefficient of spherical objects decreases with size. Note that, consistent with the Smoluchowski aggregation-fragmentation formalism in Eq. (2.14), the derivation of the Brownian aggregation kernel involves mean-field approximations. It is not possible to find an analytical solution for the Brownian aggregation kernel. Its homogeneity class is $\alpha_a = 0$, which is identical to the homogeneity class of constant aggregation kernels $K_{i,j} = \mu$. As the constant aggregation kernel admits analytic closed solutions for specific fragmentation kernels, it is used to approximate the kinetics of the Brownian aggregation kernel, in accordance with the heuristics of moment closures arguments [99, 229].

In the context of molecular polymerisation aggregation, the product kernel $K_{i,j} \propto ij$ is a popular choice for studying the merging of aggregates, only allowing aggregation via contact of functional groups [229]. This ansatz typically neglects the size dependence of the diffusivity, with a homogeneity class of $\alpha_a = 2$. It is specifically used to study gel-forming solutions, which are elaborated on in section 5.2.2. For the study of branched-chain polymerisation, the sum kernel $K_{i,j} \propto i+j$ is also studied, allowing for an-

5. Multi-scale fluctuations facilitate gelation in the innate immune response

analytic closed solutions for specific fragmentation kernels. More detailed kernels reflecting physical principles better are typically not amenable to analytic solutions [233].

Aggregation kernels are often derived from physical principles by estimating collision rates [232, 233]; however, due to the need for specific knowledge of the internal organisation of aggregates, the derivation of fragmentation rates is more complex. Consequently, a wide range of physically derived aggregation kernels can be found in the literature, see [234] and references therein, yet only a few qualitative derived fragmentation kernels have been considered. Examples of such kernels include the parabolic fragmentation kernel and the power-law fragmentation kernel:

$$F_{\text{pb}}(i, j) \propto \frac{i^{b-2}j}{i+j} \quad \text{and} \quad F_{\text{pl}}(i, j) \propto \frac{(i+j)^b}{(i+j)^{v+1}} i^v, \quad (5.3)$$

where $b > 0$ and $-2 < v \leq 0$ [229]. In particular, the choice $b = 3$ for the parabolic fragmentation kernel favours the breakage of aggregates *in the middle*, while the power-law fragmentation kernel favours the breakage of aggregates *on the side*. A detailed derivation of the fragmentation kernel can only be achieved if the detailed internal dynamics aggregates are known.

Of special interest is the combination of aggregation and fragmentation kernels, which in combination fulfil the detailed balance condition. [231] showed that the detailed balance condition presented in Eq. (2.14) using $\phi_{i,j} = K_{i,j}/F_{i,j}$ is reduced to

$$\phi_{i,j} = \frac{\prod_{n=j}^{i+j-1} \phi_{1,n}}{\prod_{n=1}^{i-1} \phi_{1,n}}. \quad (5.4)$$

With this condition, the solution in a steady state is readily determined by

$$f(s, t) = \left(\prod_{n=1}^{s-1} \phi_{1,n} \right) f(1, t)^s, \quad (5.5)$$

with the monomer concentration given by the identity

$$\mathcal{N} = \sum_{s=1}^{\infty} s f(s, t), \quad (5.6)$$

where \mathcal{N} quantifies the total mass of monomers, which is conserved by construction. This relationship is of particular interest when the fulfilment of detailed balance and the physics of the aggregation kernel are imposed. In such cases, the choice of the fragmentation kernel is restricted and only qualitative adjustments are possible, regarding whether fragmentation into equal or unequal daughters is favoured. The specific derivation of the aggregation-fragmentation kinetics for specific biomolecules is usually a major obstacle demanding quantum-chemical computation models and detailed understanding of the protein structure [191, 192]. Yet, discussing the general properties of the solutions to aggregation-fragmentation dynamics enables qualitative discussions and the estimation of extreme value statistics. We next focus in particular on the qualitative statistics of *large* aggregates, by considering *gel* forming solutions.

5.2.2. Gel-forming solutions to the Smoluchowski aggregation-fragmentation equation

In section 5.2.1, we discussed the aggregation-fragmentation dynamics from a kinetics perspective, specifying the choices of the aggregation and fragmentation kernel based on physical principles. In this section, we focus on the characteristics of the solutions, noting that aggregation and fragmentation dynamics balance each other: the absence of fragmentation leads to the formation of larger and larger clusters, whilst the absence of aggregation and infinite divisibility leads to smaller and smaller aggregates. If a moment of the size distribution diverges or vanishes, we refer to this as the appearance of gelation or shattering transitions. Throughout this chapter 5, we take monomers as minimal building blocks, thereby inhibiting shattering transitions. In this section, we will discuss the qualitative effects of gelation and specify on the definition of *large aggregates*. Recall, that we here formally defined large aggregates as aggregates larger than the average aggregate size. For this, we will first focus on a specific example, in which we illustrate the concept of gelation. Following this, we illustrate how the concept of gelation is generalised and briefly state the Carr-DaCosta criterion for non-gelling solutions.

To exemplify the concept of gelation, we closely follow [99], where a simple analytic example of aggregation-fragmentation dynamics showing gelation is presented. For this, we make use of the Kronecker-delta notation to consider the specific kernel choices of $K_{i,j} = 2\lambda$ and $F_{i,j} = 2(\delta_{i,1} + \delta_{j,1} - \delta_{ij,1})$, where fragmentation only allows the break-off of monomers, while aggregates of arbitrary sizes can merge. This kernel choice is not motivated by physical principles, but by its mathematical solvability. The polymer density, defined as the total number of aggregates, is denoted by $N = \sum_s f(s, t)$. Using the generating function $C(z, t) = \sum_j (z^j - 1)f(j, t)$, the steady state solution of the aggregation-fragmentation dynamics according to Eq (2.14), are given by non-linear Riccati differential equation

$$\frac{\partial C}{\partial t} = C^2 + 2\lambda^{-1} \frac{1-z}{z} + 2\lambda^{-1} \frac{(1-z)^2}{z} N. \quad (5.7)$$

This equation admits two different functional solutions depending on whether λ is greater or smaller than one. We define the gel mass fraction

$$g = 1 - \sum_j j f(j, t), \quad (5.8)$$

which specifies the condition of mass conservation. While the solution for $f(j, t)$ is given in [99], we here only discuss asymptotic solutions and focus on the polymer density N and the gel mass fraction g , which are

$$N = \begin{cases} 1 - \frac{\lambda}{2} & \lambda \leq 1, \\ \frac{1}{2\lambda} & \lambda > 1 \end{cases} \quad (5.9)$$

and

$$g = \begin{cases} 0 & \lambda \leq 1, \\ 1 - \lambda^{-1} & \lambda > 1. \end{cases} \quad (5.10)$$

Here, λ is an order parameter describing a kinetic phase transition. While we find that the mass is conserved for $\lambda \leq 1$ as $g = 0$, the total mass in the distribution is reduced as

5. Multi-scale fluctuations facilitate gelation in the innate immune response

$g > 0$ for $\lambda > 1$. Conversely, the total number of aggregates remains constant for $\lambda > 1$. This can be made intuitive, by thinking of an excess mass, which accumulates in a single, big aggregate above a critical density $\lambda > \lambda_c = 1$. This picture is further illustrated considering the asymptotic solutions for $s \gg 1$ with

$$f(s, t) \propto \begin{cases} \frac{(\lambda^{-1}-1)^2}{\lambda^{-1}} s^{-3/2} e^{-s(2\log \lambda^{-1} - \log(2\lambda^{-1}-1))} & \lambda \leq 1, \\ \lambda^{-1} s^{-5/2} & \lambda > 1. \end{cases} \quad (5.11)$$

Here, the size distribution shows an exponential cut-off for $\lambda \leq 1$. As λ approaches 1, the cut-off disappears. For $\lambda > 1$, the size distribution displays a power-law decay, with a single large aggregate accounting for the extra mass being referred to as a *gel*, and the species that constitute the power-law distribution being referred to as *sol*. This nomenclature is linked to the percolation threshold, although it does not have an obvious connection to an experimentally measurable viscosity. Instead, the emergence of a *gel* should be related to changes in extreme value statistics for large aggregates.

Recall that we derived a solution for gel under the assumption of only monomeric break-offs from the gel. This renders the gel a stable structure, exhibiting only small fluctuations. However, if we retain all $F_{i,j} > 0$ at finite values, then the gel structure is allowed to transiently decay into clusters of arbitrary size. This is illustrated by [235, 236], who demonstrated the appearance of *extremal* fluctuations if a critical value $\lambda > \lambda_c$ is crossed in a different aggregation-fragmentation dynamics. Without specifying the details of these dynamics, λ here refers to a general quantification of the timescale of aggregation versus the timescale of fragmentation. Inspired by the observation of a special kinetic phase transition, which alters the extreme value statistics, [237] investigate a classification of aggregation-fragmentation dynamics on the basis of the aggregation and fragmentation kernel.

The Carr-DaCosta criterion, presented in [237] and [238], provides conditions for the aggregation and fragmentation kernel, for which the moments of the size distribution converge, regardless of the value of λ , which quantifies the timescale of aggregation relative to the timescale of fragmentation. [237] refer to this regime as the *strong fragmentation* regime, where fragmentation predominates over aggregation and thus prevents the formation of *gels*. Specifically, the non-gelling is here specified as the absence of the divergence of moments

$$S_n = \sum_{j=1}^{\infty} j^n f(j, t) < \infty, \quad \forall n > 0, t > 0. \quad (5.12)$$

The aggregation-fragmentation dynamics are in the strong fragmentation regime if

$$K_{i,j} \leq K_a(i+j) \quad (5.13)$$

the aggregation kernel is bound by the summation kernel. Here $K_a > 0$ is a positive, real constant. Further, the fragmentation kernel needs to fulfil the condition

$$\sum_{j=1}^{\lfloor (r-1)/2 \rfloor} j^m F_{j,r-m} \geq C(m)r^{\gamma+m}. \quad (5.14)$$

Here $\lfloor x \rfloor$ refers to rounding to the floor of $x \in \mathbb{R}^+$. The equation needs to hold for a $\gamma > 0$ with a constant $C(m)$ for all $m \geq 0$ and $r > 3$. Formally, this criterion holds

only in the limit $N \rightarrow \infty$, where the strong fragmentation implies an exponential cut-off in the aggregate size distribution. This directly implies that all moments of the size distribution $S_n = \sum_{j=1}^n j^n f(j, t)$ converge. Conversely, [237] also proves that critical *densities*, upon which moments of the size distributions S_n diverge, occur in the weak fragmentation limit. The Carr-DaCosta criterion is widely referred to in the applied mathematics literature focusing on the question of the compactness and uniqueness of solutions to aggregation-fragmentation differential equations. A similar criterion exists in the engineering literature, known as the Vigil-Ziff criterion [229], which states that gelation occurs when $\alpha_a - \alpha_f > 2$. Note that these two criteria are not identical and that the Vigil-Ziff criterion was derived heuristically after studying 15 special cases with log-normal moment closure approximations.

From a numerical perspective, the detection of gel formation is challenging, as large gels only transiently occur. Here, we test gel formation by testing the aggregate size distribution for diverging moments in the aggregate size distribution. In simulations, we are bound to investigate finite-sized systems. We study the divergence of moments by tracking how moments change as the system size is steadily increased. Observing different cut-off statistics in the aggregate size distributions motivates us to refer to *large* aggregates, as those aggregates which form either the exponential or power-law tail. For practical considerations, we refer to large aggregates as aggregates larger than the mean aggregate size.

5.3. Reversible polymerisation subject to dynamic compartmentalisation

In chapter 2 and 3, we showed how organelle dynamics affect the response kinetics of organelle-associated signalling pathways. Here, we further specify the model presented in section 2.3. Specifically, in this chapter, we restrict the compartment dynamics, as specify the organelle dynamics to include only fusion and fragmentation. On the level of chemical reaction, we only consider reversible polymerisation kinetics. As a consequence, the dynamics in this section conserve the total compartment mass and the total mass of the aggregates summed over all compartments.

We thus consider the system as a *closed compartmentalised system*. This is in contrast to the dynamics investigated in chapter 2, where we considered the steady binding and unbinding of biomolecules to and from the organelle membranes. The conservation of the total aggregate mass does not, however, necessarily imply that the total mass of aggregates per organelle is conserved. Analogous to Eq. (2.20), we symbolically define the dynamics of the system with a Master Equation. We consider Smoluchowski aggregation-fragmentation dynamics on both the level of organelle dynamics and for reversible polymerisation kinetics. To distinguish between the dynamics on the two different spatial scales, we introduce the superscript ‘o’ for compartment dynamics² and ‘p’ for chemical reaction kinetics.

We define our compartment system in analogy to Eq. (2.19) in section 2.3 and Eq. (4.7)

²We here use ‘o’ as an abbreviation for *organelle* as we take inspiration by the application to organelle-associated signalling pathways. We avoid any potential misunderstandings with ‘c’ standing for compartment and not concentration.

5. Multi-scale fluctuations facilitate gelation in the innate immune response

in section 4.3.2 as

$$\mathbb{S} = \begin{bmatrix} \vdots \\ [\vec{s}_i, v_i] \\ \vdots \end{bmatrix}. \quad (5.15)$$

The system is characterised by a list of compartments, each of which is specified by the state of the internal stochastic many-body system and its compartment properties. The latter are fully described by the corresponding volumes, v_i . Moreover, the state of the enclosed dynamics is defined in terms of a concentration vector \vec{s}_i , which expresses the concentration of aggregates of s as $\vec{s}_i = \vec{n}_i/v_i$. Note that by this we introduced a change in notation from \vec{c} to \vec{s} , to reflect that the molecular species are all aggregates, which vary in their size. Finally, the total number of compartments in the realisation of the system \mathbb{S} is denoted by $N(\mathbb{S})$. In a semi-symbolic notation, the dynamics of the system are given in the Master-Equation framework by

$$\frac{d}{dt}P(\mathbb{S}) = \sum_i^{N(\mathbb{S})} \left(\mathcal{F}_{\text{fus},i}^{\text{p}} [P(\mathbb{S})] + \mathcal{F}_{\text{frag},i}^{\text{p}} [P(\mathbb{S})] \right) + \mathcal{F}_{\text{fus}}^{\text{o}} [P(\mathbb{S})] + \mathcal{F}_{\text{frag}}^{\text{o}} [P(\mathbb{S})] \quad (5.16)$$

Here, we refer to the aggregation-fragmentation dynamics on the level of protein polymerisation with $\mathcal{F}_{\text{fus},i}^{\text{p}}$ and $\mathcal{F}_{\text{frag},i}^{\text{p}}$. The index i indicates that the dynamics happen in parallel in all compartments. With $\mathcal{F}_{\text{fus}}^{\text{o}}$ and $\mathcal{F}_{\text{frag}}^{\text{o}}$, we refer to the dynamics of compartment fusion and fragmentation. The exact transition rates for the reversible polymerisation dynamics are specified in accordance to the formalism in section 2.2.3 and section 5.2. We adopted the symbolic notation introduced in section 2.3 and detailed out in the appendix A.2 for compartment fusion and fragmentation.

We treat the dynamics in a full stochastic framework, taking into account both reversible polymerisation kinetics and compartment dynamics as stochastic processes. As introduced and formalised in section 2.3, we consider the fragmentation of compartments as processes that introduce fluctuations in the total aggregate density per compartment, as we consider a binomial splitting process between the two daughter compartment upon fragmentation. This leads to fluctuations in the total aggregate mass per compartment. As discussed in section 4.6.1, we rescale the aggregation rate to reflect the changes in the total aggregate mass concentration per compartment.

As introduced in section 2.3, we consider the compartment dynamics to be discrete; Only fragmentation into natural multiples of a unit compartment size is possible. In appendix B.1, we argued how this approximation allows for a speed-up of the numerical simulation routine. To track the system's time evolution, we define the number density $f_i(s, t)$, which gives the abundance of molecular aggregates of size s in compartment i . The marginalised size distribution is $\tilde{f}(s, t) = \sum_i f_i(s, t)$, to which we will refer to as *aggregate size distribution*. The total molecular aggregate mass is denoted by \mathcal{N}^{p} , and the total aggregate mass in compartment i is \mathcal{N}_i^{p} . For notational simplicity, the total compartment mass is $\mathcal{N}^{\text{o}} = N$, and the size of the compartment is v_i . The aggregate density per organelle compartment is $\rho_i = \mathcal{N}_i^{\text{p}}/v_i$, with distribution $p_i(\rho)$. Note that the distributions are in general coupled.

In consistency with chapter 2, we specify on the choice for the aggregation kernel and the fragmentation kernel for the compartment dynamics. We set the aggregation kernel to be constant and independent of the compartment size and as well as independent of the

aggregate composition in the compartments, which is specified by the concentration vector \vec{s}_i for each compartment. We set the compartment fragmentation rate to be proportional to compartment size, while the position of fragmentation is uniformly distributed over the length of the compartment.

Note that these compartment dynamics are a generalisation of the compartment dynamics described in chapter 4, in which we considered how the statistics of reversible polymerisation processes are affected by either synchronous or sequential compartment fragmentation protocols. We refer to an ensemble with compartments undergoing Smoluchowski aggregation-fragmentation dynamics as a *dynamic* ensemble. We approximate the fusion and fragmentation processes, as well as subsequent mixing, we assume that they happen instantaneously, analogous to the description of the compartment dynamics in section 2.3. Between compartment fusion and fragmentation events, we consider the time evolution of the reversible polymerisation kinetics.

We contrast the *dynamic* ensemble with two compartment dynamics that do not undergo Smoluchowski aggregation-fragmentation dynamics, which we refer to *static* and *synchronous* ensembles. For the *static* compartment ensemble, we consider fragmented, independent compartments. We set all compartments to have the same total aggregate mass and compartment size, $p_i(\rho) = \delta(\rho - \mathcal{N}^p/N)$. There is no exchange of aggregates among the compartments. The reversible polymerisation kinetics evolve independently in the different compartments. In this ensemble, we have a strongly restricted possibility of aggregates reacting with each other. In the *synchronous* compartment ensemble, we evaluate how the reversible polymerisation evolves in a fully fused ensemble. To allow a direct comparison to the effects with the *dynamic* compartment and the *static* compartment ensemble, before an evaluation, we synchronously fragment the system as introduced in section 4.3.2. To record time traces, we fuse all compartments subsequent to the evaluation again.

Contrasting the *dynamic*, *static*, and *synchronous* ensemble allows us to both distinguish the effects of compartmentalising the dynamics and the effects of dynamic compartmentalisation. With this model system, we investigate the question, of to what extent compartment dynamics can alter the tail statistics of the aggregate size distribution and if compartment dynamics can effectively suppress or facilitate the formation of large aggregates. We next investigate how compartment dynamics affect the aggregate size distribution.

5.4. Dynamic compartmentalisation facilitates the formation of giant aggregates

In section 4.6.3, we demonstrated that the compartmental dynamics in general influence the aggregate size distribution of reversible polymerisation kinetics, if the polymerisation kinetics break detailed balance. We studied examples of small reaction networks which displayed differences in the aggregate size distribution if either a sequential or a synchronous fragmentation procedure was applied. While we found that the differences were not negligible, the difference between the aggregate size distributions was only a few per cent and thus marginal. Here, we explore phenomenologically the effects of dynamic compartmentalisation on reversible polymerisation dynamics in larger systems by numerical simulations, to test if the effects are strengthened or vanishing. For this, we start by investigating a specific choice of the polymerisation aggregation and fragmentation kernel

and then generalise our findings by systematically scanning other kernel choices. In the next section 5.5 we will then apply the findings of this chapter in the context of cellular anti-viral immune responses.

5.4.1. Dynamic compartmentalisation increases the frequency of large aggregates

To investigate how dynamic compartmentalisation affects the frequency of aggregates of different sizes, we first consider a specific kernel choice for the aggregation and the fragmentation kernel. With the specific kernel choice, we illustrate the effects of dynamic compartmentalisation of reversible polymerisation dynamics, as we introduce different observables. This allows us to build a first intuition about the phenomenology. We extend our investigation to other kernel choices in section 5.4.2.

In chapter 4, we gained the heuristic insight that differences induced by compartment dynamics rely on the creation of density fluctuation between compartments. For this reason, we start our investigation by focusing on aggregation-fragmentation kinetics that create *large* aggregations. In section 5.2.2, we introduced the concept of *gel formation* in the context of Smoluchowski aggregation-fragmentation dynamics. Here, we restrict to the investigation of kernel choices that fulfil the strong fragmentation criterion by Carr and DaCosta [237]. For kernel choices that fulfil the strong fragmentation criterion, we expect the absence of gel formation. Specifically, we start by investigating the kernel choices

$$K_{i,j}^p = \mu^p(i^{0.9} + j^{0.9}) \quad \text{and} \quad F_{i,j}^p = \varphi^p \left(\frac{1}{i^{0.9}} + \frac{1}{j^{0.9}} \right), \quad (5.17)$$

which fulfil the strong fragmentation criterion by Carr and DaCosta [237]. μ and φ are dimensional units specifying the timescale of aggregation and fragmentation, with $\lambda = \mu/\varphi$ the aggregation parameter. The aggregation kernel has the homogeneity class $\alpha_a = 0.9$, while the fragmentation kernel is in the homogeneity class $\alpha_f = -0.9$. Here, the kernel choice is motivated by allowing for a simple modification of the homogeneity class. We discuss how our insight translates to kernel choices motivated by physical models in section 5.4.2.

In the following, we only analyse the ensembles after they have reached a steady-state configuration. To determine if the steady state is reached, we measured moments of the aggregate size distribution $f(s, t)$. As we consider full stochastic simulation, the system fluctuates around the steady state. We compute the temporal mean of the variance $\langle \text{Var}[f(s, t)] \rangle_t$. As the system reached $\langle \text{Var}[f(s, t)] \rangle_t$ for the first time, we consider the system to have reached a steady state.

We begin our numerical investigation with an ensemble of $\mathcal{N}^o = N = 200$ compartments and a total aggregate mass of $\mathcal{N}^p = 5000$ monomeric building blocks. The aggregation parameter for the reversible polymerisation dynamics is set to $\mu^p/\varphi^p = \lambda^p = 1.5$, with the generalised collision rate being defined as $\tilde{\mu}^{o,p} = \mu^{o,p}/\mathcal{N}^{o,p}$. The molecular aggregation dynamics occur on much faster timescales with $\tilde{\mu}^p/\tilde{\mu}^o \equiv \tilde{\tau}_\mu = 5 \times 10^3 \cdot \lambda^p$. Here, we refer to $\tilde{\tau}_\mu$ as the compartment fusion time, which gives a dimensional estimate of how long the reversible polymerisation kinetics progress between two compartment events inside a compartment. We compare the steady-state aggregate size distribution of the *dynamic*, *static*, and *synchronous* ensembles, as introduced in section 5.3. For the dynamic ensemble, the compartment fragmentation rate is much larger than the aggregation rate,

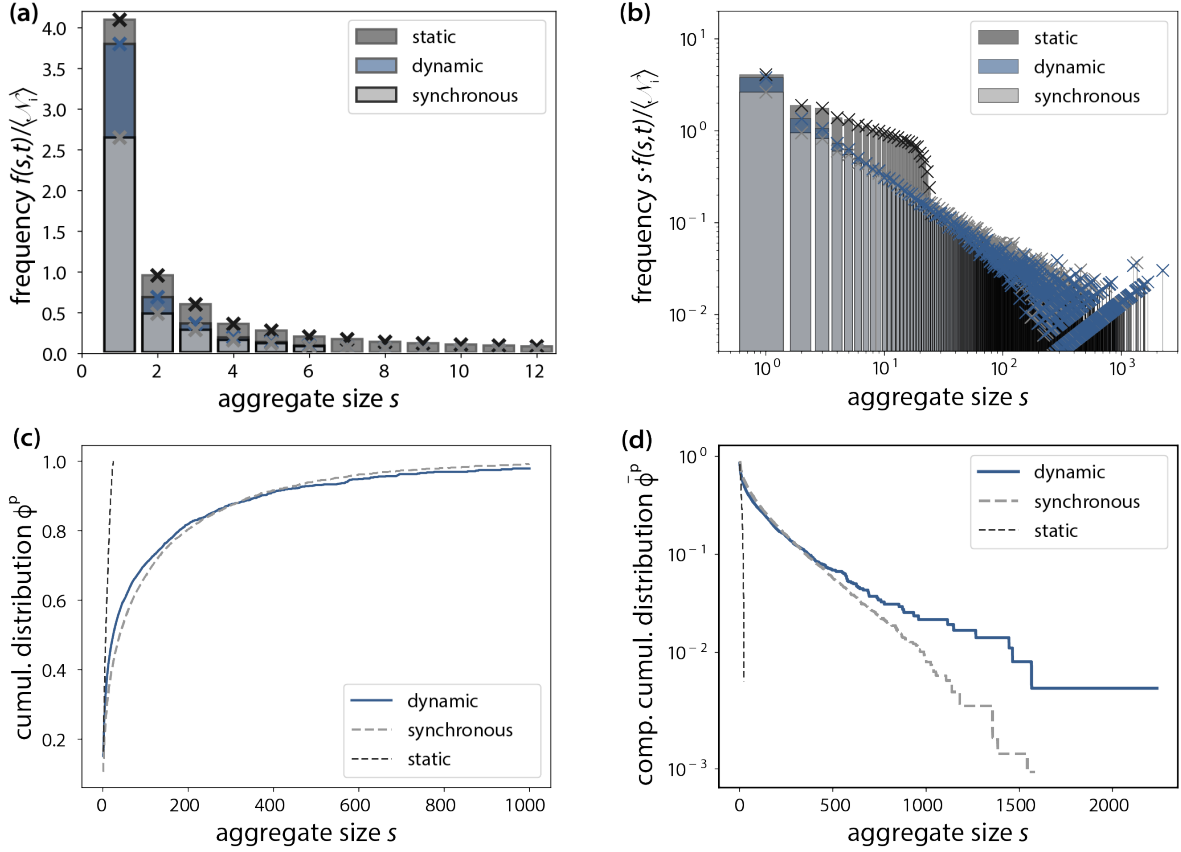


Fig. 5.1.: Compartment fusion and fragmentation facilitate the formation of large aggregates We conducted full stochastic simulations of reversible polymerisation dynamics subject to compartment fusion and fragmentation. The system has $\mathcal{N}^o = N = 200$ compartments and a total aggregate mass of $\mathcal{N}^p = 5000$. The aggregation parameter for the reversible polymerisation dynamics is set to $\lambda^p = 1.5$. The molecular aggregation dynamics occur on much faster timescales with $\tilde{\mu}^p/\tilde{\mu}^o = 5 \times 10^3 \cdot \lambda^p$. The system is motivated in section 5.4.1. All changes in the system are modelled as stochastic transitions. We compare three different compartment dynamics, as specified in section 5.3. The aggregate size is in multiples of the monomeric building block. (a) The histogram shows the aggregate size distribution normalised by the expected of organelle mass per compartment. All different compartment dynamics yield different aggregate size statistics. Only the small aggregate sizes can be analysed. (b) Plotting the histogram in a log-log scale does not make conclusions on the statistics of large aggregates. (c) The empirical cumulative distribution indicates different tail statistics when comparing the *dynamic* and *synchronous* compartment ensembles. The statistics of large aggregates are reflected in how ϕ^p approaches 1. (d) The complementary empirical cumulative distribution function allows for graphically assessing the statistics of large aggregates by using a logarithmic y-scale. We find that compartment fusion and fragmentation facilitate the formation of large aggregates.

being set to $\lambda^o = 0.001$, such that compartments are predominantly found in a fragmented state. For the *static* and *synchronous* ensembles, we consider for the evaluation the state where the compartments are fully fragmented. For presentation, we marginalise the size distribution over all compartments and normalise it such that $\sum_s s f^p(s, t) = \mathcal{N}^p/N$.

In Fig. 5.1 (a), we show the marginalised aggregate size distributions up to an aggregate size of $s = 12$. We find that the steady-state aggregate size distributions differ between

5. Multi-scale fluctuations facilitate gelation in the innate immune response

all three ensembles. While all distributions peak at $s = 1$ and rapidly fall off, we find the highest frequency of small aggregates in the *static* ensemble and the lowest frequency of small aggregates in the *synchronous* ensemble. Yet, visual inspection of the histogram is insufficient to make statements about the abundance of larger aggregates. In Fig. 5.1 (b), we plot the histogram in a log-log scale, without rescaling the bins, which each represent the abundance of aggregates of specified, discretised size s . We plot the abundance of aggregate mass with $s \cdot f(s, t)$. We find, that the *static* ensemble shows a qualitative different aggregate size distribution, where the formation of large aggregates $s > 25$ is suppressed. This is a consequence of setting a uniform aggregate mass density and inhibiting the exchange of aggregates between compartments. Contrasting the *dynamic* and *synchronous* ensemble, we find the formation of large aggregates, while assessing the statistics of the tail of the distribution is not possible from visual inspection.

We introduce the cumulative distribution function $\phi^p(k) = \sum_s^k f(s, t)/\mathcal{N}^p$ which is constrained to the interval $\phi^p(k) \in [0, 1]$. This function gives, for each aggregate size s , the mass fraction of mass in aggregates of smaller or equal size. $\phi^p(s)$ is a monotonically increasing function which approaches $\phi^p(s \rightarrow \infty) \rightarrow 1$, making it particularly useful for evaluating the tails of the distribution $f(s, t)$. As we have no access to the true distribution $f(s, t)$, we evaluate the empirical cumulative distribution function [239], as illustrated in Fig. 5.1 (c). Here, we find that the *static* ensemble rapidly approaches $\phi_{st}^p(s) \rightarrow 1$, indicating a large abundance of small aggregates, in line with our findings in Fig. 5.1 (b). In contrast, the cumulative distribution functions for the *dynamic* and *synchronous* ensembles cross. While there is more mass in small aggregates for the *dynamic* ensemble, $\phi_{dy}^p(s) \rightarrow 1$ saturates more slowly for large aggregates, $\phi_{dy}^p(s) < \phi_{sy}^p(s)$ for $s \gg 1$.

We assess the decay by evaluating the complementary cumulative distribution function $\bar{\phi}^p(s) = 1 - \phi^p(s)$, as shown in Fig. 5.1 (d). Setting the y -axis to a logarithmic scale, we observe an exponential tail in $\phi_{sy}^p(s)$, which is expected in the strong fragmentation limit. Compartment fragmentation and aggregation, on the other hand, lead to a more frequent formation of large aggregates, with an order-of-magnitude effect. We also note deviations from the exponential decay in $\bar{\phi}_{dy}^p(s)$. To determine whether these deviations are caused by fluctuations or a true effect, we examine the density distribution $p(\rho)$ over the different compartments.

We expect that changes in the aggregate size distribution will be linked to modified density fluctuation statistics in the compartments, caused by frequent compartment fusion and fragmentation. To further investigate the density fluctuations, we analyse $p_i(\rho)$ from the simulation shown in Fig. 5.1. We compute the histograms of the different ρ_i , as shown in Fig. 5.2 (a), in order to obtain an estimate for $p(\rho)$. Here, we only compare the *dynamic* and *synchronous* ensembles, as $p_{st}(\rho)$ is delta-peaked by design. We find that both $p_{dy}(\rho)$ and $p_{sy}(\rho)$ are strongly skewed distributions. The mode of $p_{dy}(\rho)$ is shifted towards the mean of the distribution when compared to $p_{sy}(\rho)$, as the number of compartments with strongly reduced density is reduced. This qualitatively resembles the emergent collective ensemble kinetics we described in section 2.5.

We expect the statistics of large aggregates examined in Fig. 5.1 (d) to coincide with the occurrence of large density fluctuations. Consequently, we are interested in the statistics of the tail of the distribution of $p(\rho)$ for large $\rho \gg 1$. However, as for the aggregate size distribution $f(s, t)$, we cannot evaluate the statistics of large fluctuations by visual inspection of the histogram. Therefore, we compute the complementary empirical cumulative distribution function for $p(\rho)$, which we refer to as $\bar{\zeta}^\rho$. In Fig. 5.2 (b) we find that the distribution over density fluctuations is shifted towards the occurrence of large fluc-

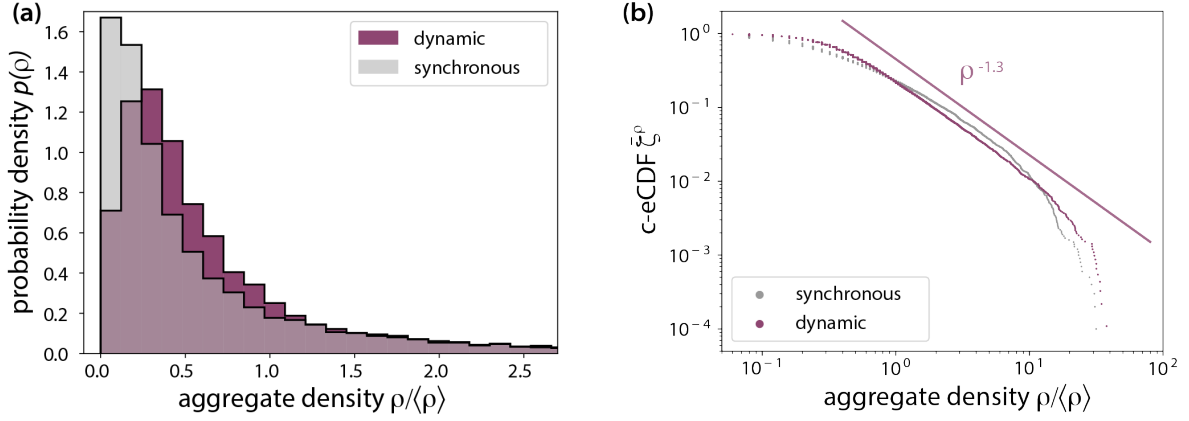


Fig. 5.2.: The density fluctuations among compartments show a power-law decay

The same simulations as in Fig. 5.1. Here, we analyse the statistics of density fluctuations, as we approximate $p(\rho)$ by building the a histogram over all ρ_i . We compare the *dynamic* and *synchronous* ensembles, as defined in section 5.3. ‘c-eCDF’ stands for the complementary empirical cumulative distribution function. (a) We find that the system has a strongly skewed distribution in $p(\rho)$ towards large density fluctuations. As the system is mass conserving, the mode of the distribution is shifted towards below-average densities $\rho_{\text{mode}} < \langle\rho\rangle$. For the dynamic and synchronous we find different distributions, with fewer compartments with strongly below-average densities. (b) To inspect the statistics of large above-average density fluctuations, we consider the complementary empirical cumulative distribution functions of the density fluctuations. We find different statistics for large density fluctuations. Specifically, the dynamic ensemble gives rise to a power-law decay with an exponent close to $\sim \rho^{-1.3}$.

tuations. In comparison to $\bar{\zeta}_{\text{sy}}^\rho$, we observe that the occurrence of low-density fluctuations is reduced while the occurrence of large density fluctuations $\rho \gg 1$ is increased. Notably, Fig. 5.1 (d) suggests that $\bar{\zeta}_{\text{dy}}^\rho$ decays with a power-law tail, in contrast to $\bar{\zeta}_{\text{sy}}^\rho$ which shows a characteristic exponential decay in a log-log plot. We estimate the power-law decay to $\sim \rho^{-1.3}$, which was evaluated by visual fitting. We find the power-law behaviour to extend over one order of magnitude in ρ . This tail behaviour is in contrast to the emergent collective ensemble kinetics described in chapters 2 and 3. We investigate how the deviations in the tail statistics originate from creating and preserving density fluctuations in section 5.4.2.2. Here, we continue to investigate the phenomenology of the system.

We next test if the results are specific to the choice $\lambda^p = 1.5$. To do so, we repeat the identical analysis to Figs. 5.1 and 5.2 for $\lambda^p = 1$, $\lambda^p = 0.5$, and $\lambda^p = 0.1$, as shown in Fig. 5.3. We find qualitatively the same results for all tested values of $\lambda^p = 1.5$, with the aggregate size distribution displaying an increased abundance of large aggregates $s \gg \langle s \rangle$ and the tail of the density fluctuations suggesting a power-law decay if the compartments undergo fusion and fragmentation dynamics. We observe that the increase in the abundance of large aggregates is more pronounced for larger λ^p , which is consistent with the difference in the density fluctuation statistics decreasing with decreasing λ^p , as shown by $\bar{\zeta}_{\text{dy}}^\rho$ and $\bar{\zeta}_{\text{sy}}^\rho$ in Fig. 5.3 (b), (d) and (f). Moreover, we find that the exponent of the power-law decreases as λ^p is decreased. By visual fitting, we estimate $\sim \rho_1^{-2.2}$, $\sim \rho_{0.5}^{-6}$, and $\sim \rho_{0.1}^{-15}$, where the subscript refers to the value of the aggregation parameter λ^p . It should be noted, however, that for $\lambda^p < 1$ the power-law decay does not extend over one order of magnitude in ρ due to the rapid decay and the finiteness of the simulated system, so the estimates of the power-laws should be treated with caution.

5. Multi-scale fluctuations facilitate gelation in the innate immune response

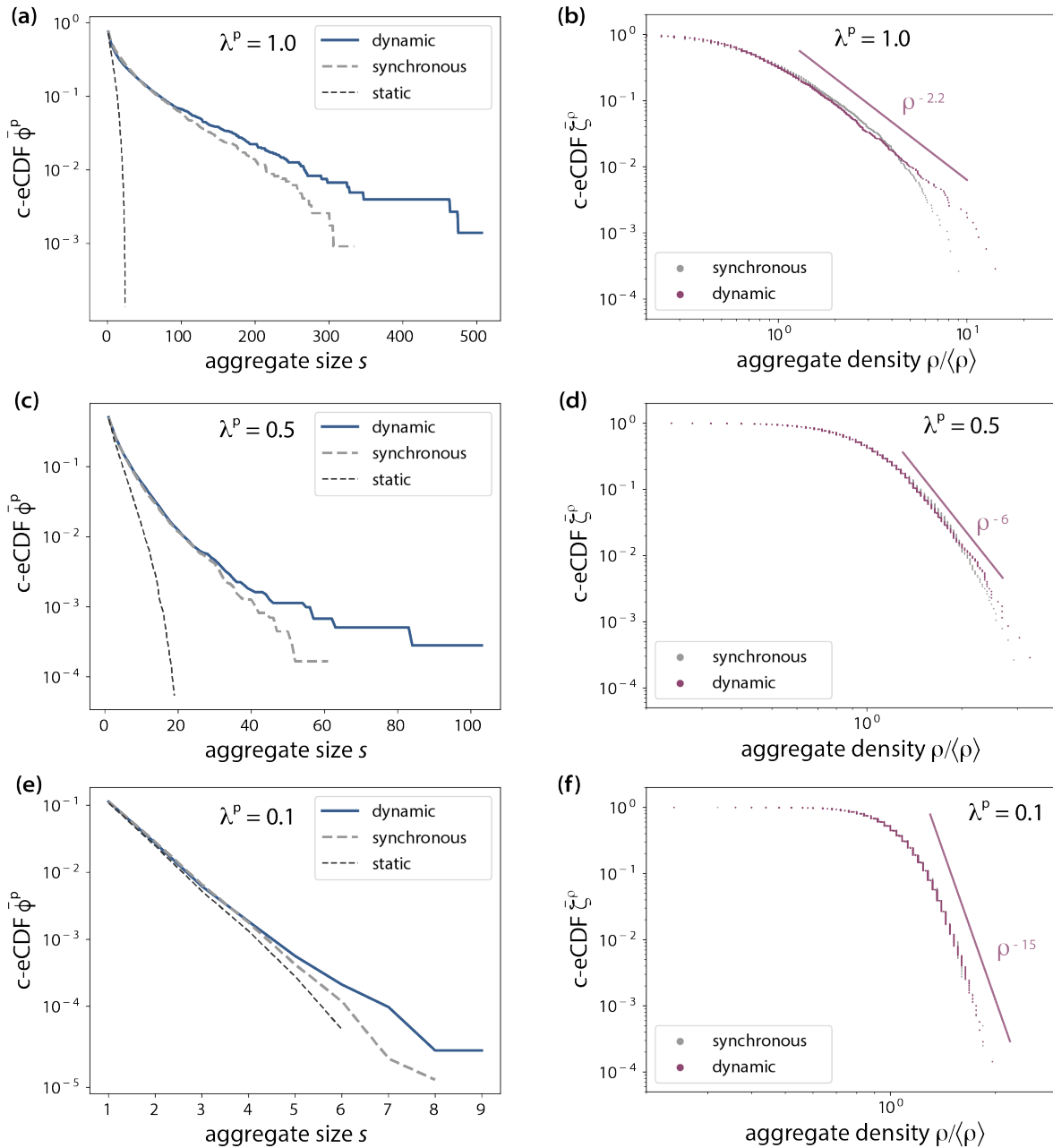


Fig. 5.3.: The qualitative findings are not specific to the choice of the aggregation parameter λ^P . Analogous simulations to Fig. 5.1 are considered with different aggregation parameters: (a,b) for $\lambda^P = 1.0$, (c,d) for $\lambda^P = 0.5$, and (e,f) with $\lambda^P = 0.1$. While we obtain the qualitative identical findings to Fig. 5.1 and Fig. 5.2, the difference in the statistics is less pronounced for lower values of λ^P . We find that the apparent power-law decays show smaller exponents for smaller values of λ^P . Note, that the decay for $\lambda^P = 0.5$ and $\lambda^P = 0.1$ extent over less than one decade and should thus be interpreted with caution. The aggregate size is in multiples of the monomeric building block. ‘c-eCDF’ stands for the complementary empirical cumulative distribution function.

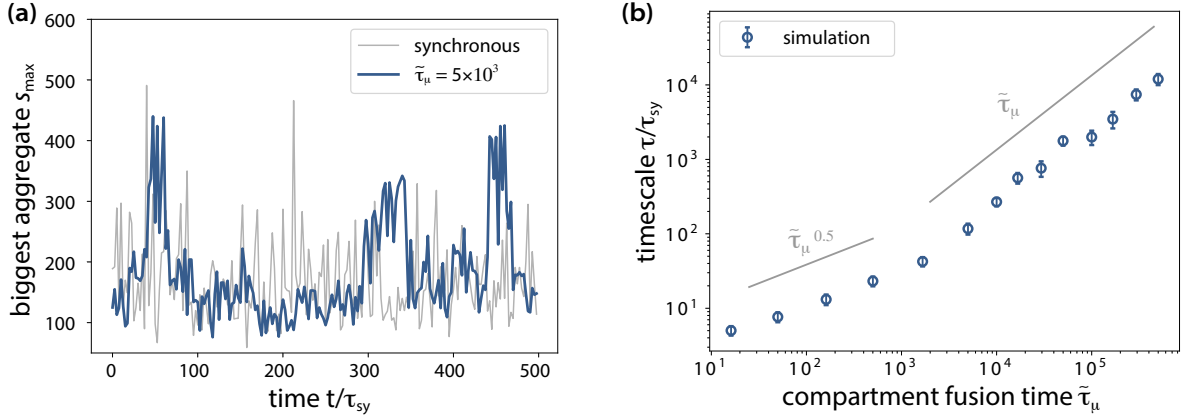


Fig. 5.4.: Compartment fusion and fragmentation affect the stability of aggregates Simulations are analogous to Fig. 5.1 with aggregation parameters for $\lambda^p = 1.0$. We track the size of the largest aggregate s_{\max} for the *dynamics* and *synchronous* ensemble dynamics. We determine the autocorrelation time as described in section 3.5. We normalise by the autocorrelation time of the largest aggregate in the *synchronous* ensemble dynamics, τ_{sy} . The aggregate size is shown in multiples of the monomeric building block. (a) Visual comparison between the *dynamics* and *synchronous* ensemble dynamics. We visually obtain that the largest aggregate is more stable in the *dynamic* ensemble, where density fluctuations are preserved. (b) We systematically change the timescale of compartment dynamics while keeping the compartment size distribution fixed. We find two different regimes which are characterised by different functional dependencies of the autocorrelation time s_{\max} on the compartment fusion time $\tilde{\tau}_{\mu}$. Slow compartment dynamics are on the right and fast compartment dynamics are on the left. Error bars are the fit errors from measuring the autocorrelation time.

We identified that compartment fusion and fragmentation dynamics give rise to the creation and preservation of density fluctuations, which ultimately lead to altered density fluctuation statistics $p(\rho)$ and aggregate size distributions $f(s, t)$. Apart from changing the steady state distributions, we find that the aggregation and fragmentation dynamics also modify the temporal persistence of aggregates, as density fluctuations are preserved in the *dynamic* ensemble in contrast to a fully fused compartment configuration. This is exemplified in Fig. 5.4 (a), where we display a time-trace of the size of the largest aggregate, using the same simulation parameters as in Fig. 5.3 (a) and (b). We calculate the autocorrelation time τ_{\max} of the time-trace and systematically change the ratio $\tilde{\mu}^p/\tilde{\mu}^o = \tilde{\tau}_{\mu}$ while keeping the other simulation parameters fixed. In Fig. 5.4 (b), it is evident that the auto-correlation time increases with increasing $\tilde{\mu}$. Plotting the auto-correlation time in a log-log scale, we detect two different regimes. For $\tilde{\mu} > \tilde{\mu}^*$, the auto-correlation time increases linearly $\tau_{\max}(\tilde{\mu}) \sim \tilde{\tau}_{\mu}$. Conversely, for $\tilde{\mu} < \tilde{\mu}^*$, the auto-correlation time increases sub-linearly $\tau_{\max}(\tilde{\mu}) \sim \tilde{\tau}_{\mu}^{0.5}$. We identify the regime with the linear increase $\tilde{\mu} > \tilde{\mu}^*$ as the regime where the reversible polymerisation dynamics inside a compartment relax faster than the rate at which compartments undergo fusion events, $\tilde{m}u^o \ll 1/\tau_{\text{rel}}^p$. In this regime, the stability of large aggregates is governed by how long density fluctuations are maintained. In contrast, the regime $\tilde{\mu} < \tilde{\mu}^*$ requires a more thorough analysis, which is also connected to an investigation of how μ^* depends on the system parameters. Note that in Fig. 5.1, Fig. 5.2 and Fig. 5.3 we considered the system parameters which are in the regime $\tilde{\mu} > \tilde{\mu}^*$, which we deem as the more physiologically probable regime.

5. Multi-scale fluctuations facilitate gelation in the innate immune response

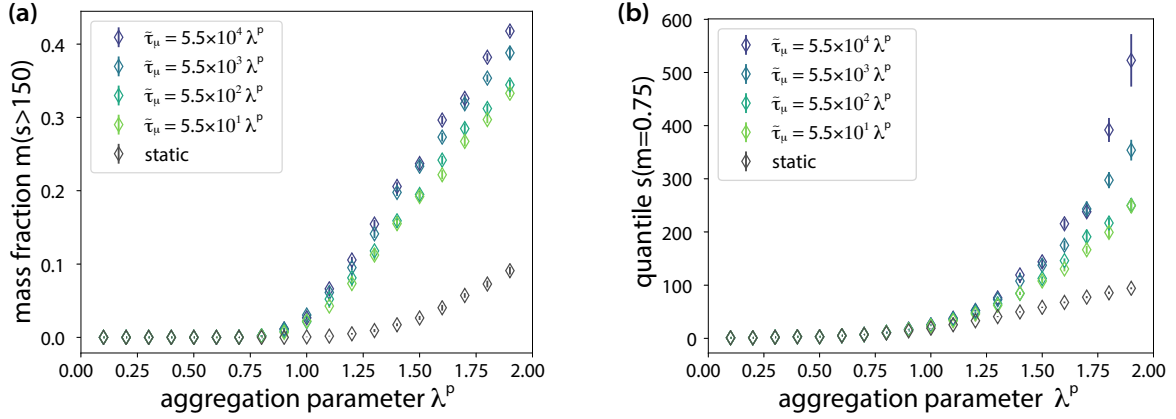


Fig. 5.5.: Increasing the aggregation parameter λ^p results in larger aggregates Analogous simulations to Fig. 5.1 are considered, but for a larger system with $\mathcal{N}^p = 5 \times 10^5$. The aggregation parameter λ^p is systematically increased. The abundance of large aggregates is quantified by considering the mass fraction $m(s > 150)$ in (a) and the quantile of the mass fraction $s(m = 0.75)$ in (b). We qualitatively test for different timescales of the compartment dynamics. Error bars are the standard error of the mean over 5 independent realisations. We find larger aggregates and for the dynamic mitochondrial ensemble with larger aggregates for smaller compartment fusion rates. The findings do not depend on the specific choices of the mass fraction threshold and the quantile [data not shown]. The aggregate size is in multiples of the monomeric building block.

Next, we quantify how variation in λ^p affects the abundance of large aggregates. To do this, we increase the system size to $\mathcal{N}^p = 5 \times 10^5$ whilst keeping $N = 200$ fixed. Fig. 5.5 compares the *static* and *dynamic* ensembles. To measure the abundance of large aggregates, we consider two different measures: the mass fraction greater than a specified aggregate size $m(s > 150)$, Fig. 5.5 (a), and the aggregate size that corresponds to a quantile of the mass fraction $s(m = 0.75)$, Fig. 5.5 (b). For both measures, we find qualitatively similar results, with larger aggregates observed when compartments are subject to fusion and fragmentation dynamics. This is consistent with the findings of Fig. 5.3, which demonstrates larger aggregates with increasing λ^p and $\tilde{\mu}$.

In this section, we have explored phenomenologically how compartment fusion and fragmentation affect the aggregate size distribution of the reversible polymerisation kinetics. For this, we considered specific system parameters and carried out numerical simulations. Our findings are not conclusive, but they provide us with initial insight into how compartment fusion and fragmentation can facilitate the formation of larger aggregates while shifting the statistics of density fluctuations to a power-law decay. In section 5.5, we will interpret these findings in the context of cellular anti-viral immune responses. We next generalise the findings of this section, by phenomenologically investigating other kernel choices for the reversible polymerisation kinetics. Subsequently, we will discuss the mechanisms underlying the facilitation of large aggregate formation, as well as the implications of the power-law decay in \bar{c}_{dy}^p . We will also consider how the results are affected by scaling of the system size, and the potential connection to *gelation*, in section 5.4.3.

5.4.2. Testing different aggregation and fragmentation kernels

In section 5.4.1, we explored the effect of compartment fusion and fragmentation on the aggregate size distribution of reversible polymerisation dynamics using numerical simulations. For this, we made specific choices for the aggregation and fragmentation kernel of the polymerisation dynamics, see Eq. (5.17). In this section, we generalise on the findings of section 5.4.1 by systematically scanning other kernel choices. Our results demonstrate that the facilitation of the formation of large aggregates is dependent on certain conditions for the aggregation and fragmentation kernels. Following our numerical investigations, we will discuss the mechanism behind this facilitation and the deviation from the steady state configuration described in chapter 2.

5.4.2.1. The facilitation of the formation of giant aggregates is specific to kernel choices

In section 5.4.1, we focused on a specific kernel choice for reversible polymerisation kinetics, with homogeneity classes of $\alpha_a = 0.9$ for the aggregation kernel and $\alpha_f = -0.9$ for the fragmentation kernel. These kernel choices are prone to the formation of large aggregates while still fulfilling the strong fragmentation criterion proposed by Carr and DaCosta [237], which predicts the absence of gel formation. Here, we systematically vary the homogeneity classes of the aggregation and fragmentation kernels to determine whether the phenomenology discussed in Section 5.4.1 is general or only valid for a particular region of the model space (α_a, α_f) . We generalise the kernel choice in Eq. (5.17) to

$$K_{i,j}^p = \mu^p(i^{\alpha_a} + j^{\alpha_a}) \quad \text{and} \quad F_{i,j}^p = \varphi^p(i^{\alpha_f} + j^{\alpha_f}). \quad (5.18)$$

Only Kernel choices with $\alpha_a < 1$ and $\alpha_f > -1$ fulfil the strong fragmentation criterion by Carr and DaCosta [237]. We expect a different phenomenology for reversible polymerisation kinetics that show the formation of gels. Here, we restrict the analysis of the model space to $(\alpha_a, \alpha_f) \in (-1, 1) \times (-1, 1)$.

Before conducting a systematic scan of the parameter region through numerical experiments, we first investigate the impact of a second specific kernel choice, setting $\alpha_a = -0.9$ and $\alpha_f = 0.9$. We expect this kernel choice to suppress the formation of large aggregates. We simulate a system with $N = 800$ compartments and a total aggregate mass of $\mathcal{N}^p = 4 \times 10^3$, setting the aggregation parameter $\lambda^p = 2$ and the ratio of timescales between the polymerisation and compartment dynamics to $\tilde{\tau}_\mu = 10^3$. As shown in Fig. 5.6 (a), the formation of large aggregates is suppressed, as aggregates of size $s > 10$ are scarce. When comparing the *dynamic* and *synchronous* ensembles, as introduced at the end of section 5.3, we find that the compartment dynamics appear to suppress the formation of large aggregates. Note that, however, the effect is smaller than the facilitation observed in section 5.4.1. The inset of Fig. 5.6 (a) shows that compartment fusion and fragmentation also affect the distribution of density fluctuations $p(\rho)$. This further supports the validity of the observed deviation in Fig. 5.6 (a) as a true effect rather than a consequence of fluctuations.

From this finding, we already conclude, that the facilitation of the formation of large aggregates is not a general property of reversible polymerisation kinetics, but specific to the kernels of the reversible polymerisation dynamics. As we conduct the parameter scan in (α_a, α_f) , we test if the compartment dynamics facilitate the formation of large aggregates. To assess if the formation of large aggregates is facilitated, we compare the

5. Multi-scale fluctuations facilitate gelation in the innate immune response

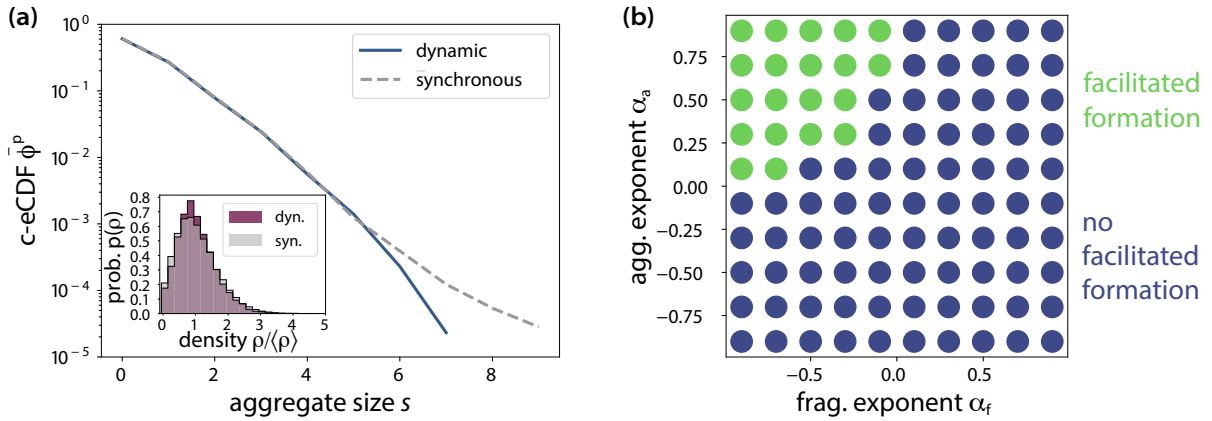


Fig. 5.6.: Systematic scanning of polymerisation kernels reveals region in the model space where compartment dynamics facilitate the formation of large aggregates (a) Test for an ensemble with $\alpha_a = -0.9$ and $\alpha_f = 0.9$ in simulations analogous to Fig. 5.1. The system parameters are specified in section 5.4.2.1. We find that the formation of large aggregates $s \gg \langle s \rangle$ is suppressed by compartment fusion and fragmentation. The inset shows the density fluctuations analogous to Fig. 5.2. Density fluctuations are also affected by the compartment dynamics. The aggregate size is in multiples of the monomeric building block. ‘c-eCDF’ stands for the complementary empirical cumulative distribution function. (b) Systematic scan over different aggregation and fragmentation kernels for the reversible polymerisation dynamics, as defined in Eq. (5.18). We evaluate the maximum of ratio of the cumulative distribution functions in the tail $s > \langle s \rangle$, q_{\max} . If $q_{\max} > 1.1$, we define to have observed the facilitated formation of large aggregates. We find that the formation of large aggregates is specific to a region in the parameter phase space.

dynamic and *synchronous* ensembles. We compute the ratio of the cumulative distribution functions and evaluate its maximum $q_{\max} = \max(\bar{\phi}_{\text{sy}}^p(s)/\bar{\phi}_{\text{dy}}^p(s))$ in the tail for $s > \langle s \rangle$. To ensure that the observed effect is not due to fluctuations in the tail of the distribution, we define an increase in the abundance of large aggregates as greater than 10%, or $q_{\max} > 1.1$. For our scan, we consider systems with $N = 200$ compartments and a total aggregate mass of $\mathcal{N}^p = 3 \times 10^5$. The compartment dynamics are set to occur at a much lower rate, with $\tilde{\mu} = 8 \times 10^5 \lambda^p$. Scanning the exponents in the range $(\alpha_a, \alpha_f) \in (-1, 1) \times (-1, 1)$, we find that the facilitation of large aggregate formation is not specific to the kernel choice $(\alpha_a, \alpha_f) = (0.9, -0.9)$, but is observable in a wider region of the model space, as shown in Fig. 5.6 (b). In particular, we observe facilitation when aggregation is facilitated and fragmentation is suppressed, with $\alpha_a > 0$ and $\alpha_f < 0$. It should be noted that this is a purely computational result at this point. Additionally, we only test for a facilitating effect. We do not make any statements about the formation of large aggregates in the region where we do not observe facilitation, as it could potentially be suppressed or compartment dynamics could have no effect. We will next discuss the mechanism that gives rise to the facilitation of large aggregate formation for the *dynamic* ensemble.

5.4.2.2. Mechanism underlying the formation of giant aggregates

In section 5.4.2.1, we conducted numerical investigations into the impact of dynamic compartmentalisation on the aggregate size distribution of reversible polymerisation dynamics. Our findings revealed an extended parameter region in which compartment dynamics

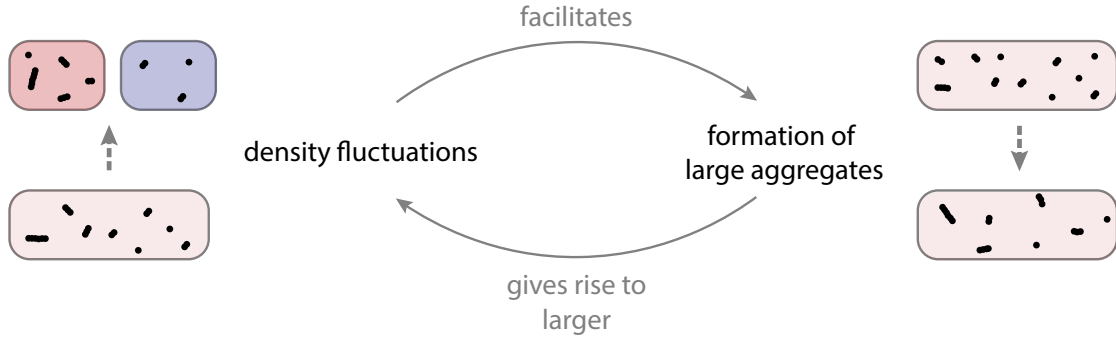


Fig. 5.7.: Schematic of a feedback loop giving rise to the facilitated formation of large aggregates. Larger aggregates give rise to larger noise in the binomial splitting procedure performed during compartment fragmentation. As density fluctuations are persevered, the above-average density fluctuations give rise to larger aggregates. In turn, larger aggregates give rise to larger density fluctuations. This sets the basis of a feedback loop. The feedback loop is counteracted by compartment fusion. The combination of compartment fusion and fragmentation gives rise to a steady-state configuration of the compartmentalised system.

facilitate the formation of large aggregates, as illustrated in Fig. 5.6 (b). In this section, we discuss the physical mechanisms through which dynamic compartmentalisation affects the steady-state aggregate size distribution. We begin by comparing the *dynamic* and *synchronous* compartment ensembles. We then discuss our findings of this chapter also in light of the effective ensemble dynamics presented in chapter 2.

From the perspective of a single aggregate, there are substantial qualitative differences in the polymerisation reaction kinetics, depending on whether we consider the *dynamic* or *synchronous* ensemble. Recall that within the *synchronous* ensemble, the reaction kinetics are performed in the fully fused compartment configuration. The large compartment is synchronously fragmented for evaluation and then fused again, meaning that in a mean-field setting, an individual aggregate can potentially fuse with every other aggregate in the system and the aggregate mass density is conserved and constant. Conversely, for compartment fusion and fragmentation, the reaction partners of an individual aggregate are restricted to those within the same compartment. Moreover, as previously demonstrated in section 5.4.1, the steady fusion and fragmentation result in fluctuations in the total aggregate density, which affect the aggregate size distribution within each compartment. Specifically, compartments with higher-than-average density shift the aggregation dynamics towards the formation of larger aggregates due to an increased collision rate $\tilde{\mu}^P$. On the other hand, compartments with lower-than-average density tend to suppress the formation of larger aggregates. We thus anticipate altered steady state aggregate size distributions if $p_{\text{dy}}(\rho)$ and $p_{\text{sy}}(\rho)$ differ. We thus find that the density fluctuations have direct feedback on the aggregate size distribution.

Conversely, the aggregate size distribution within a compartment also directly impacts the statistics of density fluctuations. This is due to the binomial splitting process that occurs during fragmentation, which involves the random assignment of each aggregate to one of two daughter compartments. Larger aggregates contribute more mass to a daughter compartment, leading to larger density fluctuations between the two daughter compartments.

We find that this gives rise to a feedback mechanism. Larger aggregate sizes give rise

5. Multi-scale fluctuations facilitate gelation in the innate immune response

to larger density fluctuations and larger density fluctuations facilitate the formation of larger aggregates. This feedback-loop is illustrated in Fig. 5.7. Note, that this heuristic is similar to the demonic scheme introduced in section 4.3.2, compare in particular with Fig. 4.1 and Fig. 4.6. There, we have also argued that density fluctuations potentially add up in the sequential fragmentation protocol. Recalling on the findings in chapter 4 further argues that the finding of facilitation of the formation of large aggregates is not a universal feature for reversible polymerisation systems subjected to dynamic compartmentalisation. In section 4.6.1, we proved that we expect no effect if the reversible polymerisation dynamics fulfils detailed balance. Furthermore, we suggested in Fig. 4.13, that the dynamic compartmentalisation further amplifies facilitation or suppression of large aggregate formation if detailed balance is broken. For further corroboration of the findings of the parameter scan in (α_a, α_f) , we thus need additional thermodynamic insight into how breaking detailed balance is amplified by compartment dynamics. While a microscopic approach can provide further insight into the thermodynamics of the system, a qualitative approach similar to the effective ensemble dynamics in section 2.5, where it described the emergence of a quasi-particle, may help to understand the power-law decay in $p_{dy}(\rho)$.

In Fig. 5.2 (a), we observed that the mode of the distribution $p_{dy}(\rho)$ is shifted towards the mean of $\langle \rho \rangle_{dy}$ compared to $p_{sy}(\rho)$. This aligns with the phenomenology of the quasi-particle described in section 2.5. However, we also find that the steady-state distribution of $p_{dy}(\rho)$ is heavily skewed and exhibits a power-law decay, which is at odds with the characteristics of the collective degree of freedom discussed in section 2.5. To better understand this discrepancy, it is useful to emphasise the differences with the dynamics in chapter 2 and re-examine the approximations made in the derivation of the localised collective ensemble state.

As previously mentioned in section 1.3, we interpret the dynamics in chapter 2 as an open system, while we consider the dynamics in this chapter as a closed system. This produces fundamentally different mechanisms for inducing *fluctuations* between the compartments. In an open system, fluctuations arise due to contact with an external reservoir, for instance, in the form of continual binding and unbinding of molecules to organelle compartments. On the other hand, in a closed system, fluctuations are purely a consequence of compartment fragmentation. Note that the fusion rate and the fragmentation rates are of the same order of magnitude for a system that exhibits a steady compartment size distribution under steady compartment fusion and fragmentation dynamics. This implies that compartment fusion cannot overpower the noise generated by fragmentation if the compartment size distribution is fixed.

We emphasise that for closed systems with mass conservation, the multiplicative noise contribution of the compartment fragmentation noise cannot be neglected, as the density fluctuations are not dominated by contact with an external reservoir. In fact, the multiplicative noise due to fragmentation is closely linked to the feedback-loop mechanism motivated in Fig. 5.7. In section 2.4.3, we have derived the multiplicative character of the fragmentation noise. Here, we refine the approximation of the fragmentation noise in the context of a closed system. While we have suggested a contribution of the fragmentation noise to every species in \vec{c} in Eq. (2.51), we here want to study density fluctuations in $p(\rho)$. For this, we marginalise the over \vec{s} to arrive to an effective one-dimensional dynamics in

ρ_i . To this end, we summarise the fragmentation noise to

$$\bar{\xi}_{\text{frag}}(t) \approx \frac{\mu}{\langle v' \rangle} \frac{\pi}{8} \left(\sum_s s f_i(s, t) \right) \xi_0(t), \quad (5.19)$$

where $\langle \xi_0(t) \rangle = 0$ and $\langle \xi_0(t) \xi_0(t') \rangle = \delta(t - t')$ is uncorrelated white Gaussian noise. We observe a direct correlation between the intensity of noise and the size distribution $f_i(s, t)$, which in turn depends on the density ρ_i . This alters the functional dependence of the fragmentation noise $\bar{\xi}_{\text{frag}}(t)$ on ρ_i . Notably, this multiplicative noise induces a skew in $p(\rho)$. To accurately determine the functional noise, we need to track how the size distribution depends on the density and so is modulated by the aggregation parameter λ^p . This necessitates solving the reversible polymerization dynamics analytically in the absence of dynamic compartmentalization, which presents its own challenges.

This suggests that deriving effective ensemble dynamics, in analogy to the effective ensemble kinetics presented in section 2.4 in Eq. (2.55), could be a potential way to approximate the power laws in $p_{\text{dy}}(\rho)$. However, Eq. (2.55) does not account for mass conservation, which is a defining characteristic of closed systems. It is important to carefully evaluate the extent to which mass conservation is necessary for the power law of $p_{\text{dy}}(\rho)$ in future research. We present the explanation of the algebraic tails of $p_{\text{dy}}(\rho)$ as an open question and consider next in section 5.4.3 how the system changes under system size scaling given the observed the power law decay in $p_{\text{dy}}(\rho)$.

5.4.3. System size scaling shows characteristics of gelation

In section 5.4.1, we have observed that a power-law decay in the statistics of the density fluctuations $p_{\text{dy}}(\rho)$ arises due to compartment fusion and fragmentation. While, we discussed in section 5.4.2.2 the physical mechanism underlying the power-law decay in $p_{\text{dy}}(\rho)$, in this section we investigate the phenomenological consequences of this decay. For this, we study how a system size scaling affects the density fluctuation statistics $p_{\text{dy}}(\rho)$ and the steady state of the aggregate size distribution $f_{\text{dy}}(s, t)$.

We begin by considering a system size scaling, whereby we increase the number of compartments N but keep the total aggregate mass \mathcal{N}^p fixed. Consequently, the average density $\langle \rho \rangle$ decreases as the number of compartments grows and, as investigated in Eq. (5.19), the noise contribution of the fragmentation noise increases. We investigate this scaling through numerical simulations, using the same simulation parameters as in Fig. 5.3 (a,b), with a total aggregate mass of $\mathcal{N}^p = 5 \times 10^3$, an aggregation parameter $\lambda = 1$, and the polymerisation dynamics $\tilde{\mu} = 5 \times 10^3$ times faster than the fusion and fragmentation of compartments. Fig. 5.8 (a) reveals an increase in the abundance of large aggregates and a decrease in the abundance of small aggregates, while the statistics of the density fluctuations $p_{\text{dy}}(\rho)$ in Fig. 5.8 (b) shows a power-law decay with a decreasing exponent for an increasing number of compartments N . This suggests that the exponent in $p_{\text{dy}}(\rho)$ is a function of the average density $\langle \rho \rangle$ and consequently the strength of noise in the system.

We next investigate how $p_{\text{dy}}(\rho)$ and $f_{\text{dy}}(s, t)$ change as the number of compartments N and the total aggregate mass \mathcal{N}^p increase, while keeping the average density $\langle \rho \rangle$ fixed. As Eq. (2.55) is derived in the continuum limit of infinitely many compartments, the exponent of the power-law decay in $p_{\text{dy}}(\rho)$ should not be affected by this system size scaling. To numerically test this, we consider the specific kernel choices $(\alpha_a, \alpha_f) = (0.9, -0.9)$ for the polymerisation dynamics, with $\langle \rho \rangle = 200$, $\lambda^p = 1$, and $\tilde{\mu} = 8 \times 10^4$. The results,

5. Multi-scale fluctuations facilitate gelation in the innate immune response

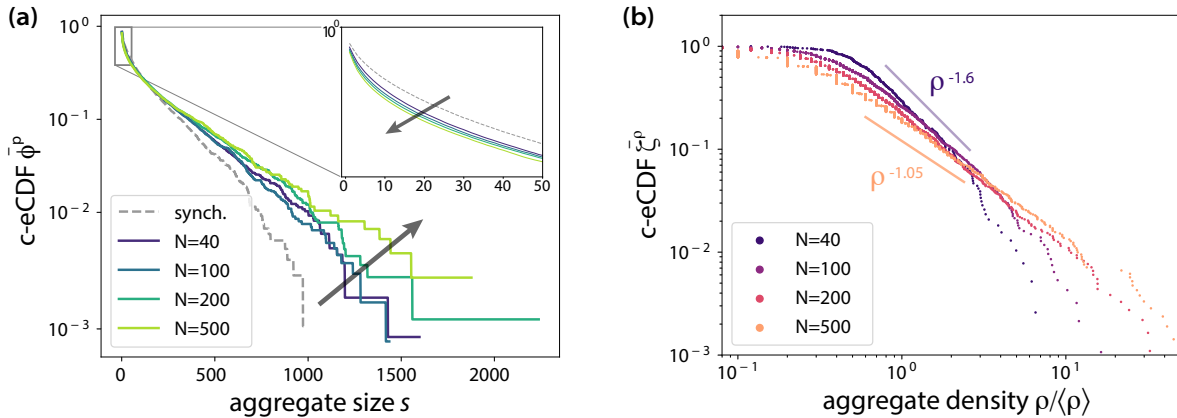


Fig. 5.8.: Increasing the number of compartments facilitates the formation of large aggregates. Simulations analogous to Fig. 5.1 with identical system parameters are performed. The system is scaled by keeping the total aggregate mass fixed, while increasing the number of compartments N . The aggregate size is in multiples of the monomeric building block. ‘c-eCDF’ stands for the complementary empirical cumulative distribution function. (a) We find that the abundance of large aggregates is increased as the number of compartments is increased. The inset shows that the abundance of small aggregates is reduced as the number of compartments is increased. (b) The density fluctuations show different power-law decay exponents. The decay component decreases as the number of compartments increases.

shown in Fig. 5.9 (a), demonstrate that the power-law exponent of the decay in $p_{\text{dy}}(\rho)$ is indeed unaffected by this system size scaling. The range over which the power-law decay is observable increases with the system size. To quantify the effect of this system size scaling on the abundance of large aggregates in $f_{\text{dy}}(s, t)$, we calculate the variance $\text{Var}[f_{\text{dy}}(s, t)] = \sigma_{\text{dy}}^2$. This is shown in Fig. 5.9 (b), where it is evident that the variance increases with the system size. In contrast, the aggregate size distribution in the *static* ensemble, which is defined in section 5.3, does not show this dependence on system size, with the variance remaining fixed. We speculate that the increase in the variance with system size is a consequence of the power-law decay in $p_{\text{dy}}(\rho)$, although this hypothesis still demands analytical confirmation.

In section 5.2.2, we elaborated on how the absence of diverging moments S_n is a defining characteristic of reversible polymerisation kinetics in the strong fragmentation limit. However, here we find that the variance of the distribution increases with system size, suggesting the diverging of moments. We observe a statistical property of the aggregate size distribution which is the defining property of *gelation*. It occurs in a region of the model space (α_a, α_f) where gelation is formally prohibited. This position in the model space is determined by the physical mechanisms underlying the aggregation and fragmentation dynamics of the reversible polymerisation kinetics. To move in the model space (α_a, α_f) implies that the *physics* of the aggregation-fragmentation dynamics are altered. For molecular polymerisation, such a modification demands strong manipulations of the system and is not plausible to occur in a biological context to control the emergence of gels.

Yet, here we observe that by subjecting reversible polymerisation dynamics to dynamic compartmentalisation, the statistics of large aggregates can be significantly altered, displaying gelation-like characteristics. Moreover, the extreme value statistics of finding large

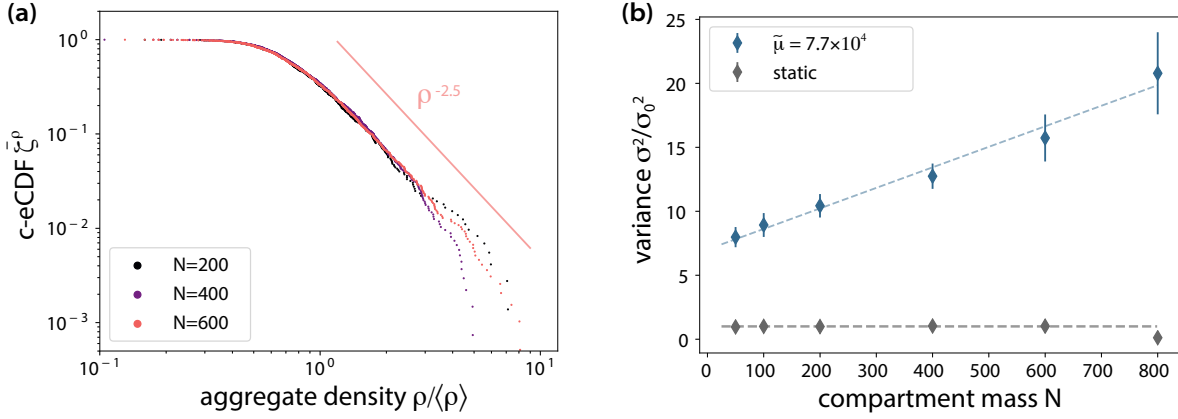


Fig. 5.9.: Increasing the system size while keeping $\langle \rho \rangle$ shows characteristics of gelation Simulations analogous to Fig. 5.1 are performed. We consider the specific kernel choices $(\alpha_a, \alpha_f) = (0.9, -0.9)$ for the polymerisation dynamics, with $\langle \rho \rangle = 200$, $\lambda^p = 1$, and $\tilde{\mu} = 8 \times 10^4$. ‘c-eCDF’ stands for the complementary empirical cumulative distribution function. (a) We find no change in the power-law exponent when analysing the tail statistics of the density fluctuations. (b) We analyse moments of the aggregate size distribution $f(s, t)$ and compare the *dynamics* and static ensemble configurations in steady state. Dotted lines are visually fitted trend lines. The variance $\langle \text{Var}[f(s, t)] \rangle_t \equiv \sigma^2$ increases with system size, which hints at diverging moments of the distribution. Notably, the Carr-DaCosta criterion states the absence of diverging moments in a strong fragmentation limit. We find here, that the apparent diverging of moments are caused by compartment dynamics. We refer to this as *multi-scale gelation*.

aggregates can be modified in a manner that cannot be replicated by simply altering the aggregation parameter λ^p . To substantiate our assertion of *multi-scale induced gelation*, further numerical simulations and an analytical theory are necessary. We next discuss our findings in the context of innate immune signalling.

5.5. Application to the cellular immune response to RNA-virus infections

While we have investigated how dynamic compartmentalisation can qualitatively alter the aggregate size distribution of reversible polymerisation dynamics, in this section we apply our findings in the context of cellular immune responses to RNA-virus infections. For this, we will first review on the biology of cellular inflammation responses to virus infection. To this end, we in particular focus on the MAVS-signalling pathway, which we have briefly introduced in section 3.9. We then apply our qualitative findings in the context of this signalling pathway in section 5.5.2.

5.5.1. Innate immune signalling

In vertebrates, the immune system is divided into the innate immune system and the adaptive immune system [240]. While the adaptive immune system can adapt and improve its response through training, the innate immune system is non-specific and responds to general characteristics of pathogens, providing the first line of defence against them. The

5. Multi-scale fluctuations facilitate gelation in the innate immune response

innate and adaptive immune systems are closely interconnected, with the proper function of the innate immune system being necessary for the adequate activation of the adaptive immune system. In the following, we will focus exclusively on the innate immune system.

The innate immune system employs a variety of cellular and multi-cellular mechanisms to prevent the infection and spread of pathogens in vertebrates. These mechanisms include the recruitment of immune cells to the site of infection, the activation of the adaptive immune system through antigen presentation, and the formation of physical and chemical barriers to block the spread of pathogens [240]. A central aspect of the innate immune response is the activation of inflammatory programs within cells. These programs are triggered when pattern recognition receptors (PRRs) detect molecules that are widely shared by pathogens but distinguishable from host bio-molecules [187]. There are various types of pattern recognition receptors that have specialized in detecting different pathogens. In this section, we will particularly focus on viral defence mechanisms [241]. For innate viral detection, toll-like receptors, which detect viral transmembrane proteins, and Rig-I-like receptors, which detect viral RNA in the cytosol, are particularly important [187]. Notably, these receptors are expressed in most cells, rather than being specific to certain cell types. Upon the detection of a virus, a type-1 interferon (IFN1) response is activated, leading to the inhibition of RNA translation, the release of cytokines that attract T-cells, and ultimately the induction of apoptosis.

Examples for Rig-I-like receptors are the proteins Rig-I and MDA-5 [187]. Both proteins detect different features of viral RNA but share the same pathway once activated by the binding to viral RNA. Upon binding to viral RNA, the activated receptors expose CARD domains, which allow for interaction with the CARD domains of the mitochondrial anti-viral signalling protein (MAVS) [189, 242, 243]. MAVS is anchored to the outer membrane of mitochondria, and the increased concentration of CARD domains leads to the accumulation of MAVS proteins to form large clusters, which function as signalling platforms for the formation of the IKK complex [187, 189, 244, 245]. This complex, in turn, synthesizes the nuclear transcription factor NF- κ B, which activates the cellular inflammation response. While the structural basis for how MAVS catalyses the formation of the IKK complex has not yet been resolved, it has been experimentally demonstrated that the formation of large MAVS protein oligomers is necessary for the IKK complex [189, 242, 243]. This pathway is illustrated in Fig. 5.10.

The formation of MAVS complexes has been extensively studied through structural biology techniques [191, 192]. It has been found that MAVS oligomers are stable in non-reducing environments [189], suggesting that their oligomerisation may be mediated by the formation of disulphide bridges. Despite being referred to as prion-like protein aggregates, X-Ray tomography measurements have shown that there are no conformational changes in the protein structure. In particular, no formation of beta-sheets in MAVS aggregates has been detected [191, 192]. This argues against a prion-like mechanism and instead suggests that MAVS undergoes reversible polymerisation processes on the outer mitochondrial membrane. Recall for this, that the cytosol is a reducing environment. From a thermodynamic perspective, the stabilisation of MAVS aggregates through disulphide bridge formation hints towards a deviation from detailed balance conditions in the polymerisation process of MAVS proteins. Yet, the details of the MAVS aggregation dynamics have to be thoroughly investigated in future research.

It has been observed that the oligomerisation of MAVS can be disrupted by interfering with the localisation of MAVS to the mitochondrial outer membrane. The NS3/4A protease expressed by Hepatitis C virus cleaves the transmembrane domain of MAVS, leading

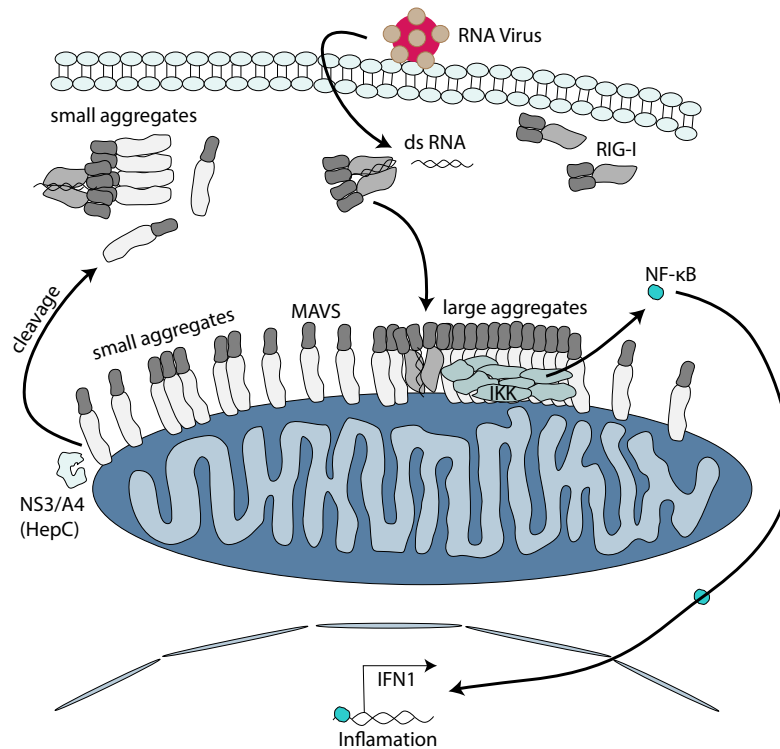


Fig. 5.10.: Schematic of signalling pathway demonstrating how inflammation responses are activated following the detection of viral RNA Figure is adapted from [242]. Rig-I-like receptors are activated following the detection of viral RNA and interact via CARD domains with MAVS proteins. MAVS proteins form aggregation on the mitochondrial membrane, on which the NF- κ B synthesising IKK-complex forms. The formation of MAVS is pivotal for the activation of inflammation responses. Hepatitis C viruses produce the NS3/A4 protease which cleaves MAVS from the membrane. MAVS forms smaller aggregates in the cytosol, which are insufficient for activating an inflammation response.

to translocation of MAVS into the cytosol [242, 243]. While MAVS still forms clusters in the cytosol, the size distribution is shifted to smaller aggregates, which impairs an efficient immune response [242]. Similarly, *in vivo* experiments have demonstrated that the inhibition of mitochondrial fusion effectively prevents the formation of large MAVS aggregates and subsequently impedes the induction of inflammatory responses [68].

Next, we elucidate the effects of organelle dynamics on the formation of large protein aggregates. As we are ignorant about the actual reaction kinetics of MAVS activation, we take the MAVS-signalling pathway as an inspiration and do not claim that we adequately modelled the MAVS aggregation dynamics in section 5.4.

5.5.2. Discussion on how multi-scale gelation facilitates cellular anti-viral responses

We now proceed to interpret our findings regarding the dynamic compartmentalisation of reversible polymerisation dynamics in the context of cellular immune signalling, with a particular focus on the Rig-I pathway and the aggregation dynamics of MAVS proteins on the mitochondrial outer membrane. In section 5.5.1, we have discussed the biology of

5. Multi-scale fluctuations facilitate gelation in the innate immune response

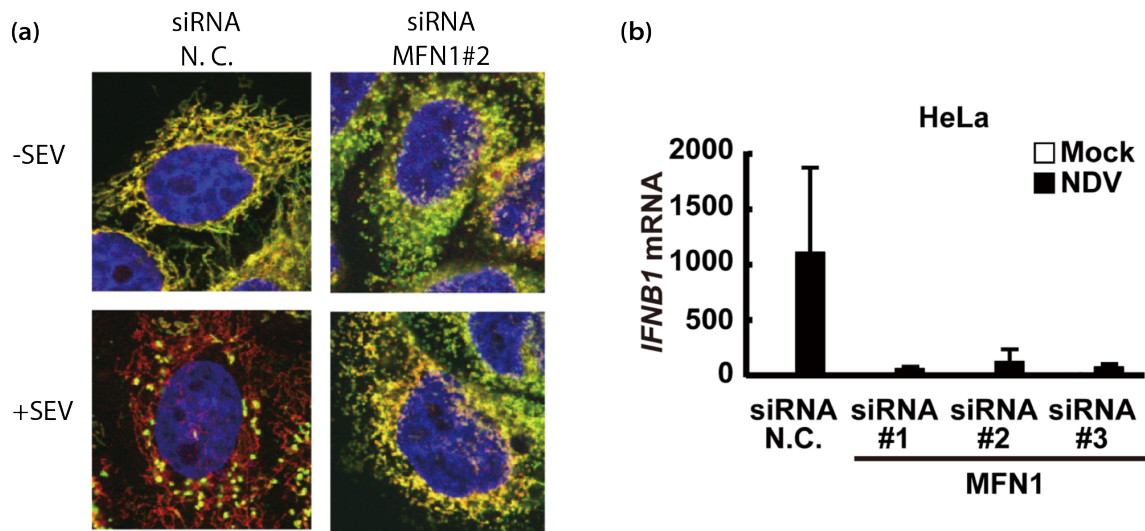


Fig. 5.11.: Inhibition of mitochondrial fusion prevents MAVS mediated ant-viral responses (a) is adapted from Fig. 11 D and (b) is adapted from Fig. 10 B from [68]. (a) IPS-1-HeLa cells transfected with negative control (N.C.) or hMFN1-targeted siRNA2 for 48 h. Cells were infected with SeV for 12 h and stained with anti-FLAG antibody (dyes MAVS) (green), MitoTracker (Mitochondria) (red), and DAPI (blue). (b) Cells transfected with siRNA were infected with Newcastle disease virus (NDV) for 12 h, and endogenous IFNB1 mRNA expression was quantified by qRT-PCR. Data represent means \pm s.d. (n=3).

innate immune signalling in response to RNA-virus infections, and have established that the formation of large MAVS aggregates is pivotal for the cellular inflammation response to detect viral RNA in the cytoplasm.

The MAVS aggregation dynamics must fulfil two biological tasks: in the absence of viral RNA, the formation of large aggregates needs to be inhibited, while the increase of a small number of activated Rig-I homo-dimer complexes must be sufficient to activate the formation of large aggregates. In this section, we show how our findings from section 5.4 can further our understanding of immune response signalling.

The major obstacle in directly applying our findings to the Rig-I innate immune signalling pathway is our lack of knowledge concerning the details of polymerisation kinetics of MAVS aggregation. Experimentally measuring the individual kinetic rates of MAVS aggregation is unfeasible, as the reaction kinetics cannot be live-tracked by in vivo microscopy. Additionally, deriving the MAVS aggregation kinetics from structural biology is also not possible. Further insight is also needed concerning the details of MAVS aggregate stabilisation mechanisms, which may be due to disulphide bridge formation and the formation of the IKK-complex. Furthermore, the details of how RIG-I facilitates aggregate formation have yet to be conclusively investigated. Consequently, we can only speculate as to whether our findings are plausible. We consider it plausible that MAVS performs reversible polymerisation dynamics, and that the aggregation parameters (α_a , α_f) are in the region of the model space where we expect facilitation of large aggregate formation by organelle fusion and fragmentation.

The over-expression of MAVS has been observed to induce the formation of MAVS aggregates sufficient for an inflammation response in the absence of activated RIG-I homo-dimers [245]. Moreover, in an in-vitro setup, MAVS aggregates have been demonstrated

to induce further aggregation of MAVS in the absence of RIG-I and mitochondrial membranes [189]. Consequently, it can be concluded that MAVS aggregate formation does not require activated RIG-I homo-dimers as a nucleation centre. Rather, the dynamics appear to hint at the formation of *large* MAVS aggregates based on the density, which is in agreement with the framework of reversible polymerisation. Upon virus detection, the additional CARD domains of the activated RIG-I complexes could lead to an increase in the density of CARD domains, resulting in the formation of large aggregates. According to the framework of reversible polymerisation dynamics, this translates to an effective increase of the aggregation parameter λ^P .

In Fig. 5.2, we have demonstrated that compartment fusion and fragmentation facilitates the formation of large aggregates on a subset of compartments. This is in agreement with the experimental observation that large MAVS aggregates only form on a subset of organelles. In the literature, it is speculated, that mitochondrial fusion and fission dynamics grant the exchange of MAVS among the organelles, which results in the accumulation of MAVS on some organelles [68]. We formalised this heuristic in Fig. 5.5, where we demonstrated that organelle dynamics strongly facilitate the formation of large aggregates. This is further corroborated by the finding that inhibiting mitochondrial fusion impedes sufficient inflammation responses to viral infections Fig. 5.11.

We compared the differences between static and dynamic ensembles, which were introduced in section 5.3. Note that a fully fused mitochondrial network is deemed to be an unphysiological state. Yet, such physiological perturbations that lead to such a configuration can be achieved by cleaving MAVS proteins from the mitochondrial outer membrane, as it happens after infection with Hepatitis C virus due to the NS3/4A protease. As demonstrated by [242], even after cleavage, MAVS can still form aggregates, albeit with an altered size distribution. This could either be due to a reduced density in the cytosol or suggest the importance of organelle dynamics in creating density fluctuations.

Our findings in Fig. 5.4 suggest that density fluctuation stabilises large aggregates. This might facilitate the function of MAVS aggregates as a signalling platform and lead to an increased formation of IKK complexes, even if the marginal aggregate size is hardly increased by organelle dynamics. Note that this stabilisation of aggregates due to density fluctuations is an effect that holds both for a fully fused and a fully fragmented compartment configuration.

To further investigate whether the mechanism of creating and preserving density fluctuations plays a central role in the formation of MAVS aggregates, additional experimental research is needed. Experimental studies focusing on the structural properties of MAVS can grant further insight into the dynamics of MAVS aggregations and its activation by RIG-I-like receptors, compare for example with [191, 192]. Reconciling with our theory, this can provide estimates of whether the expected effects of organelle fusion and fragmentation are of strong qualitative or just marginal effects. Alternatively, we suggest perturbations of the mitochondrial dynamics to assess our theory directly in experimental setups. Here, we in particular suggest investigating fused mitochondrial configurations and additional variation of MAVS concentration by setting it under the control of tunable transcription regulators.

5.6. Discussion

In this chapter, we have demonstrated how compartment dynamics can lead to extreme fluctuations in closed compartmentalised systems. We considered reversible polymerisa-

5. Multi-scale fluctuations facilitate gelation in the innate immune response

tion kinetics contained within compartments subject to stochastic fusion and fragmentation dynamics. In chapter 4, we demonstrated that breaking detailed balance on the level of the reversible polymerisation dynamics, in general, implies changed system's statistics when additionally subjecting the system to compartment dynamics. However, the effects were marginal in Fig. 4.13 as we studied small compartmentalised systems subjected to sequential fragmentation protocols. In this section, we examined systems of several orders of magnitude larger, subject to both fusion and fragmentation dynamics. Our findings showed that these dynamics can significantly increase the abundance of aggregates larger than the mean aggregate size. Our numerical results suggest altered extreme value statistics and power-law scaling of the density fluctuations. We further suggested that our findings could help elucidate the functional role of mitochondrial dynamics in cellular anti-viral immune responses.

In this chapter, we build upon the theoretical investigation of chapter 4 and pursued a phenomenological approach. We sought to identify whether the effect of compartment fusion and fragmentation dynamics on the enclosed many-body dynamics in closed compartmentalised systems vanishes or is strengthened. Our large-scale full stochastic numerical simulations suggest that compartment dynamics can have a substantial effect on the occurrence of very large aggregates, as demonstrated in section 5.4.1. Specifically, we focused on a qualitative investigation of specified reaction kinetics of a reversible polymerisation. Having chosen the kernel dynamics such that they fulfil the strong fragmentation criterion of Carr and DaCosta [237], we expected the aggregate size distribution to exhibit an exponential tail. Yet, we found that steady compartment fusion and fragmentation give rise to an increased abundance of large aggregates, a power-law decay of large density fluctuations, and increased stability of large aggregates. In section 5.4.3, we observed increasing moments of the size distribution $f(s, t)$ with increasing system size, which hints towards diverging moments of the size distribution. This is a sign of gelation formally prohibited by the strong fragmentation criterion in a mean-field description. We conclude that this effect is due to a multi-scale organisation of the dynamics. We hence refer to this observation as *multi-scale gelation*. However, as we have yet to provide analytical confirmation of our numerical findings, the multi-scale gelation is only of suggestive character. We plan to consolidate on our findings by conducting larger simulations and progressing with our analytical theories.

In section 5.4.2, we investigated whether our qualitative findings would generally hold for reversible polymerisation dynamics. We found that, when compared with reversible polymerisation dynamics that conserve detailed balance, the facilitation of the formation of large aggregates is specific to kernel choices where both aggregation of large aggregates and the fragmentation of large aggregates are suppressed. In this section, we also discussed a possible mechanism to explain the power-law decay of the density fluctuations. We suggest a feedback-loop mechanism, as illustrated in Fig. 5.7. We propose that an effective ensemble description analogous to Eq. (2.55) could be useful in providing an analytical corroboration of the observed power-law dynamics, thus posing the derivation of the power-law as an open question.

The mechanism of creating and preserving density fluctuations through compartment fusion and fragmentation dynamics has been found to be a fruitful approach to alter the statistics of closed compartmentalised systems. We have observed strong qualitative effects and, to assess a notion of work performed on the system, it may be beneficial to reconcile our theoretical findings from chapter 4 with this approach. A combined approach of detailed work contributions and phenomenology-driven analytical investigation could

be particularly insightful for further elucidating the physics of the power-law decay in the density fluctuations.

In section 5.5, we then discussed possible implications of our findings in the context of the cellular immune responses to RNA-virus infections via the signalling pathway around the MAVS proteins. Unlike the apoptotic decision-making outlined in chapter 3, MAVS proteins remain anchored to the mitochondrial membrane and there is no evidence of bi-stability. On the contrary, MAVS forms *large* aggregates in response to an RNA-virus infection. The mechanisms of MAVS aggregation are still under active investigation, yet it has been demonstrated that mitochondrial fusion dynamics are essential for the formation of such aggregates. Our numerical investigations presented in Fig. 5.5 corroborate this finding. Additionally, we suggest that the large aggregates are more stable due to the mechanism of preserved density fluctuations, as illustrated in Fig. 5.4.

Note, however, that we do not model the dynamics of the MAVS signalling pathway, but that we investigate on the qualitative effects of mitochondrial fusion and fragmentation dynamics on reversible polymerisation. We have not considered physiologically plausible parameter choices, as this would demand an increase in system size and further optimisation of the simulations. Additionally, there is still a lack of knowledge about the detailed aggregation dynamics of MAVS. Therefore, our numerical investigations are mostly of inspirational character. We suggest further experiments to investigate the role of mitochondrial dynamics on MAVS aggregate formation, such as altering the rates of mitochondrial fusion and fragmentation dynamics in combination with changing the expression level of MAVS. This could help to further elucidate the biological function of mitochondrial fusion and fragmentation dynamics.

We have restricted our numerical investigations to polymerisation kinetics that fulfil the strong fragmentation criterion by Carr and DaCosta [237]. This restriction was largely due to theoretical considerations; however, the MAVS aggregation dynamics could also occur under the weak fragmentation regime. This suggests further investigation, particularly in relation to the stability of gels.

Our findings have implications beyond cellular immune responses and organelle-associated signalling pathways, extending to the realms of the *origin of life*, where the formation of large biopolymers is of pivotal interest [246, 247]. We found that compartment fusion and fragmentation dynamics can fundamentally alter the extreme values statistics and the observed density fluctuations in the systems. This has been extensively studied in the past in connection with aerosol fusion and fragmentation in clouds [248–250]. Being subject to temperature gradients and steady forces, analysing aerosol systems may provide an interesting setup to study the formation and stabilisation of bio-molecules both in the context of the *origin of life* as well as in technical applications.

6. Conclusion and outlook

In this thesis, we have explored the dynamics of compartmentalised stochastic systems as the epitome of non-equilibrium multi-scale systems. In particular, we have investigated how active compartment dynamics affect the fluctuations in the system, with a particular focus on the effects of compartment fusion and fragmentation dynamics. We have distinguished between *open* and *closed* compartmentalised systems, and have demonstrated that they exhibit qualitatively different dynamic behaviour. In the case of open systems, we found that compartment fusion and fragmentation counteract dispersive dynamics, which are induced by contact with an external reservoir. In closed systems, on the other hand, we determined that compartment fusion and fragmentation create and preserve density fluctuations. Consequently, we consider compartment fusion and fragmentation to be a key mechanism for controlling fluctuations in compartmentalised stochastic systems.

We approached the characterisation of the dynamics of compartmentalised stochastic systems from four perspectives, dedicating chapters to the concepts of emergence, response to perturbations, work and entropy, and giant fluctuations. This demonstrated the richness of the dynamic behaviour of dynamically compartmentalised stochastic systems, which is distinct from that of statically compartmentalised systems that show no compartment dynamics. We have argued the biological relevance of our results by applying our analytical findings in the context of organelle-associated signalling pathways, which are a prime example of compartmentalized stochastic systems. Studying the example of cell death, we demonstrated how mitochondrial dynamics give rise to a kinetic low-pass filter, which allows cells to suppress responses to weak, transient stress stimuli while facilitating the response to persistent stress perturbation. Focusing on extremal fluctuations, we showed in the context of cellular innate immune responses to RNA-virus infections that mitochondrial dynamics are central for efficient immune responses.

With the findings in this thesis, we demonstrate the central importance of considering the multi-scale organisation of biological systems for gaining a mechanistic understanding of biological function. Specifically, we suggest that fundamental cell fate decisions are not controlled on a single scale of spatial organisation, but that cells rely on the interplay between dynamics on different scales of spatial organisation. To investigate the biological function of the multi-scale organisation of living matter, we suggest that combined approaches of theoretical analysis and experimental investigations can advance our understanding of living matter and identify new therapeutic strategies.

The findings in this thesis motivate further research in both the domain of physics, regarding the non-equilibrium statistical physics of compartmentalised systems, and in the domain of biology, regarding the system's biology of cell fate decisions as multi-scale processes. Next, we briefly summarise the main findings of this thesis, discussing general insights we gained on the dynamics of compartmentalised stochastic systems. After this, we argue about potential future research and the biological and technical relevance of our findings.

6.1. Discussion of the main findings of this thesis

6.1.1. Deriving effective dynamics of open compartmentalised systems

In chapter 2, we investigated the emergence of collective dynamics in open compartmentalised systems induced by compartment dynamics, which we formally defined within the framework of Master Equations. We derived effective dynamics for how the system temporally evolves and introduced a flux approximation for compartment fusion and fragmentation, which permits analytical tractability. This enables us to draw comparisons to other physical systems, and we observe an analogy to self-gravitating systems and a structural equivalence of the effective dynamics to McKean-Vlasov equations. We found that the combined action of compartment fusion and fragmentation gives rise to the emergence of a collective degree of freedom. We discussed that the collective degree of freedom is reminiscent of a quasi-particle. We derived effective equations of motion for the quasi-particle and studied its kinetic properties.

The benefit of analytical investigations is that they allow us to draw general insights into dynamics of systems without the need to solve the full dynamics explicitly or by large-scale numerical simulations. In chapter 3 we exemplified this, as we investigated the effective dynamics in the context of apoptotic decision-making. On a conceptual level, we found that compartment fusion and fragmentation counteract dispersive spread. In this context, it might be instructive to further discuss the non-equilibrium character of the collective ensemble dynamics. In particular, in light of our analysis in chapter 4, it is instructive to evaluate the work done by compartmental fusion and fragmentation and to assess the entropy production of compartmental dynamics.

Our analysis offers new perspectives on the research of resetting random walks. This connection can be best illustrated by reconsidering the one-dimensional simplification studied in section 2.4.1. In this case, the position of the random resetting is a function of the realisation of the system, as opposed to being externally implemented [251–253]. Analogous to our findings, resetting random walks show the phenomenology of approaching steady-state distributions with bound variance [251], as resetting counteracts the dispersive spread. As presented in Fig. 2.4, we have found an analytical approximation of the steady state distribution for our variation of random walks, which can qualitatively predict the shape of the distribution, give quantitative estimates for the variance and correctly predict the tail statistics, which is of central interest in the research of resetting random walks [251, 252]. More recently, interest has grown in the stochastic thermodynamics of resetting random walkers [253]; our model offers new opportunities for investigating this question, with the potential of finding general insight for the non-equilibrium thermodynamics of the resetting random walkers.

Having considered the dynamics of compartmentalised systems from a conceptual and abstract perspective, we may also discuss the applicability of our findings in a wider context. In chapter 2, we have provided a general framework and introduced an approximation scheme which allows for straightforward generalisations. We consider this framework to be useful in scenarios where the random encounter of two agents leads to a change in their internal states, regardless of whether those agents are compartments, individuals, or other entities. It is possible to modify the approximation of the fusion flux to account for modified dynamics, although the bigger challenge may lie in determining how the internal states of the interacting agents change upon an encounter. This gener-

alisation is further motivated by the structural equivalence of the effective dynamics of interacting social wasps [120].

In chapter 2, we gained a physical understanding of the effective ensemble dynamics by drawing an analogy to the effective two-body interaction potentials. Specifically, we could assign an equivalent effective interaction potential. This analogy is not only a theoretical tool but can fundamentally advance our mechanistic understanding of the dynamics and help us to gain insight into the qualitative dynamics. We, therefore, suggest that the approximation scheme introduced in this chapter can provide a fruitful approach to gaining a mechanistic understanding of multi-scale systems. Our theoretical framework has potential applications in various domains, such as in biological systems at different spatial scales or in the physics of finance when considering the fusion and splitting of deposits. Yet, we find that the prime example of compartmentalised stochastic systems is given by organelle-associated signalling pathways, which are fundamental for the functions performed by cells. We investigated this application in depth in chapter 3.

6.1.2. Collective response kinetics in the regulation of cell death

In chapter 3, we examined the quasi-particle degree of freedom in the context of the response kinetics of organelle-associated signalling pathways, using the example of cell death decisions. We reviewed the biology of organelle dynamics and signalling pathways, before presenting an effective model focusing on the regulation of the accumulation dynamics of Bax to the mitochondrial outer membrane. We demonstrated how mitochondrial dynamics gave rise to sigmoidal response kinetics to weak apoptotic stimuli and how this gave rise to a kinetic low-pass filter which suppressed transient noise fluctuations yet allowed the system to respond to changes in the environment on long timescales. To test our theoretical predictions experimentally, we explained why our predictions could not be tested one-to-one and investigated the robustness of our predictions towards non-linear pre- or post-modifications in the apoptotic signalling pathway. We predicted a transition from sigmoidal to exponential-like responses with increasing apoptotic stimulus strength, which is characteristic of the quasi-particle kinetics we derived in chapter 2. Evidence of this kinetic behaviour was found in experiments conducted by our experimental collaborators. Finally, we discussed the plausibility of our findings and their potential therapeutic implications and considered the direct translatability of our findings to other organelle-associated signalling pathways.

In section 3.8, we discussed the biological plausibility of our findings with regard to the potential separation of timescales. We emphasised that we expect different ensemble statistics for the organelles with and without fusion and fragmentation dynamics. This is a qualitative, static result that holds regardless of the specific timescales of the molecular reaction kinetics and of the organelle dynamics. Yet, we highlighted that a general discussion of the timescales of the chemical reaction kinetics and the organelle dynamics is necessary in order to assess the impact on the dynamic behaviour of the system. Depending on the specific timescales and the research question at hand, the organelle dynamics may display negligible. This, however, can only be assessed after the dynamics of the system including the organelle dynamics has been carefully discussed.

We have discussed the extent to which the findings in the context of apoptotic signalling can be generalised to other signalling pathways in section 3.9. In particular, we have assessed that the metabolic regulation of the aerobic metabolism [64] may be strongly affected by mitochondrial fusion and fragmentation dynamics, leading to a reduction in

6. Conclusion and outlook

variance and potentially a sigmoidal response dynamics - analogous to the dynamics we demonstrate for the regulation of apoptosis. We suggest that a further investigation of the lysosomal dynamics for mTorc-1 signalling [66] could be a useful experimental endeavour. Moreover, for application to endosomal maturation [186], our theoretical framework should be extended to include additional synthesis and degradation dynamics. We suggest that our theory developed in chapter 2 as suited, yet the emergence of a ‘quasi-particles’ and their kinetics need to be carefully reassessed.

In our modelling approach, we have neglected explicit feedback between the state of the signalling pathway and the organelle dynamics. However, our theoretical approach in Section 2.4.2.1 generally allows for the extension to consider this feedback. To do so, the effective equations motion in Eq. 2.72 need to be modified. This analysis will follow an analogous structure as presented in this thesis. We anticipate that explicit feedback between the state of the signalling pathway and the organelle dynamics allows for additional intricate dynamic behaviour. Note, that we considered implicit feedback on the compartment dynamics when we studied absorbing boundary conditions in Fig. 3.11, see also Appendix A.5.

While we have studied the sigmoidal response dynamics within the context of an effective bistable potential, we expect that our findings are also applicable to the transition between states in effective multi-stable potentials. We identified that the underlying mechanism of the sigmoidal response dynamics is the initial suppression of the escape dynamics, followed by the facilitation of the collective transitions, as the mean of the ensemble crosses the potential barrier. This mechanism also holds for multi-stable potentials. Throughout our analysis, we refrained from an exploration of the effects of curl fluxes on the dynamics of the signalling pathway. We anticipate that, while our analysis is also likely to be valid in the presence of stable fixed points, qualitatively new dynamics could arise if the escape from stable limit cycles or strange attractors is considered. Additionally, the emergence of single degree of freedom should be reconciled, and special attention should be paid to the correlation between the components of \vec{c} in section 2.4.2.4.

In section 3.8.2, we discussed potential therapeutic implications of our findings in the context of apoptotic decision-making. We highlighted that mitochondrial dynamics can play a central role in mitigating the side effects of therapies and improving the efficiency of cancer treatments. Moreover, we proposed that focusing on mitochondrial dynamics may be an orthogonal approach to more established therapeutic approaches. In broader terms, we consider the investigation of organelle dynamics to be instructive for future medical and biological research aimed at uncovering the systems biology of living systems. More broadly, with our findings, we have emphasised the importance of considering cell fate decisions as processes that crucially rely on the regulation of dynamics on different spatial scales of biological organisation.

6.1.3. Thermodynamics of closed compartmentalised systems

In chapter 4, we studied the thermodynamics of closed compartmentalised systems and how compartment dynamics changed the statistics of the realised system states. Specifically, we demonstrated that the extend to which compartment dynamics affect the total entropy of the system depends on the detailed of the enclosed stochastic many-body dynamics. To this end, we introduced a simple scheme to assess the work performed by compartment fusion and fragmentation, and provided a proof that the total entropy of the ideal gas is not affected by dynamic compartmentalisation. We generalised this proof

to arbitrary discrete stochastic many-body dynamics using the framework of the Second quantisation. This enabled us to predict the changes in total entropy of the system by algebraically computing a commutator relation, without the need for explicit solutions or extensive simulations. To illustrate our findings, we considered quantised ideal gas models and reversibly polymerisation dynamics and corroborated our theoretical predictions with full stochastic simulations. We investigated under which conditions compartment dynamics affected the statistics of realised system states. In this context, we demonstrated how specific fragmentation protocols perform implicit measurements on the system. Moreover, we showed that compartment dynamics generally affect the statistics of realised microstates of the system when the stochastic many-body dynamics show relations that violated detailed balance. This yields the possibility to facilitate or suppress particular particle states in the stochastic many-body dynamics by altering the compartment dynamics.

With the analysis in this chapter, we just glimpsed a peak at the non-equilibrium thermodynamics of closed compartmentalised systems. Focusing on the ideal gas, we formally presented a generalisation of Gibbs' paradox, as we introduced the notion of time by considering multiple compartments. We proofed the *entropic neutrality* of the ideal gas under dynamic compartmentalisation by discussing special statistical properties of the Dirichlet distribution. By this analysis, we strengthened the position of the Dirichlet distribution as the central distribution by which the stochastic ensemble dynamics of finite ideal gas systems should be characterised. Recall, that the Maxwell-Boltzmann distributions is derived as marginal distribution in the continuum limit, see section 4.4.4 and [216].

We demonstrated the Second quantisation as a powerful framework for investigating the thermodynamics of compartment fusion and fragmentation in general stochastic many-body dynamics. This framework links a kinetic perspective with the thermodynamics of compartment fusion and fragmentation. chapter 4.5 outlines a structured approach for investigating the effects of compartment dynamics, and offers insight into the symmetries of the stochastic dynamics in phase space and the resulting statistical properties. As an example, we find that fragmentation of compartments maps between equilibrium solutions. This framework thus enables us to gain insight into the underlying mathematical regularity of the world.

In section 4.5.2.3, we proposed a commutator relation which quantified the strength of the perturbation due to compartment fusion and fragmentation. We suggested to interpret the strength of the perturbation with a notion of work performed on the system, which requires further corroborative research. Moreover, it is possible to calculate the entropy production in the framework of Second quantisation [254]. A deeper understanding of the non-equilibrium thermodynamics of compartmentalised systems can be gained by further investigating the way in which compartment fusion and fragmentation perform work.

We have demonstrated in section 4.6.3 that compartment dynamics can have an effect on the statistics or realised system states when the stochastic many-body dynamics are out of equilibrium due to broken detailed balance relations. An analysis of how compartment fusion and fragmentation perform work on the system necessitates an understanding of these non-equilibrium processes on a fundamental level of altered stochastic fluxes in the phase space dynamics, rather than a phenomenological approach quantifying the entropy production alone. Consequently, the mechanisms by how compartment fusion and fragmentation performs work on a system require further investigation. This could potentially provide new insights into the mechanisms of non-equilibrium thermodynamics.

6. Conclusion and outlook

Furthermore, we speculate that a feedback between the compartment dynamics and the state of the enclosed many-body dynamics could introduce additional dynamics. Notably, this would constitute a full generalisation of Maxwell's demon.

We want to emphasise that our approach is similar in spirit to the approach of stochastic thermodynamics but follows formally an orthogonal approach. Stochastic thermodynamics is fundamentally centred around the investigation of canonical systems with a strong focus on the study the thermodynamics of systems described by Langevin-dynamics. Our approach of studying the non-equilibrium thermodynamics of *closed* compartmentalised systems follows the conceptual ideal of starting from isolated, microcanonical setups and gradually relaxing on the isolated setup. Moreover, we here find that the formalism of the Second quantisations is powerful in the sense, as it allows to investigate the full stochasticity and the many-body dynamics and by this gives a complete insight into how thermodynamics and the many-body dynamics in the phase-space are interrelated.

In this chapter 4, we considered mostly conceptual aspects concerning the non-equilibrium thermodynamics of closed compartmentalised systems. We discussed the experimental verifiability of our predictions and its technical and biological relevance in section 4.7, where we proposed to investigate them in micro-fluidic high through-put measurements of the reversible polymerisation dynamics of patchy colloids [218, 219]. We also suggested that our findings have direct implications for experimental setups which are a direct realisation of sequential fragmentation protocols, such as those used for building small vesicles filled with active biochemical reaction dynamics, as employed in the context of synthetic cells [222]. Moreover, we speculated that our findings have direct impact on organelle-associated signalling pathways, if the bio-molecules are anchored to the organelle membrane. We discussed a potential application of our findings in the context of the cellular immune response to RNA-virus infections in chapter 5. Here, we focus on reversible polymerisation dynamics subject to compartment fusion and fragmentation dynamics in systems several orders of magnitude larger than considered in chapter 4.

6.1.4. Extremal fluctuations and multi-scale gelation

In chapter 5, we considered systems several orders of magnitude larger than in chapter 4 and demonstrated how compartment fusion and fragmentation fortify the effects of aggregation and fragmentation. We provided a brief review of the Smoluchowski aggregation-fragmentation dynamics, and discussed the concept of gelation and its link to diverging moments in the aggregate size distributions. Our simulations illustrated how compartment fusion and fragmentation can facilitate the formation of large aggregates and increase the stability of these aggregates, as well as lead to a power-law decay in density fluctuations. We systematically scanned different aggregation and fragmentation kernels, characterising a subset of polymerisation dynamics where compartment dynamics facilitate the formation of large aggregates. We speculated that this phenomenology was due to a feedback loop created by the mechanism of creating and preserving density fluctuations by compartment fusion and fragmentation. We further observed that the variance of the aggregate size distribution increased with system size, suggesting diverging moments and multi-scale gelation. Finally, we applied our findings to the context of the signalling pathway causing inflammation responses after the infection of cells with RNA-virus. Our qualitative findings suggested that mitochondrial fusion and fragmentation dynamics are pivotal for efficient inflammation responses, as previously observed in experiments.

The investigations undertaken in this chapter were mainly numerical. Our findings,

therefore, require corroboration by analytical investigations in future research projects. Notably, the numerical simulations suggest that compartment fusion and fragmentation dynamics lead to a power-law decay in the density fluctuations. We proposed a mechanism, as discussed in section 5.4.2.2, for how this power-law might arise from a feedback-loop mechanism. However, this heuristic needs to be verified by analytical calculations. We anticipate that with this analytical investigation, we can gain a general understanding of how compartment dynamics affect the correlation statistics between the compartments. In addition, we speculate on the potential value of a description of effective ensemble dynamics, as introduced in chapter 2, and of studying the effects of mass conservation.

Our observation of *multi-scale gelation* necessitates further consolidation, which can be accomplished through additional numerical and analytical simulations. We hypothesise that the emergence of multi-scale gelation is a result of the power-law decay in the density fluctuations. Consequently, we anticipate that an analytical corroboration of the density fluctuations will be useful for elucidating the conditions of the aggregation and fragmentation kernels of the reversible polymerisation dynamics that give rise to multi-scale gelation.

In section 5.5, we investigated on the application of our qualitative findings to cellular immune responses to RNA-virus infections. Importantly, we did not model the immune response in this chapter, as we did not consider physiologically plausible parameter choices for the simulations. Nonetheless, we have demonstrated a mechanism showing how compartment dynamics can fundamentally affect the abundance of large aggregates. This leads us to speculate that mitochondrial dynamics may be pivotal for effective innate immune responses, which has also been observed in experiments [68]. Our findings may also be relevant in technical applications for the synthesis of protein aggregates, as well as in the context of the *origins of life*, where changes in the extreme values statistics of aggregate occurrence could have a profound impact on the emergence of self-organised structures [247].

6.2. Outlook and future research perspectives

The central aim of physics is to describe all observable phenomena in the universe by means of simple laws that explain its mechanisms and functioning. Despite physicists having striven for this objective for several centuries, we have yet to succeed in uncovering a unified theory. A major difficulty in this endeavour is the drastic complexity of systems when the number of constituents is increased. Characterising living matter from the perspective of physics thus is a challenging endeavour that demands research for more than a lifetime. Providing only a brief glimpse into the physics of multi-scale fluctuations in non-equilibrium systems. To this end, we focused on systems comprising stochastic many-body dynamics nested inside dynamic compartments. We demonstrated that the dynamic behaviour of these systems is fundamentally dictated by the interaction between dynamics on different spatial scales. We demonstrated how the paradigmatic example of a compartmentalised stochastic system can give us first insight into the physics of living matter. We demonstrated how compartment dynamics can give rise to collective degrees of freedom, and we studied the thermodynamics of compartmentalised stochastic systems. We found that the studying of compartmentalised systems necessitates an extension of our statistical physics methodology and a reconsideration of thermodynamic concepts that formally strictly separate between dynamics on a microscopic scale and manipulations on the constraints of systems.

6. Conclusion and outlook

Focusing on open systems, we proposed a flux approximation which not only allows us to derive effective dynamics for the system but also allows us to build effective analogues to the physics of inanimate matter. We linked compartment fusion and fragmentation to an effective steady attraction between compartments in the concentration phase space. Although the exact functional form of the effective attraction relies upon perfect mixing between fusing compartments, we argue that our approximation is more general. We suggest that deriving effective forces from the interplay between dynamics on different spatial scales is a powerful methodology for not only analytically treating and gaining mechanistic insight but for linking the dynamics of hierarchical multi-scale systems with the physics of inanimate matter.

Complementing to the effective description of multi-scale dynamics by deriving effective forces, we also followed the approach to elucidate the thermodynamics of compartmentalised stochastic systems. Traditionally, thermodynamic operations, which are the constraints on a sub-system, and thermodynamic processes, which describe the subsequent adaptation of the system, have been distinguished. However, with the multi-scale organisation of compartmentalised stochastic systems, the combined treatment of thermodynamic operations and processes is necessary. Furthermore, the compartment operations are directly affected by the outcome of previous thermodynamic processes in the system, when it comes to general compartment fusion and fragmentation protocols. We have demonstrated that the central mechanism of creating and preserving density fluctuations is the mechanism by which compartment fusion and fragmentation affect many-body dynamics. We were able to identify a special class of stochastic-many-body dynamics which are *neutral* to compartment fusion and fragmentation dynamics: If the stochastic many-body dynamics fulfils detailed balance relations, subsystems can be split and recombined without effects on the system's statistics and, consequently, on its entropy. Notably, we have found that detailed balance is sufficient but not a necessary prerequisite of entropic neutrality under dynamic compartmentalisation.

Our approach to studying the thermodynamics of compartmentalised systems offers two different perspectives on the heuristic mechanism of the creation and preservation of density fluctuations: a physical thermodynamic perspective and a mathematical statistical perspective. We argue that combining these two approaches enables a deeper understanding of the statistical symmetries of stochastic many-body dynamics in the phase space. With regard to the ideal gas, we elaborated on the special statistical properties of the Dirichlet distribution. We noted that the random splitting and rescaling of Dirichlet-distributed random variables resulted in new independent Dirichlet-distributed random variables. We argue that this statistical property is more general, as it characterises a class of probability distributions, which describe ensemble statistics of equilibrium processes. In conclusion, we suggest that further investigations could significantly advance our comprehension of the link between thermodynamic equilibrium and statistical symmetries. Furthermore, it could be instructive to also observe the fluxes of non-equilibrium stochastic many-body dynamics from the perspective of broken statistical symmetries in the concentration phase space.

In this work, we have gained theoretical insight and suggested that our findings have direct implications for understanding the dynamics of compartmentalised stochastic systems, with applications from biology to technical applications. A crucial next step would be to further examine specific applications and discuss their dynamics within the frameworks we have presented. This would enable us to corroborate our theoretical insights and determine how technical applications can be optimised, and diseases in biological systems

can be mitigated. Our findings provide a mathematical framework to discuss the dynamics of compartmentalised stochastic systems and thus propose approaches to investigate the physics of living matter. We suggest that our findings have profound implications for future research on the physics of living matter organised on multiple scales of biological organisation.

A. Mathematical concepts

A.1. Master Equation

Markov processes are processes lacking memory and are of central interest in describing a variety of systems in physics. As such, the passage to a state (a_{n+1}, t_{n+1}) depends only on the current state (a_n, t_n) , but not on the history of the path. Of central interest for this processes is the transition probability to change from one state to another. In this context it is useful to consider the Chapman-Kolmogorov relation. In the following, we closely follow [17]. Consider the probability to observe a state a at time t and an intermediate state a' at time t' given some initial state a_i at an initial time $t_i < t' < t$, $p(a, t; a', t'; a_i, t_i)$. From this, we obtain the transition probability $p(a, t; a_i, t_i)$ by integration over the intermediate states:

$$p(a, t; a_i, t_i) = \int da' p(a, t; a', t'; a_i, t_i) = \int da' p(a, t|a', t'; a_i, t_i) \cdot p(a', t'; a_i, t_i), \quad (\text{A.1})$$

which reduces for Markov processes to the Chapman-Kolmogorov relation

$$p(a, t; a_i, t_i) = \int da' p(a, t|a', t') \cdot p(a', t'; a_i, t_i). \quad (\text{A.2})$$

This description in terms of an intermediate state becomes useful. Consider the time difference $t - t' = \delta t$ infinitesimally small. Denoting the transition rate from a state a' to a state a'' during the time interval $\delta t'$ as $W(a'', a')$, we find the transition probability as $W(a'', a')\delta t$. Using this, we may write to linear order

$$p(a, t|a', t - \delta t) = \delta(a' - a) - \delta t \delta(a' - a) \int da'' W(a'', a') + \delta t W(a, a') + \mathcal{O}(\delta t^2), \quad (\text{A.3})$$

where the third term describes transition from state a' to state a and the second term describes losses from state a' to some other state a'' . Substituting this expression in the Chapman-Kolmogorov relation, and suppressing the dependence on the initial time, we find

$$p(a, t) = p(a, t')(1 - \delta t \int da'' W(a'', a')) + \delta t \int da' W(a, a') \cdot p(a', t'), \quad (\text{A.4})$$

which simplifies to

$$\frac{p(a, t) - p(a, t - \delta t)}{\delta t} = -(\int da'' W(a'', a)p(a, t')) + \int da' W(a, a') \cdot p(a', t'). \quad (\text{A.5})$$

Taking the limit $\delta t \rightarrow 0$ we find the Master Equation

$$\partial_t p(a, t) = \int da' [W(a, a')p(a', t) - W(a', a)p(a, t)]. \quad (\text{A.6})$$

A. Mathematical concepts

Here, the first term on the right hand side describes the gain of probability by transitions into the state a , while the second term describes transitions out of the state a . This balancing type of equation offers an intuitive approach to the dynamics underlying the master equation, especially if the states follow a spatial ordering.

A useful extension of this formalism arises in the context of the second quantisation, as discussed in section 4.5. In this context, it's useful to write the Master equation in form of a Matrix equation. To this end, we define the normalised, orthogonal basis vector \vec{e}_a for each accessible state of the the Master equation, such $|\vec{e}_a \cdot \vec{e}_{a'}| = \delta_{a-a'}$. We define the probability vector $\vec{p}(t) = \sum_a p(a, t) \vec{e}_a$ and write the Master equation

$$\partial_t \vec{p}(t) = \mathbf{A} \vec{p}(t), \quad (\text{A.7})$$

using the transition matrix \mathbf{A} . The entry $A_{i,j} = W(i, j)$ is given by transition rate from state j into state i for all $i \neq j$. The diagonal elements are given by $A_{i,i} = -\sum_{j \neq i} A_{j,i}$, such that each column sums to zero $\sum_j A_{j,i} = 0$. For a given initial condition, the solution of the master equation is given by the matrix exponential of A . For the application to the second quantisation, a superficial complication of this formalism becomes useful. To this end, we avoid the matrix notation and instead define basis exchange operators $\hat{o}_{j,i} \vec{e}_l = \delta(l-i) \vec{e}_j$ which maps the basis vector of state i to state j . Using this, we write

$$\partial_t \vec{p}_i(t) = \sum_j A_{i,j} \hat{o}_{i,j} \vec{p}(t)$$

and summing over all states i , we find

$$\partial_t \vec{p}(t) = \sum_i \sum_j A_{i,j} \hat{o}_{i,j} \vec{p}(t). \quad (\text{A.8})$$

We can further simplify the equation above by directly writing it in terms of the the transition rate $W(i, j)$

$$\partial_t \vec{p}(t) = \sum_i \sum_j (\hat{o}_{i,j} - \hat{o}_{j,j}) W(i, j) \vec{p}(t). \quad (\text{A.9})$$

We see in section 4.5 that this notation comes in particular handy in the context of the Second quantisation, where the rate transition rate $W(i, j)$ depends on the occupation number of state j .

A.2. Compartment dynamics in the framework of Master equations

In this section, we specify on the semi-symbolical notion used to define the compartment dynamics in the framework of Master Equations, compare in particular with section 2.3.

We start by defining the stochastic dynamics inside the compartments. We refer to these dynamics as intra-scale fluxes on the microscopic level. We define the operator

$\mathcal{Q}_{\eta(t)}$

$$\begin{aligned} \mathcal{Q}_{\eta(t)} [P(\mathbb{S})] = & \sum_i^{N(\mathbb{S})} \left(\sum_{\vec{c}'_i \neq \vec{c}_i} Q_i(\vec{c}'_i \rightarrow \vec{c}_i, \vec{o}_i) P \left(\left[\begin{array}{c} \vdots \\ [\vec{c}'_i, \vec{o}_i] \\ \vdots \end{array} \right] \right) \right) \\ & - P(\mathbb{S}) \sum_i^{N(\mathbb{S})} \left(\sum_{\vec{c}'_i \neq \vec{c}_i} Q_i(\vec{c}_i \rightarrow \vec{c}'_i, \vec{o}_i) \right). \end{aligned} \quad (\text{A.10})$$

We refer to the transition rates of the enclosed stochastic many body dynamics in compartment i with $Q_i(\vec{n}'_i \rightarrow \vec{n}_i, v_i)$. We specify on the stochastic transition rates in particular in the context of stochastic chemical reactions, as detailed out in section 2.2.1. Recall that the index $\eta(t)$ refers to the dependence of an external signal. Here, $N(\mathbb{S})$ refers to the number of compartments in the system \mathbb{S} .

In analogy, we define the intra-scale fluxes on the level of compartment dynamics with

$$\begin{aligned} \mathcal{S} [P(\mathbb{S})] = & \sum_i^{N(\mathbb{S})} \left(\sum_{\vec{o}'_i \neq \vec{o}_i} S_i(\vec{o}'_i \rightarrow \vec{o}_i, \vec{c}_i) P \left(\left[\begin{array}{c} \vdots \\ [\vec{c}_i, \vec{o}'_i] \\ \vdots \end{array} \right] \right) \right) \\ & - P(\mathbb{S}) \sum_i^{N(\mathbb{S})} \left(\sum_{\vec{o}'_i \neq \vec{o}_i} S_i(\vec{o}_i \rightarrow \vec{o}'_i, \vec{c}_i) \right). \end{aligned} \quad (\text{A.11})$$

These processes leave the concentration composition in the compartments unchanged. As for the reaction kinetics Q_i, S_i are rates happening on individual compartments, without information about the state of other compartments. Examples for these processes are compartment shape changes or the spatial translocation of compartments.

Next, we focus on inter-scale fluxes, which change both the concentration vector \vec{c}_i and compartment properties \vec{o}_i but leave the number of compartments unchanged. The prominent example of this class of processes is compartment growth, we hence define

$$\begin{aligned} \mathcal{R}_{\text{gro}} [P(\mathbb{S})] = & \sum_i^{N(\mathbb{S})} \left(\sum_{(\vec{c}'_i, \vec{o}'_i) \neq (\vec{c}_i, \vec{o}_i)} R_i^{\text{gro}}((\vec{c}'_i, \vec{o}'_i) \rightarrow (\vec{c}_i, \vec{o}_i)) P \left(\left[\begin{array}{c} \vdots \\ [\vec{c}'_i, \vec{o}'_i] \\ \vdots \end{array} \right] \right) \right) \\ & - P(\mathbb{S}) \sum_i^{N(\mathbb{S})} \left(\sum_{(\vec{c}'_i, \vec{o}'_i) \neq (\vec{c}_i, \vec{o}_i)} R_i^{\text{gro}}((\vec{c}_i, \vec{o}_i) \rightarrow (\vec{c}'_i, \vec{o}'_i)) \right). \end{aligned} \quad (\text{A.12})$$

Note, that by definition the majority of the transition rates are equal to zero for growth processes, as here the coupling between compartment property and concentration stems from the definition of the concentration as $\vec{c}_i = \vec{n}_i/s_i$, where s_i refers to the size of the compartment and \vec{n}_i to the number of chemical species in the compartment. Here, we generalised on the notation of the dynamics.

For compartment creation and degradation, both the compartment with properties \vec{o} and a concentration \vec{c} are to be considered. We introduce notation to refer to the admissible states that can be accessed by compartment degradation processes. We define

A. Mathematical concepts

the set $\mathcal{J}_{\text{deg}}(\mathbb{S}) = \{\mathbb{S}' | N(\mathbb{S}') - 1 = N(\mathbb{S}) \wedge \mathbb{S}_{1:N} = \mathbb{S}_{1:N}\}$. By definition, we demand that \mathbb{S}' has one compartment more, and that $1 : N$ compartments coincide. Without loss of generality, we refer to the one compartment in \mathbb{S}' which is not present in \mathbb{S} with the index $N + 1$. With this notation, we find for the birth term:

$$\mathcal{R}_{\text{D}}[P(\mathbb{S})] = \sum_{\mathbb{S}' \in \mathcal{J}_{\text{deg}}(\mathbb{S})} R^{\text{D}}([\vec{c}_{N+1}, \vec{o}_{N+1}] \rightarrow \emptyset) P(\mathbb{S}') - P(\mathbb{S}) \sum_i^{N(\mathbb{S})} R^{\text{D}}([\vec{c}_i, \vec{o}_i] \rightarrow \emptyset). \quad (\text{A.13})$$

Here, $R^{\text{D}}([\vec{c}_i, \vec{o}_i] \rightarrow \emptyset)$ refers to the rate with which a compartment with characteristics $[\vec{c}_i, \vec{o}_i]$ is degraded. In analogy, for the compartment creation we define the set $\mathcal{J}_{\text{cre}}(\mathbb{S}) = \{\mathbb{S}' | N(\mathbb{S}') + 1 = N(\mathbb{S}) \wedge \mathbb{S}_{1:N-1} = \mathbb{S}_{1:N-1}\}$. Again, we consider all admissible permutations, such that without loss of generality we refer to the created compartment with the index N . This yields

$$\mathcal{R}_{\text{B}}[P(\mathbb{S})] = \sum_{\mathbb{S}' \in \mathcal{J}_{\text{cre}}(\mathbb{S})} R^{\text{B}}(\emptyset \rightarrow [\vec{c}_{N+1}, \vec{o}_{N+1}]) P(\mathbb{S}') - P(\mathbb{S}) \sum_{[\vec{c}, \vec{o}]} R^{\text{B}}(\emptyset \rightarrow [\vec{c}, \vec{o}]). \quad (\text{A.14})$$

Here, $R^{\text{B}}(\emptyset \rightarrow [\vec{c}_i, \vec{o}_i])$ refers to the rate with which a compartment with characteristics $[\vec{c}_i, \vec{o}_i]$ is created from the void.

As discussed in depth in section 2.3, we understand that compartment fusion and fragmentation pose as inter-scale fluxes, as these processes alter both the compartment properties and the concentration composition. As for the creation and degradation terms, we define a set for compartment fusion $\mathcal{J}_{\text{fus}}(\mathbb{S}) = \{\mathbb{S}' | N(\mathbb{S}') - 1 = N(\mathbb{S}) \wedge \mathbb{S}_{1:N-1} = \mathbb{S}_{1:N-1}\}$. Here, we again state that $N - 1$ compartments between the two systems must be identical. Without loss of generality, we refer to the compartments not coinciding, with index N and for \mathbb{S} and $N, N + 1$ for \mathbb{S}' . This yields

$$\begin{aligned} \mathcal{R}_{\text{fus}}[P(\mathbb{S})] &= \sum_{\mathbb{S}' \in \mathcal{J}_{\text{fus}}(\mathbb{S})} R^{\text{fus}}([\vec{c}_N, \vec{o}_N], [\vec{c}_{N+1}, \vec{o}_{N+1}] \rightarrow [\vec{c}_N, \vec{o}_N]) P(\mathbb{S}') \\ &\quad - P(\mathbb{S}) \sum_{i,j}^{N(\mathbb{S})} \sum_{[\vec{c}, \vec{o}]} R^{\text{fus}}([\vec{c}_i, \vec{o}_i], [\vec{c}_j, \vec{o}_j] \rightarrow [\vec{c}, \vec{o}]), \end{aligned} \quad (\text{A.15})$$

where we symbolically defined the rate for two compartments to fuse. We define also for the fragmentation an a set $\mathcal{J}_{\text{frag}}(\mathbb{S}) = \{\mathbb{S}' | N(\mathbb{S}') + 1 = N(\mathbb{S}) \wedge \mathbb{S}_{1:N-1} = \mathbb{S}_{1:N-1}\}$ and also allow for all possible permutations such that we refer to the non-coinciding compartments with index $N - 1, N$ and for \mathbb{S} and N for \mathbb{S}' . This yields

$$\begin{aligned} \mathcal{R}_{\text{frag}}[P(\mathbb{S})] &= \sum_{\mathbb{S}' \in \mathcal{J}_{\text{frag}}(\mathbb{S})} R^{\text{frag}}([\vec{c}_N, \vec{o}_N] \rightarrow ([\vec{c}_{N-1}, \vec{o}_{N-1}], [\vec{c}_{N+1}, \vec{o}_{N+1}])) P(\mathbb{S}') \\ &\quad - P(\mathbb{S}) \sum_i^{N(\mathbb{S})} \sum_{([\vec{c}_k, \vec{o}_k], [\vec{c}_l, \vec{o}_l])} R^{\text{frag}}([\vec{c}, \vec{o}] \rightarrow ([\vec{c}_k, \vec{o}_k], [\vec{c}_l, \vec{o}_l])), \end{aligned} \quad (\text{A.16})$$

where we symbolically defined the rate for the fragmentation of compartments.

We do not claim that the list of compartment dynamics is extensive, but rather a selection of compartment processes inspired by the dynamics of organelles. Also note, that the complexity of the terms above effectively hinder further analytical treatment of the compartment dynamics on the basis of the Master Equation framework. In section 2.4.1 we thus proceeded to further investigate the dynamics in the continuum limit of infinitely

large system sizes in the framework of population balance equations.

A.3. Stochastic two-body interaction dynamics

In this section, we derive a Fokker-Planck approximation for a many-body system of particles performing Brownian motion while being subject to two-body interaction. Here, we closely follow [101]. Consider N interacting particles performing Brownian motion with a two-body interaction. \vec{x} denotes the N positions of the particles x_i , and the two-body interactions create a potential

$$V(\vec{x}) = \frac{1}{2} \sum_{i \neq j} v(x_i - x_j),$$

where the two body interactions are symmetric with $v(x) = v(-x)$. μ denotes the mobility and D denotes the diffusion constant. The Fokker-Planck equation describing this system is

$$\partial_t P(\vec{x}, t) = \sum_i \partial_{x_i} (D \partial_{x_i} P(\vec{x}, t) + \mu P(\vec{x}, t) \partial_{x_i} V(\vec{x})).$$

We are interested in the one-particle density and the pair-particle density defined by

$$P^{(1)}(x, t) = \int dx_2 \cdots dx_N P(x, x_2, \dots, x_N)$$

$$P^{(2)}(x, x', t) = \int dx_3 \cdots dx_N P(x, x', x_3, \dots, x_N).$$

The many-body Fokker-Planck equation obeys a BBGKY hierarchy. The first equation of the hierarchy reads

$$\partial_t P^{(1)}(x, t) = \partial_x \left(D \partial_x P^{(1)}(x, t) + (N-1) \mu \int dx' P^{(2)}(x, x', t) \partial_{x'} v(x-x') \right). \quad (\text{A.17})$$

Using a mean field approximation and scaling μ accordingly, we find:

$$\partial_t P(x, t) = \partial_x \left(D \partial_x P(x, t) + \tilde{\mu} P(x, t) \int dx' P(x', t) \partial_{x'} v(x-x') \right). \quad (\text{A.18})$$

Note, that the derivative of the two-body interaction potential $-\partial_x v(x-x')$ enters into the integral. We draw the derivative out of the integral and define the interaction potential

$$\Phi[P(x, t)] = \tilde{\mu} \int dx' P(x', t) \partial_{x'} v(x-x'), \quad (\text{A.19})$$

such that

$$\partial_t P(x, t) = \partial_x \left(D \partial_x P(x, t) - (\partial_x \Phi[P(x, t)]) P(x, t) \int dx' P(x', t) \partial_{x'} v(x-x') \right). \quad (\text{A.20})$$

This allows to link interaction potentials $\Phi[P(x, t)]$ with elementary two-body interaction potential $v(x-x')$ and hence serves as a guide to establish correspondence between dynamics.

A.4. Waddington’s epigenetic landscape as a metaphor for signalling pathways

The chemical Master Equation, its Fokker-Planck approximation and the chemical Langevin Equation provide a general framework for describing the dynamics of signalling pathways, taking into account the stochastic nature of chemical reactions at small copy numbers. In this general framework, we have not specified chemical reactions and hence left the drift vector \vec{F} and the diffusion matrix \mathbf{D} generic. Notably, the drift vector \vec{F} is associated with highly non-linear dynamics, which renders intuitive understanding of the dynamics difficult and necessitates detailed analysis of the model for the purpose of predicting the qualitative dynamics. Fixed point analysis can be employed as a useful toolbox for characterising the dynamics encoded by the drift vector \vec{F} in a specified region of the phase space.

Particularly important from a biological perspective is the description of stable fixed points and limit cycles. While fixed points are individual points in the phase space, limit cycles represent periodic solutions of the non-linear dynamics. Stable fixed points and limit cycles are characterised by a ‘region of attraction’, meaning that the dynamics within this region relax to the fixed point, making them stable against small fluctuations [5]. However, alterations in system parameters can cause changes in the position of fixed points, regions of attraction and the presence of fixed points themselves. Catastrophe theory, which is a branch of mathematics concerned with the study of dynamical systems, provides formalisation of how fixed points change as system parameters are altered [255].

The connection between catastrophe theory and biological systems was first discussed by biologist Conrad Hal Waddington and mathematician René Thom in the context of Waddington’s epigenetic landscape. Waddington developed the notion of an epigenetic landscape in the context of cell type evolution, and this picture has been frequently employed in the context of gene regulatory networks [256–258] and signalling pathways to provide an intuitive approach to non-linear dynamics encoded in reaction networks. However, it is important to acknowledge the limitations of Waddington’s landscape and to interpret it cautiously. We give a brief discussion on Waddington’s landscape and related concepts, highlighting the situations in which it offers a useful illustration of the dynamics of reaction networks and wherein it can be a misleading picture.

Conrad Hal Waddington proposed the concept of an epigenetic landscape as a qualitative model to describe the dedifferentiation dynamics of stem cells [256]. In this model, cells are represented as a ball sliding down a landscape of bifurcating valleys. Different valleys correspond to different cell states, with the sliding of the ball symbolising the temporal evolution of the cell. At bifurcation points, the ball randomly continues in one of the two branching valleys. Waddington’s landscape illustrates how cells of the same stem cell type differentiate into various cell types and suggests that differentiation is a uni-directional process. This metaphor implies that the development of a biological system is given by a gradient descent dynamics. Whilst the y-axis in Waddington’s landscape can be linked to the progression of time, the x-axis and the potential landscape have only an abstract, qualitative notion. Specifically, the x-axis displays a scalar quantity which allows for the distinction between different cell types, which may not have a measurable biological analogue, and the height of the potential is arbitrary. In terms of the analysis of dynamical systems using fixed points, the bottom of a valley denoting a cell type corresponds to stable fixed points. As the ball rolls down to the bottom of valleys in this landscape picture, valleys represent the *regions of attraction* around the stable fixed

points. The bifurcation of valleys corresponds to a change in the number of stable fixed points as system parameters change over time. The greatest advantage of Waddington's landscape is its capacity to illustrate intricate dynamics in a captivating and intuitive manner.

In the context of reaction networks, stable fixed points correspond to protein compositions associated with biological states of signalling networks [259]. Variations in system parameter can include changes in chemical reaction rates $k_j(\eta(t))$ over time, as induced by signals $\eta(t)$. Consequently, these signals $\eta(t)$ allow for transitions between stable states of the signalling pathway, leading to changes in a cell's function. Investigating the dynamics of signalling pathways thus requires an analysis of transitions between states. To this end, the metaphor of Waddington's landscape provides an intuitive approach.

The notion of Waddington's landscape as gradient dynamics is generally misleading. Although an extension to include stochastic transition between states due to barrier crossing events can be considered, this is not the case for high-dimensional systems, which require rotational flows to be taken into account. The metaphor of Waddington's landscape only includes singular fixed points, but ignores other attractors such as limit cycles and strange attractors, which cannot be represented adequately in a landscape picture. Quasi-potentials have been proposed as a means of incorporating rotational flows into landscape metaphors [256], however, these have not been followed as literal interpretations of Waddington's metaphor are avoided.

Similar to the notion of Waddington's landscape, which shows as potential, Lyapunov functions which are commonly employed in dynamical systems analysis to assess the stability of fixed points. Lyapunov functions are scalar functions $V(\vec{x})$ defined on a region \mathcal{D} around some stable fixed point \vec{x}_s which are semi-definite and have a continuous first derivative [5]. If there exists a function $V(x)$ such that $\nabla V(\vec{x})\vec{F}(\vec{x}) \leq 0$ the fixed point \vec{x}_s is called asymptotically stable. Note that all stable singular fixed points are asymptotically stable. The condition $\nabla V(\vec{x})\vec{F}(\vec{x}) \leq 0$ implies that $V(\vec{x}(t))$ is steadily decreasing along every deterministic trajectory following $d/dt\vec{x} = \vec{F}(\vec{x})$, such that $V(x)$ is scalar function with a minimum at \vec{x}_s . While this suggests, that a potential function can be locally defined around every fixed point, the condition $\nabla V(\vec{x})\vec{F}(\vec{x}) \leq 0$ does not imply that trajectories $\vec{x}(t)$ follow the steepest descent of $V(\vec{x})$ and hence does not imply the dynamics are gradient dynamics around stable fixed points. As rotational fluxes are not excluded, such as the spiralling into a stable fixed point, Lyapunov functions grants the existence of so called generalised gradient dynamics. If all fixed points of a system can be described by the same Lyapunov function, $V(\vec{x})$ is called a global Lyapunov functions. For $d/dt\vec{x} = -\nabla\Phi(\vec{x})$, the potential $\Phi(\vec{x})$ is by construction a global Lyapunov function. Note, that conversely the existence of a global Lyapunov $V(\vec{x})$ function is not implying $\nRightarrow d/dt\vec{x} = -\nabla V(\vec{x})$. Analysis of chemical reaction networks fulfilling detailed balance in steady states proofed that stable fixed points are necessary singular points in the phase space and hence proofed the absence of limit cycles and strange attractors in these dynamical systems. Furthermore, it has been proofed that these systems allow for global Lyapunov functions characterising a potential landscape, without implying actual gradient dynamics. In the context of signalling pathways which fulfil detailed balance in steady states of the dynamics, Lyapunov functions represent a formalisation of Waddington's landscape metaphor.

Concluding this section, the metaphor of Waddington's landscape can serve as an illustration to provide an intuitive approach to the dynamics encoded in signalling pathways. However, potential landscapes only adequately describe dynamical systems if the system

can conform to a gradient dynamics, which is generally not true for chemical reaction networks. As such, the illustration of dynamics using potential landscapes, such as Waddington's landscape picture or global Lyapunov functions, can be misleading. In this thesis, analysis will only be performed on the level of drift vectors \vec{F} and care will be taken to indicate and comment when potential dynamics are used for illustrative purposes.

A.5. Modification of Kramer's escape rate due to compartment dynamics

In section 3.4, we elaborated that the effective dynamics demand modifications to account for absorbing boundary condition placed at the separatrix of regions of attraction. Here, we discuss how in particular the stable-tail-long-range approximation of the fusion flux, Eq. (2.35), allows to map effects of organelle fusion and fragmentation to a simple modification of the barrier escape rate. For this, we make use of the interpretation presented in appendix A.3, where we discussed the interpretation of the fusion flux in terms of effective two-body interaction potentials, $\phi_{\text{eff}}[f(\vec{c}, t), \vec{c}^\dagger]$. Here, we will in particular focus on the stable-tail-long-range approximation, which we have shown to approximation in particular the tail of the distribution $f(\vec{c}, t)$ well in steady state. To derive effective dynamics in the context of an absorbing boundary condition, we make use of mathematical proof presented in [104].

[104] Proofed mathematically that the stochastic escape of individual, stochastic particles subject to diffusion, drift, and an effective two-body interaction potential, is captured by a Kramer's escape in an effective potential. While [104] discuss also the special case of general drift dynamics, here, we focus for didactic reasons on gradient dynamics where $\vec{F}(\vec{c}, t) = -\nabla V\vec{c}$. We define \vec{c}_s as a stable fixed point from which compute the stochastic escape rate through the absorbing boundary \mathcal{D} . Setting the diffusivity to D , the expectation of the mean first passage time $\langle\tau_{\mathcal{D}}\rangle$ of a single particle is given by

$$\lim_{D \rightarrow 0} D \log(\langle\tau_{\mathcal{D}}\rangle) = \inf_{\vec{z} \in \mathcal{D}} 2(V(\vec{z}) - V(\vec{c}_s) + \phi_{\text{eff}}[f_{ss}(\vec{c}, t), \vec{z} - \vec{c}_s]), \quad (\text{A.21})$$

where we made use of the steady state solution of the distribution $f_{ss}(\vec{c}, t)$. Note that this approximation of the Kramer's escape rate is only valid for vanishing $D \rightarrow 0$, hence the barrier position is located in the tail of the distribution and we a posteriori justify the use of the stable tail long-range approximation of the fusion flux. To the knowledge of the authors a generalisation of multiplicative noise has not been mathematically proven, yet. Generalisation of the Kramer's escape to account for multiplicative noise has, however, been discussed in the literature [164]. Next, we use this modification of the Kramer's rate to compute the escape from a simple quadratic potential well.

To this end, we consider effective one-dimensional dynamics. We let $\delta\eta(t) = \eta t - \eta(0)$ be the fluctuating extrinsic signal. We define the steepness of the potential k and define $\eta(0) = c_s k$. The effective potential is

$$V_{\text{eff}}(c) = \frac{1}{2}kc^2 - \eta(t)c \quad (\text{A.22})$$

A.6. Modification of Kramer's escape rate due to heterogeneous size distributions

and the effective potential in the modified Kramer's rate with an absorption at $z > c_s$

$$Q(z) = kz^2 - 2z\eta(t) + \frac{\delta\eta(t)^2}{k} + 2\mu_{\text{eff}} \left(z - \frac{\eta(t)}{k} \right). \quad (\text{A.23})$$

The Kramer's escape rate τ_z^{-1} in the limit $D \rightarrow 0$ is

$$\tau_z^{-1} = \tilde{\omega}_0 \exp\left(-\frac{kz^2}{D}\right) \cdot \exp\left(-\mu_{\text{eff}} \frac{z - \frac{\eta(t)}{k}}{D}\right) \cdot \exp\left(-\frac{\frac{\delta\eta(t)^2}{k} - 2z\eta(t)}{D}\right), \quad (\text{A.24})$$

where accounted for the dimensional prefactor $\tilde{\omega}_0$, see for example [164]. According to the Smoluchowski aggregation dynamics discussed in section 2.2.3, we account for the fusion flux to be a linear function of the total organelle mass m , and define $\mu_{\text{eff}}(m) \equiv \mu_0 m$. We next introduce the abbreviated notation

$$\tau_z^{-1}(V_{\text{eff}}, m, \eta(t)) = \tilde{\omega}_0 \exp(-\Gamma_{\text{Kramer}}) \cdot \exp(-m\Gamma_{\text{Int}}) \cdot \exp(-\Gamma_{\eta(t)}). \quad (\text{A.25})$$

With this modified Kramer's escape rate, we find a simple differential equation quantifying the mass of absorbed mitochondria in the picture of Fig. 3.11 (b). To account for fluctuating signals $\eta(t)$ we in particular assume that the quasi-statistic approximation, such that $\tau_z > \tau_\eta$. We normalise the initial organelle mass to $m(t=0) = 1$, which yields

$$\partial m = -\tau_z^{-1}(V_{\text{eff}}, m, \eta(t))m = -\omega(V_{\text{eff}}, \eta(t)) \cdot \exp(-m\Gamma_{\text{Int}}) m. \quad (\text{A.26})$$

This differential equation admit analytic solutions in terms of the inverse of the exponential integral function Ei^{-1} , making use of the effective Kramer's rate $\omega(V_{\text{eff}}, \eta(t))$ and the rescaled interaction potential evaluated at the position of the absorbing boundary condition, with

$$m(t) = \frac{1}{\Gamma_{\text{Int}}} \text{Ei}^{-1}(-\omega(V_{\text{eff}}, \eta(t))t + \text{Ei}(\Gamma_{\text{Int}})). \quad (\text{A.27})$$

By construction, the amount of mitochondrial mass absorbed is given by $\bar{m}(t) = 1 - m(t)$. This solution in particular nicely illustrates how organelle fusion and fission effectively suppresses the stochastic switching to the high concentration state and illustrates how the vanishing suppression with the progression of time gives rise to sigmoidal response kinetics.

A.6. Modification of Kramer's escape rate due to heterogeneous size distributions

Heterogeneous size distributions of organelle ensembles without organelle dynamics changing the sizes of individual organelles suggest treating organelle subpopulations of identical sizes independently, rather than marginalising over organelle sizes. In the context of the random switching dynamics due to apoptotic stimuli, as presented in Section 3.4, separate Kramer's escape problems can be considered for each subpopulation of a specified organelle size. The backward reaction from the high concentration state to the low concentration state is assumed to be negligible. The Kramer's rate can be computed using standard methods, such as those outlined in [260]. The Kramer's escape rate for the

A. Mathematical concepts

subpopulation of size s is symbolically denoted by $\omega(s)$, and the total mass in a subpopulation is defined as m_s . Then, the time evolution of mitochondrial mass in the low concentration state yields

$$m(t) = \sum_s m_s \exp(-\omega(s)t). \quad (\text{A.28})$$

Defining the high concentration state at c_h and the low concentration state at c_l , and assuming that the Kramer's limit is met for all s , we approximate the mean of the distributions in response to an apoptotic stimulus

$$\langle c(t) \rangle \approx c_l \cdot \left(\sum_s \frac{m_s}{m(0)} \exp(-\omega(s)t) \right) + c_h \cdot \left(1 - \sum_s \frac{m_s}{m(0)} \exp(-\omega(s)t) \right). \quad (\text{A.29})$$

For given potentials, this equation yields analytic solutions with no free fit parameter.

A.7. Pre- and post-modifications in apoptotic signalling pathway

In section 3.7, the predicted kinetics of the quasi-particle in cell culture experiments were elaborated on, discussing the extent to which the sigmoidal dynamics are robust towards the including of additional dynamics before and after the release of Cyt c . This section provides a brief description of how qualitative arguments are corroborated by numerical simulations.

As we consider not direct inducers of apoptosis, we assume that the apoptotic stimulus applied to the cell is already the consequence of stochastic processes. To account for this pre-modification, we assume that the start of the apoptotic stimulus is a random variable. Specifically, we assume that the onset of the apoptotic stimulus is exponentially distributed. Furthermore, we assume that also the strength of the stimulus is subject to variations. We capture this by assuming fixed stimuli, but with the strength of the stimulus distributed like a Gaussian variable around a specified mean. This translates to our model, as we assume the skew of the bistable potential to be Gaussian distributed. To account for the post-modification, we note that a partial release of Cyt c from a mitochondrial subpopulation $> 10\%$ has so far not been observed experimentally [153–155]. We translate this insight to our model, as we assume that a release from a mitochondrial ensemble $> 10\%$ to be sufficient for a cell to undergo apoptosis.

We translate these conditions into a model, taking into account the theoretical models from Fig. 3.10 (a) with the associated parameters and averaging over many realisations. Specifically, we consider for the variable apoptotic onset an exponential distribution with $t_0 \sim \text{Exp}(60t_r)$ and a variation of the skew of $\sigma_\eta \approx 20\%E_B$, where E_B is the height of the potential barrier. We then digitalise the predicted trajectory at the threshold values $\Theta(\langle c \rangle / c_h^* > 0.1)$. Finally, we compare the solution for the equations of motion for the quasi-particle with the modified Kramer's escape dynamics in the absence of mitochondrial fusion and fragmentation. The results are shown in Fig. 3.14 (e,f).

B. Numerical routines

B.1. Numerical routine for the simulation of compartmentalised systems

In order to investigate the multi-scale dynamics of compartmentalised stochastic reaction kinetics systems, we sample random trajectories of the dynamics specified by the Master equation (2.20). For this purpose, we employ the direct method of the *stochastic simulation algorithm* [261, 262]. This formulation enables us to implement the dynamics straightforwardly. However, due to the multi-scale nature of the dynamics, the computational costs tend to become prohibitively high when large systems with large concentration vectors \vec{c}_i are simulated, as this drastically slows down the run time. Therefore, we introduce additional approximations, which allow for a drastic reduction in computational time by assuming that compartmental dynamics typically proceed at slower timescales than chemical reactions.

In order to implement the dynamics specified by the Master equation Eq. (2.20), we associate each possible transition with a rate $\mathcal{T}_{\mathbb{S} \rightarrow \mathbb{S}'} \equiv \mathcal{T}_j$, which is commonly referred to as the propensity of transition j [262]. The ratio $\mathcal{T}_j / \sum_l \mathcal{T}_l$ represents the probability of taking transition j in order to move to the subsequent step, with the sum running over all possible transitions between state \mathbb{S} and another state \mathbb{S}' . By drawing two random uniform numbers r_1 and r_2 the system changes its state after the time step

$$\tau = \frac{1}{\sum_l \mathcal{T}_l} \log \left(\frac{1}{r_1} \right) \quad (\text{B.1})$$

according to the transition specified by the j , which fulfils being the smallest integer satisfying

$$\sum_l^j \mathcal{T}_l > r_2 \sum_l^j \mathcal{T}_l. \quad (\text{B.2})$$

This routine updates the system in sequential order without making any assumption on the timescale of the specific reactions. Due to the large number of possible transitions, the stochastic evolution of this dynamics typically shows long run times prohibiting extensive simulations of large systems.

In order to enhance the efficiency of our code, we account explicitly for the multi-scale organisation of compartmentalised stochastic reaction kinetics systems. We make a distinction between compartment dynamics and inter-scale fluxes resulting from chemical reactions. The compartment dynamics are simulated using the Master equation, along with a stochastic simulation algorithm, while the concentration \vec{c}_i in each compartment is evolved parallel to this, at intervals of duration τ_o . By splitting the code in this way, it can be parallelised, thus significantly reducing the execution time. This is especially beneficial when the dynamics of the compartments are often slower than those on the

molecular level.

We might further optimise the run time of the algorithm by additionally parallelising the compartment dynamics. To do this, we discretise the evolution steps of the compartment dynamics to a fixed τ_o , and assign for each compartment probabilities for undergoing compartment dynamics after the next step, for example fusion with another compartment. This routine accurately recreates the size distribution predicted by the compartment aggregation-fragmentation dynamics presented section 2.2.3. Additionally, for large systems with large concentration vectors \vec{c}_i , memory management is optimised by assigning compartments of discrete sizes. For each *elementary* compartment block, memory capacities are pre-allocated, in which the composition vector and the transition matrix of the chemical reaction network are stored and updated. We have implemented the multi-scale dynamics both in Python and C++; while Python allows for simple and intuitive exploration of the phenomena encoded in the multi-scale dynamics, C++ provides opportunities for efficiency optimisation of the code through controlling and pre-allocating the memory demands.

B.2. Optimisation of the numerical routine to account for gelation dynamics

In Eq. (5.16) we gave a description of the system’s dynamics in terms of a Master Equation, analogous to the dynamics described in section 2.3. Here, we simulate both the organelle dynamics and chemical reaction kinetics explicitly on the level of stochastic transitions. For this, we extend on the numerical routine introduced in appendix B.1 and additionally focus on how to allocation of memory, which allows for the optimisation of the run time.

We simulate the organelle kinetics and the reversible polymerisation kinetics using stochastic simulation algorithms (SSAs) with the direct method [261, 262]. The time-step between stochastic compartment fusion and fragmentation events is determined on the level of compartments, and the stochastic reversible polymerisation kinetics is evolved on all compartments in parallel for the duration of the time-step. Following this, compartment fusion or fragmentation is performed before the time-step to the next compartment fusion and fragmentation event is determined. This time-evolution procedure is repeated until the final simulation time is reached, making this numerical routine especially suited to handling organelle compartments of varying sizes.

By simulating all chemical reaction steps explicitly, the simulation quickly increases in run time and memory demands. We implemented the algorithm in C++ which enables us to manage memory allocation. A significant slow-down of the algorithm is caused by the handling of the individual reaction rate propensities of the aggregation reactions for accounting for all aggregates of different sizes. The total number of possible reactions scales as N_{\max}^2 , where N_{\max} is the size of the largest aggregate, and the reaction rates must be re-calculated between individual update steps of the SSA. However, only those rates that are affected by the previous update step are re-calculated, reducing the computation of the duration of the time-step. This also results in updating individual columns and rows of a reaction propensity matrix. In order to store the reaction rate propensity matrices, memory is pre-allocated for each compartment at the start of the simulation. To prevent frequent copying of the large reaction propensity matrices, the fusion and fragmentation of compartments are simulated using pointer variables. This approximation of compartment dynamics as discrete Smoluchowski aggregation-fragmentation dynamics, combined with

the conservation of total organelle mass, provides a substantial speed up of the simulation run time. While allowing the full stochastic simulation of Master-Equation Eq. (5.16), this numerical routine has a poor scaling with the system size, setting bounds on the numerical investigation of systems with large total aggregate mass. As the total aggregate mass increases, the number of possible reactions is increased and the time-step of an individual update step is reduced. The former effect increases the run time for each update step, while the latter necessitates the increase in total number of updating steps required to reach a specified final time, thus resulting in strongly increased run times when larger systems are analysed.

We initiate a dynamic and synchronous ensemble by first performing temporal evolution in the configuration of fully fused compartments. To improve the statistics, we create multiple sets of data from simulations runs, combining the statistics from different time points with a difference of $\Delta t \gg \tau_r$ that is much larger than the system's auto-correlation time. We pay particular attention to ensure that the statistics are not quantitatively affected by this procedure.

B.3. Routine for the efficient numerical investigation of finite-sized ideal gas ensembles

There are different options for simulating an ideal gas in the context of dynamic compartmentalisation. The most prominent choice is simulating a 2D hard disk gas in a rectangular chamber by solving the equations of motion for each particle in the ensemble. While coding this implementation of the problem is feasible, the model does indeed show the full dynamics in both the concentration and volume phase space and provides beautiful visualizations as a bonus. However, these simulations quickly become computationally expensive and require a long run time to ensure relaxation to equilibrium. Furthermore, as we want to map out the statistics of the ensemble, we need a large number of repetitions of these simulations. Under these constraints, simulating the full dynamics is not an ideal choice.

As we introduced in section 4.3.2, for sequential fragmentation s_{seq} , we set the timescale of partition insertion be much larger than the relaxation timescale, $\Delta t \tau$. To speed up the simulations by orders of magnitude, we make use of the statistics derived in the previous section 4.4.2: instead of simulating the time evolution, we directly sample the statistics from a Dirichlet distribution. In fact, [216] showed that the statistics of molecular dynamics simulations of hard sphere gases can be captured by the statistics derived in section 4.4.2. The algorithms for sequential fragmentation (s_{seq}) and synchronous frag-

Algorithm 1 Synchronous fragmentation

```

1: function FRAGSYNC( $\vec{E}, N$ )      ▷  $\vec{E}$ : energy vector of size  $\mathcal{N}$ ;  $N$ : number of rooms.
2:    $M \leftarrow \{(\mathcal{E}_i, \mathcal{N}_i) \leftarrow (0, 0)\}$     ▷ Initialise the system.  $M$ : list of compartments.
3:   for  $i \leftarrow 1$  to  $\mathcal{N}$  do                ▷ Assign particles to random compartments.
4:      $u \sim U(0, 1)$ 
5:     find  $\mu$  the smallest integer, such that  $u < \sum_{k=1}^{\mu} \frac{1}{N}$ 
6:      $\mathcal{N}_{\mu} \leftarrow \mathcal{N}_{\mu} + 1$ 
7:      $\mathcal{E}_{\mu} \leftarrow \mathcal{E}_{\mu} + E_i$ 
8:   return  $M$ 

```

Algorithm 2 Sequential fragmentation

```

1: function BINOMSPLIT( $\vec{E}$ ,  $p$ )           ▷  $\vec{E}$ : energy vector;  $p$ : splitting probability.
2:    $(\mathcal{E}_1, \mathcal{N}_1), (\mathcal{E}_2, \mathcal{N}_2) \leftarrow (0, 0), (0, 0)$            ▷ Initialise the system.
3:   for  $i \leftarrow 1$  to  $\mathcal{N}$  do           ▷ Assign particles to random compartments.
4:      $u \sim U(0, 1)$ 
5:     if  $u \leq p$  then
6:        $\mathcal{N}_1 \leftarrow \mathcal{N}_1 + 1$ 
7:        $\mathcal{E}_1 \leftarrow \mathcal{E}_1 + E_i$ 
8:     else
9:        $\mathcal{N}_2 \leftarrow \mathcal{N}_2 + 1$ 
10:       $\mathcal{E}_2 \leftarrow \mathcal{E}_2 + E_i$ 
11:   return  $(\mathcal{E}_1, \mathcal{N}_1), (\mathcal{E}_2, \mathcal{N}_2)$ 
12:
13: function FRAGSEQU( $\vec{E}, N$ )           ▷  $\vec{E}$ : energy vector of size  $\mathcal{N}$ ;  $N$ : number of rooms.
14:    $M \leftarrow \{(\mathcal{E}_i, \mathcal{N}_i) \leftarrow (0, 0)\}$            ▷ Initialise the system.  $M$ : list of compartments.
15:    $(\mathcal{E}_I, \mathcal{N}_I) \leftarrow (E, \mathcal{N})$            ▷ Initialise the intermediate macrostate  $I$ 
16:   for  $i \leftarrow 1$  to  $N$  do
17:      $p \leftarrow \frac{i}{N}$ 
18:     sample a microstate  $\vec{E}$  that corresponds to macrostate  $I$ 
19:      $(\mathcal{E}_i, \mathcal{N}_i), (\mathcal{E}_I, \mathcal{N}_I) \leftarrow \text{BINOMSPLIT}(\vec{E}, p)$ 
20:   return  $M$ 

```

mentation (s_{syn}) are given in Alg.1 and Alg.2, respectively. Note, that both algorithms can be straightforwardly generalised from the setting of the ideal gas to general stochastic many-body dynamics.

List of Figures

1.1.	Self-similarity of inanimate matter	2
1.2.	Organelles compartmentalise the interior of cells	4
1.3.	The functioning of living matter relies on the interplay between dynamics on different scales	5
1.4.	Difference between open and closed compartmentalised systems	8
2.1.	Schematic illustration of compartment dynamics	15
2.2.	Illustration of the multi-scale organisation of compartmentalised systems .	21
2.3.	Graphical illustration of the fusion flux approximation	24
2.4.	The fusion flux approximation is corroborated by full stochastic simulations	28
2.5.	Accounting for finite fragmentation rates in the fusion flux approximation .	32
2.6.	Compartment fusion and fragmentation gives rise to quasi-particle like state	41
2.7.	Dynamics of the quasi-particle in the concentration phase space	42
2.8.	Mechanic analogue of the quasi-particle	48
2.9.	The quasi-particle exhibits altered kinetic properties	50
3.1.	Schematic of a signalling pathway	57
3.2.	Mitochondria inside a cell shows as multiple compartments	60
3.3.	Schematic of the Bcl-2 reaction network	61
3.4.	The Bax accumulation dynamics are effectively captured by a bistable po- tential	64
3.5.	Effective model of the intrinsic apoptotic signalling pathway	67
3.6.	Comparison of Bcl-2 reaction kinetics between simulated and experimental timescales	68
3.7.	Mitochondrial dynamics give rise to a localisation of the apoptotic sig- nalling pathway in the concentration phase space	70
3.8.	Graphical analysis of the equations of motion for the quasi-particle	71
3.9.	Simulation of system's response to strong and weak apoptotic stimuli . . .	73
3.10.	The equations of motion for the quasi-particle agrees with full stochastic simulations	75
3.11.	Sigmoidal relaxation dynamics are robust to accounting for the degradation of mitochondria	76
3.12.	Sigmoidal relaxation kinetics give rise to a kinetic low-pass filter	79
3.13.	Mitochondrial dynamics improve the quality of apoptotic decision-making .	82
3.14.	Observing the sigmoidal progression of apoptosis in cell culture experiments	89
4.1.	Dynamic compartmentalisation gives rise to the creation and preservation density fluctuation	98
4.2.	A single particle system subject to a cyclic process	102
4.3.	Illustration of Gibbs' paradox	103
4.4.	Schematic of Maxwell's demon	106

List of Figures

4.5. Connection between compartment fusion and fragmentation and barrier insertion	107
4.6. Time protocols for the fragmentation of multiple compartments	110
4.7. Comparing synchronous and sequential fragmentation for an ideal gas . . .	117
4.8. Sequential fragmentation of an ideal gas with varying total particle number	118
4.9. Sequential fragmentation of an ideal gas in systems with varying total compartment number	119
4.10. Quantised gases with two body interaction rules respecting detailed balance are unaffected by sequential fragmentation	135
4.11. Sequential fragmentation affects chemical reaction systems with reaction rates independent of the fragmentation process	139
4.12. The effects of sequential fragmentation on chemical reaction systems vanishes for rescaled aggregation rates	144
4.13. The effects of sequential fragmentation on chemical reaction systems with broken detailed balance do not vanish for rescaled aggregation rates	147
4.14. System size dependence of the effect of sequential fragmentation	149
4.15. Quantised gases with globally coupled reaction rates are affected by sequential fragmentation processes	150
4.16. Sequential compartmentalisation affects the statistics of total energy per compartment	151
4.17. Experimental setups for investigating dynamic compartmentalisation . . .	153
5.1. Compartment fusion and fragmentation facilitate the formation of large aggregates	169
5.2. The density fluctuations among compartments show a power-law decay . .	171
5.3. The qualitative findings are robust to variations in the aggregation parameter	172
5.4. Compartment fusion and fragmentation affect the stability of large aggregates	173
5.5. Increasing the aggregation parameter results in larger aggregates	174
5.6. Systematic scanning of polymerisation kernels reveals region in the model space where compartment dynamics facilitate the formation of large aggregates	176
5.7. Schematic of a feedback loop giving rise to the facilitated formation of large aggregates	177
5.8. Increasing the number of compartments facilitates the formation of large aggregates	180
5.9. System size scaling shows scaling characteristics of gelation	181
5.10. Schematic of RIG-I pathway	183
5.11. Inhibition of mitochondrial fusion prevents MAVS mediated ant-viral responses	184

Bibliography

- [1] *Encyclopaedia Britannica*. Encyclopaedia Britannica, Chicago, Ill., 2004. ISBN 978-0-85229-066-8.
- [2] J. L. E. Dreyer. *A History of Astronomy from Thales to Kepler*. Dover Publications Inc., New York, N.Y, new ed edition edition, June 1953. ISBN 978-0-486-60079-6.
- [3] Geoffrey Gorham, Benjamin Hill, Edward Slowik, and C. Kenneth Waters. *Language of Nature: Reassessing the Mathematization of Natural Philosophy in the Seventeenth Century*. University of Minnesota Press, Minneapolis (Minn.), illustriert edition, June 2016. ISBN 978-0-8166-9950-6.
- [4] Max Planck. *The Philosophy of Physics*. Minkowski Institute Press, November 2019. ISBN 978-1-927763-62-9.
- [5] Steven H. Strogatz. *Nonlinear Dynamics and Chaos: With Applications to Physics, Biology, Chemistry, and Engineering: With Applications to Physics, Biology, Chemistry, and ... Second Edition*. Westview Press, Boulder, CO, 2 edition, July 2014. ISBN 978-0-8133-4910-7.
- [6] Richard C. Tolman. *The Principles of Statistical Mechanics*. Dover Publications Inc., New York, new ed edition edition, November 1979. ISBN 978-0-486-63896-6.
- [7] A. Khinchin. *Mathematical Foundations of Statistical Mechanics*. Martino Fine Books, June 2014. ISBN 978-1-61427-642-5.
- [8] R. Kubo. The fluctuation-dissipation theorem. *Rep. Prog. Phys.*, 29(1):255, January 1966. ISSN 0034-4885. doi: 10.1088/0034-4885/29/1/306.
- [9] L. D. Landau and E. M. Lifshitz. *Statistical Physics, Part 1*. Pergamon Press, Oxford ; New York, 3 edition, January 1980. ISBN 978-0-08-023038-2.
- [10] J. B. Johnson. Thermal Agitation of Electricity in Conductors. *Phys. Rev.*, 32(1):97–109, July 1928. doi: 10.1103/PhysRev.32.97. Publisher: American Physical Society.
- [11] Joseph G. Hoffman. The fluctuation dissipation theorem. *Physics Today*, 15(1):30–36, January 1962. ISSN 0031-9228. doi: 10.1063/1.3057971. Publisher: American Institute of Physics.
- [12] Andrei Nikolaevich Kolmogorov, V. Levin, Julian Charles Roland Hunt, Owen Martin Phillips, and David Williams. Dissipation of energy in the locally isotropic turbulence. *Proceedings of the Royal Society of London. Series A: Mathematical and Physical Sciences*, 434(1890):15–17, January 1997. doi: 10.1098/rspa.1991.0076. Publisher: Royal Society.
- [13] Stephen B. Pope. *Turbulent Flows*. Cambridge University Press, Cambridge ; New York, new edition edition, August 2000. ISBN 978-0-521-59886-6.
- [14] Arkady Tsinober. *The Essence of Turbulence as a Physical Phenomenon: With Emphasis on Issues of Paradigmatic Nature*. Springer, New York, NY, 2nd ed. 2019 edition edition, January 2019. ISBN 978-3-319-99530-4.
- [15] J. M. Yeomans. *Statistical Mechanics of Phase Transitions*. Clarendon Press, Oxford England : New York, 1st edition edition, June 1992. ISBN 978-0-19-851730-6.
- [16] Nigel Goldenfeld. *Lectures On Phase Transitions And The Renormalization Group*. CRC Press, Boca Raton, June 2019. ISBN 978-0-429-49349-2. doi: 10.1201/9780429493492.
- [17] Alexander Altland and Ben D. Simons. *Condensed Matter Field Theory*. Cambridge University Press, Cambridge ; New York, 2 edition, 2010. ISBN 978-0-521-76975-4.

Bibliography

- [18] Leo Kadanoff, Wolfgang Goetz, David Hamblen, Robert Hecht, E. A. S. Lewis, V. V. Palciauskas, Martin Rayl, J. Swift, David Aspnes, and Joseph Kane. Static Phenomena Near Critical Points: Theory and Experiment. *Rev. Mod. Phys.*, 39(2):395–431, April 1967. doi: 10.1103/RevModPhys.39.395. Publisher: American Physical Society.
- [19] C. Fukushima and J. Westerweel. English: This picture is a false-color image of the far-field of a submerged turbulent jet, made visible by means of laser induced fluorescence (LIF)., November 2007. The Technical University of Delft, https://commons.wikimedia.org/wiki/File:False_color_image_of_the_far_field_of_a_submerged_turbulent_jet.jpg.
- [20] Damian Owls. English: Ising model very near the critical temperature. Note the fractal structure of the domains - a signature of scale invariance as the correlation length diverges. The longevity of structures is a result of the divergence of the correlation time., December 2020. https://commons.wikimedia.org/wiki/File:Ising_Criticality2.gif.
- [21] Robert H. Swendsen. *Swendsen, R: Introduction to Statistical Mechanics and Therm.* OUP Oxford, Oxford ; New York, 2012. ISBN 978-0-19-964694-4.
- [22] Lars Onsager. Reciprocal Relations in Irreversible Processes. I. *Phys. Rev.*, 37(4):405–426, February 1931. doi: 10.1103/PhysRev.37.405. Publisher: American Physical Society.
- [23] Robert Zwanzig. *Nonequilibrium Statistical Mechanics.* Oxford University Press, Oxford ; New York, 1st edition edition, April 2001. ISBN 978-0-19-514018-7.
- [24] Ilya Prigogine. *Non-Equilibrium Statistical Mechanics.* Dover Publications Inc., Mineola, New York, reprint edition edition, April 2017. ISBN 978-0-486-81555-8.
- [25] Miroslav Grmela. Thermodynamics of driven systems. *Phys. Rev. E*, 48(2):919–930, August 1993. doi: 10.1103/PhysRevE.48.919. Publisher: American Physical Society.
- [26] S. C. Takatori and J. F. Brady. Towards a thermodynamics of active matter. *Phys. Rev. E*, 91(3):032117, March 2015. doi: 10.1103/PhysRevE.91.032117. Publisher: American Physical Society.
- [27] Thomas Speck. Stochastic thermodynamics for active matter. *EPL*, 114(3):30006, June 2016. ISSN 0295-5075. doi: 10.1209/0295-5075/114/30006. Publisher: EDP Sciences, IOP Publishing and Societ  Italiana di Fisica.
- [28] Frank Juelicher, Stephan W. Grill, and Guillaume Salbreux. Hydrodynamic theory of active matter. *Rep. Prog. Phys.*, 81(7):076601, June 2018. ISSN 0034-4885. doi: 10.1088/1361-6633/aab6bb. Publisher: IOP Publishing.
- [29] Etienne Fodor, Cesare Nardini, Michael E. Cates, Julien Tailleur, Paolo Visco, and Frederic van Wijland. How Far from Equilibrium Is Active Matter? *Phys. Rev. Lett.*, 117(3):038103, July 2016. doi: 10.1103/PhysRevLett.117.038103. Publisher: American Physical Society.
- [30] Neil Thomas, Yasuhiro Imafuku, and Katsuhisa Tawada. Molecular motors: thermodynamics and the random walk. *Proceedings of the Royal Society of London. Series B: Biological Sciences*, 268(1481):2113–2122, October 2001. doi: 10.1098/rspb.2001.1764. Publisher: Royal Society.
- [31] John Toner and Yuhai Tu. Flocks, herds, and schools: A quantitative theory of flocking. *Phys. Rev. E*, 58(4):4828–4858, October 1998. doi: 10.1103/PhysRevE.58.4828. Publisher: American Physical Society.
- [32] Cesare Nardini, Etienne Fodor, Elsen Tjhung, Fr d ric van Wijland, Julien Tailleur, and Michael E. Cates. Entropy Production in Field Theories without Time-Reversal Symmetry: Quantifying the Non-Equilibrium Character of Active Matter. *Phys. Rev. X*, 7(2):021007, April 2017. doi: 10.1103/PhysRevX.7.021007. Publisher: American Physical Society.
- [33] M. C. Marchetti, J. F. Joanny, S. Ramaswamy, T. B. Liverpool, J. Prost, Madan Rao, and R. Aditi Simha. Hydrodynamics of soft active matter. *Rev. Mod. Phys.*, 85(3):1143–1189, July 2013. doi: 10.1103/RevModPhys.85.1143. Publisher: American Physical Society.

- [34] Lennart Dabelow, Stefano Bo, and Ralf Eichhorn. Irreversibility in Active Matter Systems: Fluctuation Theorem and Mutual Information. *Phys. Rev. X*, 9(2):021009, April 2019. doi: 10.1103/PhysRevX.9.021009. Publisher: American Physical Society.
- [35] Tamas Vicsek, Andras Czirok, Eshel Ben-Jacob, Inon Cohen, and Ofer Shochet. Novel Type of Phase Transition in a System of Self-Driven Particles. *Phys. Rev. Lett.*, 75(6):1226–1229, August 1995. doi: 10.1103/PhysRevLett.75.1226. Publisher: American Physical Society.
- [36] Jacob Klein and Eugenia Kumacheva. Confinement-Induced Phase Transitions in Simple Liquids. *Science*, 269(5225):816–819, August 1995. doi: 10.1126/science.269.5225.816. Publisher: American Association for the Advancement of Science.
- [37] Nancy R. Gough. Emerging roles for organelles in cellular regulation. *Science Signaling*, 9(457):eg11–eg11, December 2016. doi: 10.1126/scisignal.aal4031. Publisher: American Association for the Advancement of Science.
- [38] Tatjana Kleine and Dario Leister. Retrograde signaling: Organelles go networking. *Biochimica et Biophysica Acta (BBA) - Bioenergetics*, 1857(8):1313–1325, August 2016. ISSN 0005-2728. doi: 10.1016/j.bbabi.2016.03.017.
- [39] Kelvinsong. English: A reworked version of File:Biological_cell.svg., December 2012. https://commons.wikimedia.org/wiki/File:Animal_Cell.svg.
- [40] Gary A. Clawson, Gail L. Matters, Ping Xin, Christopher McGovern, Eric Wafula, Claude de-Pamphilis, Morgan Meckley, Joyce Wong, Luke Stewart, Christopher D’Jamoos, Naomi Altman, Yuka Imamura Kawasawa, Zhen Du, Loren Honaas, and Thomas Abraham. "Stealth dissemination" of macrophage-tumor cell fusions cultured from blood of patients with pancreatic ductal adenocarcinoma. *PLOS ONE*, 12(9):e0184451, September 2017. ISSN 1932-6203. doi: 10.1371/journal.pone.0184451. Publisher: Public Library of Science.
- [41] Florian J. Bock and Stephen W. G. Tait. Mitochondria as multifaceted regulators of cell death. *Nat Rev Mol Cell Biol*, 21(2):85–100, February 2020. ISSN 1471-0080. doi: 10.1038/s41580-019-0173-8. Number: 2 Publisher: Nature Publishing Group.
- [42] Denise Pumain, editor. *Hierarchy in Natural and Social Sciences*. Springer, Dordrecht, The Netherlands, 2006th edition edition, November 2005. ISBN 978-1-4020-4126-6.
- [43] Andre Pires-daSilva and Ralf J. Sommer. The evolution of signalling pathways in animal development. *Nat Rev Genet*, 4(1):39–49, January 2003. ISSN 1471-0064. doi: 10.1038/nrg977. Number: 1 Publisher: Nature Publishing Group.
- [44] Cole Trapnell, Davide Cacchiarelli, Jonna Grimsby, Prapti Pokharel, Shuqiang Li, Michael Morse, Niall J. Lennon, Kenneth J. Livak, Tarjei S. Mikkelsen, and John L. Rinn. The dynamics and regulators of cell fate decisions are revealed by pseudotemporal ordering of single cells. *Nat Biotechnol*, 32(4):381–386, April 2014. ISSN 1546-1696. doi: 10.1038/nbt.2859. Number: 4 Publisher: Nature Publishing Group.
- [45] Jonathan A Griffiths, Antonio Scialdone, and John C Marioni. Using single-cell genomics to understand developmental processes and cell fate decisions. *Molecular Systems Biology*, 14(4):e8046, April 2018. ISSN 1744-4292. doi: 10.15252/msb.20178046. Publisher: John Wiley & Sons, Ltd.
- [46] Kathryn N. Ivey and Deepak Srivastava. MicroRNAs as Regulators of Differentiation and Cell Fate Decisions. *Cell Stem Cell*, 7(1):36–41, July 2010. ISSN 1934-5909. doi: 10.1016/j.stem.2010.06.012.
- [47] Jenny Hsieh and Fred H Gage. Epigenetic control of neural stem cell fate. *Current Opinion in Genetics & Development*, 14(5):461–469, October 2004. ISSN 0959-437X. doi: 10.1016/j.gde.2004.07.006.
- [48] Victoria V. Lunyak and Michael G. Rosenfeld. Epigenetic regulation of stem cell fate. *Human Molecular Genetics*, 17(R1):R28–R36, April 2008. ISSN 0964-6906. doi: 10.1093/hmg/ddn149.

Bibliography

- [49] Yan Zhang and Kim L. Good-Jacobson. Epigenetic regulation of B cell fate and function during an immune response. *Immunological Reviews*, 288(1):75–84, 2019. ISSN 1600-065X. doi: 10.1111/imr.12733. _eprint: <https://onlinelibrary.wiley.com/doi/pdf/10.1111/imr.12733>.
- [50] Allon M. Klein, Linas Mazutis, Ilke Akartuna, Naren Tallapragada, Adrian Veres, Victor Li, Leonid Peshkin, David A. Weitz, and Marc W. Kirschner. Droplet Barcoding for Single-Cell Transcriptomics Applied to Embryonic Stem Cells. *Cell*, 161(5):1187–1201, May 2015. ISSN 0092-8674. doi: 10.1016/j.cell.2015.04.044.
- [51] Sabrina M. Lewis, Marie-Liesse Asselin-Labat, Quan Nguyen, Jean Berthelet, Xiao Tan, Verena C. Wimmer, Delphine Merino, Kelly L. Rogers, and Shalin H. Naik. Spatial omics and multiplexed imaging to explore cancer biology. *Nat Methods*, 18(9):997–1012, September 2021. ISSN 1548-7105. doi: 10.1038/s41592-021-01203-6. Number: 9 Publisher: Nature Publishing Group.
- [52] Yong Wang and Nicholas E. Navin. Advances and Applications of Single-Cell Sequencing Technologies. *Molecular Cell*, 58(4):598–609, May 2015. ISSN 1097-2765. doi: 10.1016/j.molcel.2015.05.005.
- [53] Rebecca Heald and Orna Cohen-Fix. Morphology and function of membrane-bound organelles. *Current Opinion in Cell Biology*, 26:79–86, February 2014. ISSN 0955-0674. doi: 10.1016/j.ccb.2013.10.006.
- [54] Navdeep S. Chandel. Mitochondria as signaling organelles. *BMC Biology*, 12(1):34, May 2014. ISSN 1741-7007. doi: 10.1186/1741-7007-12-34.
- [55] Jonathan C. Kagan. Signaling Organelles of the Innate Immune System. *Cell*, 151(6):1168–1178, December 2012. ISSN 0092-8674. doi: 10.1016/j.cell.2012.11.011.
- [56] Halime Kalkavan and Douglas R Green. MOMP, cell suicide as a BCL-2 family business. *Cell Death Differ*, 25(1):46–55, January 2018. ISSN 1350-9047. doi: 10.1038/cdd.2017.179.
- [57] Rashu B. Seth, Lijun Sun, Chee-Kwee Ea, and Zhijian J. Chen. Identification and Characterization of MAVS, a Mitochondrial Antiviral Signaling Protein that Activates NF- κ B and IRF3. *Cell*, 122(5):669–682, September 2005. ISSN 0092-8674. doi: 10.1016/j.cell.2005.08.012.
- [58] Stephanie Bleicken, Olatz Landeta, Ane Landajuela, Gorka Basanez, and Ana J. Garcia-Saez. Proapoptotic Bax and Bak Proteins Form Stable Protein-permeable Pores of Tunable Size. *Journal of Biological Chemistry*, 288(46):33241–33252, November 2013. ISSN 0021-9258. doi: 10.1074/jbc.M113.512087.
- [59] Laura M. Westrate, Jeffrey A. Drocco, Katie R. Martin, William S. Hlavacek, and Jeffrey P. MacKegan. Mitochondrial Morphological Features Are Associated with Fission and Fusion Events. *PLoS ONE*, 9(4):e95265, April 2014. ISSN 1932-6203. doi: 10.1371/journal.pone.0095265. Publisher: Public Library of Science.
- [60] O. Guillery, F. Malka, P. Frachon, D. Milea, M. Rojo, and A. Lombès. Modulation of mitochondrial morphology by bioenergetics defects in primary human fibroblasts. *Neuromuscul. Disord.*, 18(4):319–330, April 2008. ISSN 0960-8966. doi: 10.1016/j.nmd.2007.12.008.
- [61] Michal Cagalinec, Dzhamilja Safiulina, Mailis Liiv, Joanna Liiv, Vinay Choubey, Przemyslaw Wareski, Vladimir Veksler, and Allen Kaasik. Principles of the mitochondrial fusion and fission cycle in neurons. *J Cell Sci*, 126(10):2187–2197, May 2013. ISSN 0021-9533, 1477-9137. doi: 10.1242/jcs.118844. Publisher: The Company of Biologists Ltd Section: Research Article.
- [62] Veronica Eisner, Guy Lenaers, and Gyoergy Hajnoczky. Mitochondrial fusion is frequent in skeletal muscle and supports excitation-contraction coupling. *Journal of Cell Biology*, 205(2):179–195, April 2014. ISSN 0021-9525. doi: 10.1083/jcb.201312066.
- [63] Veronica Eisner, Ryan R. Cupo, Erhe Gao, Gyoergy Csordas, William S. Slovinsky, Melanie Pailard, Lan Cheng, Jessica Ibeti, S. R. Wayne Chen, J. Kurt Chuprun, Jan B. Hoek, Walter J. Koch, and Gyoergy Hajnoczky. Mitochondrial fusion dynamics is robust in the heart and depends on calcium oscillations and contractile activity. *Proceedings of the National Academy of Sciences*,

- 114(5):E859–E868, January 2017. doi: 10.1073/pnas.1617288114. Publisher: Proceedings of the National Academy of Sciences.
- [64] Vitaly A. Selivanov, Tatyana V. Votyakova, Jennifer A. Zeak, Massimo Trucco, Josep Roca, and Marta Cascante. Bistability of Mitochondrial Respiration Underlies Paradoxical Reactive Oxygen Species Generation Induced by Anoxia. *PLoS Comput Biol*, 5(12):e1000619, December 2009. ISSN 1553-734X. doi: 10.1371/journal.pcbi.1000619.
- [65] Vitaly A. Selivanov, Marta Cascante, Mark Friedman, Mark F. Schumaker, Massimo Trucco, and Tatyana V. Votyakova. Multistationary and Oscillatory Modes of Free Radicals Generation by the Mitochondrial Respiratory Chain Revealed by a Bifurcation Analysis. *PLOS Computational Biology*, 8(9):e1002700, September 2012. ISSN 1553-7358. doi: 10.1371/journal.pcbi.1002700. Publisher: Public Library of Science.
- [66] Liron Bar-Peled and David M. Sabatini. Regulation of mTORC1 by amino acids. *Trends in Cell Biology*, 24(7):400–406, July 2014. ISSN 0962-8924. doi: 10.1016/j.tcb.2014.03.003.
- [67] Suchithra Menon, Christian C. Dibble, George Talbott, Gerta Hoxhaj, Alexander J. Valvezan, Hidenori Takahashi, Lewis C. Cantley, and Brendan D. Manning. Spatial Control of the TSC Complex Integrates Insulin and Nutrient Regulation of mTORC1 at the Lysosome. *Cell*, 156(4):771–785, February 2014. ISSN 0092-8674. doi: 10.1016/j.cell.2013.11.049.
- [68] Kazuhide Onoguchi, Koji Onomoto, Shiori Takamatsu, Michihiko Jogi, Azumi Takemura, Shiho Morimoto, Ilkka Julkunen, Hideo Namiki, Mitsutoshi Yoneyama, and Takashi Fujita. Virus-Infection or 5’ppp-RNA Activates Antiviral Signal through Redistribution of IPS-1 Mediated by MFN1. *PLOS Pathogens*, 6(7):e1001012, July 2010. ISSN 1553-7374. doi: 10.1371/journal.ppat.1001012. Publisher: Public Library of Science.
- [69] Peter S. Swain, Michael B. Elowitz, and Eric D. Siggia. Intrinsic and extrinsic contributions to stochasticity in gene expression. *Proceedings of the National Academy of Sciences*, 99(20):12795–12800, October 2002. doi: 10.1073/pnas.162041399. Publisher: Proceedings of the National Academy of Sciences.
- [70] Johan Elf and Mans Ehrenberg. Fast Evaluation of Fluctuations in Biochemical Networks With the Linear Noise Approximation. *Genome Res.*, 13(11):2475–2484, November 2003. ISSN 1088-9051, 1549-5469. doi: 10.1101/gr.1196503. Company: Cold Spring Harbor Laboratory Press Distributor: Cold Spring Harbor Laboratory Press Institution: Cold Spring Harbor Laboratory Press Label: Cold Spring Harbor Laboratory Press Publisher: Cold Spring Harbor Lab.
- [71] Erhan Cinlar. *Introduction to Stochastic Processes*. Dover Publications, Mineola, New York, illustrated edition edition, February 2013. ISBN 978-0-486-49797-6.
- [72] Lorenzo Duso and Christoph Zechner. Stochastic reaction networks in dynamic compartment populations. *Proceedings of the National Academy of Sciences*, 117(37):22674–22683, September 2020. doi: 10.1073/pnas.2003734117. Publisher: Proceedings of the National Academy of Sciences.
- [73] Lionel Foret, Jonathan E. Dawson, Roberto Villasenor, Claudio Collinet, Andreas Deutsch, Lutz Brusch, Marino Zerial, Yannis Kalaidzidis, and Frank Juelicher. A General Theoretical Framework to Infer Endosomal Network Dynamics from Quantitative Image Analysis. *Current Biology*, 22(15):1381–1390, August 2012. ISSN 0960-9822. doi: 10.1016/j.cub.2012.06.021.
- [74] A. D. Randolph and E. T. White. Modeling size dispersion in the prediction of crystal-size distribution. *Chemical Engineering Science*, 32(9):1067–1076, January 1977. ISSN 0009-2509. doi: 10.1016/0009-2509(77)80144-9.
- [75] Doraiswami Ramkrishna and Meenesh R. Singh. Population Balance Modeling: Current Status and Future Prospects. *Annual Review of Chemical and Biomolecular Engineering*, 5(1):123–146, 2014. doi: 10.1146/annurev-chembioeng-060713-040241. _eprint: <https://doi.org/10.1146/annurev-chembioeng-060713-040241>.

Bibliography

- [76] Marco Millies and Dieter Mewes. Interfacial area density in bubbly flow. *Chemical Engineering and Processing: Process Intensification*, 38(4):307–319, September 1999. ISSN 0255-2701. doi: 10.1016/S0255-2701(99)00022-7.
- [77] S. Rigopoulos. Population balance modelling of polydispersed particles in reactive flows. *Progress in Energy and Combustion Science*, 36(4):412–443, August 2010. ISSN 0360-1285. doi: 10.1016/j.pecs.2009.12.001.
- [78] P. W. Anderson. More Is Different. *Science*, 177(4047):393–396, August 1972. doi: 10.1126/science.177.4047.393. Publisher: American Association for the Advancement of Science.
- [79] Philip W. Anderson. *Basic Notions Of Condensed Matter Physics*. CRC Press, March 2018. ISBN 978-0-429-97374-1. Google-Books-ID: 9HhQDwAAQBAJ.
- [80] J. M. Ziman. *Principles of the Theory of Solids*. Cambridge University Press, Cambridge, 2 edition, 1972. ISBN 978-0-521-29733-2. doi: 10.1017/CBO9781139644075.
- [81] Tom Lancaster. *The Emergence of Excitations in Quantum Fields*. Routledge Handbooks Online, March 2019. ISBN 978-1-138-92508-3 978-1-315-67521-3. doi: 10.4324/9781315675213-23.
- [82] Luciano Pietronero. Complexity ideas from condensed matter and statistical physics. *Europhysics News*, 39(6):26–29, November 2008. ISSN 0531-7479, 1432-1092. doi: 10.1051/epn:2008603. Number: 6 Publisher: EDP Sciences.
- [83] Daniel T. Gillespie. The chemical Langevin equation. *J. Chem. Phys.*, 113(1):297–306, July 2000. ISSN 0021-9606. doi: 10.1063/1.481811. Publisher: American Institute of Physics.
- [84] Ramon Grima, Philipp Thomas, and Arthur V. Straube. How accurate are the nonlinear chemical Fokker-Planck and chemical Langevin equations? *J. Chem. Phys.*, 135(8):084103, August 2011. ISSN 0021-9606. doi: 10.1063/1.3625958. Publisher: American Institute of Physics.
- [85] Lucy Ham, Megan A. Coomer, and Michael P. H. Stumpf. The chemical Langevin equation for biochemical systems in dynamic environments. *J. Chem. Phys.*, 157(9):094105, September 2022. ISSN 0021-9606. doi: 10.1063/5.0095840. Publisher: American Institute of Physics.
- [86] Alessandro Ceccato and Diego Frezzato. Remarks on the chemical Fokker-Planck and Langevin equations: Nonphysical currents at equilibrium. *J. Chem. Phys.*, 148(6):064114, February 2018. ISSN 0021-9606. doi: 10.1063/1.5016158. Publisher: American Institute of Physics.
- [87] Federico Sporleder, Zsolt Borka, Jannike Solsvik, and Hugo A. Jakobsen. On the population balance equation. *Reviews in Chemical Engineering*, 28(2-3):149–169, July 2012. ISSN 2191-0235. doi: 10.1515/revce-2011-0013. Publisher: De Gruyter.
- [88] M. V. Smoluchowski. Drei Vortrage uber Diffusion, Brownsche Bewegung und Koagulation von Kolloidteilchen. *Zeitschrift fur Physik*, 17:557–585, January 1916. ADS Bibcode: 1916ZPhy...17..557S.
- [89] Hugo A. Jakobsen. *Chemical Reactor Modeling: Multiphase Reactive Flows*. Springer, Cham, 2nd ed. 2014 edition edition, April 2014. ISBN 978-3-319-05091-1.
- [90] Mark Z. Jacobson. *Fundamentals of Atmospheric Modeling*. Cambridge University Press, Cambridge, 2 edition, 2005. ISBN 978-0-521-54865-6. doi: 10.1017/CBO9781139165389.
- [91] Marco Lattuada, Alessio Zaccone, Hua Wu, and Massimo Morbidelli. Population-balance description of shear-induced clustering, gelation and suspension viscosity in sheared DLVO colloids. *Soft Matter*, 12(24):5313–5324, June 2016. ISSN 1744-6848. doi: 10.1039/C6SM01097K. Publisher: The Royal Society of Chemistry.
- [92] Gerardo Odriozola. Ion-specific colloidal aggregation: Population balance equations and potential of mean force. *J. Chem. Phys.*, 135(13):134704, October 2011. ISSN 0021-9606. doi: 10.1063/1.3644769. Publisher: American Institute of Physics.

- [93] Venkataramana Runkana, P. Somasundaran, and P. C. Kapur. A population balance model for flocculation of colloidal suspensions by polymer bridging. *Chemical Engineering Science*, 61(1):182–191, January 2006. ISSN 0009-2509. doi: 10.1016/j.ces.2005.01.046.
- [94] Steffen Waldherr. Estimation methods for heterogeneous cell population models in systems biology. *Journal of The Royal Society Interface*, 15(147):20180530, October 2018. doi: 10.1098/rsif.2018.0530. Publisher: Royal Society.
- [95] Mostafa Adimy, Fabien Crauste, and Shigui Ruan. A Mathematical Study of the Hematopoiesis Process with Applications to Chronic Myelogenous Leukemia. *SIAM J. Appl. Math.*, 65(4):1328–1352, January 2005. ISSN 0036-1399. doi: 10.1137/040604698. Publisher: Society for Industrial and Applied Mathematics.
- [96] Che-Chi Shu, Anushree Chatterjee, Wei-Shou Hu, and Doraiswami Ramkrishna. Role of Intracellular Stochasticity in Biofilm Growth. Insights from Population Balance Modeling. *PLOS ONE*, 8(11):e79196, November 2013. ISSN 1932-6203. doi: 10.1371/journal.pone.0079196. Publisher: Public Library of Science.
- [97] Niccolo Totis, Cesar Nieto, Armin Kueper, Cesar Vargas-Garcia, Abhyudai Singh, and Steffen Waldherr. Cell size statistics in cell lineages and population snapshots with different growth regimes and division strategies, May 2020. Pages: 2020.05.15.094698 Section: New Results.
- [98] Jincheng Wu and Emmanuel S. Tzanakakis. Distinct Allelic Patterns of Nanog Expression Impart Embryonic Stem Cell Population Heterogeneity. *PLOS Computational Biology*, 9(7):e1003140, July 2013. ISSN 1553-7358. doi: 10.1371/journal.pcbi.1003140. Publisher: Public Library of Science.
- [99] Pavel L. Krapivsky, Sidney Redner, and Eli Ben-Naim. *A Kinetic View of Statistical Physics*. Cambridge University Press, Cambridge, 2010. ISBN 978-0-521-85103-9. doi: 10.1017/CBO9780511780516.
- [100] Samlesh Choudhury, Vaishnavi Ananthanarayanan, and K. GanapathyÂ Ayappa. Coupling of mitochondrial population evolution to microtubule dynamics in fission yeast cells: a kinetic Monte Carlo study. *Soft Matter*, 18(23):4483–4492, 2022. doi: 10.1039/D2SM00155A. Publisher: Royal Society of Chemistry.
- [101] Nicolas Martzel and Claude Aslangul. Mean-field treatment of the many-body Fokker-Planck equation. *J. Phys. A: Math. Gen.*, 34(50):11225, December 2001. ISSN 0305-4470. doi: 10.1088/0305-4470/34/50/305.
- [102] Pierre-Emmanuel Jabin and Zhenfu Wang. Mean Field Limit for Stochastic Particle Systems. In Nicola Bellomo, Pierre Degond, and Eitan Tadmor, editors, *Active Particles, Volume 1*, pages 379–402. Springer International Publishing, Cham, 2017. ISBN 978-3-319-49994-9 978-3-319-49996-3. doi: 10.1007/978-3-319-49996-3_10. Series Title: Modeling and Simulation in Science, Engineering and Technology.
- [103] Peter M. Kotelenez and Thomas G. Kurtz. Macroscopic limits for stochastic partial differential equations of McKean-Vlasov type. *Probab. Theory Relat. Fields*, 146(1-2):189, January 2010. ISSN 0178-8051, 1432-2064. doi: 10.1007/s00440-008-0188-0.
- [104] Samuel Herrmann, Peter Imkeller, and Dierk Peithmann. Large deviations and a Kramers’ type law for self-stabilizing diffusions. *Ann. Appl. Probab.*, 18(4):1379–1423, August 2008. ISSN 1050-5164, 2168-8737. doi: 10.1214/07-AAP489.
- [105] Luca Gammaitoni, Peter Haenggi, Peter Jung, and Fabio Marchesoni. Stochastic resonance. *Rev. Mod. Phys.*, 70(1):223–287, January 1998. doi: 10.1103/RevModPhys.70.223. Publisher: American Physical Society.
- [106] Wei Liu, Liming Wu, and Chaoen Zhang. Long-Time Behaviors of Mean-Field Interacting Particle Systems Related to McKean Vlasov Equations. *Commun. Math. Phys.*, 387(1):179–214, October 2021. ISSN 1432-0916. doi: 10.1007/s00220-021-04198-5.

Bibliography

- [107] L. D. Salem and H. S. Wio. Quantum corrections to the Vlasov description of collective modes. *Physics Letters B*, 248(1):5–9, September 1990. ISSN 0370-2693. doi: 10.1016/0370-2693(90)90005-Q.
- [108] O. Boine-Frankenheim, I. Hofmann, and G. Rumolo. Simulation and Observation of the Long-Time Evolution of the Longitudinal Instability in a Cooler Storage Ring. *Phys. Rev. Lett.*, 82(16):3256–3259, April 1999. doi: 10.1103/PhysRevLett.82.3256. Publisher: American Physical Society.
- [109] Theodore Kolokolnikov, Jose A. Carrillo, Andrea Bertozzi, Razvan Fetecau, and Mark Lewis. Emergent behaviour in multi-particle systems with non-local interactions. *Physica D: Nonlinear Phenomena*, 260:1–4, October 2013. ISSN 0167-2789. doi: 10.1016/j.physd.2013.06.011.
- [110] P. H. Chavanis. Phase transitions in self-gravitating systems. *Int. J. Mod. Phys. B*, 20(22):3113–3198, September 2006. ISSN 0217-9792. doi: 10.1142/S0217979206035400. Publisher: World Scientific Publishing Co.
- [111] P. H. Chavanis and L. Delfini. Phase transitions in self-gravitating systems and bacterial populations with a screened attractive potential. *Phys. Rev. E*, 81(5):051103, May 2010. doi: 10.1103/PhysRevE.81.051103. Publisher: American Physical Society.
- [112] Jan Maas and Alexander Mielke. Modeling of Chemical Reaction Systems with Detailed Balance Using Gradient Structures. *J Stat Phys*, 181(6):2257–2303, December 2020. ISSN 1572-9613. doi: 10.1007/s10955-020-02663-4.
- [113] Efthimios Kaxiras. *Atomic and Electronic Structure of Solids*. Cambridge University Press, Cambridge, UK ; New York, 1st edition edition, January 2003. ISBN 978-0-521-52339-4.
- [114] P. G. De Gennes and J. Matricon. Collective Modes of Vortex Lines in Superconductors of the Second Kind. *Rev. Mod. Phys.*, 36(1):45–49, January 1964. doi: 10.1103/RevModPhys.36.45. Publisher: American Physical Society.
- [115] F. Iachello. New Class of Low-Lying Collective Modes in Nuclei. *Phys. Rev. Lett.*, 53(15):1427–1429, October 1984. doi: 10.1103/PhysRevLett.53.1427. Publisher: American Physical Society.
- [116] Paul Romatschke and Michael Strickland. Collective modes of an anisotropic quark-gluon plasma. *Phys. Rev. D*, 68(3):036004, August 2003. doi: 10.1103/PhysRevD.68.036004. Publisher: American Physical Society.
- [117] S. A. Kivelson and D. S. Rokhsar. Bogoliubov quasiparticles, spinons, and spin-charge decoupling in superconductors. *Physical Review, B: Condensed Matter; (USA)*, 41:16, June 1990. ISSN 0163-1829. doi: 10.1103/PhysRevB.41.11693.
- [118] Jonas Denk, Simon Kretschmer, Jacob Halatek, Caroline Hartl, Petra Schwillie, and Erwin Frey. MinE conformational switching confers robustness on self-organized Min protein patterns. *Proceedings of the National Academy of Sciences*, 115(18):4553–4558, May 2018. doi: 10.1073/pnas.1719801115. Publisher: Proceedings of the National Academy of Sciences.
- [119] Tom Burkart, Manon C. Wigbers, Laeschkir Wuerthner, and Erwin Frey. Control of protein-based pattern formation via guiding cues. *Nat Rev Phys*, 4(8):511–527, August 2022. ISSN 2522-5820. doi: 10.1038/s42254-022-00461-3. Number: 8 Publisher: Nature Publishing Group.
- [120] Solenn Patalano, Adolfo Alsina, Carlos Gregorio-Rodriguez, Martin Bachman, Stephanie Dreier, Irene Hernando-Herraez, Paulin Nana, Shankar Balasubramanian, Seirian Sumner, Wolf Reik, and Steffen Rulands. Self-organization of plasticity and specialization in a primitively social insect. *Cell Systems*, 13(9):768–779.e4, September 2022. ISSN 2405-4712. doi: 10.1016/j.cels.2022.08.002.
- [121] Definition of signaling pathway - NCI Dictionary of Cancer Terms - NCI, February 2011. Archive Location: nciglobal,ncicenterprise.
- [122] Julian Daniel Schwab, Lea Siegle, Silke Daniela Kuehlwein, Michael Kuehl, and Hans Armin Kestler. Stability of Signaling Pathways during Aging-A Boolean Network Approach. *Biology (Basel)*, 6(4):46, December 2017. ISSN 2079-7737. doi: 10.3390/biology6040046.

- [123] Arnau Montagud, Jonas Beal, Luis Tobalina, Pauline Traynard, Vigneshwari Subramanian, Bence Szalai, Robert Alfoeldi, Laszlo Puskas, Alfonso Valencia, Emmanuel Barillot, Julio Saez-Rodriguez, and Laurence Calzone. Patient-specific Boolean models of signalling networks guide personalised treatments. *eLife*, 11:e72626, February 2022. ISSN 2050-084X. doi: 10.7554/eLife.72626. Publisher: eLife Sciences Publications, Ltd.
- [124] Md Humayun Kabir, Ralph Patrick, Joshua W. K. Ho, and Michael D. O'Connor. Identification of active signaling pathways by integrating gene expression and protein interaction data. *BMC Systems Biology*, 12(9):120, December 2018. ISSN 1752-0509. doi: 10.1186/s12918-018-0655-x.
- [125] Jignesh R. Parikh, Bertram Klinger, Yu Xia, Jarrod A. Marto, and Nils Bluethgen. Discovering causal signaling pathways through gene-expression patterns. *Nucleic Acids Res*, 38(Web Server issue):W109–W117, July 2010. ISSN 0305-1048. doi: 10.1093/nar/gkq424.
- [126] J. Bachmann, A. Raue, M. Schilling, V. Becker, J. Timmer, and U. Klingmueller. Predictive mathematical models of cancer signalling pathways. *Journal of Internal Medicine*, 271(2):155–165, 2012. ISSN 1365-2796. doi: 10.1111/j.1365-2796.2011.02492.x. [_eprint: https://onlinelibrary.wiley.com/doi/pdf/10.1111/j.1365-2796.2011.02492.x](https://onlinelibrary.wiley.com/doi/pdf/10.1111/j.1365-2796.2011.02492.x).
- [127] E. Z. Bagci, Y. Vodovotz, T. R. Billiar, G. B. Ermentrout, and I. Bahar. Bistability in Apoptosis: Roles of Bax, Bcl-2, and Mitochondrial Permeability Transition Pores. *Biophysical Journal*, 90(5):1546–1559, March 2006. ISSN 0006-3495. doi: 10.1529/biophysj.105.068122.
- [128] Tingzhe Sun, Xuzhu Lin, Yinna Wei, Yichen Xu, and Pingping Shen. Evaluating bistability of Bax activation switch. *FEBS Letters*, 584(5):954–960, March 2010. ISSN 0014-5793. doi: 10.1016/j.febslet.2010.01.034.
- [129] Jun Cui, Chun Chen, Haizhu Lu, Tingzhe Sun, and Pingping Shen. Two Independent Positive Feedbacks and Bistability in the Bcl-2 Apoptotic Switch. *PLOS ONE*, 3(1):e1469, January 2008. ISSN 1932-6203. doi: 10.1371/journal.pone.0001469. Publisher: Public Library of Science.
- [130] Angelica Aguilera-Gomez and Catherine Rabouille. Membrane-bound organelles versus membraneless compartments and their control of anabolic pathways in *Drosophila*. *Developmental Biology*, 428(2):310–317, August 2017. ISSN 0012-1606. doi: 10.1016/j.ydbio.2017.03.029.
- [131] Liting Duan, Daphne Che, Kai Zhang, Qunxiang Ong, Shunling Guo, and Bianxiao Cui. Optogenetic Control of Molecular Motors and Organelle Distributions in Cells. *Chemistry & Biology*, 22(5):671–682, May 2015. ISSN 1074-5521. doi: 10.1016/j.chembiol.2015.04.014.
- [132] Seok-Yong Choi, Ping Huang, Gary M. Jenkins, David C. Chan, Juergen Schiller, and Michael A. Frohman. A common lipid links Mfn-mediated mitochondrial fusion and SNARE-regulated exocytosis. *Nat Cell Biol*, 8(11):1255–1262, November 2006. ISSN 1476-4679. doi: 10.1038/ncb1487. Number: 11 Publisher: Nature Publishing Group.
- [133] Mafalda Escobar-Henriques and Fabian Anton. Mechanistic perspective of mitochondrial fusion: Tubulation vs. fragmentation. *Biochimica et Biophysica Acta (BBA) - Molecular Cell Research*, 1833(1):162–175, January 2013. ISSN 0167-4889. doi: 10.1016/j.bbamcr.2012.07.016.
- [134] Mitochondrion | Definition, Function, Structure, & Facts | Britannica, January 2023.
- [135] Samantha W. Jones, Amy L. Ball, Amy E. Chadwick, and Ana Alfirevic. The Role of Mitochondrial DNA Variation in Drug Response: A Systematic Review. *Frontiers in Genetics*, 12, 2021. ISSN 1664-8021.
- [136] Marcin Chlystun, Michelangelo Campanella, Ah-Lai Law, Michael R. Duchon, Lux Fatimathas, Tim P. Levine, Volker Gerke, and Stephen E. Moss. Regulation of Mitochondrial Morphogenesis by Annexin A6. *PLOS ONE*, 8(1):e53774, January 2013. ISSN 1932-6203. doi: 10.1371/journal.pone.0053774. Publisher: Public Library of Science.
- [137] Louisa Howard. Transmission electron microscope image of a thin section cut through an area of mammalian lung tissue. The high magnification image shows a mitochondria., 2023. https://commons.wikimedia.org/wiki/File:Mitochondria,_mammalian_lung_-_TEM.jpg.

Bibliography

- [138] Alexander M. van der Blik, Qinfang Shen, and Sumihiro Kawajiri. Mechanisms of Mitochondrial Fission and Fusion. *Cold Spring Harb Perspect Biol*, 5(6), June 2013. ISSN 1943-0264. doi: 10.1101/cshperspect.a011072.
- [139] Randy J. Giedt, Douglas R. Pfeiffer, Anastasios Matzavinos, Chiu-Yen Kao, and B. Rita Alevriadou. Mitochondrial Dynamics and Motility Inside Living Vascular Endothelial Cells: Role of Bioenergetics. *Ann Biomed Eng*, 40(9):1903–1916, September 2012. ISSN 1573-9686. doi: 10.1007/s10439-012-0568-6.
- [140] Pradeep K. Mouli, Gilad Twig, and Orian S. Shirihai. Frequency and Selectivity of Mitochondrial Fusion Are Key to Its Quality Maintenance Function. *Biophysical Journal*, 96(9):3509–3518, May 2009. ISSN 0006-3495. doi: 10.1016/j.bpj.2008.12.3959.
- [141] Der-Fen Suen, Kristi L. Norris, and Richard J. Youle. Mitochondrial dynamics and apoptosis. *Genes Dev.*, 22(12):1577–1590, June 2008. ISSN 0890-9369, 1549-5477. doi: 10.1101/gad.1658508.
- [142] Antonina J. Kruppa and Folma Buss. Motor proteins at the mitochondria-cytoskeleton interface. *Journal of Cell Science*, 134(7):jcs226084, April 2021. ISSN 0021-9533. doi: 10.1242/jcs.226084.
- [143] Andrew S Moore and Erika LF Holzbaur. Mitochondrial-cytoskeletal interactions: dynamic associations that facilitate network function and remodeling. *Current Opinion in Physiology*, 3:94–100, June 2018. ISSN 2468-8673. doi: 10.1016/j.cophys.2018.03.003.
- [144] Francisca Diaz and Carlos T. Moraes. Mitochondrial Biogenesis and Turnover. *Cell Calcium*, 44(1):24–35, July 2008. ISSN 0143-4160. doi: 10.1016/j.ceca.2007.12.004.
- [145] Xingguo Liu, David Weaver, Orian Shirihai, and Gyoergy Hajnoczky. Mitochondrial 'kiss-and-run': interplay between mitochondrial motility and fusion-fission dynamics. *The EMBO Journal*, 28(20):3074–3089, October 2009. ISSN 0261-4189. doi: 10.1038/emboj.2009.255. Publisher: John Wiley & Sons, Ltd.
- [146] David Weaver, Veronica Eisner, Xingguo Liu, Peter Varnai, Laszlo Hunyady, Atan Gross, and Gyoergy Hajnoczky. Distribution and Apoptotic Function of Outer Membrane Proteins Depend on Mitochondrial Fusion. *Molecular Cell*, 54(5):870–878, June 2014. ISSN 1097-2765. doi: 10.1016/j.molcel.2014.03.048.
- [147] Valerii M. Sukhorukov, Daniel Dikov, Andreas S. Reichert, and Michael Meyer-Hermann. Emergence of the Mitochondrial Reticulum from Fission and Fusion Dynamics. *PLOS Computational Biology*, 8(10):e1002745, October 2012. ISSN 1553-7358. doi: 10.1371/journal.pcbi.1002745. Publisher: Public Library of Science.
- [148] Shiqi Wang, Weiming Xiao, Sicong Shan, Chunsun Jiang, Ming Chen, Yan Zhang, Shouqin Lue, Juan Chen, Chuanmao Zhang, Quan Chen, and Mian Long. Multi-Patterned Dynamics of Mitochondrial Fission and Fusion in a Living Cell. *PLOS ONE*, 7(5):e19879, May 2012. ISSN 1932-6203. doi: 10.1371/journal.pone.0019879. Publisher: Public Library of Science.
- [149] Xin Niu, Hetal Brahmabhatt, Philipp Mergenthaler, Zhi Zhang, Jing Sang, Michael Daude, Fabian G. R. Ehlert, Wibke E. Diederich, Eve Wong, Weijia Zhu, Justin Pogmore, Jyoti P. Nandy, Maragani Satyanarayana, Ravi K. Jimmidi, Prabhat Arya, Brian Leber, Jialing Lin, Carsten Culmsee, Jing Yi, and David W. Andrews. A Small-Molecule Inhibitor of Bax and Bak Oligomerization Prevents Genotoxic Cell Death and Promotes Neuroprotection. *Cell Chemical Biology*, 24(4):493–506.e5, April 2017. ISSN 2451-9456. doi: 10.1016/j.chembiol.2017.03.011.
- [150] Justin Kale, Elizabeth J. Osterlund, and David W. Andrews. BCL-2 family proteins: changing partners in the dance towards death. *Cell Death Differ*, 25(1):65–80, January 2018. ISSN 1476-5403. doi: 10.1038/cdd.2017.186. Number: 1 Publisher: Nature Publishing Group.
- [151] D. Westphal, R. M. Kluck, and G. Dewson. Building blocks of the apoptotic pore: how Bax and Bak are activated and oligomerize during apoptosis. *Cell Death Differ*, 21(2):196–205, February 2014. ISSN 1476-5403. doi: 10.1038/cdd.2013.139. Number: 2 Publisher: Nature Publishing Group.

- [152] Stephen W. G. Tait, Melissa J. Parsons, Fabien Llambi, Lisa Bouchier-Hayes, Samuel Connell, Cristina Munoz-Pinedo, and Douglas R. Green. Resistance to Caspase-Independent Cell Death Requires Persistence of Intact Mitochondria. *Developmental Cell*, 18(5):802–813, May 2010. ISSN 1534-5807. doi: 10.1016/j.devcel.2010.03.014.
- [153] Gabriel Ichim, Jonathan Lopez, Shafiq U. Ahmed, Nathiya Muthalagu, Evangelos Giampazolias, M. Eugenia Delgado, Martina Haller, Joel S. Riley, Susan M. Mason, Dimitris Athineos, Melissa J. Parsons, Bert van de Kooij, Lisa Bouchier-Hayes, Anthony J. Chalmers, Rogier W. Rooswinkel, Andrew Oberst, Karen Blyth, Markus Rehm, Daniel J. Murphy, and Stephen W. G. Tait. Limited Mitochondrial Permeabilization Causes DNA Damage and Genomic Instability in the Absence of Cell Death. *Molecular Cell*, 57(5):860–872, March 2015. ISSN 1097-2765. doi: 10.1016/j.molcel.2015.01.018.
- [154] Gabriel Ichim and Stephen W. G. Tait. A fate worse than death: apoptosis as an oncogenic process. *Nat Rev Cancer*, 16(8):539–548, August 2016. ISSN 1474-1768. doi: 10.1038/nrc.2016.58. Number: 8 Publisher: Nature Publishing Group.
- [155] Kai Cao, Joel S. Riley, Rosalie Heilig, Alfredo E. Montes-Gomez, Esmee Vringer, Kevin Berthenet, Catherine Cloix, Yassmin Elmasry, David G. Spiller, Gabriel Ichim, Kirsteen J. Campbell, Andrew P. Gilmore, and Stephen W. G. Tait. Mitochondrial dynamics regulate genome stability via control of caspase-dependent DNA damage. *Developmental Cell*, 57(10):1211–1225.e6, May 2022. ISSN 1534-5807. doi: 10.1016/j.devcel.2022.03.019.
- [156] Sabrina L. Spencer and Peter K. Sorger. Measuring and Modeling Apoptosis in Single Cells. *Cell*, 144(6):926–939, March 2011. ISSN 0092-8674. doi: 10.1016/j.cell.2011.03.002.
- [157] Katia Cosentino and Ana J. Garcia-Saez. Bax and Bak Pores: Are We Closing the Circle? *Trends in Cell Biology*, 27(4):266–275, April 2017. ISSN 0962-8924. doi: 10.1016/j.tcb.2016.11.004.
- [158] Lieven P. Billen, Candis L. Kokoski, Jonathan F. Lovell, Brian Leber, and David W. Andrews. Bcl-XL Inhibits Membrane Permeabilization by Competing with Bax. *PLoS Biology*, 6(6):e147, June 2008. ISSN 1545-7885. doi: 10.1371/journal.pbio.0060147. Publisher: Public Library of Science.
- [159] Chaoxiang Chen, Xiang Zhang, Shuyue Zhang, Shaobin Zhu, Jingyi Xu, Yan Zheng, Jinyan Han, Jin-Zhang Zeng, and Xiaomei Yan. Quantification of protein copy number in single mitochondria: The Bcl-2 family proteins. *Biosensors and Bioelectronics*, 74:476–482, December 2015. ISSN 0956-5663. doi: 10.1016/j.bios.2015.06.057.
- [160] Kerstin Weiss, Andreas Neef, Qui Van, Stefanie Kramer, Ingo Gregor, and Joerg Enderlein. Quantifying the Diffusion of Membrane Proteins and Peptides in Black Lipid Membranes with 2-Focus Fluorescence Correlation Spectroscopy. *Biophysical Journal*, 105(2):455–462, July 2013. ISSN 0006-3495. doi: 10.1016/j.bpj.2013.06.004.
- [161] Margaret E. Maes, Cassandra L. Schlamp, and Robert W. Nickells. Live-cell imaging to measure BAX recruitment kinetics to mitochondria during apoptosis. *PLoS ONE*, 12(9):e0184434, September 2017. ISSN 1932-6203. doi: 10.1371/journal.pone.0184434. Publisher: Public Library of Science.
- [162] Frank Edlich, Soojay Banerjee, Motoshi Suzuki, Megan M. Cleland, Damien Arnoult, Chunxin Wang, Albert Neutzner, Nico Tjandra, and Richard J. Youle. Bcl-xL Retrotranslocates Bax from the Mitochondria into the Cytosol. *Cell*, 145(1):104–116, April 2011. ISSN 0092-8674. doi: 10.1016/j.cell.2011.02.034.
- [163] Miguel V. Moreno, Daniel G. Barci, and Zochil Gonzalez Arenas. State-dependent diffusion in a bistable potential: Conditional probabilities and escape rates. *Phys. Rev. E*, 101(6):062110, June 2020. doi: 10.1103/PhysRevE.101.062110. Publisher: American Physical Society.
- [164] Alexandre Rosas, Italo'Ivo Lima Dias Pinto, and Katja Lindenberg. Kramers' rate for systems with multiplicative noise. *Phys. Rev. E*, 94(1):012101, July 2016. doi: 10.1103/PhysRevE.94.012101. Publisher: American Physical Society.

Bibliography

- [165] Mariusz Karbowski, Damien Arnoult, Hsiuchen Chen, David C. Chan, Carolyn L. Smith, and Richard J. Youle. Quantitation of mitochondrial dynamics by photolabeling of individual organelles shows that mitochondrial fusion is blocked during the Bax activation phase of apoptosis. *Journal of Cell Biology*, 164(4):493–499, February 2004. ISSN 0021-9525. doi: 10.1083/jcb.200309082.
- [166] M. E. Maes, J. A. Grosser, R. L. Fehrman, C. L. Schlamp, and R. W. Nickells. Completion of BAX recruitment correlates with mitochondrial fission during apoptosis. *Sci Rep*, 9(1):16565, November 2019. ISSN 2045-2322. doi: 10.1038/s41598-019-53049-w. Number: 1 Publisher: Nature Publishing Group.
- [167] Guoping Feng and Neil Kaplowitz. Mechanism of staurosporine-induced apoptosis in murine hepatocytes. *American Journal of Physiology-Gastrointestinal and Liver Physiology*, 282(5):G825–G834, May 2002. ISSN 0193-1857. doi: 10.1152/ajpgi.00467.2001. Publisher: American Physiological Society.
- [168] Joerg Kleeff, Marko Kornmann, Harneet Sawhney, and Murray Korc. Actinomycin D induces apoptosis and inhibits growth of pancreatic cancer cells. *International Journal of Cancer*, 86(3):399–407, 2000. ISSN 1097-0215. doi: 10.1002/(SICI)1097-0215(20000501)86:3<399::AID-IJC15>3.0.CO;2-G. _eprint: <https://onlinelibrary.wiley.com/doi/pdf/10.1002/%28SICI%291097-0215%2820000501%2986%3A3%3C399%3A%3AAID-IJC15%3E3.0.CO%3B2-G>.
- [169] Reut Yosef, Noam Pilpel, Ronit Tokarsky-Amiel, Anat Biran, Yossi Ovadya, Snir Cohen, Ezra Vadai, Liat Dassa, Elisheva Shahar, Reba Condiotti, Ittai Ben-Porath, and Valery Krizhanovsky. Directed elimination of senescent cells by inhibition of BCL-W and BCL-XL. *Nat Commun*, 7(1):11190, April 2016. ISSN 2041-1723. doi: 10.1038/ncomms11190. Number: 1 Publisher: Nature Publishing Group.
- [170] Nethmi M.B. Yapa, Valerie Lisnyak, Boris Reljic, and Michael T. Ryan. Mitochondrial dynamics in health and disease. *FEBS Letters*, 595(8):1184–1204, 2021. ISSN 1873-3468. doi: 10.1002/1873-3468.14077. _eprint: <https://onlinelibrary.wiley.com/doi/pdf/10.1002/1873-3468.14077>.
- [171] David C. Chan. Mitochondrial Dynamics and Its Involvement in Disease. *Annual Review of Pathology: Mechanisms of Disease*, 15(1):235–259, 2020. doi: 10.1146/annurev-pathmechdis-012419-032711. _eprint: <https://doi.org/10.1146/annurev-pathmechdis-012419-032711>.
- [172] Timothy Wai and Thomas Langer. Mitochondrial Dynamics and Metabolic Regulation. *Trends in Endocrinology & Metabolism*, 27(2):105–117, February 2016. ISSN 1043-2760. doi: 10.1016/j.tem.2015.12.001.
- [173] Ayman W. El-Hattab, Adekunle M. Adesina, Jeremy Jones, and Fernando Scaglia. MELAS syndrome: Clinical manifestations, pathogenesis, and treatment options. *Molecular Genetics and Metabolism*, 116(1):4–12, September 2015. ISSN 1096-7192. doi: 10.1016/j.jmgme.2015.06.004.
- [174] Jenq-Lin Yang, Sujira Mukda, and Shang-Der Chen. Diverse roles of mitochondria in ischemic stroke. *Redox Biology*, 16:263–275, June 2018. ISSN 2213-2317. doi: 10.1016/j.redox.2018.03.002.
- [175] Simone Fulda, Lorenzo Galluzzi, and Guido Kroemer. Targeting mitochondria for cancer therapy. *Nat Rev Drug Discov*, 9(6):447–464, June 2010. ISSN 1474-1784. doi: 10.1038/nrd3137. Number: 6 Publisher: Nature Publishing Group.
- [176] Sunil Nath. The thermodynamic efficiency of ATP synthesis in oxidative phosphorylation. *Biophysical Chemistry*, 219:69–74, December 2016. ISSN 0301-4622. doi: 10.1016/j.bpc.2016.10.002.
- [177] F. Guillaud, S. Droese, A. Kowald, U. Brandt, and E. Klipp. Superoxide production by cytochrome bc1 complex: A mathematical model. *Biochimica et Biophysica Acta (BBA) - Bioenergetics*, 1837(10):1643–1652, October 2014. ISSN 0005-2728. doi: 10.1016/j.bbabi.2014.05.358.
- [178] Brittany Angarola and Shawn M. Ferguson. Coordination of Rheb lysosomal membrane interactions with mTORC1 activation. *F1000Res*, 9:F1000 Faculty Rev–450, May 2020. ISSN 2046-1402. doi: 10.12688/f1000research.22367.1.

- [179] Golam T. Saffi and Roberto J. Botelho. Lysosome Fission: Planning for an Exit. *Trends in Cell Biology*, 29(8):635–646, August 2019. ISSN 0962-8924. doi: 10.1016/j.tcb.2019.05.003.
- [180] Bernadette Carroll, Dorothea Maetzel, Oliver DK Maddocks, Gisela Otten, Matthew Ratcliff, Graham R Smith, Elaine A Dunlop, Joao F Passos, Owen R Davies, Rudolf Jaenisch, Andrew R Tee, Sovan Sarkar, and Viktor I Korolchuk. Control of TSC2-Rheb signaling axis by arginine regulates mTORC1 activity. *eLife*, 5:e11058, January 2016. ISSN 2050-084X. doi: 10.7554/eLife.11058. Publisher: eLife Sciences Publications, Ltd.
- [181] Ulrike Rehbein, Mirja Tamara Prentzell, Marti Cadena Sandoval, Alexander Martin Heberle, Elizabeth P. Henske, Christiane A. Opitz, and Kathrin Thedieck. The TSC Complex-mTORC1 Axis: From Lysosomes to Stress Granules and Back. *Frontiers in Cell and Developmental Biology*, 9, 2021. ISSN 2296-634X.
- [182] Marisol Estrella Armijo, Emilia Escalona, Daniela Pena, Alejandro Farias, Violeta Morin, Matthias Baumann, Bert Matthias Klebl, Roxana Pincheira, and Ariel Fernando Castro. Blocking the Farnesyl Pocket of PDE1 γ Reduces Rheb-Dependent mTORC1 Activation and Survival of Tsc2-Null Cells. *Frontiers in Pharmacology*, 13, 2022. ISSN 1663-9812.
- [183] Andrew R. Tee, Diane C. Fingar, Brendan D. Manning, David J. Kwiatkowski, Lewis C. Cantley, and John Blenis. Tuberous sclerosis complex-1 and -2 gene products function together to inhibit mammalian target of rapamycin (mTOR)-mediated downstream signaling. *Proceedings of the National Academy of Sciences*, 99(21):13571–13576, October 2002. doi: 10.1073/pnas.202476899. Publisher: Proceedings of the National Academy of Sciences.
- [184] Thomas Wilhelm. The smallest chemical reaction system with bistability. *BMC Systems Biology*, 3(1):90, September 2009. ISSN 1752-0509. doi: 10.1186/1752-0509-3-90.
- [185] Willem Stoorvogel, Ger J. Strous, Hans J. Geuze, Viola Oorschot, and Alan L. Schwartz. Late endosomes derive from early endosomes by maturation. *Cell*, 65(3):417–427, May 1991. ISSN 0092-8674. doi: 10.1016/0092-8674(91)90459-C.
- [186] Angela Wandinger-Ness and Marino Zerial. Rab Proteins and the Compartmentalization of the Endosomal System. *Cold Spring Harb Perspect Biol*, 6(11):a022616, November 2014. ISSN , 1943-0264. doi: 10.1101/cshperspect.a022616. Company: Cold Spring Harbor Laboratory Press Distributor: Cold Spring Harbor Laboratory Press Institution: Cold Spring Harbor Laboratory Press Label: Cold Spring Harbor Laboratory Press Publisher: Cold Spring Harbor Lab.
- [187] Jan Rehwinkel and Michaela U. Gack. RIG-I-like receptors: their regulation and roles in RNA sensing. *Nat Rev Immunol*, 20(9):537–551, September 2020. ISSN 1474-1741. doi: 10.1038/s41577-020-0288-3. Number: 9 Publisher: Nature Publishing Group.
- [188] Celine Castanier, Dominique Garcin, Aime Vazquez, and Damien Arnoult. Mitochondrial dynamics regulate the RIG-I-like receptor antiviral pathway. *EMBO reports*, 11(2):133–138, February 2010. ISSN 1469-221X. doi: 10.1038/embor.2009.258. Publisher: John Wiley & Sons, Ltd.
- [189] Fajian Hou, Lijun Sun, Hui Zheng, Brian Skaug, Qiu-Xing Jiang, and Zhijian J. Chen. MAVS Forms Functional Prion-like Aggregates to Activate and Propagate Antiviral Innate Immune Response. *Cell*, 146(3):448–461, August 2011. ISSN 0092-8674. doi: 10.1016/j.cell.2011.06.041.
- [190] Ming-Shih Hwang, Jerome Boulanger, Jonathan D. Howe, Anna Albecka, Mathias Pasche, Leila Muresan, and Yorgo Modis. MAVS polymers smaller than 80 nm induce mitochondrial membrane remodeling and interferon signaling. *The FEBS Journal*, 286(8):1543–1560, 2019. ISSN 1742-4658. doi: 10.1111/febs.14772. __eprint: <https://onlinelibrary.wiley.com/doi/pdf/10.1111/febs.14772>.
- [191] Hui Xu, Xiaojing He, Hui Zheng, Lily J Huang, Fajian Hou, Zhiheng Yu, Michael Jason de la Cruz, Brian Borkowski, Xuewu Zhang, Zhijian J Chen, and Qiu-Xing Jiang. Structural basis for the prion-like MAVS filaments in antiviral innate immunity. *eLife*, 3:e01489, February 2014. ISSN 2050-084X. doi: 10.7554/eLife.01489. Publisher: eLife Sciences Publications, Ltd.

Bibliography

- [192] Lichun He, Benjamin Bardiaux, Mumdooh Ahmed, Johannes Spehr, Renate Koenig, Heinrich LÄ¼nsdorf, Ulfert Rand, Thorsten Luehrs, and Christiane Ritter. Structure determination of helical filaments by solid-state NMR spectroscopy. *Proceedings of the National Academy of Sciences*, 113(3):E272–E281, January 2016. doi: 10.1073/pnas.1513119113. Publisher: Proceedings of the National Academy of Sciences.
- [193] Thermodynamics | Laws, Definition, & Equations | Britannica, January 2023.
- [194] Peter Atkins and Julio de Paula. *Atkins' Physical Chemistry*. Oxford University Press, Oxford ; New York, 10 edition, January 2014. ISBN 978-0-19-969740-3.
- [195] Artemy Kolchinsky and David H. Wolpert. Work, Entropy Production, and Thermodynamics of Information under Protocol Constraints. *Phys. Rev. X*, 11(4):041024, November 2021. doi: 10.1103/PhysRevX.11.041024. Publisher: American Physical Society.
- [196] Stefan Hilbert, Peter Haenggi, and Joern Dunkel. Thermodynamic laws in isolated systems. *Phys. Rev. E*, 90(6):062116, December 2014. doi: 10.1103/PhysRevE.90.062116. Publisher: American Physical Society.
- [197] Jose M. G. Vilar and J. Miguel Rubi. Communication: System-size scaling of Boltzmann and alternate Gibbs entropies. *J. Chem. Phys.*, 140(20):201101, May 2014. ISSN 0021-9606. doi: 10.1063/1.4879553. Publisher: American Institute of Physics.
- [198] Joern Dunkel and Stefan Hilbert. Consistent thermostatics forbids negative absolute temperatures. *Nature Phys*, 10(1):67–72, January 2014. ISSN 1745-2481. doi: 10.1038/nphys2815. Number: 1 Publisher: Nature Publishing Group.
- [199] Entropy | Definition & Equation | Britannica, January 2023.
- [200] Jos Uffink. Bluff Your Way in the Second Law of Thermodynamics. *Studies in History and Philosophy of Science Part B: Studies in History and Philosophy of Modern Physics*, 32(3):305–394, September 2001. ISSN 1355-2198. doi: 10.1016/S1355-2198(01)00016-8.
- [201] Pasko Zupanovic and Domagoj Kuic. Relation between Boltzmann and Gibbs entropy and example with multinomial distribution. *J. Phys. Commun.*, 2(4):045002, April 2018. ISSN 2399-6528. doi: 10.1088/2399-6528/aab7e1. Publisher: IOP Publishing.
- [202] J. Willard Gibbs. *The Scientific Papers of J. Willard Gibbs, Vol. 1: Thermodynamics*. Dover Publications, Woodbridge, Conn, January 1961. ISBN 978-0-486-60721-4.
- [203] E. T. Jaynes. The Gibbs Paradox. In C. Ray Smith, Gary J. Erickson, and Paul O. Neudorfer, editors, *Maximum Entropy and Bayesian Methods: Seattle, 1991*, Fundamental Theories of Physics, pages 1–21. Springer Netherlands, Dordrecht, 1992. ISBN 978-94-017-2219-3. doi: 10.1007/978-94-017-2219-3_1.
- [204] Andrew Rex. Maxwell's Demon-A Historical Review. *Entropy*, 19(6):240, June 2017. ISSN 1099-4300. doi: 10.3390/e19060240. Number: 6 Publisher: Multidisciplinary Digital Publishing Institute.
- [205] L. Szilard. ueber die Entropieverminderung in einem thermodynamischen System bei Eingriffen intelligenter Wesen. *Z. Physik*, 53(11):840–856, November 1929. ISSN 0044-3328. doi: 10.1007/BF01341281.
- [206] Rolf Landauer. Information is a physical entity. *Physica A: Statistical Mechanics and its Applications*, 263(1):63–67, February 1999. ISSN 0378-4371. doi: 10.1016/S0378-4371(98)00513-5.
- [207] R. Landauer. Irreversibility and Heat Generation in the Computing Process. *IBM Journal of Research and Development*, 5(3):183–191, July 1961. ISSN 0018-8646. doi: 10.1147/rd.53.0183. Conference Name: IBM Journal of Research and Development.
- [208] L. Brillouin. Maxwell's Demon Cannot Operate: Information and Entropy. I. *Journal of Applied Physics*, 22(3):334–337, March 1951. ISSN 0021-8979. doi: 10.1063/1.1699951. Publisher: American Institute of Physics.

- [209] L. Brillouin. Physical Entropy and Information. II. *Journal of Applied Physics*, 22(3):338–343, March 1951. ISSN 0021-8979. doi: 10.1063/1.1699952. Publisher: American Institute of Physics.
- [210] Leo Touzo, Matteo Marsili, Neri Merhav, and Edgar Roldan. Optimal work extraction and the minimum description length principle. *J. Stat. Mech.*, 2020(9):093403, September 2020. ISSN 1742-5468. doi: 10.1088/1742-5468/abac3. Publisher: IOP Publishing and SISSA.
- [211] Qian Zeng and Jin Wang. New fluctuation theorems on Maxwell’s demon. *Science Advances*, 7(23):eabf1807, June 2021. doi: 10.1126/sciadv.abf1807. Publisher: American Association for the Advancement of Science.
- [212] Gonzalo Manzano, Diego Subero, Olivier Maillet, Rosario Fazio, Jukka P. Pekola, and Edgar Roldan. Thermodynamics of Gambling Demons. *Phys. Rev. Lett.*, 126(8):080603, February 2021. doi: 10.1103/PhysRevLett.126.080603. Publisher: American Physical Society.
- [213] B. Ahmadi, S. Salimi, and A. S. Khorashad. Irreversible work and Maxwell demon in terms of quantum thermodynamic force. *Sci Rep*, 11(1):2301, January 2021. ISSN 2045-2322. doi: 10.1038/s41598-021-81737-z. Number: 1 Publisher: Nature Publishing Group.
- [214] Nathanael Cottet, Sebastien Jezouin, Landry Bretheau, Philippe Campagne-Ibarcq, Quentin Ficheux, Janet Anders, Alexia Auffeves, Remi Azouit, Pierre Rouchon, and Benjamin Huard. Observing a quantum Maxwell demon at work. *Proceedings of the National Academy of Sciences*, 114(29):7561–7564, July 2017. doi: 10.1073/pnas.1704827114. Publisher: Proceedings of the National Academy of Sciences.
- [215] James Clerk Maxwell. IV. On the dynamical theory of gases. *Philosophical Transactions of the Royal Society of London*, 157:49–88, January 1997. doi: 10.1098/rstl.1867.0004. Publisher: Royal Society.
- [216] Enrico Scalas, Adrian T. Gabriel, Edgar Martin, and Guido Germano. Velocity and energy distributions in microcanonical ensembles of hard spheres. *Phys. Rev. E*, 92(2):022140, August 2015. doi: 10.1103/PhysRevE.92.022140. Publisher: American Physical Society.
- [217] Ilja N. Bronstein, K. A. Semendjajew, Gerhard Musiol, and Heiner Muehlig. *Taschenbuch der Mathematik*. Deutsch, Frankfurt am Main, July 2008. ISBN 978-3-8171-2007-9.
- [218] Naresh Yandrapalli, Julien Petit, Oliver Baeumchen, and Tom Robinson. Surfactant-free production of biomimetic giant unilamellar vesicles using PDMS-based microfluidics. *Commun Chem*, 4(1):1–10, June 2021. ISSN 2399-3669. doi: 10.1038/s42004-021-00530-1. Number: 1 Publisher: Nature Publishing Group.
- [219] Marlous Kamp, Bart de Nijs, Marjolein N. van der Linden, Isja de Feijter, Merel J. Lefferts, Antonio Aloi, Jack Griffiths, Jeremy J. Baumberg, Ilja K. Voets, and Alfons van Blaaderen. Multivalent Patchy Colloids for Quantitative 3D Self-Assembly Studies. *Langmuir*, 36(9):2403–2418, March 2020. ISSN 0743-7463. doi: 10.1021/acs.langmuir.9b03863. Publisher: American Chemical Society.
- [220] Emory M. Payne, Daniel A. Holland-Moritz, Shuwen Sun, and Robert T. Kennedy. High-throughput screening by droplet microfluidics: perspective into key challenges and future prospects. *Lab Chip*, 20(13):2247–2262, June 2020. ISSN 1473-0189. doi: 10.1039/D0LC00347F. Publisher: The Royal Society of Chemistry.
- [221] Emanuela Bianchi, Ronald Blaak, and Christos N. Likos. Patchy colloids: state of the art and perspectives. *Phys. Chem. Chem. Phys.*, 13(14):6397–6410, April 2011. ISSN 1463-9084. doi: 10.1039/C0CP02296A. Publisher: The Royal Society of Chemistry.
- [222] Etienne Loiseau, Jochen A. M. Schneider, Felix C. Keber, Carina Pelzl, Gladys Massiera, Guillaume Salbreux, and Andreas R. Bausch. Shape remodeling and blebbing of active cytoskeletal vesicles. *Science Advances*, 2(4):e1500465, April 2016. doi: 10.1126/sciadv.1500465. Publisher: American Association for the Advancement of Science.

Bibliography

- [223] A. A. Hyman, S. Salser, D. N. Drechsel, N. Unwin, and T. J. Mitchison. Role of GTP hydrolysis in microtubule dynamics: information from a slowly hydrolyzable analogue, GMPCPP. *Mol Biol Cell*, 3(10):1155–1167, October 1992. ISSN 1059-1524. doi: 10.1091/mbc.3.10.1155.
- [224] WHO. A world at risk - annual report on global preparedness for health emergencies. Technical report, Global Preparedness Monitoring Board Geneva, 2019.
- [225] Bojan Basrak. Fisher-Tippett Theorem. In Miodrag Lovric, editor, *International Encyclopedia of Statistical Science*, pages 525–526. Springer, Berlin, Heidelberg, 2011. ISBN 978-3-642-04898-2. doi: 10.1007/978-3-642-04898-2_254.
- [226] Rint P. Sijbesma, Felix H. Beijer, Luc Brunsveld, Brigitte J. B. Folmer, J. H. K. Ky Hirschberg, Ronald F. M. Lange, Jimmy K. L. Lowe, and E. W. Meijer. Reversible Polymers Formed from Self-Complementary Monomers Using Quadruple Hydrogen Bonding. *Science*, 278(5343):1601–1604, November 1997. doi: 10.1126/science.278.5343.1601. Publisher: American Association for the Advancement of Science.
- [227] Zoe Budrikis, Giulio Costantini, Caterina A. M. La Porta, and Stefano Zapperi. Protein accumulation in the endoplasmic reticulum as a non-equilibrium phase transition. *Nat Commun*, 5(1):3620, April 2014. ISSN 2041-1723. doi: 10.1038/ncomms4620. Number: 1 Publisher: Nature Publishing Group.
- [228] Sourabh Lahiri, Yang Wang, Massimiliano Esposito, and David Lacoste. Kinetics and thermodynamics of reversible polymerization in closed systems. *New J. Phys.*, 17(8):085008, August 2015. ISSN 1367-2630. doi: 10.1088/1367-2630/17/8/085008. Publisher: IOP Publishing.
- [229] R. Dennis Vigil and Robert M Ziff. On the stability of coagulation-fragmentation population balances. *Journal of Colloid and Interface Science*, 133(1):257–264, November 1989. ISSN 0021-9797. doi: 10.1016/0021-9797(89)90300-7.
- [230] David P. Brown, Esko I. Kauppinen, Jorma K. Jokiniemi, Stanley G. Rubin, and Pratim Biswas. A method of moments based CFD model for polydisperse aerosol flows with strong interphase mass and heat transfer. *Computers & Fluids*, 35(7):762–780, August 2006. ISSN 0045-7930. doi: 10.1016/j.compfluid.2006.01.012.
- [231] R. Dennis Vigil. On equilibrium solutions of aggregation-fragmentation problems. *Journal of Colloid and Interface Science*, 336(2):642–647, August 2009. ISSN 0021-9797. doi: 10.1016/j.jcis.2009.04.061.
- [232] Sheldon K. Friedlander. *Smoke, Dust, and Haze: Fundamentals of Aerosol Dynamics*. Oxford University Press, New York, second edition edition, 2000. ISBN 978-0-19-512999-1.
- [233] Jacek Banasiak, Wilson Lamb, and Philippe Laurecot. *Analytic Methods for Coagulation-Fragmentation Models, Volume I & II*. CRC Press, 1st edition edition, September 2019. ISBN 978-0-367-23544-4.
- [234] F. P. da Costa. Mathematical Aspects of Coagulation-Fragmentation Equations. In Jean-Pierre Bourguignon, Rolf Jeltsch, Alberto Adrego Pinto, and Marcelo Viana, editors, *Mathematics of Energy and Climate Change*, CIM Series in Mathematical Sciences, pages 83–162, Cham, 2015. Springer International Publishing. ISBN 978-3-319-16121-1. doi: 10.1007/978-3-319-16121-1_5.
- [235] E. Ben-Naim and P. L. Krapivsky. Kinetics of ring formation. *Phys. Rev. E*, 83(6):061102, June 2011. doi: 10.1103/PhysRevE.83.061102. Publisher: American Physical Society.
- [236] E. Ben-Naim and P. L. Krapivsky. Phase transition with nonthermodynamic states in reversible polymerization. *Phys. Rev. E*, 77(6):061132, June 2008. doi: 10.1103/PhysRevE.77.061132. Publisher: American Physical Society.
- [237] J. Carr and F. P. da Costa. Asymptotic behavior of solutions to the coagulation-fragmentation equations. II. Weak fragmentation. *J Stat Phys*, 77(1):89–123, October 1994. ISSN 1572-9613. doi: 10.1007/BF02186834.

- [238] J. Carr. Asymptotic behaviour of solutions to the coagulation-fragmentation equations. I. The strong fragmentation case. *Proceedings of the Royal Society of Edinburgh Section A: Mathematics*, 121(3-4):231–244, 1992. ISSN 1473-7124, 0308-2105. doi: 10.1017/S0308210500027888. Publisher: Royal Society of Edinburgh Scotland Foundation.
- [239] Frederik Michel Dekking, Cornelis Kraaikamp, Hendrik Paul Lopuhaae, and Ludolf Erwin Meester. *A Modern Introduction to Probability and Statistics*. Springer Texts in Statistics. Springer London, London, 2005. ISBN 978-1-85233-896-1 978-1-84628-168-6. doi: 10.1007/1-84628-168-7.
- [240] Rachael Clark and Thomas Kupper. Old Meets New: The Interaction Between Innate and Adaptive Immunity. *Journal of Investigative Dermatology*, 125(4):629–637, October 2005. ISSN 0022-202X. doi: 10.1111/j.0022-202X.2005.23856.x.
- [241] Zhe Ma, Guoxin Ni, and Blossom Damania. Innate Sensing of DNA Virus Genomes. *Annual Review of Virology*, 5(1):341–362, 2018. doi: 10.1146/annurev-virology-092917-043244. __eprint: <https://doi.org/10.1146/annurev-virology-092917-043244>.
- [242] Natalia Zamorano Cuervo, Quentin Osseman, and Nathalie Grandvaux. Virus Infection Triggers MAVS Polymers of Distinct Molecular Weight. *Viruses*, 10(2):56, February 2018. ISSN 1999-4915. doi: 10.3390/v10020056. Number: 2 Publisher: Multidisciplinary Digital Publishing Institute.
- [243] Stacy M. Horner and Michael Gale. Regulation of hepatic innate immunity by hepatitis C virus. *Nat Med*, 19(7):879–888, July 2013. ISSN 1546-170X. doi: 10.1038/nm.3253. Number: 7 Publisher: Nature Publishing Group.
- [244] Wen-Hai Shao, Daniel H. Shu, Yuxuan Zhen, Brendan Hilliard, Stephen O. Priest, Matteo Cesaroni, Jenny P.-Y. Ting, and Philip L. Cohen. Prion-like Aggregation of Mitochondrial Antiviral Signaling Protein in Lupus Patients Is Associated With Increased Levels of Type I Interferon. *Arthritis & Rheumatology*, 68(11):2697–2707, 2016. ISSN 2326-5205. doi: 10.1002/art.39733. __eprint: <https://onlinelibrary.wiley.com/doi/pdf/10.1002/art.39733>.
- [245] Nan Qi, Yuheng Shi, Rui Zhang, Wenting Zhu, Bofeng Yuan, Xiaoyan Li, Changwan Wang, Xuewu Zhang, and Fajian Hou. Multiple truncated isoforms of MAVS prevent its spontaneous aggregation in antiviral innate immune signalling. *Nat Commun*, 8(1):15676, June 2017. ISSN 2041-1723. doi: 10.1038/ncomms15676. Number: 1 Publisher: Nature Publishing Group.
- [246] Manfred Eigen and Peter Schuster. A principle of natural self-organization. *Naturwissenschaften*, 64(11):541–565, November 1977. ISSN 1432-1904. doi: 10.1007/BF00450633.
- [247] Norio Kitadai and Shigenori Maruyama. Origins of building blocks of life: A review. *Geoscience Frontiers*, 9(4):1117–1153, July 2018. ISSN 1674-9871. doi: 10.1016/j.gsf.2017.07.007.
- [248] Adrian Tuck. The Role of Atmospheric Aerosols in the Origin Of Life. *Surveys in Geophysics*, 23(5):379–409, September 2002. ISSN 1573-0956. doi: 10.1023/A:1020123922767.
- [249] Christopher M. Dobson, G. Barney Ellison, Adrian F. Tuck, and Veronica Vaida. Atmospheric aerosols as prebiotic chemical reactors. *Proceedings of the National Academy of Sciences*, 97(22):11864–11868, October 2000. doi: 10.1073/pnas.200366897. Publisher: Proceedings of the National Academy of Sciences.
- [250] Ali Fallah-Araghi, Kamel Meguellati, Jean-Christophe Baret, Abdeslam El Harrak, Thomas Mangeat, Martin Karplus, Sylvain Ladame, Carlos M. Marques, and Andrew D. Griffiths. Enhanced Chemical Synthesis at Soft Interfaces: A Universal Reaction-Adsorption Mechanism in Microcompartments. *Phys. Rev. Lett.*, 112(2):028301, January 2014. doi: 10.1103/PhysRevLett.112.028301. Publisher: American Physical Society.
- [251] Martin R. Evans, Satya N. Majumdar, and Gregory Schehr. Stochastic resetting and applications. *J. Phys. A: Math. Theor.*, 53(19):193001, April 2020. ISSN 1751-8121. doi: 10.1088/1751-8121/ab7cfe. Publisher: IOP Publishing.

Bibliography

- [252] Shuang Wang, Hanshuang Chen, and Feng Huang. Random walks on complex networks with multiple resetting nodes: A renewal approach. *Chaos*, 31(9):093135, September 2021. ISSN 1054-1500. doi: 10.1063/5.0064791. Publisher: American Institute of Physics.
- [253] Jaco Fuchs, Sebastian Goldt, and Udo Seifert. Stochastic thermodynamics of resetting. *EPL*, 113(6):60009, April 2016. ISSN 0295-5075. doi: 10.1209/0295-5075/113/60009. Publisher: EDP Sciences, IOP Publishing and Societ  Italiana di Fisica.
- [254] D. M. Busiello and A. Maritan. Entropy production in master equations and Fokker-Planck equations: facing the coarse-graining and recovering the information loss. *J. Stat. Mech.*, 2019(10):104013, October 2019. ISSN 1742-5468. doi: 10.1088/1742-5468/ab363e. Publisher: IOP Publishing and SISSA.
- [255] Peter Timothy Saunders. *An Introduction to Catastrophe Theory*. Cambridge University Press, Cambridge Eng. ; New York, 1st edition edition, June 1980. ISBN 978-0-521-29782-0.
- [256] Jin Wang, Kun Zhang, Li Xu, and Erkang Wang. Quantifying the Waddington landscape and biological paths for development and differentiation. *Proceedings of the National Academy of Sciences*, 108(20):8257–8262, May 2011. doi: 10.1073/pnas.1017017108. Publisher: Proceedings of the National Academy of Sciences.
- [257] James E. Ferrell. Bistability, Bifurcations, and Waddington’s Epigenetic Landscape. *Current Biology*, 22(11):R458–R466, June 2012. ISSN 0960-9822. doi: 10.1016/j.cub.2012.03.045.
- [258] Meritxell Saez, Robert Blassberg, Elena Camacho-Aguilar, Eric D. Siggia, David A. Rand, and James Briscoe. Statistically derived geometrical landscapes capture principles of decision-making dynamics during cell fate transitions. *Cell Systems*, 13(1):12–28.e3, January 2022. ISSN 2405-4712. doi: 10.1016/j.cels.2021.08.013.
- [259] Nicole Radde. Analyzing fixed points of intracellular regulation networks with interrelated feedback topology. *BMC Systems Biology*, 6(1):57, June 2012. ISSN 1752-0509. doi: 10.1186/1752-0509-6-57.
- [260] Peter Haenggi, Peter Talkner, and Michal Borkovec. Reaction-rate theory: fifty years after Kramers. *Rev. Mod. Phys.*, 62(2):251–341, April 1990. doi: 10.1103/RevModPhys.62.251. Publisher: American Physical Society.
- [261] Daniel T Gillespie. A general method for numerically simulating the stochastic time evolution of coupled chemical reactions. *Journal of Computational Physics*, 22(4):403–434, December 1976. ISSN 0021-9991. doi: 10.1016/0021-9991(76)90041-3.
- [262] Daniel T. Gillespie. Exact stochastic simulation of coupled chemical reactions. *J. Phys. Chem.*, 81(25):2340–2361, December 1977. ISSN 0022-3654. doi: 10.1021/j100540a008. Publisher: American Chemical Society.

Versicherung

Hiermit versichere ich, dass ich, Felix Jonathan Meigel, die vorliegende Arbeit ohne unzulässige Hilfe Dritter und ohne Benutzung anderer als der angegebenen Hilfsmittel angefertigt habe. Die aus fremden Quellen direkt oder indirekt übernommenen Gedanken sind als solche kenntlich gemacht. Die Arbeit wurde bisher weder im Inland noch im Ausland in gleicher oder ähnlicher Form einer anderen Prüfungsbehörde vorgelegt. Die vorgelegte Arbeit wurde im Zeitraum von Februar 2019 bis Februar 2023 unter Betreuung durch Prof. Dr. Steffen Rulands und Prof. Dr. Frank Jülicher am Max-Planck-Institut für Physik komplexer Systeme durchgeführt. Ich versichere, dass ich bisher keine erfolglosen Promotionsverfahren unternommen habe. Ich erkenne die Promotionsordnung der Fakultät der Mathematik und Naturwissenschaften der Technischen Universität Dresden an.

Felix Jonathan Meigel

Ort, Datum